Gholam Reza Darvish

Physical Effects Controlling Mass Transfer in Matrix Fracture System During CO_2 Injection into Chalk Fractured Reservoirs

PhD Thesis

April 2007

Faculty of Engineering Science and Technology

Department of Petroleum Engineering and Applied Geophysics

NTNU

Acknowledgements

I wish to express my sincere gratitude to my supervisor, Professor Jon Kleppe and co-supervisor Dr. Erik Lindeberg. With their enthusiasm, their inspiration, and their great efforts to explain things clearly and simply, they helped to make my research life full of hope for the future. Throughout my research, they provided encouragement, sound advice, good teaching, good company, and numerous good ideas.

I would like to thank, my previous colleagues at Sintef Petroleum Research Dr. Torleif Holt and Dr. Frode Vassenden and my M.Sc. supervisors Professor Curtis H. Whitson and Professor Ole Torsæter for their kind assistance with work in the laboratory, giving wise advice, helping with various applications, and so on.

I wish to thank in addition Oddmund Frigård, Svein Arild Utne, and other colleagues at Sintef Petroleum Research for their technical assistance, and also the secretaries in the Department of Petroleum Engineering and Applied Geophysics for their help during my career at Sintef Petroleum Research.

I also acknowledge the editorial assistance from Stewart Clark, Norwegian University of Science and Technology and Robert Drysdale from Sintef.

For financial support, I thank the National Iranian Oil Company (NIOC) and Sintef Petroleum Research

I wish to thank my father and my mother and entire family for providing a loving environment to complete my research.

Lastly, and most importantly, I wish to thank my wife Armin for her kindness and help. I would have been lost without her help.

Summary

Tertiary recovery or Improved Oil Recovery (IOR) methods are key processes to replace or upgrade reserves, which can be economically recovered, beyond conventional methods. Therefore, the application of IOR methods offers opportunities to increase the hydrocarbon reserves that have been produced in addition to those coming from exploration and reservoir appraisal.

The purpose of this thesis is to combine experiments, computations, and theory to make fundamental advances in our ability to predict transport phenomena as well as the IOR potential involved in tertiary CO_2 injection at the lab scale in a matrix fracture system. This is done by using rock and fluid samples similar to one of the chalk fractured reservoirs in the North Sea.

The work involves a review of key physical mechanisms and calculation methods for the modelling of fluid flow in fractured reservoirs. The main matrix fracture fluid exchange mechanisms described are gravity drainage, capillary imbibition and molecular diffusion. Also described are the estimation of the recovery performance for a single block and a stack of blocks surrounded by gas. The effect of interfacial tension on the ultimate recovery has been discussed and the definition of the minimum miscibility pressure for single porosity and dual porosity system is described.

Numerical modelling of gravity drainage for a matrix blocks surrounded by gas has been described. Numerical estimation of gas-oil gravity drainage by reducing the number of grid blocks in vertical direction in a draining matrix column is common practice in order to reduce the simulation time. However this can lead to systematic numerical errors and consequently underestimation of the recovery.

In order to minimize the underestimation of the reservoir performance, a set of pseudo functions needs to be developed that not only satisfy the actual responses in the fine grid simulation but also reduce the simulation time. The effectiveness and the accuracy of such pseudo functions are extensively discussed and the different simulation models have been run to quantify the underestimation of recovery by coarse griding in the numerical modelling of gravity drainage.

The importance of the molecular diffusion to recover oil from a high fracture intensity system is described as well as the basic concept for calculating the molecular diffusion based on the Fick's second law. Corresponding laboratory methods for the estimation and measurement of the oil and gas diffusion coefficients are reviewed. The effect of molecular diffusion on the interfacial tension and eventually on the gas-oil capillary pressure is presented.

A compositional study of a non-equilibrium gas injection process such as CO_2 requires an equation of state (EOS) model which can predict the CO_2/oil phase behaviour. In order to make such EOS model, a set of pVT experiments using fluids involved in the core flooding has been performed and finally the EOS models were tuned against experimental pVT data. The necessary steps to perform pVT experiments including making live reservoir oil, constant composition expansion, single flash, viscosity measurements and CO_2-oil swelling are described.

Gas injection is known to have a significant potential for high ultimate recovery in many oil fractured reservoirs with tall matrix blocks. The high ultimate recovery in these reservoirs could be due to the effectiveness of the gravity drainage mechanism.

Fractured chalk reservoirs in the North Sea have a very high porosity (up to 45%), and low matrix permeability (3-4 mD) with small matrix block size. In order to quantify the dominant transport mechanisms and potential of Improved Oil Recovery (IOR) in the case of CO_2 injection in the North Sea chalk fractured reservoirs, CO_2 injection experiments at reservoir conditions have to be performed in the laboratory.

The feasibility of such laboratory experiments initially has been verified by performing compositional simulation. In these simulations by varying the experimental parameters, such as core height and fracture size, the optimum matrix and fracture geometry were designed and the summary of the task is presented in Paper 1- Appendix A.

CO_2 injection experiments under reservoir conditions in the presence of different water saturation at reservoir conditions have been carried out. A unique technique has been developed for saturating the matrix system with reservoir fluids. This method ensures a homogeneous fluid composition within the pore system before the fracture system is initialized with the CO_2.

A complete description of, rock and fluids, experimental procedure and experimental results is given in Chapters 3, 4 and Papers 2 and 3 in Appendices B, C. In order to investigate the effect of temperature on the oil recovery mechanism, CO_2 injection experiments were carried out at initial reservoir temperature (130 ºC) and a low temperature 60 ºC which representing the water flooded parts in the reservoir. The effect of initial water saturation also was investigated at reservoir temperature 130 ºC by performing two experiments with different initial water saturation.

Results from these experiments show a high potential for oil recovery in all experiments. In the high temperature experiments, the produced oil had a variable composition during CO_2 injection, while at the low temperature condition, the produced oil initially had a constant composition and then it started to change. Different behaviour of produced oil composition in the high and low temperature might be due to dominant of diffusion mechanism in the high temperature experiments.

In the low temperature (60 ºC) experiment, at the early stage of CO_2 injection the produced oil had constant composition for a short period of time and then it changed to variable composition similar to the high temperature case. This behaviour maybe is due to high solubility of CO_2 into oil and consequently more oil swelling than the high temperature condition.

In order to quantify the above mechanisms, several attempts have been done to history match the experiments by using compositional simulator. But in all cases, it was not possible to history match the experiments.

The weakness of the simulator was due to the improper formulation which was used for calculating the cross phase diffusion between the oil and gas phase in the matrix and fracture system. The details of simulation work as well as the cross phase diffusion issue are discussed in Chapter 5 and Paper 2 in Appendix B.

Table of Contents

1. Introduction

For most producing oil fields a conventional approach to enhanced oil recovery (EOR) is the use of water or hydrocarbon gas. However in the most cases applying these methods does not fulfil the social benefits in the form of environmental considerations. The unique properties of supercritical carbon dioxide (CO_2) not only is able to improve the oil production in the final (tertiary) phase of reservoir life, but also has respectable environmental benefits for minimizing greenhouse gas (GHG) emissions.

The injection of CO_2 in various forms has been applied by the oil industry since the early 1960s (Ramsay and Small, 1964). Based on the published empirical rough screening criteria (Nelms and Burke 2004), oil reservoir characteristics found to be most favourable for CO_2 miscible flooding are summarized below:

- Oil reservoirs that have demonstrated good water flood response are the best candidates for CO_2 flooding.
- Prior to the application of CO_2 miscible flooding, the water flood oil recovery factor should be greater than 20% of the OOIP but less than 50% of the OOIP.
- The oil reservoir depth must be greater than 2,500 ft to reach CO_2 minimum miscibility pressure (MMP), which is a function of lithostatic pressure, bottom hole temperature, and oil composition.
- An oil gravity greater than 27 degrees API with an oil viscosity less than 10 centipoises (cp) at reservoir conditions is ideal.
- Formation porosity greater than 12% with an effective permeability to oil of greater than 10 millidarcies (mD) is ideal

A major part of the world oil reserves are present in naturally fractured reservoirs. Preliminary recoveries of all fractured reservoirs are accompanied by rising fracture water oil contact thus the residual oil saturation is still high and this residual oil can be targeted for more advanced CO_2 injection EOR projects. Based on classical fractured reservoir production mechanism, when an oil-saturated matrix block is surrounded by CO_2 in the fracture, oil and water will drain from the matrix as a result of density difference between the CO_2 and the oil/water.

The Warren and Root model is used in most commercial simulators for studying and simulating fractured reservoirs. This model is a dual continua model in which one continuum contains the fracture domain and the other contains the matrix domain. Even using the Warren and Root (1963) model for the matrix-fracture system, the calculation of the ultimate oil recovery from a single matrix when it is surrounded by CO_2 is very difficult. This difficulty comes from the large compositional space existing between the oil and the CO_2 in the matrix domain and fracture domain respectively.

Several authors like Van Golf-Racht (1982), Saidi (1987) tried to approach matrix fluid displacement through the use of simplified dynamics models, where more attention has been given to the forces involved in the process and less attention to the compositional effects between both domains. Depending on the matrix and fracture fluid properties, the compositional effects will change the balance of all forces and this may change the displacement results to a completely opposite direction from what was initially expected.

Understanding complex mechanisms and actual dynamics of field scale CO_2 injection for fractured reservoirs must be investigated by performing a set of complete core and laboratory analysis of rock and reservoir fluids that mimic actual reservoir conditions and mass transfer effects as realistically as possible during the injection of CO_2.

The input from these laboratory experiments could be in the form of the recovery performance for a single matrix blocks as well as better understanding of the contribution of each individual force in the recovery mechanism. In addition the results could also be scaled up to a larger block size and finally development of the necessary transfer functions for any field scale simulation.

However performing these kinds of laboratory experiments at the reservoir conditions will face with many challenges. One of the most important challenges for performing these experiments is saturating the matrix and fracture fluids with the representative reservoir fluids.

Because of the large permeability contrast between the matrix and the fracture it is difficult to saturate the matrix by simply flooding the system with live oil. Oil will flow through the fracture and only partially saturate the core. A literature review shows that in most of the previous experiments live oil has not been used for core initialization.

For example in the CO_2 gravity drainage experiments performed by Li et al. (2000), the core was saturated with dead oil while the experiment was supposed to be done under reservoir conditions.

Dry gas injection in fractured chalk by Øyno et al. (1995) was conducted by saturating the matrix system with live oil, but their method for initialization of the pore system with live oil is not certain. In their experiment the oil recombination was carried out in the core holder where the matrix and fracture were placed. The oil/gas mixture was circulated in the system and the pressure was monitored. Once pressure had stabilized, they assumed that the pore system is saturated with the live oil. In this method, since the pore system was saturated with oil by a very slow diffusion mechanism, pressure stabilization over a short time interval will not guarantee homogeneous initialization of the pore system with representative reservoir fluids

The main objective of this PhD thesis work has been to perform laboratory CO_2 injection experiments at the reservoir conditions in fractured chalk cores focussing on the performance of CO_2 injection in water flooded chalk fractured reservoirs. In these experiments, a unique technique has been developed for saturating the matrix system with representative reservoir fluids while the fractures are saturated by CO_2.

Different CO_2 injection scenarios into fractured cores were carried out and the component exchange between the oil in the matrix and CO_2 in the fracture was monitored. The recovery profiles as well as the produced fluid compositions were used to construct a compositional numerical model. By using the developed compositional numerical model special attention has been given to the compositional effects between both the matrix and fracture domains. The magnitude of all forces as well as their contribution to the displacement mechanism during the experiments was studied.

1.1 Organization

As outlined in Section 1 the objective of the thesis is (1) to perform laboratory CO_2 injection experiments at reservoir conditions in fractured chalk cores (2) simulating the displacement mechanisms by compositional simulators.

The following chapter (Chapter 2) discusses fluid flow and all possible displacement mechanisms in fractured reservoirs. Chapter 3 explains fluid and rock characterization, all pVT measurements and finally gives a description of the equation of state (EOS).

In Chapter 4 the CO_2 injection experiments in an artificially fractured chalk core at reservoir conditions are explained. In Chapter 5, the history matching and numerical simulation of the first has been explained. The published papers regarding the numerical and laboratory experiments are given in Appendices A, B and C.

1.2 References

1) Hujun, Li. “Experimental Investigation of CO2 Gravity Drainage in a Fractured System,” paper SPE 64510 presented at the SPE Asia Pacific Oil and Gas Conference and Exhibition held in Brisbane, Australia, 16–18 October 2000

2) Nelms, Ralph L., and Burke, Randolph. B., (2004). “Evaluation of Oil Reservoir Characteristics to Assess North Dakota Carbon Dioxide Miscible Flooding Potential”, 12th Williston Basin Horizontal Well and Petroleum Conference 2-4 May, 2004 Minot, North Dakota.

3) Øyno, L, Uleberg K., Whitson C.H. “Dry Gas Injection in Fractured Chalk Reservoirs- an Experimental Approach”, Paper SCA1995-27 presented at the International Symposium of the Society of Core Analysts held in San Fransisco.

4) Ramsay, H.J. and Small, F.R., (1964). “Use of Carbon Dioxide for Water Injectivity Improvement”, Journal of Petroleum Technology

5) Saidi A.M. (1987). “Reservoir engineering of fractured reservoirs (Fundamental and practical aspects)”, Total Edition Presse, Paris

6) Van Golf-Racht, T.D. (1982). “Fundamentals of Fractured Reservoir Engineering, Developments in Petroleum Science, no. 12, Elsevier Scientific Publishing Company, Netherlands.

7) Warren, J.E. and Root, P.J. "The Behaviour of Naturally Fractured Reservoirs," SPEJ (Sept. 1963) 245-255.

2. Displacement mechanisms in the case of non-equilibrium gas injection in naturally fractured reservoirs

This chapter reviews the main governing equations and the key physical mechanisms for modelling gravity drainage. The main matrix fracture fluid exchange mechanisms described are gravity drainage and molecular diffusion. Important issues such as, gas/oil interfacial tension and its dependency on the composition of the fluid, minimum miscibility pressure and finally the importance of molecular diffusion in fractured reservoirs are also addressed.

2.1 Introduction

In fractured reservoirs carbon dioxide, nitrogen, or hydrocarbons can be used as injection gas for increasing oil recovery. Based on classical fractured reservoir production mechanism, when an oil-saturated matrix block is surrounded by gas in the fracture, oil and water will drain (gravity drainage) from the matrix because of the density difference between the gas and the oil/water. The drainage rate depends on the magnitude of capillary force (interfacial tension), gravity forces and in displacement front. Interfacial tension (IFT) and diffusion forces are compositionally dependent and the magnitude of these forces is variable as the displacement front is moving inside the matrix blocks. These variations depend on the component exchange between the gas and oil inside the displacement front.

Variation in frontal interfacial tension can potentially have a significant impact on the flow behaviour in the matrix fracture system. The high frontal interfacial tension prevents entering of the gas into the matrix blocks and causing the early gas breakthrough, wherein the case of low frontal interfacial tension, the flow of gas into matrix blocks will be easier than previous case and high drainage rate with late gas breakthrough.

Diffusion forces are controlled by the concentration gradient of each component inside the displacement front as well as the component concentration gradient between the gas and oil inside the fracture and matrix respectively.

Injection of non-equilibrium gas into fracture system is accompanied by compositional effects between the gas in the fractures and oil in the matrix and consequently changing frontal composition Stubos (1999). These changes are sometimes favourable or unfavourable for displacement. Appling this compositional effect into the flow equations complicates the estimation of ultimate recovery during non-equilibrium gas injection in fractured reservoirs.

Several authors like Van Golf-Racht (1982), Saidi (1987) have tried to approach matrix fluid displacement through the use of simplified dynamics models, where more attention has been given to the forces involved in the process and less attention to the compositional effects between gas and oil in the displacement front.

2.2 Dual porosity permeability concept

Barenblatt et al. (1960) introduced the dual porosity permeability concept. In his concept, he assumed the existence of two porous regions of distinctly different porosities and permeabilities within the formation. In addition, one continuum was assumed, where any small volume contains a large proportion of both media. Hence

each point in space should have two pressure values, P_f and P_m associated with it for high permeable and less permeable media respectively.

This concept was completed and introduced for the modelling of fractured reservoirs in an idealized manner by Warren and Root (1963). The Warren and Root model is a dual continua model in which one continuum contains the fracture domain and the other contains the matrix domain. In this model the porous system of any reservoir is divided into two parts:

- Primary Porosity (Matrix)
- Secondary Porosity (Fracture)

The matrix is a portion of the porous system that is inter-granular and controlled by the deposition method. This media contributes significantly to fluid storage but because of low permeability, its contribution to fluid flow is low.

Secondary porosity or fractures are the portion of the porous system that is caused by fracturing, solution or other post-depositional phenomena. This media is highly permeable and hence contributes significantly to the fluid flow as it is not very porous, its contribution to fluid storage is negligible.

2.3 Gas oil gravity drainage displacement mechanism

Gas-oil gravity drainage takes place when gas from gas saturated fractures displaces oil in the matrix. The free gas may be gas liberated from the oil that has segregated in the fractures, gas from an expanding gas cap, or gas from gas injection. The density difference between the oil and gas phases provides the energy for the gravity drainage mechanism.

Knowledge of the mechanism that is taking place in fractured reservoirs has been progressively improved since the 1960s when large research projects on major issues were initiated. The world knowledge on fractured reservoirs was extremely poor prior to the 1960s.

This can be noted among other improper practices from the comments made by a group of experts from several major oil companies who investigated Iranian fractured reservoirs in 1954. They stated “In the Iranian field, gravity drainage may be small .The dominant reservoir mechanism in these fields were then believed to be dissolved gas-expansion from matrix into the fissure.” The same concept was initially used to produce the Speraberry field in Texas in early fifties. It is now evident that the solution gas derived mechanism in Iranian fracture reservoirs caused recovery losses due to oil shrinkage, and the recovery mechanism is essentially gravity drainage. (A.M. Saidi, 1979).

2.4 Gas-oil gravity drainage for a single block

During the production of a fractured reservoir, the fractures may be invaded either by gas or by water. If the matrix block is surrounded by gas, the gravity forces tend to drain oil from the matrix and the capillary forces to retain the oil. If the gas in the fracture system is immiscible with the oil in the matrix and both phases are in thermodynamic equilibrium, the saturation profile within the matrix block at the end of the production may be derived by equating gravity and capillary forces:

$$P_c(S_g) = \left(\rho_o - \rho_g\right).h.g \quad \text{.....2-1}$$

Where $P_c(S_g)$ is the capillary pressure, ρo and ρg are the densities of oil and gas, g is the gravitational acceleration, h is the height of the matrix block by saturation Sg. Figure 2.1 shows the oil saturation profile in a matrix block surrounded with gas in the fracture.

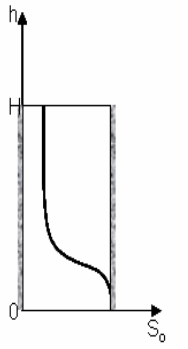

Figure 2.1 The oil saturation profile in a matrix block surrounded with gas

Van Golf (1982) presented the mathematical model for a single matrix block saturated by oil and surrounded by gas in the fracture system. In his model, the following assumptions have been made:

- The gas was considered to be the non-wetting phase
- The gas compressibility was ignored
- Immiscible displacement
- One dimensional flow
- The capillary pressure at the interface was assumed constant.

For each matrix block with the above assumptions two cases can be considered:

- Oil saturated block is totally surrounded by gas. This case corresponds to the blocks located in the gas invaded zone as shown in Figure 2.2.
- An oil saturated block, is partially surrounded by gas. This case corresponds to the blocks located in the interval between gas invaded zones in Figure 2.2.

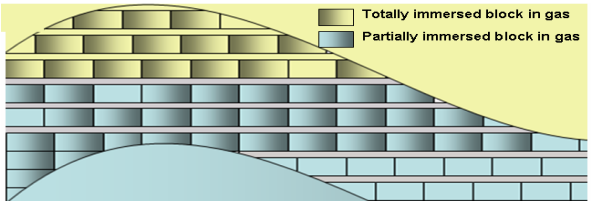

Figure 2.2 Fracture reservoir invaded by gas-cap.

2.4.1 Block is totally surrounded by gas

A block initially saturated by oil and totally surrounded by gas is shown in Figure 2.3.

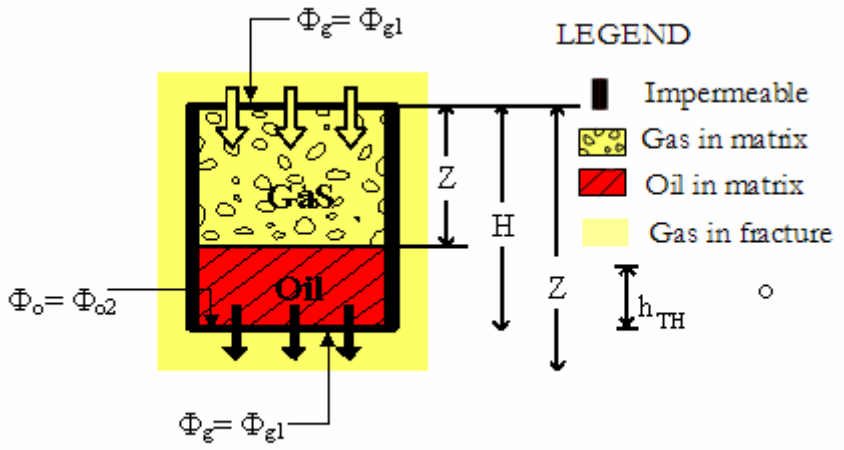

Figure 2.3 Schematic of a matrix block when totally immersed in gas (After Van Golf, 1982).

The initial pressure of the gas column is considered to be above the threshold pressure; therefore, gas can enter the block and oil velocity can be calculated by Eq.2-2.

$$U = \frac{g(H-Z)\Delta\rho - P_c}{\frac{\mu_g}{KK_{rg}}\left[MH + (1-M)Z\right]} \quad \text{.....2-2}$$

In Eq. 2-2, H and Z are the matrix block height and gas level in the matrix block respectively, M = (μ_o/K_o)/ (μ_g/K_g) is mobility ratio.

In the displacement of oil by gas, the capillary pressure has a negative effect on oil recovery. Oil can be produced when the gravitational forces exceed capillary forces and the gas level in fracture, Hg is higher than the threshold height, $H_g > h_{TH}$. Depending on the value of the capillary pressure and the block height, when H_g is equal to h_{TH} equilibrium is reached and oil will no longer be displaced. The relationship between the fraction of the recovered oil and time is obtained by substituting $U = \Phi \cdot dz/dt$ in Eq. 2-2 and integrating with initial conditions t = 0, Z = 0, the results obtained are:

$$t_{D,G,P_c} = Z_D(M-1) - \left[M + (1-M)(1 - \frac{P_c}{gH\Delta\rho})\right] \ln\left(1 - \frac{P_c}{gH\Delta\rho} - Z_D\right) \quad \text{.....2-3}$$

Where the dimensionless height $Z_D = Z/H$ is fraction of oil produced and $t_{D.G.P_c} = K \cdot K_{rg_{\max}} \cdot g \cdot \Delta\rho / \Phi\mu_g H$ is dimensionless time. When the capillary pressure P_c is much smaller than the gravity force, Eq. 2-3 becomes:

$$t_{D,G,P_c} = Z_D(M-1) - \ln(1-Z_D) \quad \text{.....2-4}$$

Eq. 2-4 is the basic analytical solution for estimation of the recovery Z_D as a function of dimensionless time for the case where the capillary pressure P_c is much smaller than the gravity force.

2.4.2 Block is partially surrounded by gas

Figure 2.4 shows a case in which the oil saturated block is partially surrounded by gas. This case corresponds to the gas front which did not reach the lower face of the block, and thus the problem will be the same as in the case of totally immersed block.Displacement will start when the column of gas in the fractures is higher than the threshold height.

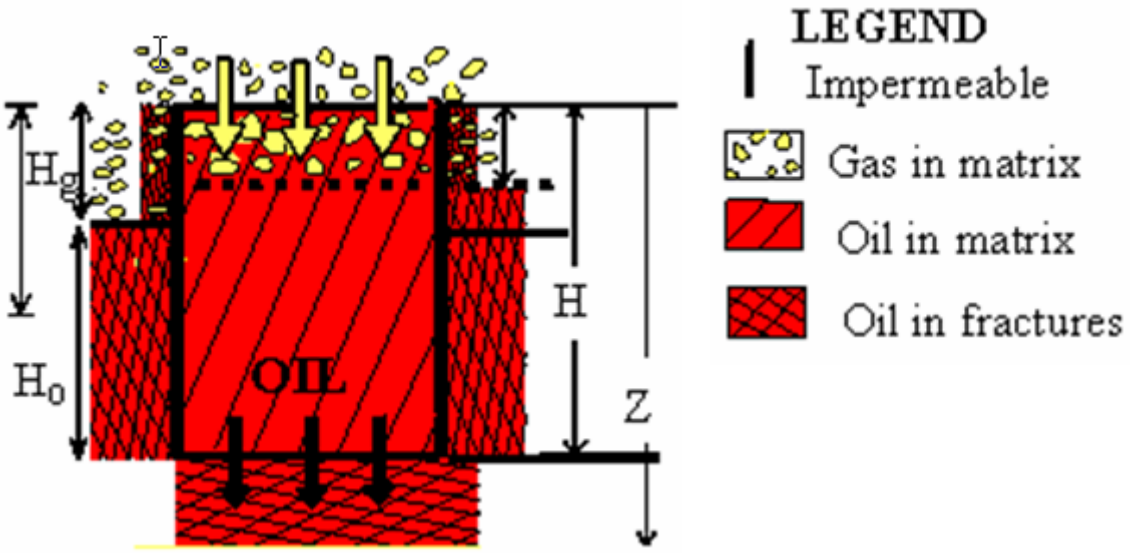

Figure 2.4 Schematic of a matrix block when partially immersed in gas (After Van Golf, 1982

In this case displacement will cease when the gas-oil contact in the matrix reaches the threshold height. The velocity of oil in this case can be obtained by Eq. 2-5

$$U = \frac{g\left[H_g - (H - Z)\right]\Delta\rho - P_c}{\frac{\mu_g}{KK_{rg}}\left[MH + (1-M)Z\right]} \quad \text{.....2-5}$$

It is obvious from Figure 2.1, the matrix recovery depends on the balance of gravity and capillary forces. Figure 2.5 shows that for a given capillary pressure curve; four singlematrix blocks of different heights will behave differently. Block 1 will contain unrecoverable oil, block 2 will be recovered slightly, and more and more oil will be recovered in blocks 3 and 4. This means that in taller blocks the gravity forces could overcome the capillary resistance to the entrance of the displacing fluid.

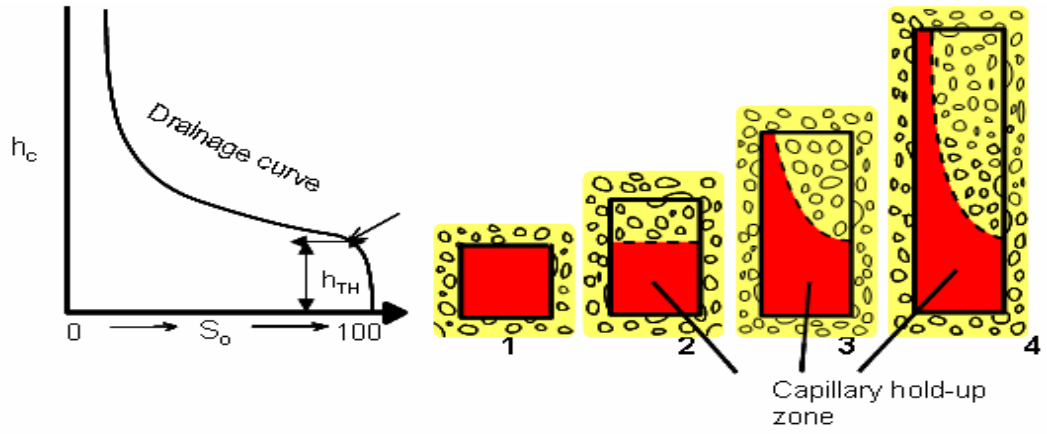

Figure 2.5 Effect of block height on the displacement of oil by gas (After Van Golf, 1982)

2.5 Numerical evaluation of gas-oil gravity drainage

The matrix-block concept is used for simulating gas-oil gravity drainage (GOGD) in a gas cap of a naturally fractured reservoir. In this concept, a draining matrix rock column is considered to be a stack of individual matrix blocks with low permeability surrounded by fractures with high permeability. A dual-permeability approach where the matrix blocks and fractures are simulated as continua superimposed on each other can be used to simulate the performance of these reservoirs.

In these circumstances performing a dual permeability dual porosity simulation in field scale requires simulation time that may not be as reasonable and sometimes it is impossible. To achieve reasonable simulation times in a field scale simulation, the number of grid blocks has to be minimized. However, reducing the number of grid blocks in a vertical direction in a draining matrix column in gas-oil gravity drainage simulations lead to systematic underestimation of the oil drainage rate. In order to minimize the underestimation of the reservoir performance, it is necessary to develop a set of pseudo functions that not only satisfy the actual responses in the fine grid simulation but also reduce the simulation time.

Krijn (2002) presented pseudo-relative permeability relations for numerical grid cells in gas-oil gravity drainage simulations. Using these pseudo relations, the fine vertical grid cells system in a draining matrix block was converted to a coarse grid cells without any effect on the drainage performance of the matrix block (in the extreme case only one numerical grid cell can be used).

Depending on the position of cells, in this method, a different pseudo relative permeability relation is assigned and consequently it is possible to largely reduce and in some cases completely remove the simulation error. The procedure developed by Krijn (2002) for calculating the pseudo-relative permeability functions in a coarse grid simulation is discussed in the following sections.

2.5.1 Development of pseudo-relative permeability relations

The idea of developing pseudo-relative permeability relations comes from the fact that the finite difference methods have been used for solving the flow equations in all reservoir simulators (Krijn 2002). In the finite difference approximation the simulation

model or the draining column which consists of several individual matrix blocks (located on the top of each other) are subdivided into a number of discrete numerical grid cells so-called a block-cantered grid system. In this system, the mid point of each grid cell represents the average property of the grid cell.

The average grid property approaches the local property when the number of the numerical grid approaches infinite or uses a fine grid system. The fine grid simulation will eliminate the mismatch between average and local grid property and consequently eliminates all possible numerical errors involved in the finite difference approximation.

Considering the long simulation time in the case of fine grid simulation, and the need to solve the flow equation, the modelling must be performed by using a course grid system. In this condition proper pseudo functions have to be used to relate the average grid property to the local property. This will reduce the risk of using any coarse grid simulation.

These pseudo relations should be applicable to a variety of cases where different forces like capillary and gravity are involved in the displacement mechanism. The most important cases where these kinds of pseudo relations are applicable can be defined as follows:

- A single isolated matrix block surrounded by fractures filled with gas
- A draining column consisting of several matrix blocks located on top of each other with permeability contrast

Pseudo relative permeability relations in a homogeneous draining matrix block

Consider a homogeneous matrix block saturated with oil with height H and surrounded by fractures which are filled with gas. The numerical grid model for the matrix block is shown in Figure 2.6. For this system the gravity drainage can be simulated by using the rock relative permeability relation and capillary pressure using the finite difference approximation considering the following assumptions (Krijn 2002):

- One-dimensional vertical flow
- Immiscible gas
- Infinite gas mobility
- Corey exponent type oil relative permeability
- No capillary pressure (for simplicity)

Figure 2.6 shows the matrix block is divided by N equal grid cells with $\Delta Z = H/N$ and average initial oil saturation of $\overline{S}_{oi}$ Considering infinite gas mobility, the value of mobility ratio M in Eq. 2-2 becomes much larger than one (M>>1) and therefore it can be simplified to Eq. 2-6.

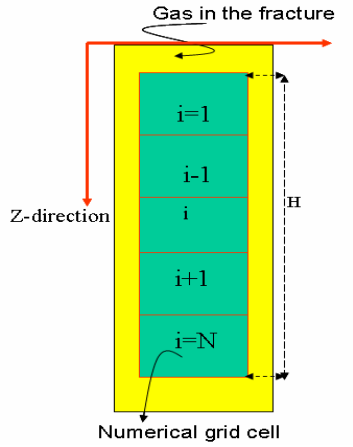

Figure 2.6 A draining single matrix block divided to N number of numerical grid cells and having initial average saturation of S_{oi}

$$U_o(z,t)=\frac{\Delta\rho.g.k_m}{\mu_o}\left[S_o(z,t)\right]^n=U_m.\left[S_o(z,t)\right]^n \quad \text{2-6}$$

$$U_m=\frac{\Delta\rho\cdot g\cdot k_m}{\mu_o} \quad \text{2-7}$$

The local material balance for any arbitrary point in the column can be written as indicated in Eq.2-8.

$$\frac{\partial U_o}{\partial z}=-\varphi\frac{\partial S_o}{\partial t} \quad \text{2-8}$$

Defining, $T=\frac{\varphi\cdot H}{U_m}$, $U_m=\frac{\Delta\rho\cdot g\cdot k_m}{\mu_o}$, $y=\frac{z}{H}$, and the dimensionless time as $\tau=\frac{t}{T}$ Eq. 2-8 can be written as:

$$n.S_o^{n-1}.\frac{\partial S_o}{\partial y}=-\frac{\partial S_o}{\partial \tau} \quad \text{2-9}$$

From exact differential equation relations:

$$\left(\frac{dy}{d\tau}\right)_{S_o}=-\frac{\frac{\partial S_o}{\partial \tau}}{\frac{\partial S_o}{\partial y}} \quad \text{2-10}$$

Applying Eq. 2-10 into Eq. 2-9, the material balance equation can be written as:

$$\frac{dy}{d\tau}=n.S_o^{n-1} \quad \text{2-11}$$

Using the method of characterization for solving partial differential equation for a specific time the saturation profile in the column can be obtained by integration of Eq. 2-11, this result is:

$$\frac{dy}{d\tau}=n.S_o^{n-1}\Rightarrow y(S_o)=n.S_o^{n-1}\cdot\tau \quad \text{2-12}$$

Considering Eq.2-12, the following important results can be obtained:

- The gas front $(S_o = 1)$ has a dimensionless velocity $\frac{dy}{d\tau} = n$
- The gas front will arrive at the bottom of the column $y = 1$ at $\tau = \frac{1}{n}$
- For $\tau \leq \frac{1}{n}$, the drainage rate at the bottom of the column is at its maximum value (U_m) where the oil saturation S_{ob} at the bottom is equal to one.
- For the dimensionless time $\tau \rangle \frac{1}{n}$, the bottom oil saturation S_{ob} declines below one and consequently the bottom drainage rate U_{ob} become smaller than U_m.

Inserting $y = 1$ in Eq. 2-12 gives S_{ob} as a function of τ and results in:

$$\frac{U_{ob}}{U_m} = S_{ob}^n = \left(\frac{1}{n\tau}\right)^{\frac{n}{n-1}}, \text{ for } \tau \rangle \frac{1}{n} \quad \text{..... 2-13}$$

$$\frac{U_{ob}}{U_m} = 1, \textit{for } \tau \leq \frac{1}{n} \quad \text{..... 2-14}$$

For $\tau \rangle \frac{1}{n}$ the oil saturation profile is given by:

$$y(S_o) = \left(\frac{S_o}{S_{ob}}\right)^{n-1} \quad \text{..... 2-15}$$

Let us now consider an arbitrary interval of the column between $z = z_1$ and $z = z_2$ with the oil saturation profile for $\tau \rangle \frac{1}{n}$:

$$\frac{z}{H} = \left(\frac{S_o(z)}{S_{ob}}\right)^{n-1} \text{ or } \frac{z}{z_2} = \left(\frac{S_o(z)}{S_o(z_2)}\right)^{n-1} \quad \text{..... 2-16}$$

Using Eq.2-16, the average oil saturation of the interval (z_1, z_2) as a function of oil saturation at the bottom can be obtained by integration of oil saturation over that interval as shown in Eq.2-17.

$$\overline{S}_o = \frac{\int_z^{z_2} S_o(z_2).\left(\left(\frac{z}{z_2}\right)^{\frac{1}{n-1}}\right).dz}{z_2 - z_1} \quad \text{..... 2-17}$$

$$\overline{S}_o = S_o(z_2).\frac{z_2}{z_2 - z_1}\left[1 - \left(\frac{z_1}{z_2}\right)^{\frac{n}{n-1}}\right].\frac{n-1}{n}$$

In the finite difference approximation or numerical method for solving the continuity Eq. 2-8 a vertical continuous rock column is described by a limited number of grid layers as shown in Figure 2.6. By this approach, the actual oil saturation profile is replaced by oil saturation at the grid centre point, representing the average saturation of each grid layer or interval. In such a simulation, the drainage rate of an individual grid cell is calculated from the relative permeability at the grid cell oil saturation.

The actual drainage rate at the bottom of a grid cell however, is based on the relative permeability at the oil saturation at the bottom of that block, which is always higher, in view of the shape of the actual oil saturation profile. The ratio f between the interval average oil saturation $\overline{S}_o$ and the oil saturation at the bottom of such interval can be obtained from Eq. 2-18. Knowing this value, we can correct for this error by applying this factor f to the oil saturation of a grid block.

$$f = \frac{\overline{S}_o}{S_o(z_2)} = \frac{z_2}{z_2 - z_1}\left[1 - \left(\frac{z_1}{z_2}\right)^{\frac{n}{n-1}}\right].\frac{n-1}{n} \quad \text{..... 2-18}$$

A more practical approach is to introduce this factor f directly into the relative permeability relation itself, giving rise to a pseudo relative permeability relation (Krijn 2002):

$$k_{or_{ps}}(\overline{S}_o) = k_{or}(\overline{S}_o / f) \quad \text{..... 2-19}$$

The factor f is different for each interval in the column, as it depends on both z_1 and z_2. Consequently, each interval or grid cell requires a separate pseudo-relative permeability relation. By introducing for each interval (or grid block):

$$i = \frac{z_2}{z_2 - z_1} \quad \text{..... 2-20}$$

The following relation between f_i and i can be derived by substituting Eq. 2-20 into Eq. 2-18.

$$f_i = \frac{n-1}{n}.i.\left[1 - \left(\frac{i-1}{i}\right)^{\frac{n}{n-1}}\right] \quad \text{..... 2-21}$$

If the rock column is divided in N equally spaced grid blocks, the parameter i coincides with the grid block number, counted downwards.

The top block $i = 1$ always has a value of $f_1 = n-1/n$. For very large N, the factor f for the bottom blocks approaches 1, indicating that the pseudo-relative permeability relation approaches the rock relative permeability relation for such a block.

When the actual oil saturation profile is such that the gas front $(S_o = 1)$ has not yet reached the bottom of a particular grid cell, the average oil saturation in that grid cell is between f and 1, while the actual oil saturation at its bottom is still 1, i.e. an effective relative permeability of 1, despite reduced (average) oil saturation. The relation in Eq. 2-19 therefore has to be extended to:

$$k_{or_{ps}}(\bar{S}_o) = k_{or}(\bar{S}_o / f) \text{ For } \bar{S}_o \langle f \quad \text{2-22}$$

$$k_{or_{ps}}(\bar{S}_o) = 1 \text{ For } f \le \bar{S}_o \le 1 \quad \text{2-23}$$

Using the above pseudo relations, the actual drainage rate of each grid cell is correctly calculated from its average oil saturation.

Pseudo relations for several matrix blocks with permeability contrast

The pseudo relative permeability relations (Krijn 2002) in the case of several matrix blocks with permeability contrast can be obtained by using the same approach as described in the previous section. Figure 2.7 shows the oil saturation profile in a heterogeneous stack of draining blocks. The assumptions and boundary conditions for the derivation of the pseudo relations are as follow:

- One-dimensional vertical flow
- In the case of over flow, the drained oil from the top most permeable will go to the vertical fracture. Therefore there is no restriction of drainage for cases where the top block is more permeable than the lower block.
- Oil relative permeability is calculated using $k_{ro} = S_o^n$

Eq. 2-17 is used for relating the average oil saturation in each block and the oil saturation in its bottom

Based on the above assumptions and using Eq. 2-12, the time that gas front arrives at the bottom of each matrix block when there is permeability contrast is calculated by:

$$\tau_i = \frac{1}{n} \cdot \left(1 + \frac{K_1}{\varphi_1 \cdot H_1} \cdot \sum_{j=2}^{j=i} \frac{\varphi_j H_j}{K_j} \right) \text{ for } i \ge 2 \quad \text{2-24}$$

$$\tau = \frac{1}{n} \text{ for i} = 1 \quad \text{2-25}$$

In Eqs. 2-24 and 2-25 the dimensionless time is calculated based on the first matrix block which means $T = \varphi_1 \cdot H_1 / U_{1_m}$ and $\tau = t / T$.

Using the defined dimensionless time for each block, the proper rate equation can be put inside the material balance equation.

The derivation of the pseudo relations for several blocks on the top of each other has been described extensively by Krijn (2002). The summary of the most important results are as follows:

The drainage performance in a stack of two blocks with a permeability contrast indicates that pseudo-relative permeability relations that include a constant reduction factor f in the saturation can be effectively used. However the value of factor f_i for block i is no longer a unique function of i and should be corrected according to the position of the block in the stack.

If in a heterogeneous stack of blocks, block *i* has permeability k_i, porosity φ_i and block height H_i , the following relation holds for the effective block number i_{ef} and f_i.

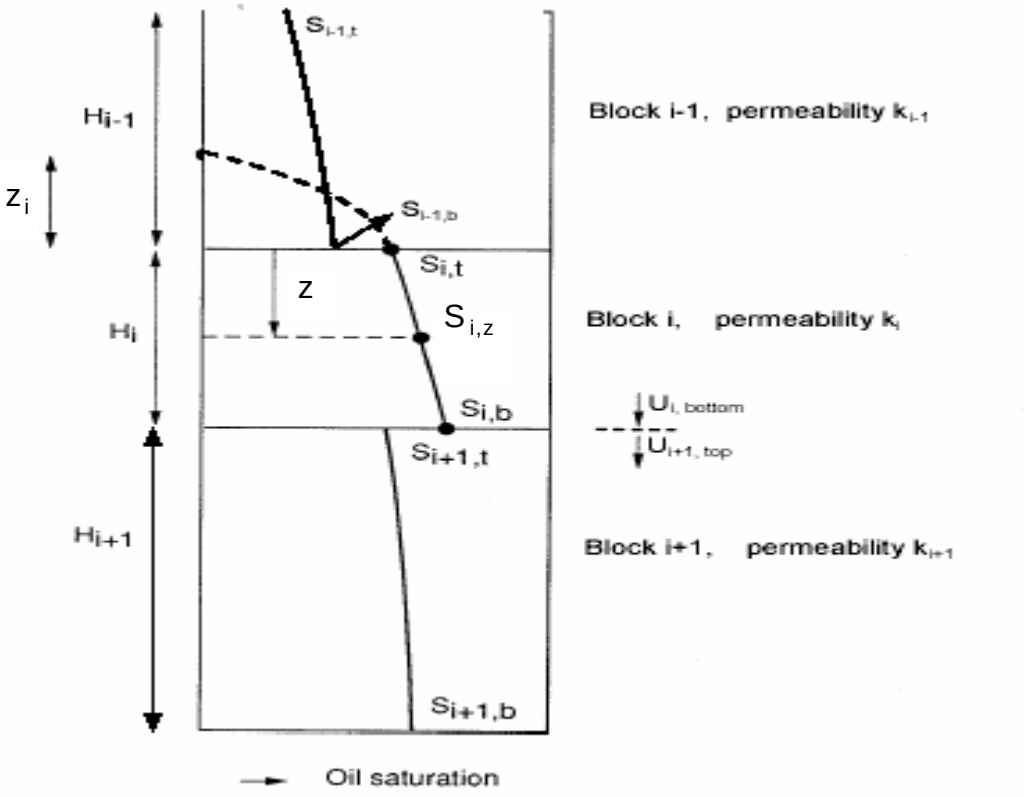

Figure 2.7 Oil saturation profiles in a heterogeneous stack of draining blocks (after Krijn 2002)

$$i_{eff} = \frac{k_i^{\frac{1}{n}}}{H_i \cdot \varphi_i} \sum_{j=1}^{j=i} \frac{H_j \cdot \varphi_j}{k_j^{\frac{1}{n}}} \quad \text{2-26}$$

$$f_i = \left(\frac{n-1}{n}\right) \cdot i_{eff} \cdot \left[1 - \left(\frac{i_{eff}-1}{i_{eff}}\right)^{\frac{n}{n-1}}\right] \quad \text{2-27}$$

It is important to note that the above procedures are only applicable to gravity drainage without capillary hold-up effects in the individual blocks and for free drainage of oil towards fixed gas-oil contact at the bottom of the column. For cases where the capillary pressure exists the pseudo relations should be corrected using f_i^* which can be calculated by using Eq.2-28.

$$k_{ior_{pseudo}}(\overline{S}_o) = k_{or}\left(\frac{\overline{S}_o}{f_i^*}\right) \quad \text{2-28}$$

$$f_i^* = f_i + (1 - f_i) \cdot \overline{S}_{o_{ult_i}}$$

In Eq. 2-28 the correction factor f_i is the factor where there is no capillary pressure for block i and $\overline{S}_{o_{ult_i}}$ is the ultimate capillary hold-up average oil saturation for each block in the column.

2.6 Analytical gravity drainage performance of two matrix blocks

In order to check the numerical drainage performance of two matrix blocks by the above pseudo functions, the analytical gravity drainage performance of two matrix blocks by the same procedure as given by Krijn (2002) is developed in the following section.

Derivation of the analytical drainage equations by considering all parameters in the process would be very complicated, therefore for simplicity the analytical drainage of a simple system consist of two matrixes blocks as it is shown Figure 2.8 is considered.

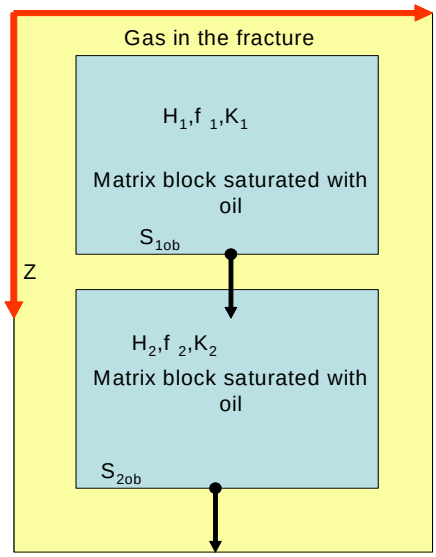

Figure 2.8 Two draining matrix blocks with different properties

Figure 2.8 shows two draining matrix blocks with different properties. It is assumed that the oil relative permeability for each block is calculated by Corey exponent type oil relative permeability relation $k_{ro} = S_o^n$ and that each block has a different block height (H), porosity (φ) and permeability (K). Using Eqs. 2-24 and 2-25 the time that gas front arrives at the bottom blocks 1 and 2 is $\frac{1}{n}$ and $\frac{1}{n}\cdot\left(1+\frac{K_1}{\varphi_1\cdot H_1}\cdot\frac{\varphi_2.H_2}{K_2}\right)$ respectively.

For $\tau \le \frac{1}{n}$ the oil saturation at the bottom of the upper matrix block S_{o_b} is equal to 1 therefore if a semi-steady state condition is assumed the material balance for the upper block will be:

$$U_{1top} - U_{1bottom} = \varphi_1 \cdot H_1 \cdot \frac{d\overline{S}_o}{dt} \quad \text{.....2-29}$$

Assume that there is no flow from the top of the block $U_{1top} = 0$. The flow from the bottom of the top block is calculated by:

$$U_{1bottom} = \frac{\Delta\rho \cdot g \cdot K_1}{\mu_o} \cdot S_{1o_b}^{\ n} \quad \text{2-30}$$

The bottom oil saturation for block1 in this time interval $0 \le \tau \le \frac{1}{n}$ is equal to 1. Assume $U_{1_m} = \frac{\Delta\rho \cdot g \cdot K_1}{\mu_o}$, $T = \frac{\varphi_1 \cdot H_1}{U_{1_m}}$ and $\tau = \frac{t}{T}$ applying them in Eq.2-29, the material balance equation for block 1 will be:

$$d\overline{S}_{1_b} = -d\tau \quad \text{2-31}$$

Integration of Eq. 2-31 gives the drainage performance for time $0 \le \tau \le \frac{1}{n}$ as:

$$\overline{S}_{1_o} = 1 - \tau \text{ for } 0 \le \tau \le \frac{1}{n} \quad \text{2-32}$$

Or in terms of the recovery factor R:

$$R = \tau \text{ for } 0 \le \tau \le \frac{1}{n} \quad \text{2-33}$$

Applying the material balance of block1 for time $\tau \rangle \frac{1}{n}$:

$$S_{1ob}^{\ n} = -\frac{d\overline{S}_{1o}}{d\tau} \quad \text{2-34}$$

Eq. 2-34 can be solved if the relation between the average oil saturation $\overline{S}_{1o}$ and the block bottom oil saturation S_{1_b} is known. The relation between the average oil saturation $\overline{S}_{1o}$ and the block bottom oil saturation is calculated by using Eqs. 2-20 and 2-21 where i=1.

$$f_1 = \frac{\overline{S}_{1o}}{S_{1ob}} = \frac{n-1}{n} \Rightarrow S_{1ob} = \left(\frac{n}{n-1}\right) \cdot \overline{S}_{1o} \quad \text{2-35}$$

Applying Eq. 2-35 into Eq. 2-34 we will have:

$$\left(\frac{n}{n-1}\right)^n \cdot \overline{S}_{1o}^{\,n} = -\frac{d\overline{S}_{1o}}{d\tau} \quad \text{2-36}$$

Integration of Eq. 2-36 with the boundary conditions gives:

$$\left(\frac{n}{n-1}\right)^n \cdot \int_{\frac{1}{n}}^{\tau} d\tau = -\int_{1-\frac{1}{n}}^{\overline{S}_{1oo}} \frac{d\overline{S}_{1o}}{\overline{S}_{1o}^{\,n}}$$

$$\overline{S}_{1o} = \left[\left(1-\frac{1}{n}\right)^{1-n} + \left(\frac{n}{n-1}\right)^{n-1} \cdot \left(n \cdot \tau - 1\right)\right]^{\frac{1}{1-n}} \quad \text{2-37}$$

Eq. 2-37 in terms of recovery will be:

$$R = 1 - \left[\left(1 - \frac{1}{n}\right)^{1-n} + \left(\frac{n}{n-1}\right)^{n-1} \cdot \left(n \cdot \tau - 1\right) \right]^{\frac{1}{1-n}} \quad \text{2-38}$$

Eqs. 2-37 and 2-38 are for the top block and have drainage performance after $\tau > \frac{1}{n}$.

The same methodology can be applied for the second block to find its gravity drainage performance.

For lower block, (block no 2), in the time interval $0 \le \tau \le \frac{1}{n}$ there are three possibilities:

- Case 1 The maximum drainage of the second block is equal to the first block, therefore all drained oil from top block will go to lower the block and there is no saturation change in this block until time $\tau = \frac{1}{n}$.
- Case 2 The maximum drainage rate of the second block is smaller than the first block, therefore the saturation of the second block will not change and the over rate from the first block will drained through the fracture system and the saturation of the second block start to change after time $\tau > \frac{1}{n}$.
- Case 3 The maximum drainage rate of the second block is larger than the first block; therefore the saturation of the second block will start to change from time $\tau < \frac{1}{n}$.

The gravity performance of the second block for case 1 is discussed in detail and for the other cases the analysis is the same as case 1.

Case 1: The maximum drainage of the second block is equal to the first block; therefore the following conditions should be satisfied:

The second block average oil saturation $\overline{S}_{2o}$ is equal to 1 for time $\tau \le \frac{1}{n}$ and therefore the second block recovery factor $R = 0$.

$$\frac{K_1}{H_1 \cdot \varphi_1} = \frac{K_2}{H_2 \cdot \varphi_2} \quad \text{2-39}$$

Applying Eq. 2-39 into Eq. 2-24 the time of gas break through for the bottom of the second block is:

$$\tau_{2gas\_brek} = \frac{2}{n} \quad \text{2-40}$$

In this condition the second block bottom oil saturation S_{2ob} is equal to 1 for time $\tau \le \frac{2}{n}$. The material balance for the second block for time $\frac{1}{n} < \tau \le \frac{2}{n}$ can be written as:

$$U_{1b} - U_{2b} = \varphi_2 \cdot H_2 \frac{d\overline{S}_{2o}}{dt} \quad \text{2-41}$$

In Eq.2-41, U_{1b} is the first block drainage rate coming into the second block and U_{2b} is the second block drainage rate coming out from the bottom of the second block and it is calculated by its bottom oil saturation. Using the drainage performance from the first block, the U_{1b} can be written as:

$$U_{1b} = U_{1m} \cdot \left(\frac{1}{n\tau}\right)^{\frac{n}{n-1}} \quad \text{2-42}$$

For the second block U_{2b} is equal to:

$$U_{2b} = U_{2m} \cdot \bar{S}_{2ob}^{n} \quad \text{2-43}$$

Applying both Eqs. 2-43 and 2-42 into Eq.2-41, it gives:

$$\left(\frac{1}{n\tau}\right)^{\frac{n}{n-1}} - 1 = \frac{d\bar{S}_{2o}}{d\tau} \quad \text{2-44}$$

Solving Eq. 2-44 gives the second block drainage performance for time period $\frac{1}{n} < \tau \le \frac{2}{n}$.

$$\bar{S}_{2o} = 1 + \frac{1}{n} + (1-n)\left(\frac{1}{n}\right)^{\frac{n}{n-1}} \cdot \left(\tau^{\frac{1}{1-n}} - \left(\frac{1}{n}\right)^{\frac{1}{1-n}}\right) - \tau \quad \text{2-45}$$

For time $\tau > \frac{2}{n}$ the oil saturation at the bottom of the second block starting to decline below 1. In this condition the material balance for the second block is the same as Eq.2-41, but the oil saturation at the bottom of the block is not equal to 1. Therefore it is important to find the relation between the average oil saturation and bottom oil saturation for the second block.

Using Eqs. 2-26 and 2-27 the relation between the average oil saturation and bottom oil saturation for the second block is calculated as:

$$\frac{\bar{S}_{2o}}{S_{2ob}} = f_2 = 2 \cdot \left(\frac{n-1}{n}\right)\left(1 - \left(\frac{1}{2}\right)^{\frac{n}{n-1}}\right) \quad \text{2-46}$$

Using Eq. 2-46 the material balance Eq. 2-41 will be:

$$\left(\frac{1}{n\tau}\right)^{\frac{n}{n-1}} - \left(\frac{\bar{S}_{2o}}{f_2}\right)^{n} = \frac{d\bar{S}_{2o}}{d\tau} \quad \text{2-47}$$

By solving Eq.2-47, the second block average oil saturation for time $\tau > \frac{2}{n}$ can be found and consequently the recovery performance of the second block can be calculated.

2.7 Case studies using pseudo-relative permeability relations

The accuracy of the developed pseudo relations by Krijn (2002) for the following cases has been investigated by a simple black oil model using the Eclipse 100 version (2004):

- A single draining matrix block
- Two draining matrix blocks with permeability contrast

For each case the simulated results have been compared with the analytical solution developed in the previous section.

2.7.1 Single matrix block

One isolated matrix block 15 feet in height, saturated with oil and surrounded with fractures filled with gas has been considered. The recovery of the matrix block was modelled with fine grid modelling using the rock relative permeability and the results are compared with coarse grid modelling using pseudo relations for the oil relative permeability.

In the fine grid model (base case) 50 grid cells in the Z-direction $\left(N_z = 50\right)$ with the rock relative permeability with Corey exponent $n = 2$ were used. Then the number of grid cells in the Z-direction was reduced from 50 to 6 in one case, and in another extreme case, the number of grid cells in the Z-direction was reduced from 50 to 1. In all three cases, the capillary force assumed to be zero, matrix permeability was 2 mD and fracture permeability was 500 mD. The oil and gas properties are indicated in Table 2.1.

Table 2.1 Oil and gas properties used in all simulations

Gas viscosity	0.003	cp
Gas density	0.169	kg/m^3
Oil viscosity	1.50	cp
Oil density	600	kg/m^3

The matrix oil relative permeability for the base case $\left(N_z = 50\right)$ is calculated by $k_{ro} = S_o^2$ and the fracture oil relative permeability is assumed to have a linear relation with oil saturation.

Using Eq. 2-21 and applying n=2, the value of *f* for different cases can be calculated. The calculated values for *f* for different number of grid block in the Z-direction are given in Table 2.2. The rock and pseudo relative permeability for each case are calculated and shown in Figure 2.9

The pseudo-relative permeabilities are generated by using Eqs. 2-18 and 2-19 with the Cory exponent n=2.

The simulated results are compared in Figure 2.10. This figure shows that in the case of using the rock relative permeability without any modification, the underestimation of the drainage performance increases as the number of grid cells in the Z-direction

decreases. This figure also shows that using the pseudo relations for the oil relative permeability reduces the underestimation of the drainage performance.

Table 2.2 The f factor for different grid number in the Z-direction calculated using Equation 5-15.

Case	N_Z	f
Base Case	50	1.00
N_Z=6	6	0.92
N_Z=1	1	0.5

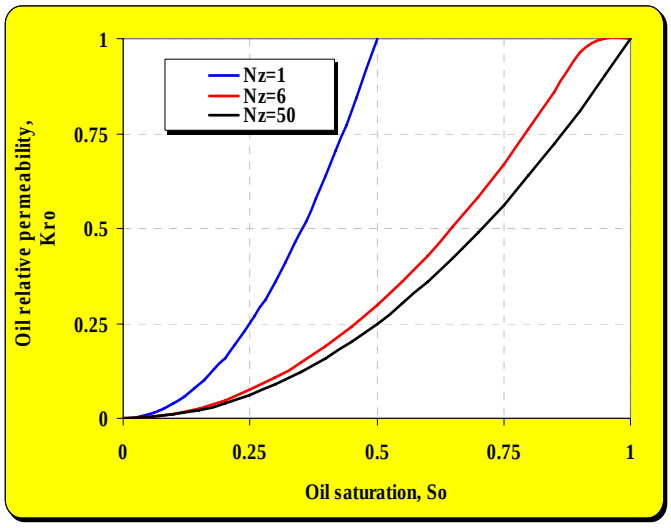

Figure 2.9 The rock relative permeability used in the simulations for three cases Nz = 50, 6 and 1.

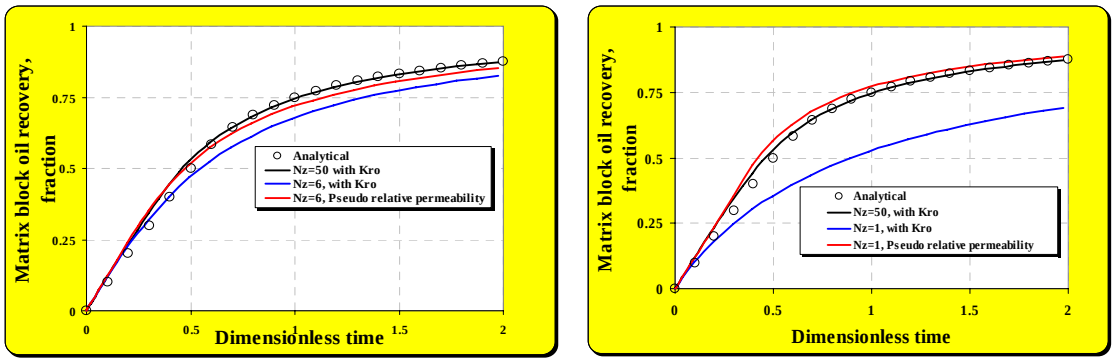

Figure 2.10 The drainage performance for the case with one grid cell in the Z-direction and using pseudo relations for calculating relative permeability

In Figure 2.10 the analytical values are calculated by using Eq. 2-48 in which the Corey exponent is n=2.

$$\begin{cases} R = \tau & \text{for } \tau \le \dfrac{1}{n} \\ R = 1 - \dfrac{n-1}{n} \cdot \left(\dfrac{1}{n\tau} \right)^{\frac{1}{n-1}} & \text{for } \tau \rangle \dfrac{1}{n} \end{cases} \quad \text{..... 2-48}$$

Table 2.3 The simulated oil recovery at dimensionless time for a single matrix block for a different girding system and with and without pseudo relative permeability relations

Case	Oil recovery at dimensionless time τ=2		Oil recovery at dimensionless time τ=2	
	Simulated without modifying K_{ro}	Error (%)	Simulated with modifying K_{ro}	Error (%)
Fine grid Nz= 50	87 %	0.00	87 %	0.00
Coarse grid Nz= 6	83 %	5.66	85 %	2.40
Coarse grid Nz= 1	69 %	26.18	89 %	1.65

Table 2.3 shows that the maximum value of error for simulated oil recovery at dimensionless time $\tau = 2$ is equal to 26.2 % and this error is reduced to 1.67 % after modifying the relative permeability by using pseudo relation function.

2.7.2 Two draining block

In this section the accuracy of the pseudo relation for the system consists of two matrix blocks on the top of each other has been investigated. The configuration for this system was shown in Figure 2.8 and the corresponding pseudo relations were shown in Eqs. 2-26 and 2-27.

Considering two matrix blocks with equal height on the top of each other, the following cases can be considered:

- Both blocks have the same absolute permeability (K_1=K_2)
- The permeability of the top block is more than the lower block (K_1=4K_2)
- The permeability of the top block is less than the lower block (K_2=4K_1)

For all three cases, in the base case simulation model the number of numerical grid cells in the Z-direction is N_z =50 and for coarse girds the number of grid cells in the Z-direction is reduced to one. The other simulation parameters for each case are shown in Table 2.4.

Eqs. 2-27 and 2-28 have been used to calculate the corresponding pseudo-relative permeability relation for coarse grid simulations.

Both blocks have the same absolute permeability

The fluid property for this case is the same as the previous case and was shown in Table 2.1. The rock permeability is calculated by $k_{ro} = S_o^2$. The capillary pressure inside the fractures and the matrix blocks assumed to be zero. The factors *f*=0.5 and *f*=0.75 for the first and second matrix blocks have been calculated by using Eqs. 2-26 and 2-27.

The pseudo relative permeability for each matrix block with *f*=0.5 and *f*=0.75 is shown in Figure 2.11. The rock curve (black) was used in the fine grid simulation of the model where each matrix block was assumed to have 50 grid blocks in the Z-direction. The pseudo curves (blue and red) were used in the coarse grid simulation where each matrix block was considered as one grid cell.

Table 2.4 The matrix properties for the simulation of the two matrix block on the top of each other.

Case	Top block			Bottom block		
	Matrix permeability (mD)	Porosity %	Block height (ft) ft	Matrix permeability (mD)	Porosity %	Block height (ft) ft
Case 1	2	20	15	2	20	15
Case 2	8	20	15	2	20	15
Case 3	2	20	15	8	20	15

By using Eqs. 2-33 and 2-38, the analytical drainage performance of each block has been calculated. The drainage performance of each block and the stack by using pseudo relative permeability functions was shown in Figure 2.13.

Figure 2.13, Figure 2.13 and Table 2.4 clearly show the advantage of using pseudo relative permeability curves to minimize the simulation error. The simulation results for the lower and upper blocks show a significant improvement when the pseudo relations have been used in a coarse grid simulation whereas the rock relations lead to systematically underestimated recovery.

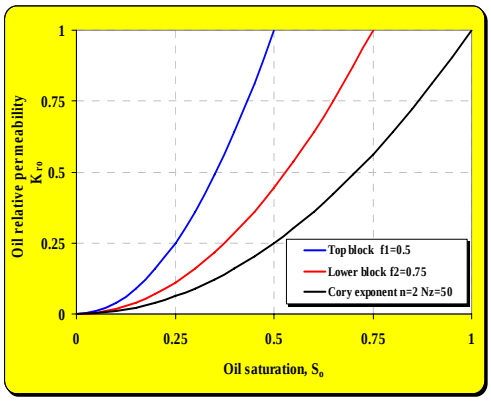

Case 1 $K_1=K_2$

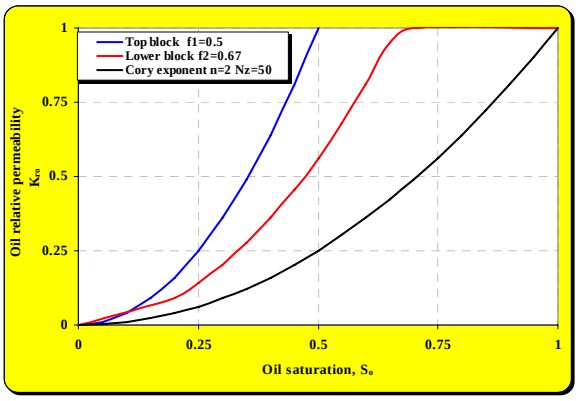

Case 2 $K_1=4K_2$

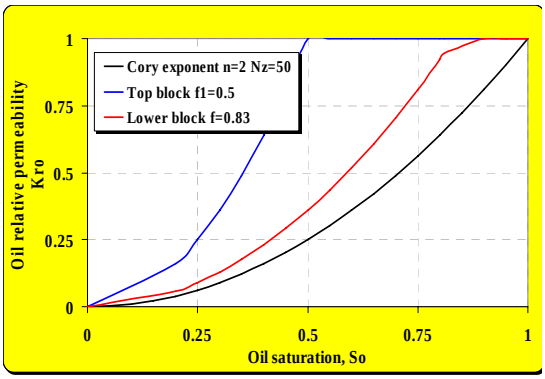

Case 3, $K_2=4K_1$

Figure 2.11 *Pseudo relative permeability used for the top and bottom blocks in the case of coarse grid simulation and oil relative permeability calculated by Eqs. 2-26 and 2-27*

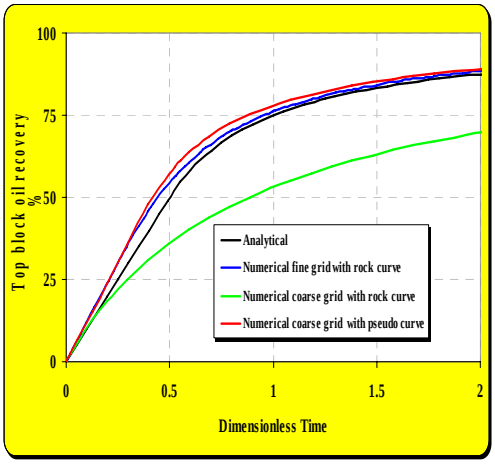

Top block

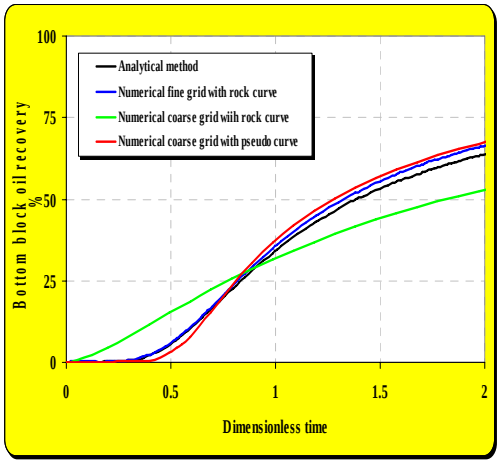

Bottom block

Figure 2.12 *The drainage performance vs. dimensionless time for the upper and lower blocks for case1 $K_1=K_2$*

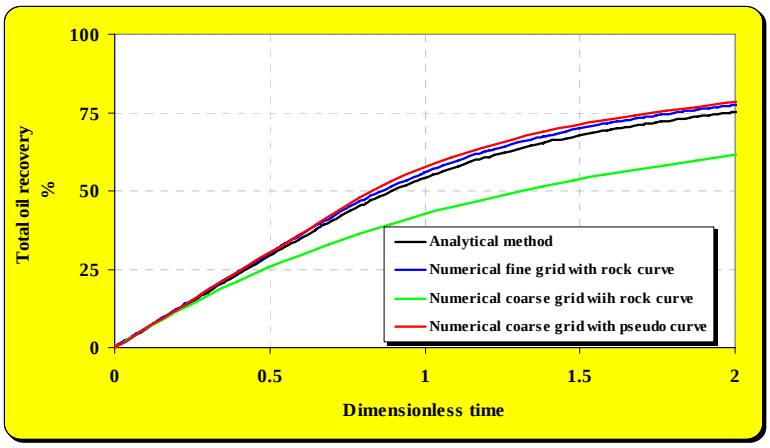

Figure 2.13 The stack drainage performance vs. dimensionless time for Case 1 (K_1=K_2)

The top block is the most permeable ($K_1 = 4K_2$)

The fluid property for this case is the same as the previous case and was shown in Table 2.1. The rock permeability is calculated by $k_{ro} = S_o^2$. The capillary pressure inside the fractures and the matrix blocks is assumed to be zero. Factors $f = 0.5$ and $f = 0.67$ for the first and second matrix blocks have been calculated by using Eqs. 2-26 and 2-27. The pseudo relative permeability for each matrix block with $f = 0.5$ and $f = 0.67$ are shown in Figure 2.11.

The rock curve (black) was used in the fine grid simulation of the model where each matrix block was assumed to have 50 grid blocks in the Z-direction. The pseudo curves (blue and red) were used in the coarse grid simulation where each matrix block was considered as one grid cell.

The drainage performance of each block and the stack by using pseudo-relative permeability functions are shown in Figure 2.14 and Figure 2.15. These figures clearly show the advantage of using pseudo relative permeability curves to minimize the simulation error. The simulation results for the lower and upper blocks show the significant improvement when the pseudo relations have been in a coarse grid simulation whereas the rock relations lead to systematic underestimated recovery.

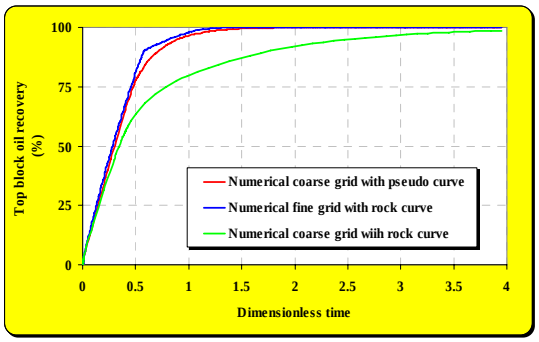

Top block

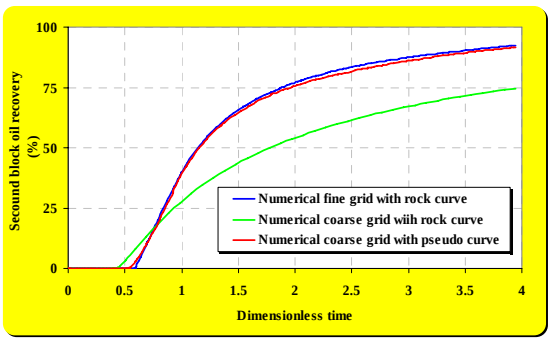

Bottom block

Figure 2.14 The drainage performance vs. dimensionless time for the upper and lower blocks for case K_1= $4K_2$

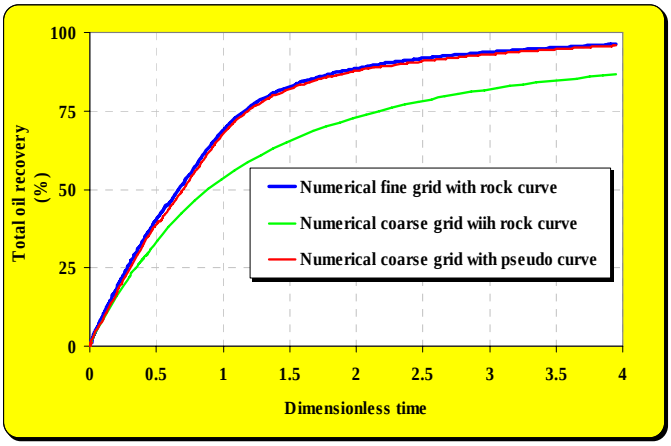

Figure 2.15 The stack drainage performance vs. dimensionless time for case: $K_1=4K_2$

The second block is the most permeable ($K_2=4K_1$)

The fluid property for this case is the same as the previous case and was shown in Table 2.1. The rock permeability is calculated by $k_{ro} = S_o^2$. The capillary pressure inside the fractures and the matrix blocks is assumed to be zero. The factors f=0.5 and f=0.83 for the first and second matrix blocks have been calculated by using Eqs. 2-26 and 2-27.

The pseudo-relative permeability for each matrix block with f=0.5 and f=0.83 is shown in Figure 2.11. The rock curve (black) was used in the fine grid simulation of the model where each matrix block was assumed to have 50 grid blocks in the Z-direction. The pseudo curves (blue and red) were used in the coarse grid simulation where each matrix block was considered to be one grid cell.

The drainage performance of each block and the stack by using pseudo relative permeability functions are shown in Figure 2.16 and Figure 2.17. These figures clearly indicate the advantage of using pseudo relative permeability curves to minimize the simulation error. The simulation results for the lower and upper blocks show the significant improvement when the pseudo relations have been in a coarse grid simulation whereas the rock relations lead to systematic underestimated recovery.

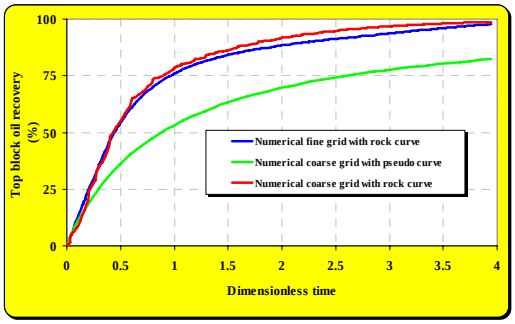

Top block

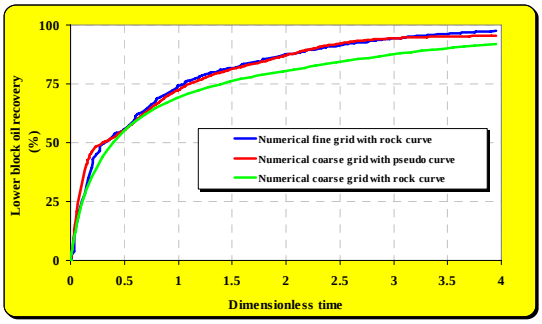

Bottom block

Figure 2.16 The drainage performance vs. dimensionless time for upper and lower block for case $K_2=4K_1$

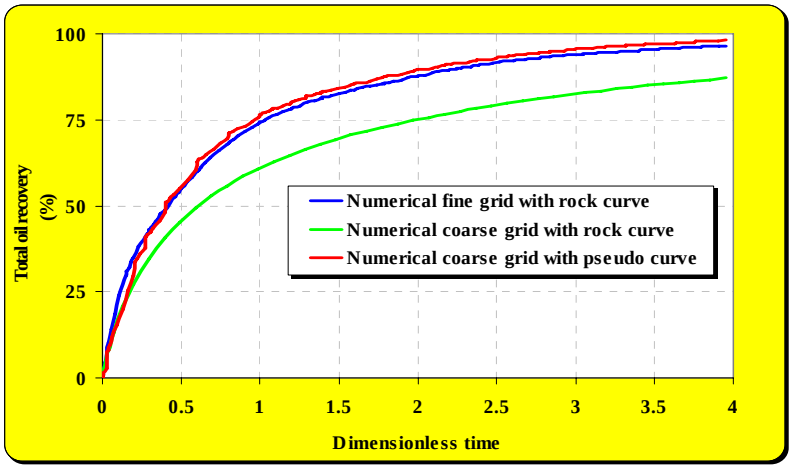

Figure 2.17 The stack drainage performance vs. dimensionless time for case $K_2=4K_1$

Simulation of gravity drainage by using the finite difference approximation will lead to systematic error. This error comes from the fact that the actual oil saturation profile (front) is replaced by oil saturation at the grid points, representing the average saturation of each grid layer or interval. In such simulation, the drainage rate of an individual grid layer is calculated from the relative permeability at the grid block oil saturation where the saturation is less than the front saturation. To minimize this error there are two possibilities:

First increasing the number of numerical grids, this minimizes the difference between the actual oil saturation profile and the average oil saturation of each grid layer. As discussed by Krijn (2002) the error is inversely proportional to $\sqrt{N}$ (N= number of grid cells) since a large number of grid blocks have to be used to make this error negligible, in the field scale simulation this will involve a lengthy simulation time which is unacceptable from a practical point of views.

Second, correcting the average oil saturation of each grid cell, which will have a direct effect on the calculation of the drainage rate for an individual grid layer. This method needs to develop a set of pseudo relations or transfer function. However the introduction of complicating factors such as permeability contrast and capillary hold-up in the system may affect the accuracy of such pseudo relations.

2.8 Interfacial tension and its effect on gas-oil gravity drainage

While most thermodynamic properties refer to individual fluid phases, interfacial tension (IFT) is unique in the sense that it is a property of the interface between the fluid phases. Being a sensitive property strongly dependent on the composition of the interacting phases (Al-Rub 1999), the IFT is a good indicator of mass transfer effects between the phases. Numerous methods have been proposed to estimate the surface tension of pure liquids and liquid mixtures. An extensive revision of these methods is given by Hirschfelder, et al. (1964). One of the simplest is the empirical formula proposed by Macleod (1923). It expresses the surface tension of a liquid in equilibrium with its own vapour as a function of the liquid- and vapour-phase densities as:

$$\sigma=K.\left(\rho_l-\rho_v\right)^4 \quad \text{..... 2-49}$$

In Eq. 2-49 K is a constant which is independent of temperature but is characteristic of the liquid under consideration. Sugden (1924) modified this expression as follows:

$$\sigma=\left[\left[P\right].\left(\rho_l-\rho_v\right)\right]^4 \quad \text{2-50}$$

In Eq. 2-50 $P=K^{\frac{1}{4}}$, Sugden called this temperature-independent parameter [P] the parachor, and indicated a way to estimate it from the molecular structure. Quayle (1953) used experimental surface tension and density data for numerous compounds to calculate the parachors of hydrocarbons. He was able to suggest an additive procedure to correlate the parachors [P] with a structural contribution. The right-hand side of Eq. 2-50 implies that surface tension is very sensitive to the value of the parachor and liquid density. It has been shown that the parachor is a weak function of temperature for a variety of fluids and within wide ranges of temperature (Macleod, 1923; Sugden, 1924; Quayle, 1953), and thus it is generally assumed to be a constant.

Eq. 2-50 has been shown to be good for surface tension prediction, as long as experimental data for the parachor and equilibrium densities are employed. Thus, it may be considered as an equation of state for the interface. The good performance and extreme simplicity of its analytical form have made Eq. 8-2 a very popular method for surface tension calculation (Weinaug and Katz, 1943; Lee and Chien, 1984; Hugill and van Welsenes, 1986; Gasem et al., 1989; Fanchi, 1985, 1990; Ali, 1994).

The McLeod-Sugden equation was extended to mixtures by Weinaug and Katz (1943) as it is shown in Eq. 2-51.

$$\sigma^{1/4}=\sum_{i=1}^{N}\left(\rho_l.\left[P\right]_i.X_i-\rho_v.\left[P\right]_i.Y_i\right) \quad \text{2-51}$$

In Eq. 2-51, X*i* and Y*i* are the mole fractions of component *i* in the liquid and vapour phases, respectively, and [P]*i* is the parachor of component *i*.

Danesh et al. (1991) reviewed some of the major contributions for predicting the surface tension of multi-component systems, observing that Eq. 2-51 is still one of the most widely used for this purpose. Danesh et al. (1991) also proposed a modification of the surface tension exponent, which was assumed to be a function of the difference between the density of the liquid and the vapour phases:

$$\sigma^{1/E}=\sum_{i=1}^{N}\left(\rho_l.\left[P\right]_i.X_i-\rho_v.\left[P\right]_i.Y_i\right) \quad \text{2-52}$$

Where parameter E is given by:

$$E=3.583+0.16\left(\rho_l-\rho_v\right) \quad \text{2-53}$$

The molar densities depend on temperature, phase pressure, and mole fractions. Therefore, the derivatives of the surface tension model may depend on terms that come from the equation of state adopted for the system (Ali J K 1994). Eqs. 2-52 and 2-53 are most widely used in the petroleum industry to estimate the interfacial tension between fluids. This requires an equation of state model EOS which is tuned based on the experimental data.

For a matrix block that is surrounded by the gas phase, the gravity forces tend to drain oil from the matrix and the capillary forces retain the oil. The capillary force is the

normal stress developed on the phase boundaries of curved objects (drops, bubbles, lamellae) which correlate with the principal radii of curvatures R_1 and R_2 and the surface or interfacial tension of phases. At pore level, the curvature of the interface is often assumed to be equal to the pore size, denoted by R. Thus, the capillary pressure between the fluids in a pore of size R is approximated by using the Young-Laplace equation (Lee, 1989; Tester and Modell, 1996; Sychev, 1981) in which the droplet assumed to be a perfect sphere with radius R.

$$P_c = \frac{2\sigma}{\mathrm{R}} \quad \text{2-54}$$

It is obvious from Eq. 2-54 that the capillary force is proportional to the interfacial tension between each phase. Any increase on the gas-oil interfacial tension causes increases in the capillary pressure and consequently increases the retaining force to keep the oil inside the pore system. In the extreme case the capillary force is balanced by the gravity force and no oil recovery can be expected from the matrix block from the gravity drainage mechanism. This was clearly was shown in the Figure 2.5 for block number 1 where the capillary forces are of the same order of magnitude of block height or gravity force.

Based on Eq. 2-54, capillary pressures must also go to zero as the surface tension vanishes, and here one would expect a linear dependence as shown in Eq. 2-55.

$$P_{cog}^{corr} = \left(\frac{\sigma}{\sigma_{ref}} \right) . P_{cog} \quad \text{2-55}$$

where P_{cog} the capillary pressure is measured at the reference surface tension σ_{ref} and P_{cog}^{corr} is the corrected capillary pressure for new surface tension σ. In the most reservoir simulations, Eq. 2-55 is considered for the scaling of the capillary pressure curves.

Based on Eq. 2-55 the capillary forces can be reduced to a minimum if the interfacial tension between the injected gas and the oil in the matrix is reduced to zero. In a miscible gas injection scheme, the interfacial tension between the injected gas and the oil can be minimized. This concept is explained in the following section.

2.9 Miscibility

More than half of the crude oil found in petroleum reservoirs is left behind at the end of primary recovery and secondary water flooding. This is due to rock–fluid interactions, including capillary forces, which prevent the oil from flowing within the pores of the reservoir rock, trapping huge amounts of residual oil in the reservoirs.

These capillary forces can be reduced to a minimum if the interfacial tension between the injected fluid and the trapped crude oil is reduced to zero. Thus there is a need for miscibility development between the gas injected (natural gas or CO_2) and the crude oil to remobilize these huge amounts of trapped oil and improve the oil recovery.

An injected gas becomes miscible with oil when enough light hydrocarbons concentrated in the gas enable the gas and liquid to become mutually soluble. Enriched hydrocarbon gas, carbon dioxide, flue gas or nitrogen can be used as injection gas to develop miscibility.

All of these gases become miscible only when their density at reservoir condition is high, generally greater than 0.5 g/cc. Thus, they work best at high pressure. For carbon dioxide, the minimum pressure is 75 barg at 31 ºC, i.e., when CO_2 becomes supercritical and its gas and liquid are no longer separate phases. At these conditions the density of carbon dioxide is high enough for it to be a good solvent for oil which contains a significant volume of light hydrocarbons.

As the temperature increases (CO_2 density decreases), or the API gravity decreases (light hydrocarbons decrease), the pressure needed to attain miscibility increases. So at 75 ºC, carbon dioxide develops miscibility at pressures greater than 172 barg.

Nitrogen on the other hand becomes an efficient miscible displacement only for light oils, temperatures greater than 115 ºC and pressures greater than 345 barg, where its density is high enough to extract light-hydrocarbons from the oil. Flue-gas works well at lower pressure and temperature, since it contains around 13 % carbon dioxide.

In conventional reservoirs, the miscible displacement process depends on fluid properties alone. In these reservoirs miscibility develops mainly due to three types of mass transfer mechanisms between the injected gas and the fluids in the reservoir, namely vaporizing gas drive, condensing gas drive and combined condensing vaporizing gas drive.

In the vaporizing gas injection process, the injected gas is relatively lean consisting mostly of methane and other hydrocarbons with low molecular weight. As the injected fluid moves through the reservoir, it comes in contact with the reservoir oil many times and becomes enriched in composition by vaporizing the intermediate components (C_2–C_4) in the crude oil. This process continues until the injected gas attains miscibility with reservoir oil.

In the condensing gas injection process, the injected gas contains significant amounts of intermediates (C_2–C_4). During the multiple contacts of the injected gas with crude oil in the reservoir, the intermediates condense from the gas phase into the oil phase. The continuation of this process modifies the reservoir oil composition to become miscible with additional injected gas, resulting in miscible displacement.

In the combined condensing/vaporizing process, the light intermediate compounds in the injected gas (C_2–C_4) condense into the reservoir oil, while the middle intermediate compounds (C_5–C_{10} to C_{30}) in the crude oil vaporize into the injected gas. This prevents miscibility between fluids near the injection point as the oil becomes heavier. As the injection of gas continues, there will be no further condensation of light intermediates from the injected gas into this saturated oil.

However, the vaporization of middle intermediates continues from the oil enriching the injected gas further. As this condensation/vaporization process continues farther into the reservoir, the gas becomes enriched to greater and greater extents as it comes into contact with more and more oil and eventually becomes miscible with the reservoir oil.

This mechanism, involving simultaneous counter-directional mass transfer of components between the phases, is shown to be the one that most frequently occurs during the displacements of oil by gas (Zick 1986).

2.9.1 Predication of minimum miscibility pressure in conventional reservoirs

For conventional reservoirs, the true minimum miscibility pressure (MMP), at a specific temperature can be obtained accurately using a series of slim tube displacement experiments. By definition, the recovery at 1.2 hydrocarbon pore volumes of injected gas is called ultimate recovery. The ultimate recoveries for various displacement pressures corresponding to average reservoir pressure are recorded for a given oil and injection gas. The recovery for an immiscible process increases with pressure.

The recovery versus pressure curve starts to flatten out when the displacement processes approach miscibility (Høier, 1997). The breakpoint recovery defines the minimum miscibility pressure, and is theoretically 100 percent. An alternative to experimental determination of miscibility is numerical simulation based on an equation of state (EOS) model (Høier, 1997). The accuracy of EOS predicated MMP/MME is strongly dependent on the accuracy of the EOS description of the actual fluid system, as well as the method used to simulate miscibility.

The slim tube experiment can be simulated by using an EOS based on a compositional reservoir simulator (Høier, 1997). In this method, a series of slim tube simulations should be made and the recoveries after 1.2 pore volumes of injected gas are recorded for each run. However numerical dispersion involved in the MMP calculation is a serious problem and needs to be eliminated.

Grid effect and numerical dispersion

Numerical dispersion and selection of grid sizes are common problems in most of the numerical simulation studies. In order to determine MMP by slim tube simulation, numerical dispersion can play an important role in the simulated results. The consequence of fine grid simulations gives a significant over prediction of MMP (Høier, 1997). On the other hand, slim tube simulation by several thousand grids, is time consuming especially in the case of compositional simulation. To compensate for this problem, Stalkup (1992) recommended a method to eliminate errors to predict true MMP. His method is described by the following procedure:

Step 1 An EOS characterization model that can predicate the relevant pVT properties for the system has to be prepared in advance.

Step 2 Using a compositional simulator to initialize one-dimensional 100 grid cells saturated with reservoir fluid using the same EOS model found in Step 1.

Step 3 Run six to eight slim tube simulations with 100 grids at different pressure in such a way that 3 to 4 selected pressures give recovery factor at 1.2 pore volume injected gas ($RF_{1.2}$) in the region 0.6 to 0.9 and other pressures give higher $RF_{1.2}$. The recovery factor at 1.2 pore volume injected gas ($RF_{1.2}$) is defined as:

$$RF_{1.2} = \frac{a-b}{a} \quad \text{2-56}$$

where a is initial oil volume at reservoir conditions after converting it to surface conditions, and b equals the remaining oil at reservoir conditions which is converted to surface conditions and after injecting 1.2 pore volumes (PV) of gas.

Repeat step 3 changing the number of grids from 100 to 500 and 1000 grids in the simulation model and performing the simulation with the same pressure in as used in Step 3 and record $RF_{1.2}$ for each run.

Step 4 Plot the $RF_{1.2}$ versus $\frac{1}{\sqrt{N}}$ (N = number of grids) for each pressure.

Step 5 From the graph obtained in the Step 4 extrapolate $RF_{1.2}$ to an infinite number of grids for each pressure.

Step 6 Plot the result obtained (RF_{∞}) in Step 5 versus pressure. At MMP the recovery (RF_{∞}) versus pressure curve starts to flatten out when the displacement is miscible.

It should be noticed that in one-dimensional system for the single porosity systems or conventional reservoirs, selection of rock properties such as grid size, porosity, permeability has no effect on the determination of MMP.

2.9.2 Predication of minimum miscibility pressure for a matrix-fracture system

In the matrix-fracture system, the miscible displacement process no longer depends on fluid properties alone. The fracture matrix geometry, size and interaction, and other physical phenomena also play an important role. The existence of high permeable fractures will help to override the well-defined displacement of oil by gas and consequently the fracture gas surrounds the matrix blocks being filled with oil. Depending on the fluids and the matrix-fracture network characteristics, different types of oil displacement mechanisms will start.

When dry gas is injected in a highly fractured/highly under-saturated oil reservoir, gas will be dissolved in the matrix oil, resulting in increasing saturation pressure and oil swelling. This can be together with decreasing oil viscosity, interfacial tensions, and a high amount of mass transfer from the matrix oil into matrix gas and vice versa. In these situations, the gas composition gradient inside the fracture and matrix becomes an essential parameter to develop miscibility. In this circumstance the molecular diffusion of gas dispersed through the fractures can change the miscible behaviour.

By considering the gas diffusion effect, the gas composition inside the matrix blocks is usually different from the composition in the fractures and this motivates component exchange between phases inside the matrix.

All this suggest that the total composition, and hence the miscibility process near the displacement front will be different from one-dimensional slim tube displacement.

Away from injectors on a fractured reservoir, the fracture gas composition may be influenced by the upstream matrix-fracture fluid exchange. As a result, the gas entering the matrix blocks some distance away from the injectors will be richer than original injection gas. This leads to expect more favourable conditions for the development of miscibility and recoveries from the matrix blocks in reservoir regions away from the injectors.

Another effect that might play an important role on the recovery and developed miscibility is oil re-infiltration from one matrix block to another one (block-to-block interaction).

Knut Ulberg (2002) recommended a new approach based on Zick's (1986) concept of an extrapolated historical minimum miscibility indicator. He proposed simulating the actual multi-dimensional flow process using a compositional reservoir simulator. In this approach instead of recording the final recovery, grid block physical properties such as saturation, equilibrium phase compositions, densities and gas-oil interfacial tensions are reported throughout the simulation run. A minimum miscibility indicator (MMI) is recorded at each report step. A dispersion free miscibility indicator (MMI∞) is found by extrapolation by Pade's (1978) approximation.

The system which Ulberg (2002) has simulated was a matrix block surrounded by fractures in a 2-D Cartesian system. The gas injection well was located at top of the matrix block, injecting with a constant pressure. The production well was located at the bottom of matrix block producing at a constant rate.

For a single matrix block, interfacial tension was recorded for two grid blocks at the top bottom of the matrix block. In this situation, the corresponding pressure when interfacial tension approaches zero is, considered to be the MMP.

Typical dispersion-free minimum miscibility indicators such as function of system pressure for the upper and lower parts of a matrix block which was subjected to gas injection in its fracture system is shown in Figure 2.18. This figure illustrates that dispersion-free minimum miscibility indicators approach zero at pressure 450 bara. Therefore the calculated MMP for 2-D system can be assumed 450 bara, while the calculated MMP based on a 1-D condensing and vaporizing mechanism for the same gas and oil and using slim tube simulation was calculated to be at 330 bar.

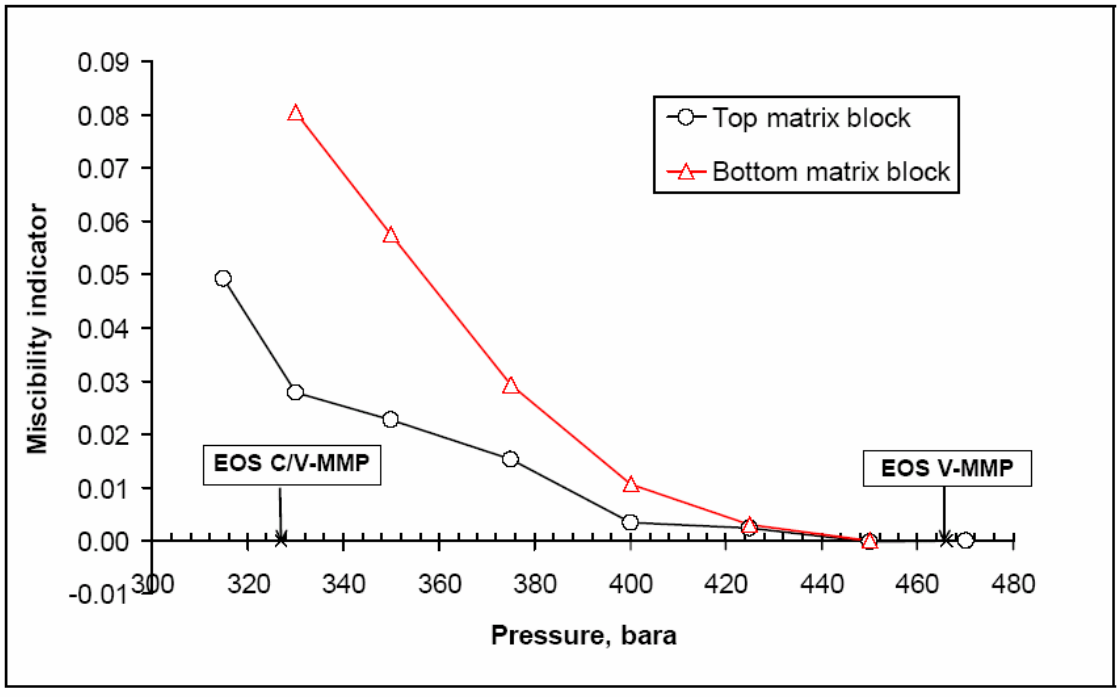

Figure 2.18 Dispersion free minimum miscibility indictors as function of system pressure for the upper and lower grid block in a matrix block surrounded by fracture and is subjected to gas injection into fracture system (After Ulberg, 2002).

Therefore the minimum miscibility pressure MMP calculated by using Ulberg's (2002) method for a matrix-fracture system is significantly higher than the calculated MMP based on 1-D condensing and vaporizing mechanism by using slim tube simulation. This can be due to multi-dimensional flow behaviour as well as molecular diffusion. Ulberg (2002) suggest that in a matrix fracture system even if true miscible conditions are not obtained, high 'miscible-like' recoveries can be achieved far below the calculated 2-D MMP/MME due to a complex capillary- driven recovery process.

2.10 Molecular diffusion in a matrix-fracture system

Molecular diffusion is defined as the movement of ions or molecules from regions of high concentration to low concentration within an isotropic media. Diffusion is caused by random molecular motion that leads to complete mixing. Figure 2.19 shows three flow regimes from Perkins and Johnston (1963).

Diffusion can occur in gases, liquids and dense phases. It can be a slow process. In gases, diffusion progresses at a rate of about 10 cm/min; in liquids, its rate is about 0.05 cm/min; in solids its rate may be only about 0.00001 cm/min.

Study of the diffusion process started with research on the diffusion of gases in the early 19^{th} century by Graham (1833). His research depended most strongly on the apparatus shown in Figure 2.20. This apparatus, or "diffusion tube", consisted of a straight glass tube, one end of which is closed with a dense stucco plug. In a typical experiment, the tube was initially filled with hydrogen, and the end sealed with water as shown. Hydrogen diffuses through the plug out of the tube.

At the same time, air diffuses back into the tube. Because the flux of hydrogen does not equal the flux of air, the water level in this tube will rise during diffusion. This change in water level would lead to a pressure gradient which alters the diffusion. To avoid this pressure gradient, Graham (1833) continuously lowered the tube so that the water level stayed constant.

His experimental results showed that the amount of volume change is characteristic of each gas originally held in the tube. Graham (1833) further showed that this volume change was inversely proportional to the square root of density of the gas. In other words, diffusion is inversely proportional to the square root of the molecular weight of the gas.

The experiments can be successfully explained as the result of the zero pressure difference across the porous plug, without ever mentioning Fick's law (1855) or any concept of diffusion coefficient (Mason and Krastadt, 1967).

Earlier studies of the diffusion process in the liquids were confusing because of using membranes in the experiments. Bruke (1843) placed turpentine and olive oil on opposite sides of a leather membrane, and measured volume changes across the membrane by diffusion. The presence of the membrane obscured analysis of the diffusion process.

.

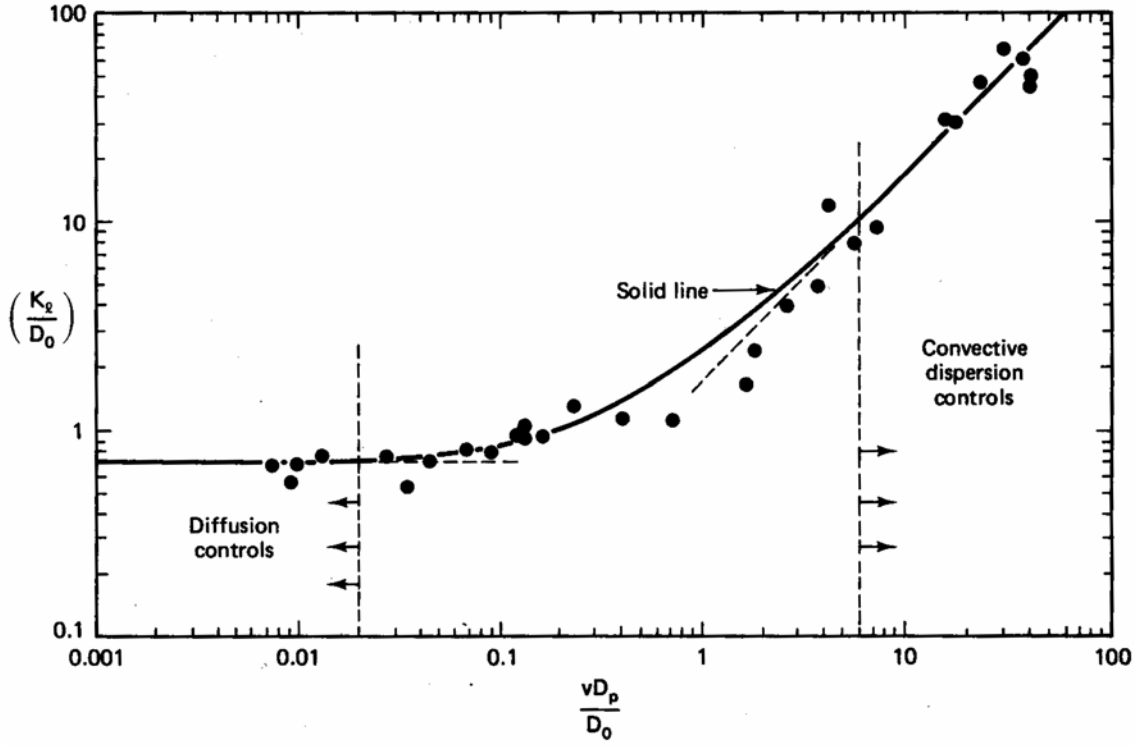

Figure 2.19 Longitudinal dispersion coefficients in permeable media flow. D_0 is the effective diffusion coefficient, D_P is an average particle diameter, K_o is longitudinal dispersion coefficient, v is interstitial velocity. (After Perkins Johnston, 1963)

Graham (1850) removed the membrane from the experiments. He did his studies by the equipment shown in Figure 2.21. In one series of his experiments, he connected two bottles initially containing solutions of different concentrations. In another series of experiments, he placed a small bottle containing a solution of known concentration in a large jar containing only water. After several days, he removed the bottle and measured its concentration

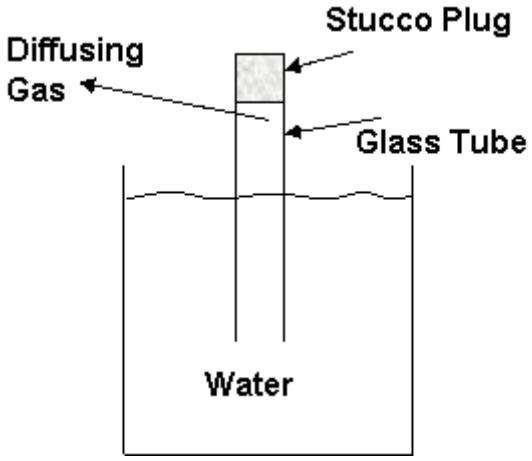

Figure 2.20 Graham's diffusion tube for gases. The tube is lowered as diffusion occurs so that the water level remains constant. (After Cussler,1976)

He showed that diffusion in liquids was at least several thousand times slower than diffusion in gases. He concluded that the diffusion got slower as the experiment progressed. Graham understood that the flux concentration difference in liquids was linearly related, and that diffusion was a differential process. However he did not make the natural connection between the diffusion of mass and the diffusion of heat. As a result, he never tried to describe diffusion in terms of Fourier's theory of thermal conduction (Cussler 1976).

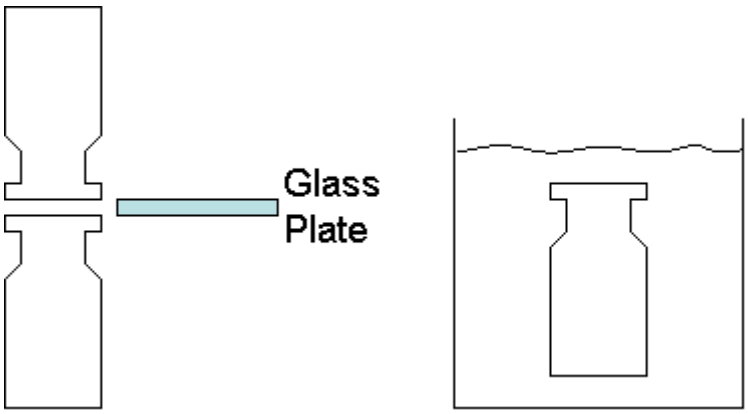

Figure 2.21 Graham's diffusion apparatus for liquids. (After Cussler, 1976)

2.10.1 Fick's laws of diffusion

Fick finally put Graham's experiments on to a quantitative basis. In other words, diffusion can be described on the same mathematical basis as Fourier's law of heat conduction. Fick quickly developed the laws of diffusion by means of analogies with Fourier's work. He defined one-dimensional steady state flux *J*. The general forms of Fick's and Fourier's laws are:

J=-D.∇c 2-57

q=-C.∇T 2-58

Where c is the concentration, D is the diffusion coefficient and C is the coefficient of thermal conductivity, both coefficients are properties of the particular substance.

The first equation is called the Fick's first law of diffusion; the two equations are fully analogous. In fact Eq. 2-57 is the most commonly used form of the binary constitutive relationship.

Fick also paralleled Fourier's development to form a more general conservation equation:

$$\frac{\delta c}{\delta t} = D\left(\frac{\delta^2 c}{\delta^2 z} + \frac{1}{A}\frac{\delta A}{\delta z}\frac{\delta c}{\delta z}\right) \quad \text{..... 2-59}$$

When the area A is constant, this becomes the basic equation for one-dimensional unsteady-state diffusion, and it is well known as Fick's second law. The solution for Fick's second law when the area of diffusion is constant and two fluids have not any movements can be presented as:

$$c = \frac{1}{2}\left[1 \pm erf\left(\frac{z}{2\sqrt{Dt}}\right)\right] \quad \text{2-60}$$

In terms of the error function, the initial and boundary condition values need to be specified. When two fluids are moving at the same velocity v, the distance z can be replaced by the effective distance:

$$\bar{z} = z - vt \quad \text{2-61}$$

Eq. 2-57 is more popular than the others: first of all, because the concentration gradient usually leads to the diffusivity; and second, it can be easily modified for porous media. However this equation is not the most convenient one to be used in practical design problems because under non-isothermal conditions, the molar concentration gradients will vary with composition and temperature. Another form of Fick's first law is related to the mass gradient:

$$J = -\rho D.\nabla\omega \quad \text{2-62}$$

Where ω is the mass fraction of species *i* and ρ is the density of solution. This form of Fick's law is more convenient when we have to solve the mass continuity equation simultaneously with the equation of motion and when the liquid density is constant. The third expression for Fick's law is related to the mole fraction gradient, *X*:

$$J = -\rho D.\nabla x \quad \text{2-63}$$

Eq. 2-63 is the best equation for ideal gases where the molar concentration c is constant. Stefan-Maxwell (1974) presented a different form of the diffusion equation:

$$\nabla x_1 = \frac{x_1 x_2}{D}(v_1 - v_2) \quad \text{2-64}$$

In the above equation *X* is the molar fraction of species *i*, and *v* is the average velocity of species *i*. All defined diffusion coefficients, D in Eqs. 2-57 to 2-64 are identical.

2.10.2 Diffusion coefficients

The diffusion coefficient is generally not constant. It varies with pressure, temperature and to some degree concentration and interfacial tension.

The effect of concentration on the diffusion coefficient varies depending on the nature and conditions of the diffusing components of molecules. For example for the binary gas mixture, it is almost independent of the gas concentration at low pressure.

In the majority of reservoir engineering applications, the diffusion coefficient can be considered to be constant. Diffusion in porous media is described by the general diffusion equation with the introduction of an effective diffusion coefficient D_{eff}, which depends on the texture of the porous medium. The presence of porous media essentially reduces the diffusion coefficient, due to the variable area of contact between two fluids, while the mechanism of diffusion remains the same. This is because the diffusing molecules have to travel through a longer path as well as through the throats and the wider areas of the pores. It takes a longer time for the molecules to travel an apparent distance in porous media than in a conduit without a porous medium conduit.

Measurements of molecular diffusion coefficients

Measurement of molecular diffusion coefficients (MDC) is one of the most important parts in the modelling and prediction of diffusion processes in fractured reservoirs. Measurement of MDC in porous media is more complex and should be modified against the rock parameters such as porosity and the tortuosity factor. Experimental and theoretical investigations reveal that diffusion coefficients depend on:

- The pressure and temperature of the system.
- The composition of phases and changes of the phases for mixture.
- The fluid saturation.
- And in the porous media, the molecular diffusion coefficients are dependent in addition on:
    - The pore connectivity which is characterized by the tortuosity factor (τ).
    - The porosity (Φ).
    - The matrix geometry in terms of fractured reservoirs.

Generally for a typical hydrocarbon mixture system in fractured porous media, the diffusion coefficient is a function of the temperature T, the pressure P, the composition X or Y, the tortuosity τ, the matrix's porosity Φ_m, the fracture's porosity Φ_f, the shape factor σ and the fluid saturation in the porous medias S_f.

$$\text{Diffusion coefficients} = f\left(T, P, X_i, Y_i, \tau, \phi_m, \phi_f, \sigma, S_f\right)$$

In fractured reservoirs, any laboratory measurement of diffusion coefficient should be modified for matrix geometry and also should be scaled up to reservoir pressure and temperature.

The gas and liquid diffusion coefficients can be measured by different methods; the following methods are described in the following sections.

1) By application of Fick's second law
2) By measurement of global pressure system (Luna et al. 2003)

Measurement and estimation of the effective diffusion coefficients by application of Fick's Second law

In this method, Fick's second law for diffusion is modified for the diffusion coefficient and is applied to measure the diffusion coefficients. It can be written as:

For the liquid phase:

$$\frac{\partial C_l}{\partial t} = D_{l,eff} \cdot \frac{\partial^2 C_l}{\partial x^2} \quad \text{2-65}$$

And for the gas phase:

$$\frac{\partial C_g}{\partial t} = D_{g,eff} \cdot \frac{\partial^2 C_g}{\partial x^2} \quad \text{2-66}$$

In the above equations C_g and C_l are functions of time and distance, by substitution C_g and C_l in Eqs. 2-65 and 2-66, the liquid-liquid diffusion coefficients ($D_{l,eff.}$) and the gas-gas diffusion coefficients $D_{g,eff.}$ are determined. The method is described by the following steps:

- Measurement of the concentration of components in a fixed position in the system versus time for both liquid and gas phases.
- Measurement of the concentration in different positions in the system at a typical time.
- Plotting measured data from steps 1 and 2
- Finding the best curves which can be accurately fitted and determine the corresponding equation by regression.
- Derive relevant derivatives and substitute in Eqs. 2-65 and2-66
- Solve the equations to find $D_{g,eff}$ and $D_{g,eff}$

The experimental set up for measuring diffusion coefficients is formed by following parts:

- PVT Cell.
- Transporting valves.
- Chromatography setup.
- Typical porous media.
- An instrument to keep all set ups to constant temperature (to have an isothermal process).

Figure 2.22 and Figure 2.23 show the diagrams for a pVT cell and experimental set up. Valves are shown in Figure 2.22 in different positions and transport fluid samples with different concentration.

By using the chromatographic technique it is possible to analyse the concentration of the obtained fluids from different positions. Usually, the pressure of injected gas which is injected at the top of the pVT cell is recorded by using a pressure gauge and a Sentonec system which is connected to a computer.

All the process is set to be isothermal by putting all of the set up inside an oven. For most of the experiments, the PVT cell is filled with an artificial porous medium such as a packed sand column.

The measurement of the effective molecular diffusion coefficients in a real porous medium by this method is difficult. For more detail see an example of the application of this method by Islas-Juarez (2004).

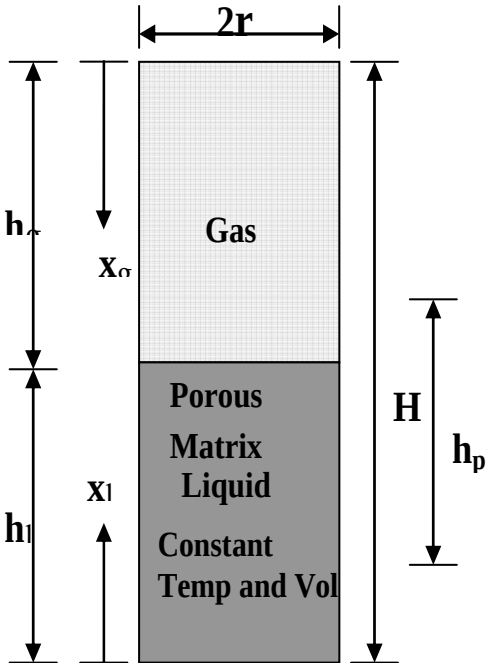

Figure 2.22 Diagram of the pVT cell and reference system used to determine the effective diffusion coefficient in porous media. (After Islas-Juarez, 2004)

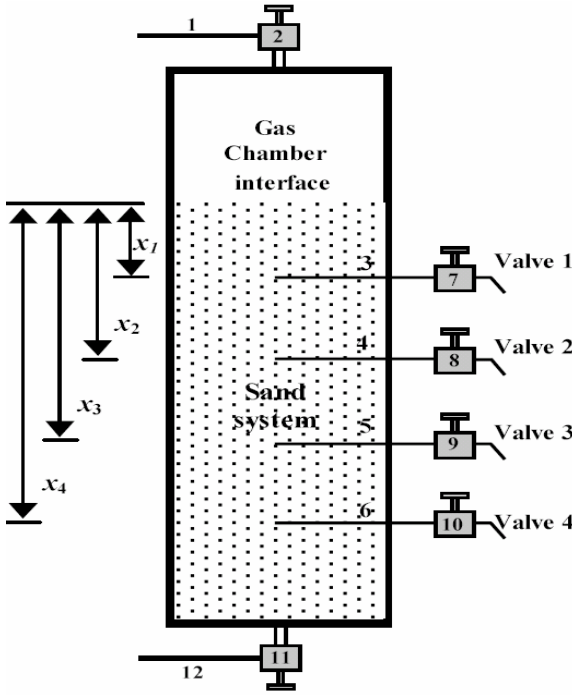

Figure 2.23 Diagram of the experimental setup (After Islas-Juarez,2004)

Measurement effective diffusion coefficients by measurement of global pressure system (Luna et al. 2003)

Based on the method which was developed by Luna et al. (2003), Eq. 2-67 was derived by EOS .

$$\frac{dp}{dt} = \frac{(Z_g\phi - Z_i).RT}{H}\left(D_g \left[\frac{\partial C_{C_n}}{\partial x_g}\right]_{X_g = h_g} - D_{l,eff}\left[\frac{\partial C_g}{\partial x_l}\right]_{x_l = h_l}\right)$$

$$P(t=0) = P_{ini} \qquad \text{..... 2-67}$$

$$P(t \to \infty) = P_{eq}$$

where P is the global pressure system, Z_g and Z_l are the compressibility of the gas and liquid phases respectively, T is the temperature of the system, Φ is the porosity of the medium, R is the universal constant of gases, P_{ini} is the initial pressure and P_{eq} is the equilibrium pressure.

The theory behind this equation is demonstrated easily. The changes in the chemical composition of the liquid and gaseous phases cause changes in the global pressure of the system .These changes in pressure can be studied through the equations of state.

The solution of the problem for the global pressure is defined by Eq. 2-68, as following:

$$P=P_{eq}+\frac{8a_1}{\pi^2}\left(P_{ini}-P_{eq}\right).\sum_{m=0}^{\infty}\left[\frac{\left(1+\frac{1}{a_1}\right).\exp\left[-\left(\frac{2m+1}{2}\pi\right)^2 d_l t\right]-\exp\left[-\left(\frac{2m+1}{2}\right)^2 d_g t\right].}{\left(2m+1\right)^2}\right] \quad \text{2-68}$$

Where, the parameters a_l ,d_l and d_g are defined as:

$$a_1=\frac{C_{g,eq}\left(Z_g\phi-Z_l\right)RTh_g}{\left(P_{ini}-P_{eq}\right).H}$$

$$d_l=\frac{D_{l,eff}}{h_l^2} \quad \text{2-69}$$

$$d_g=\frac{D_g}{h_g^2}$$

Eq. 2-68 reveals that the pressure of the system is a function of a variety of parameters and generally:

$$P=\left(\mathrm{t},\mathrm{P_{ini}},P_{eq},a_1,d_l,d_g\right) \quad \text{2-70}$$

This means that the pressure depends on its initial value and four more parameters. These parameters are unknown for the problem and they are determined by applying Least Squares method. Mathematically it can be written as:

$$Min\,P_{eq,a1,dl,dg}=\sum\left\{P_{eq}-P\left(P_{ini}:P_{eq},a_1,d_l,d_g\right)\right\}^2 \quad \text{2-71}$$

By finding d_l and d_g applying Eqs. 2-70 and 2-71, the gas-gas and liquid-liquid effective molecular diffusions are determined. The experimental set up is similar to previous methods and the main parameter measured here, is recording the global pressure versus time and plotting it. By fitting the experimental data and changing the parameters mentioned in Eq .2-68 (analytical solution), the molecular diffusions coefficients are determined.

2.10.3 Calculations of the diffusion coefficients of components by correlation

Reservoir oil is mixture of many heavy and light hydrocarbon and non-hydrocarbon components. Depending on the state of the reservoir these components may be all in the liquid phase or in the gas phase or in a two- phase condition at equilibrium.

For any compositional analysis of matrix fracture component exchange including diffusion, the value of the diffusion coefficients for all components in the gas and liquid phases is the key parameter in such analysis. The diffusion coefficients of the components in the gas and liquid phases can be calculated by using the correlations to calculate the binary diffusion coefficients as well as the properties of the components.

Correlations for the calculation of the binary diffusion coefficients which have been introduced by different authors are different to each other because they have been derived based on different measurements and variety models. In other words, even if different models are applied for a similar measurement set up experiment, the correlations are not the same. The most used equations in gas and oil systems are described now.

The standard engineering approach uses the effective diffusion coefficient (EDC) for component *i* in a mixture, D_{im} where it can be calculated in one of two ways:

- From binary diffusion coefficients and mixture coefficients and mixture composition.
- From component *i* properties and mixture viscosity

The first approach uses the Wilke formula (1955) to calculate:

$$D_{im} = \frac{1 - y_i}{\sum_{j \neq i=1}^{N} \frac{y_i}{D_{ij}}} \quad \text{2-72}$$

where y_i is mixture mole fraction and $D_{ij} = D_{ji}$ is the binary diffusivity at the pressure and temperature of the mixture.

Sigmund (1976) correlates the effect of pressure and temperature on diffusion coefficients using a corresponding-state approach with reduced density:

$$\frac{\rho_M D_{ij}}{\rho_M^o D_{ij}^o} = 0.99589 + 0.096016.\rho_{pr} - 0.22035.\rho_{pr}^2 + .03287.\rho_{pr}^3 \quad \text{2-73}$$

where D_{ij} is the diffusion coefficients for pressure and temperature, ρ_{pr} is pseudo-reduced density = $\frac{\rho_M}{\rho_{M_{pc}}} = \left(\frac{\rho}{M}\right).v_{pc}$, ρ_M is mixture molar density, $\rho_M^o.D_{ij}^o$ is low pressure density-diffusivity product, and v_{pc} is pseudo-critical molar volume calculated by mixing rule. Note that the ratio $\frac{\rho_M.D_{ij}}{\rho_M^o.D_{ij}^o}$ is the same for all binary pairs in a mixture because ρ_{pr} is only a function mixture density and composition.

Da Silva and Berely (1987) noted that the Sigmund correlation does not work well for liquid systems and proposed the following extrapolation for ρ_{pr} >3:

$$\frac{\rho_M D_{ij}}{\rho_M^o D_{ij}^o} = \exp\left(3 - \rho_{pr}\right) \quad \text{2-74}$$

which avoids negative D_{ij} for oils at ρ_{pr} >3.7 as estimated by the Sigmund correlation.

Chapman and Cowling (1970) gave the most common theoretical estimation of gaseous diffusion. Their theory depends on the assumption that molecular interaction involves collision between only two molecules at the same time.

This theory is best illustrated for a gas of rigid sphere of very small molecular dimensions and it gives accurate to an average of about eight percent, leads to the equation.

$$D = \frac{1.86.10^{-3} T^{3/2} \left(1/M_1 + 1/M_2\right)^{1/2}}{P\delta_{12}^2 \Omega} \quad \text{2-75}$$

In the above equation, D is the diffusion coefficient measured in cm^2/sec.T is the absolute temperature in degrees Kelvin, P is the pressure in atmospheres, and Mi is the

molecular weight of component i. δ_{12} is the collision diameter in angstrom and it is define as the arithmetic average of the two present species .where

$$\delta_{12} = \frac{1}{2}(\delta_1 + \delta_2)$$

The dimensionless quantity is usually order of one and it depends on an integration of the interaction between the two species and it is calculated from energy of interaction . The methods for calculating δ_1 , δ_2 , Ω the values for different gases were given by Hirschfelder et al. (1954) .

Renner (1988) proposed a generalized correlation for effective diffusion coefficients of light hydrocarbons and CO_2 in reservoir fluids that can be used as an alternative to the Sigmund-type correlation.

$$D_{im} = 10^{-9}\mu_o^{-1.4562} M_i^{-0.6898} \rho_{Mi}^{1.706} .T^{4.524} .P^{-1.83} \quad \text{.....2-76}$$

with D in $\frac{cm^2}{s}$ and μ_o is oil viscosity in cp, M_i is molecular weight, ρ_{Mi}, molar density of component *i* at P and T in $\frac{gmol}{cm^3}$, P is pressure in psia ,and T is temperature in K. This correlation is based on 141 experimental data and statistical analyses with the following property ranges:

0.2< μo<134 cp; 16<Mi<44; 0.04< ρMi<7 $\frac{kmol}{m^3}$; 14.7<P<2560 psia, and 273<T<333 K and *i* is CO_2, C_1, C_2 and C_3. Renner also gives a correlation for diffusivity of CO_2 in water brine system as:

$$D_{CO_2-w} = \left(6.39210^3\right)\mu_{CO_2}^{6.911} .\mu_w^{-0.1584} \quad \text{.....2-77}$$

2.10.4 Formulation of the effective diffusion coefficient

If in Eq. 2-61 the interstitial velocity $v = q/(\phi.A)$ is used instead of the fluid velocity $u = \frac{q}{A}$ for moving fluids, the effective diffusivity coefficient D_e should be used in the general solution of the diffusivity equation. The term *q* is the volumetric flow rate and Φ the formation porosity. Fried et al. (1971) argued that molecular diffusion is similar to the conduction of electricity and molecular concentration, mass flux, and diffusion coefficient are analogous to electrical potential, intensity and conductivity, respectively. He gave the equation:

$$D_e = \frac{D}{F.\phi} \quad \text{.....2-78}$$

Perkins et al. (1984) published data for the effective coefficient in porous media and showed that the value F.Φ typically ranges from 1.25 to 1.65 depending on the texture of the medium. The electrical resistivity factor-porosity term (F.Φ) is sometimes replaced by the tortuosity factor. It is reported by Ruthven (1984) that the experimental

tortuosity factor for porous media varies between 2 to 6. Saidi (1986) presented some experimental procedures for calculating D_e. All his experiments showed that the measured D_e/D were lower than the corresponding measured values of 1/F.Φ. The higher permeable rock has the smaller difference and the lower permeable sample has the largest difference. Figure 2.24 shows the result of the experiments.

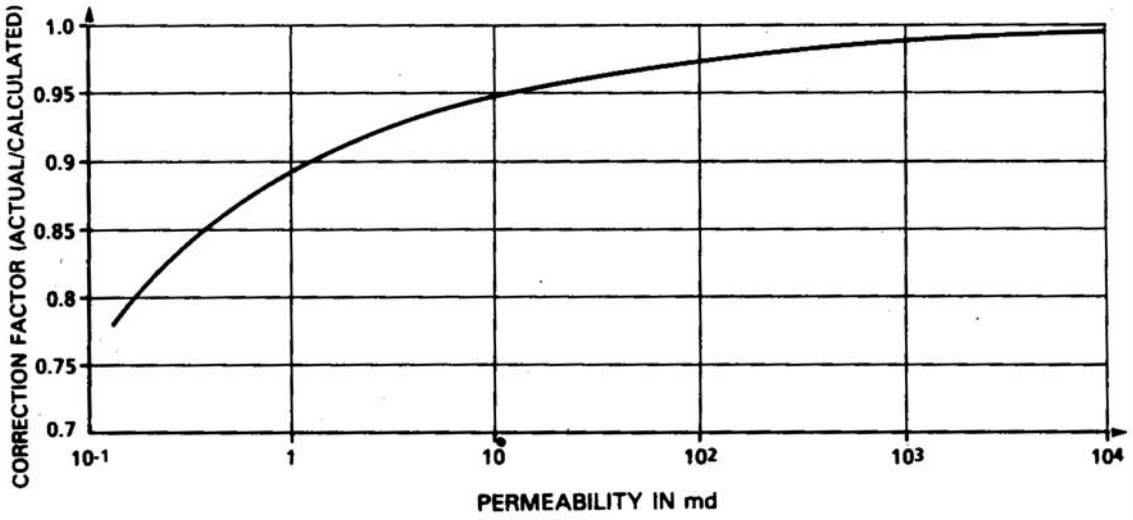

Figure 2.24 Correction factor for calculating effective diffusion coefficient in porous media versus permeability. (After Riazi, 1987)

In porous media, the effective diffusion coefficient is (Cussler 1997):

$$D_{eff} = \varepsilon \frac{D}{\tau} \quad \text{.....2-79}$$

where D is the diffusion coefficient within the pores ($m^2\ s^{-1}$), ε is the valid fraction or porosity, and τ is the tortuosity. The tortuosity is the length travelled by a particle divided by the net distance travelled.

2.11 References

1) Ali J.K. (1994). Predictions of parachors and petroleum cuts and pseudo components Fluid Phase Equilib. 95383–98.
2) Al-Rub, F.A.A. and Datta, R., Theoretical Study of Vapour-Liquid Equilibrium inside Capillary Porous Plates, Fluid Phase Equilibria, 162, 83 (1999).
3) Barenblatt, et al. (1960). G. E. Barenblatt, I. P. Zheltov, and I. N. Kochina. Basic Concepts in the Theory of Seepage of Homogeneous Liquids in Fractured Rocks. 1960. J. Appl. Math. (USSR). 24 (5). 1286-1303
4) Buckley, S. E. and Leverett, M. C. Mechanism of fluid displacement in sands, Transactions, American Institute of Mining, Metallurgical and Petroleum Engineers, 1942, 146, 107-1 16
5) Chapman,S.,and Cowling,T.G.(1970).The Mathematical Theory of Non-uniform Gases,3rd ed. Cambridge University Press
6) Cussler, E.L. (1976) Multi component Diffusion Amsterdam: Elsevier.
7) Danesh, A.S., Dandekar, A.Y., Todd, A.C., and Sarkar, R., A Modified Scaling Law and Parachor Method Approach for Improved Prediction of Interfacial Tension of Gas-Condensate Systems. SPE 22710, Dallas, TX, Oct (1991).
8) Fanchi J R. (1990). Calculation of parachors for compositional simulation: an update SPE Reservoir Eng. 5 433–6.
9) Fanchi, J.R. "Calculation of Parachors for Compositional Simulation," SPE J., November, 2049 (1985).
10) Gasem, K.A.M., P.B. Dulcamara, B.K. Dickson, and R.L. Robinson, Jr., "Test of Prediction AIChE Journal, Volume 42, No. 5, pp. 1425-1433, May 1996 Methods for Interfacial Tensions of CO2 and Ethane in Hydrocarbon Solvents," Fluid Phase Equil., 53, 39 (1989).
11) Høier, Lars. " Miscibility Variation in Compositional Grading Petroleum Reservoirs," Dr.ing Thesis Norwegian University of Science and Technology, NTNU, Nov.,1997
12) Hirschfelder JO, Curtiss CF and Bird R.B. (1964) Molecular Theory of Gases and Liquids (New York: Jain P C, Jody B J and Saxena S C 1975 Chem.
13) Hugill, J.A., and A.J. van Welsenes, "Surface Tension: A Simple Correlation for Natural Gas Condensate Systems," Fluid Phase Equil., 29, 383 (1986). Jasper, J.J., "The Surface Tension of Pure Liquid Compounds," J. Phys. Chem. Ref. Data, 1, 841 (1972).
14) Luna,R.E.,S.M.,Pineda,M.A.Hernandez,E.L. and Serrano,S.E.”Medicion del coefficient de Diffusion a Traves de Cambios de Presion en una Celda PVT”Technical report,Project D.02101,from Mexican petroleum Instriute(2003).
15) Lake L.W. (1989). Enhanced Oil Recovery (Englewood Cliffs, NJ: Prentice-Hall) p 234.

16) Lee J.I. and Reitzel G.A. (1982). High pressure, dry gas miscible flood, Brazeau River Nisku Oil Pools J. Petroleum Technol. 34 (November) 2503–9.

17) Lee, S.-T., and M.C.H. Chien, "A New Multi component Surface Tension Correlation Based on Scaling Theory," SPE/DOE 12643. Paper presented at SPE/DOE 4th Symp. on EOR. Tulsa, OK, April 15-18, (1984).

18) Lee, S-T., Capillary-Gravity Equilibrium for Hydrocarbon Fluids in Porous Media. SPE 19650, San Antonio, TX, Oct (1989).

19) Leverett, M.C. Capillary Behaviour in Porous Solids, Trans AIME, 142, 152 (1941).

20) McLeod, D.B., On a relation between Surface Tension and Density, Trans. Faraday Soc., 19, 38 (1923).

21) Nelms, Ralph L., and Burke, Randolph. B., (2004). "Evaluation of Oil Reservoir Characteristics to Assess North Dakota Carbon Dioxide Miscible Flooding Potential", 12th Williston Basin Horizontal Well and Petroleum Conference May 2-4, 2004 Minot, North Dakota.

22) Perkins, T.K. and Johnston, O.C.: A Review of Diffusion and Dispersion in Porous Media, SPEJ (March 1963)70-84.

23) Quayle, O.R., "Surface Tension and Parachor of Hydrocarbons," Chem. Rev., 53, 439 (1953).

24) Ramsay, H.J. and Small, F.R. (1964). "Use of Carbon Dioxide for Water Injectivity Improvement", Journal of Petroleum Technology.

25) Reid, C.R., J.M. Prausnitz, and B.F. Poling. The Properties of Gases and Liquids. McGraw-Hill, 4th Edition, New York, NY. 632-655 (1988).

26) Renner, T.A. (1988). Measurement and correlation of diffusion coefficients for CO_2 and rich-gas applications. SPE 15391 may 1988.

27) Riazi,M.R.,1996.:" A New Method for Experimental Measurement of diffusion Coefficients in Reservoir. Fluids. Journal of Petroleum Science and Engineering 14,235-250

28) Riazi, M.R., and G.A. Mansoori, "Simple Equation of State Accurately Predicts Hydrocarbon Densities," Oil and Gas J., July 12, 108 (1993).

29) Reid, R.C., Prausnitz, J.M., and Poling, B.E., The Properties of Gases and Liquids, McGraw Hill, N.Y. (1987).

30) Saidi A.M. (1987). "Reservoir engineering of fractured reservoirs (Fundamental and practical aspects)", TOTAL Edition Presses, Paris.

31) Schechter D S and Guo B. (1998). Parachors based on modern physics and their uses in IFT prediction of reservoir fluids SPE Reservoir Eval. Eng. 1 207–17.

32) Sigmund. (1976). Prediction of molecular diffusion at reservoir conditions. Part I – measurement and prediction of binary dense gas diffusion coefficients. The Journal of Canadian Petroleum Technology. April-June 1976, pp 48-57.

33) Sigmund, P.M., Dranchuk, P.M., Morrow, N.R. and Purvis, R.A., Retrograde Condensation in Porous Media, Soc. Pet. Eng. J., 93, April (1973).

34) Sugden, S. The Parachors and Valency. A List of Parachors, Brit. Assoc. Report (1932).

35) Sugden, S., "The Variation of Surface Tension with Temperature and some Related Functions," J. Chem. Soc., 125, 32 (1924).

36) Tester, J.W. and Modell, M., Thermodynamics and its Applications, Prentice Hall International Series, 3rd edition (1996).

37) Thomas, L.K., T.N. Dixon, R.G. Pierson, Hroar Hermansen, 1991. Ekofisk Nitrogen Injection. SPE 19839

38) Van Golf-Racht, T.D. (1982) “Fundamentals of Fractured Reservoir Engineering, Developments in Petroleum Science, no. 12, Elsevier Scientific Publishing Company, Netherlands.

39) Warren, J.E. and Root, P.J.: "The Behaviour of Naturally Fractured Reservoirs," SPEJ (Sept. 1963) 245-255.

40) Weinaug C F and Katz D.L. (1943). Surface tensions of methane–propane mixtures Indust. Eng. Chem. 35 239–46.

41) Zick A.A. (1986). A combined condensing/vaporizing mechanism in the displacement of oil by enriched gases SPE 61st Annual Technical Conf. and Exhibition (New Orleans, LA, Oct. 1986 Paper SPE 15493).

3. Fluid and EOS characterization

3.1 Introduction

The physical properties and phase behaviour of petroleum fluids are very significant factors impacting the accuracy of any compositional numerical modelling of gas injection experiments. The hydrocarbon fluid system is adequately described by assuming one (dry gas) or two (crude oil, natural gas) hydrocarbon components, and correlating their physical fluid properties based upon the subsurface temperatures and pressures encountered. However, when encountering abnormal compositions (such as when injecting CO_2) or conditions (such as being near the "critical" pressure and temperature) these simple correlations fail.

Chapter 4 presents CO_2 injection experiments in a matrix fracture system using rock and fluids samples similar to one of the North Sea chalk fracture reservoirs. The goal of these experiments was to specify and quantify the contribution of all forces involved in the recovery mechanism during CO_2 injection in fractured cores. This was done by compositional modelling of the experiments using the Soave-Redlich-Kwong (SRK) Equation of State (EOS).

When performing compositional simulations using a cubic equation of state, the EOS characterization may have a large influence on the results. At the heart of the EOS model is an equation that defines a set of parameters for each fluid component in the fluid system. Some of these parameters are constants while others are "adjusted" to "tune" the EOS model to produce the desired results. To ensure that the EOS can correctly predict the phase behaviour of mixtures occurring during the component transfer between matrix and fracture system, relevant pVT experiments should be performed. The EOS should be tuned to match the experimental results.

This chapter discusses the necessary steps to generate an EOS model which is able to calculate the CO_2-oil phase behaviour. These include the procedures for making live reservoir oil and the corresponding pVT experiments on the mixture of the oil-CO_2 system.

3.2 Reservoir oil

The reservoir oil used for saturating the matrix block in all experiments was similar to one of the North Sea chalk fractured reservoirs. The initial bubble point pressure of the oil was 383 bar at 130 ºC. Production history of the field under study shows that the reservoir pressure was reduced from its initial pressure of 495 bar to a minimum value of 247 bar and then water was injected into the reservoir and the reservoir pressure was increased to 300 bar. Therefore the present bubble point pressure of the oil would be 242 bar at 130 ºC (assuming the separated gas in the reservoir was produced from the gas cap before the start of water injection). The initial gas oil ratio (GOR) for the oil was reported to be 261. Sm^3/sm^3. The initial composition of the reservoir oil is shown in Table 3.1. The C_{7+} density and molecular weights (C_{7+}) are 0.8578 g/cm^3 and 228 g/gmol respectively.

The oil composition shown in Table 3.1 was selected as a base to make the initial reservoir oil by recombination of the stock tank oil (STO) and the synthetic gas. The present reservoir oil was made by flashing the initial reservoir oil to 242 bar at 130 ºC and the resulting fluid was used in all CO_2 injection experiments. The procedure for

recombining the oil and preparing the present reservoir oil is explained in the following sections.

Table 3.1 The initial reservoir oil composition

Component name	N_2	CO_2	C_1	C_2	C_3	i-C_4	n-C_4	i-C_5	n-C_5	C_6	C_{7+}
mol%	0.21	0.93	58.77	7.57	4.09	0.91	2.09	0.77	1.15	1.75	21.76

3.2.1 The procedure for making live reservoir oil

The process for making live reservoir oil from stock tank oil (STO) is complicated and has the following steps:

1. Preparing the field STO
2. Extended compositional analysis (C_{30+} or greater)
3. Molecular weight (MW) by freezing point depression
4. Density at standard condition
5. Nominating target reservoir oil composition
6. Based on a recipe for initial reservoir oil composition given in Table 3.1 calculate the number of moles of components which is required to add up to the STO to turn into the target initial oil composition
7. Recombination operation
8. Flashing the recombined oil to the present reservoir pressure and temperature and separate the oil phase for use in all experiments as reservoir oil.

Preparing the field stack tank oil sample

The stack tank oil sample must be collected from well/wells where the gas-oil ratio (GOR) is the same as the reservoir oil. Sometimes some wells are producing oil with a high GOR which is not equally descriptive of the reservoir fluid. This high GOR characteristic makes the STO to be condensate enriched and consequently the measured C_{7+} molecular weight (MW) and density of condensate enriched STO are lower than the current reservoir oil. The condensate enrichment of STO could be especially detrimental to an EOR study and result in misleading data.

Once the proper field STO sample is collected, it must be centrifuged to precisely remove BS&W-type material. Enough oil should be centrifuged to provide a single batch of STO from which all intended experiments can be successfully conducted. From elevated temperature pVT work, generally a relatively mild centrifuging of about 2000 rpm for 30 minutes should be applied. For core flooding work, more precise centrifuging may be appropriate. The weight percent of material removed should be recorded for future reference.

Using the above procedure, 100 cm^3 of STO oil has been centrifuged. There was no indication of any BS&W-type material after centrifuging. The sample compositions after and before centrifugation have been compared and are shown in the Table 3.2.

Table 3.2 The stock tank oil composition before and after centrifugation

Comp name	Before centri.	After centri.	Comp name	Before centri.	After centri.
	Weight fraction			Weight fraction	
Methane	0.000	0.000	C_{18}	0.026	0.027
Ethane	0.000	0.000	C_{19}	0.024	0.025
Propane	0.001	0.001	C_{20}	0.022	0.023
Iso Butane	0.001	0.001	C_{21}	0.021	0.022
n-Butane	0.004	0.004	C_{22}	0.019	0.020
Iso pentane	0.004	0.004	C_{23}	0.016	0.018
n-Pentane	0.006	0.007	C_{24}	0.016	0.017
C_6	0.015	0.015	C_{25}	0.015	0.016
C_7	0.030	0.031	C_{26}	0.014	0.016
C_8	0.042	0.043	C_{27}	0.014	0.016
C_9	0.037	0.038	C_{28}	0.015	0.015
C_{10}	0.036	0.037	C_{29}	0.015	0.018
C_{11}	0.031	0.032	C_{30}	0.019	0.021
C_{12}	0.029	0.030	C_{31}	0.022	0.023
C_{13}	0.031	0.032	C_{32}	0.025	0.027
C_{14}	0.031	0.032	C_{33}	0.028	0.029
C_{15}	0.034	0.035	C_{34}	0.026	0.028
C_{16}	0.027	0.028	C_{35+}	0.283	0.247
C_{17}	0.026	0.027	Sum	1	1

This table shows that the STO oil before and after centrifugation has almost the same composition. Because of the difficulty of centrifuging a large volume of STO oil and the similarity of the compositions shown in Table 3.2 as well as the absence of any BS&W material for centrifuged sample, it was decided not to centrifuge the STO oil for all the intended experiments. However the STO oil bottle was left under static conditions for almost two months which allowed settling of all possible BS&W material at the bottom of the oil bottle.

The molecular weight of the STO was measured by the freezing point depression method. The measured STO oil molecular weight was MW=237.85.

Based on the measured STO molecular weight (MW=237.85) and STO analysed (weight fraction) given in Table 3.2, the composition of STO (mole %) is calculated and the result is given in Table 3.3. Using the measured STO oil molecular weight and the

STO oil composition, the C_{7+} molecular weight for the STO oil was calculated MW= 237.85 g/gmol.

The STO oil density at laboratory conditions (T=20°C and P=1.0 atm) was measured 0.8554 g/cm^3. Using the density correction factor for thermal expansion of hydrocarbon liquid given by Standing (1977) the density at standard conditions (T=15.56 °C and p=1 atm) was calculated to be 0.8586 g/cm^3.

Table 3.3 The STO analysis (mol %), calculated based on the measured STO molecular weight (MW=237.856) and the weight fraction analysis given in Table 3.2

Component	MW g/gmol	Composition (mol %)
Nitrogen	28.02	0.00
Carbon dioxide	44.01	0.00
Methane	16.04	0.00
Ethane	30.07	0.09
Propane	44.09	0.61
Isobutane	58.12	0.36
n-Butane	58.12	1.56
Isopentane	72.15	1.27
n-Pentane	72.15	2.10
Hexanes	85.11	4.01
Heptanes	93.52	7.57
Octanes	106.37	9.35
Nonanes	118.81	7.38
C_{10+}	311.79	65.68
Total	237.86	100.00

Nominating target reservoir oil composition

The initial reservoir oil composition for the field under study was given by the field operator and shown in Table 3.1. This fluid was determined to have a bubble point of 383 bar at 130 ºC.

Calculation of the recipe of gas components for recombination

The STO oil composition before centrifugation and the reservoir oil composition which were shown in Table 3.2 andTable 3.1 have been used to calculate the recipe of the gas composition for recombination process.

The recipe of C_{4-} gas and the liquid (C_5 and C_6) were calculated by performing an overall and component material balance. The calculated gas composition and C_{6-}/STO weight ratio to get the correct reservoir oil composition are shown in Table 3.4 andTable 3.5.

Table 3.4 The calculated gas composition (mole %) which should be added to STO oil to get initial reservoir oil shown in Table 3.1

Component	Calculated Synthetic gas composition with no C_5 and C_6	Calculated liquid mixture of C_5/C_6	Calculated Synthetic gas composition with C_6&C_5
Nitrogen	0.28	0.00	0.28
Carbon dioxide	1.26	0.00	1.23
Methane	79.49	0.00	77.51
Ethane	10.21	0.00	9.96
Propane	5.33	0.00	5.20
Isobutane	1.11	0.00	1.08
n-Butane	2.32	0.00	2.26
Isopentane	0.00	24.52	0.61
n-Pentane	0.00	34.03	0.85
Hexanes	0.00	41.45	1.03
Total	100.00	100.00	100.00

Table 3.5 The C_{6-}/STO weight ratio for recombination operation to get initial reservoir oil shown in Table 3.1

Item	Number of mol	Molecular weight	Weight
	gmol	gmol	g
STO oil	0.00420	237.86	1.000
The mixture of light components	0.01119	20.79	0.233
The mixture of IC_5 and NC_5	0.00017	72.15	0.012
NC_6	0.00012	86.17	0.010
Recombined reservoir oil	0.01688	74.36	1.255

Table 3.5 shows the corresponding mass of C_{4-} ,C_5 and C_6 which are required for making 1.255 g of reservoir from 1 g of STO oil.

Recombination to bubble point pressure (Pb)

Recombination operation was performed by stepwise addition of STO oil to the pVT cell initially charged with a gas mixture with composition given in Table 3.4 (last column). The initial conditions of the pVT cell before oil addition is shown in Table 3.6.

Table 3.6 Initial condition of the recombination cell which was charged with gas contains up to C_6 with composition shown in Table 3.4

pVT cell pressure (bar)	pVT cell temperature (ºC)	Gas MW g/gmol	Gas compressibility @T,p	Cell volume cm^3	Mass of gas (g)
88.1	130.21	22.11	0.91	127.88	8.17

Based on the values given in Table 3.5, for each 8.17 g of the gas (containing C_5 and C_6), almost 27.89 g of STO oil should be used. The stepwise addition of the oil to the pVT cell was performed and the bubble point of the recombined oil was measured. The measured bubble point versus the mass ratio of added STO and the gas inside the pVT cell for each step is shown in Figure 3.1.

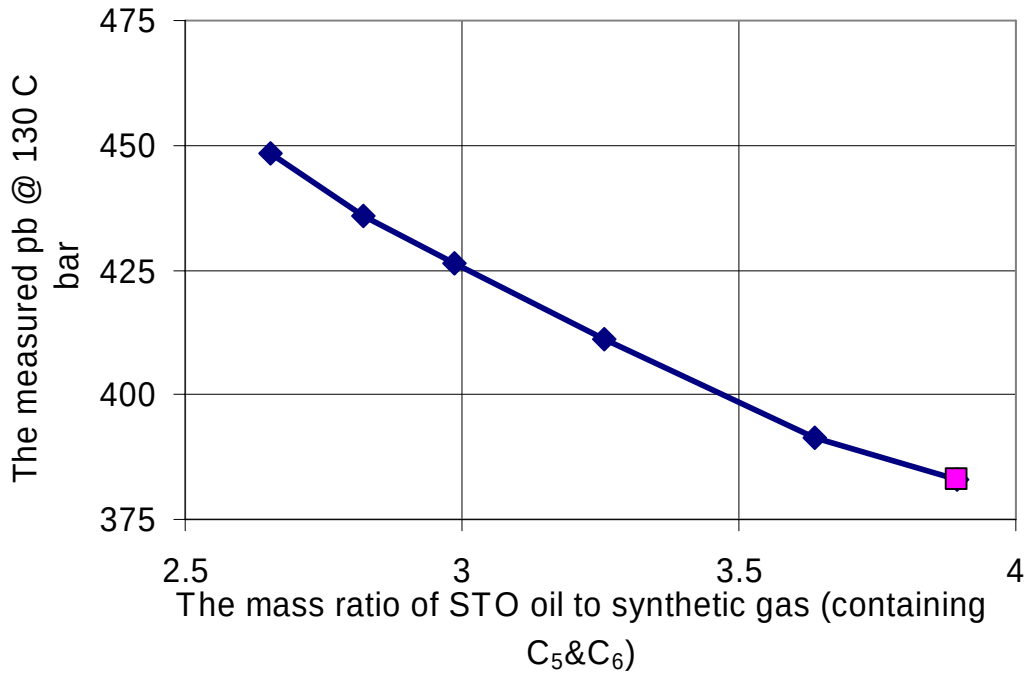

Figure 3.1 The measured bubble point versus the mass ratio of added STO and the gas inside the pVT cell for each step. The last point is corresponding to the calculated mass ratio given in Table 3.5

Figure 3.1 shows that the recombined fluid based on the recipe given in Table 3.5 has a bubble point pressure of 383 bar at 130 ºC. The last point data have been used for making the necessary amount of live oil for all pVT and core flooding experiments.

Flashing the recombined oil to the lowest reservoir pressure

Based on production history of the field, the reservoir pressure was reduced from its initial pressure of 497 bar to 242 bar. Therefore the present bubble point of the reservoir fluid is 242 bar at 130 ºC. Thus to obtain a reservoir fluid with this bubble point, the recombined oil in the previous step must be flashed out to these conditions. This was done by lowering the pressure of the fluid and pushing off the gas cap. It was preferable to due this in a stepwise manner in pressure steps of approx 35 bar. After removing the flashed gas at constant pressure, the remaining liquid (oil) will have the required bubble point specification. The set up for step wise lowering of the oil pressure is shown in Figure 3.2.

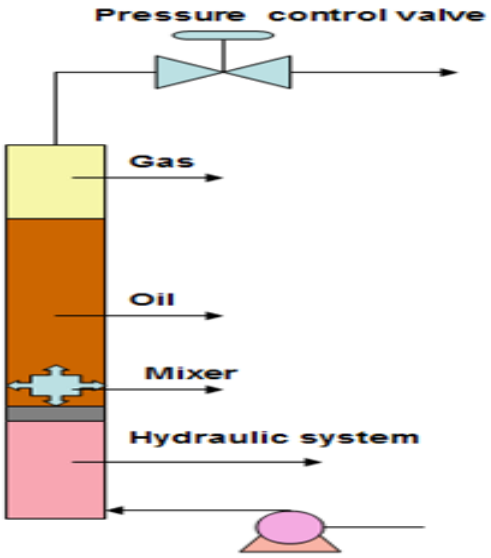

Figure 3.2 The set up for stepwise flashing of the oil from initial bubble point of 383 bar to 242 bar. All equipment installed in the heating cabinet operates at 130 ºC.

The initial pressure for the system was set to 350 bar at 130 ºC which was lower than the fluid bubble point pressure. The proper mixing in this operation is an essential factor which brings both separated gas and oil in equilibrium conditions. After removing all gas in each pressure step the remaining liquid has a bubble point pressure of 242 bar.

3.3 Reservoir oil characterization

When performing compositional simulations using a cubic equation of state, the EOS-characterization may have large influence on the results. To ensure that the EOS can correctly predict the phase behaviour of mixtures occurring during the matrix and fracture mass transfer, relevant experiments should be performed and tune the EOS parameter accordingly. The most important experiments for this purpose are:

- Single flash experiments for measuring:
  - Oil density
  - Oil molecular weight

  - Gas-oil ratio (GOR)
  - Oil formation volume factor Bo
  - Oil composition
- Constant composition expansion experiment for measuring:
  - Bubble point pressure
  - Pressure-volume behaviour at constant temperature
  - Gas to liquid volume ratio at pressure steps below the bubble point
- The multi-contact swelling experiments
  - Measure the critical point for the mixture of CO_2 and oil
- Viscosity measurements

3.3.1 Characterization of the initial reservoir oil

For initial reservoir oil the single flash, oil-CO_2 swelling and constant composition expansion experiments were performed and the results are shown in the following sections.

Single flash

The pVT cell was charged with initial reservoir oil at pressure and temperature of 400 bar and 130 ºC respectively. The single flash operation was performed by flashing a known volume of the reservoir oil to atmospheric conditions. The weight, volume, composition, and molecular weight of the flashed oil and gas were measured. The single flash fluid compositions and the resulting initial reservoir oil composition are shown in Table 3.7.

By performing corresponding mathematical recombination, the composition of the recombined initial reservoir oil was determined and the results shown in Table 3.7. The corresponding volumetric data obtained in the single flash experiment for initial reservoir oil are shown Table 3.8.

Constant composition expansion experiments

Constant composition experiments (CCE) were performed and the density, compressibility, and bubble point pressure of the initial reservoir oil at 130 ºC was determined. Using the oil density measured in the single flash and the oil compressibility data, the oil density was calculated as a function of pressure and the result is shown in Figure 3.3.

CO_2/oil swelling experiments

A pVTx diagram for the oil and CO_2 system have be determined by mixing a known amount of initial reservoir oil and CO_2 in the pVT cell. The pVT cell was charged with known quantities of the initial reservoir as shown in Table 3.9, the known amount of CO_2 was added in separate steps as given in

Table 3.10.

Table 3.7 The fluid compositions measured in the single flash of the initial reservoir oil composition

Component	MW	Flashed gas composition	Flashed oil composition	Reservoir oil composition
	g/gmol	mol%	mol%	mol%
Nitrogen	28.01	0.31	0.00	0.23
Carbon dioxide	44.01	1.30	0.00	0.98
Hydrogen sulphide	34.08	0.00	0.00	0.00
Methane	16.04	77.95	0.05	58.85
Ethane	30.07	10.24	0.19	7.77
Propane	44.10	4.70	0.59	3.69
i-Butane	58.12	0.90	0.31	0.75
n-Butane	58.12	2.02	1.11	1.80
i-Pentane	72.15	0.60	0.87	0.67
n-Pentane	72.15	0.80	1.60	1.00
Hexanes	85.54	0.72	4.15	1.56
Heptanes	93.24	0.35	5.68	1.66
Octanes	106.16	0.11	8.81	2.24
Nonanes	120.90	0.01	7.00	1.72
C_{10+}	294.35	0.00	69.65	17.08

Table 3.8 The single flash results for the initial reservoir fluid. The bubble point pressure was determined in the CCE experiments at reservoir temperature 130 ºC

Item	Initial fluid	Unit
Bubble point pressure	383.00	bar
The oil density at p_b	0.58	g/cm^3
Oil molecular weight	74.19	g/gmol
Gas oil ratio	265.53	sm^3/sm^3
Oil formation volume factor at p_b	1.90	cm^3/scm^3

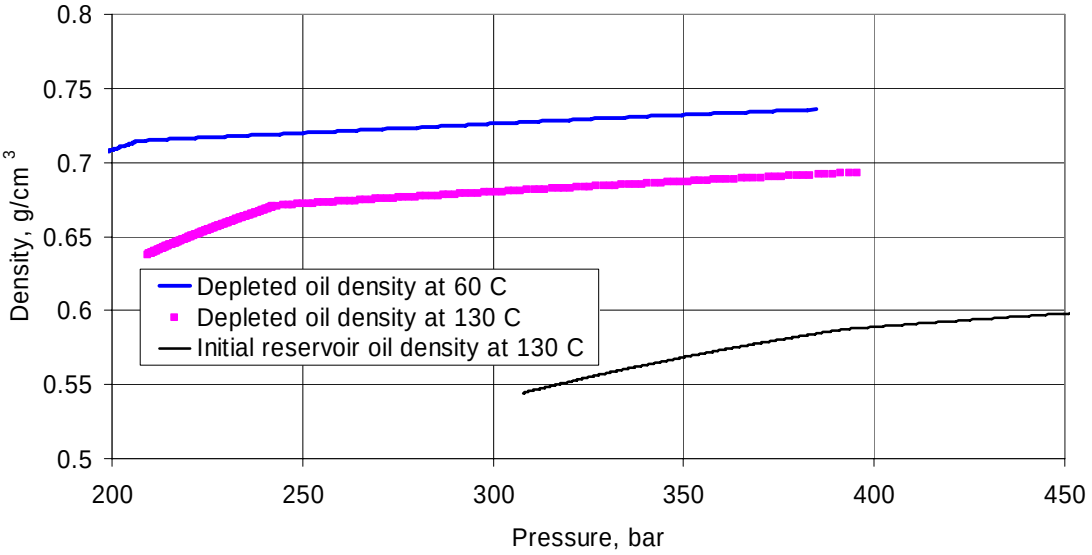

Figure 3.3 *Oil density as function of pressure at the reservoir temperature 130 ºC and 60 ºC for the initial and depleted reservoir oil. All measured densities below the bubble point are the density of the two phase fluid*

Table 3.9 *The pVT cell initial conditions before addition of any CO_2 at 130 ºC*

Pressure	450.0	bara
Temperature	130.4	º C
pVT cell volume	32.9	ml
Molar volume of oil:@450 bar	126.5	ml/mole
Oil molecular weight	74.2	g/gmol
Mole of oil in the pVT cell	0.26	gmol

For each step in

Table 3.10 the oil and CO_2 were mixed and the system pressurized into the one phase region. A constant mass expansion was performed. Below the bubble point the gas and liquid volumes were measured at several pressures. The percentage of the liquid volume versus pressure for each step is shown in Figure 3.4. As shown in this figure, all points having 100 % liquid volume are placed in the bubble point.

Finally similar tests have been done by starting with pure CO_2 in the cell for several successive oil additions. The pVT cell initial conditions before addition of any oil is shown in Table 3.11.

Table 3.10 The mole fraction of the CO_2 in the pVT cell after addition of CO_2 in each step

Step	Mole of oil:	Cumulative mole of added CO_2	X, Mole fraction of CO_2
	gmol	gmol	fraction
0	0.26	0	0
1	0.26	0.026	0.09
2	0.26	0.051	0.163
3	0.26	0.097	0.272
4	0.26	0.111	0.3
5	0.26	0.128	0.329
6	0.26	0.174	0.401
7	0.26	0.251	0.491
8	0.26	0.451	0.634

Table 3.11 The pVT cell initial conditions before addition of any oil

Pressure	450.0	bara
Temperature	130.4	^{o} C
pVT cell volume	33.1	ml
CO_2 density at T, P	0.702	g/cm^3
Molecular weight	44.0	g/gmol
Mole of CO_2	0.529	gmol

Starting with pure CO_2 in the pVT cell as shown in Table 3.11 known amount of mole of oil were added in separate steps as given in Table 3.12.

Table 3.12 The mole fraction of the CO_2 in the pVT cell after each addition of oil

Step	Mole of CO_2	Cumulative mole of added oil	X, Mole fraction of CO_2
	gmol	gmol	fraction
9	0.529	0.129	0.80
10	0.529	0.189	0.74
11	0.529	0.503	0.51

For each step given in Table 3.12 the oil and CO_2 were mixed and the system pressurized into the one phase region (gas phase). A constant mass expansion was performed. Below the dew point the gas and oil volumes were measured at several pressures. The results for each step are shown in Figure 3.4

Using the volumetric values given in Figure 3.4, the phase diagram for CO_2-oil system was made and the results are shown in Figure 3.5. This figure shows that the critical point for this system is at $X_{CO2} = 0.43$. As shown in this figure all data with zero percent liquid volume are in the dew point line

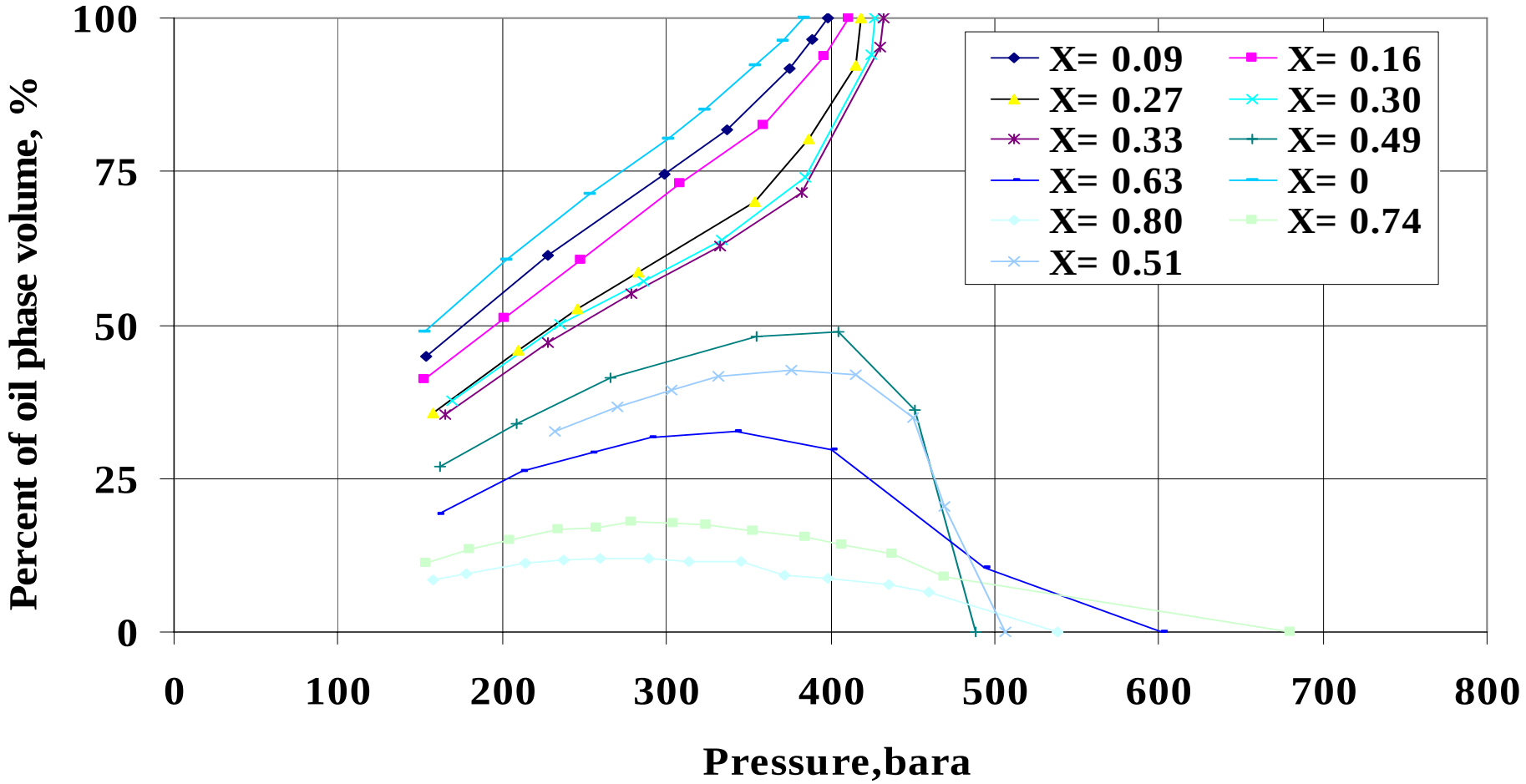

Figure 3.4 *The oil-CO_2 volumetric values measured in swelling followed by CCE experiment. The experiments were conducted at 130 ºC and using the initial reservoir fluid.*

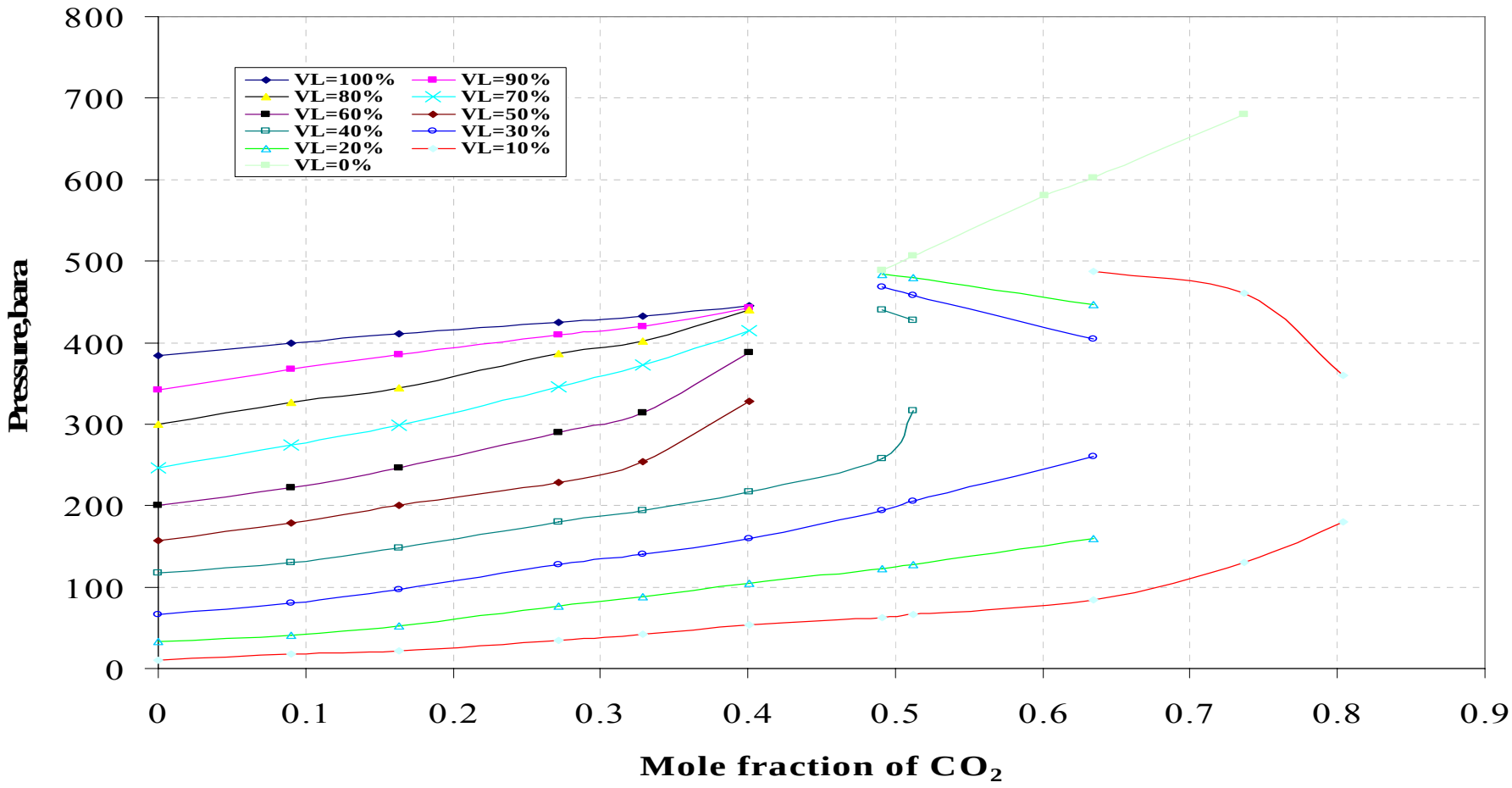

Figure 3.5 The pVTx diagram for the initial reservoir fluid with pb=384.4 bar @T=130.4 ° C

3.3.2 Characterization of depleted reservoir oil at 130 ºC

For depleted reservoir oil the single flash, oil-CO_2 swelling and constant composition expansion experiments were performed and the results are shown in the following:

Single flash

The pVT cell was charged with depleted reservoir oil at pressure and temperature of 350 bar and 130 ºC respectively. The single flash operation was performed by flashing a known volume of the reservoir oil to atmospheric conditions. The weight, volume, composition, and molecular weight of the flashed oil and gas were measured. The single flash fluid compositions and the resulting initial reservoir oil composition are shown in Table 3.13.

Table 3.13 The fluid compositions measured in the single flash of the depleted reservoir oil composition

Component	MW	Flashed gas composition	Flashed oil composition	Reservoir oil composition
	g/gmol	mol%	mol%	mol%
Nitrogen	28.01	0.20	0.00	0.12
Carbon dioxide	44.01	1.37	0.00	0.83
Hydrogen	34.08	0.00	0.00	0.00
Methane	16.04	72.62	0.03	44.15
Ethane	30.07	12.32	0.18	7.56
Propane	44.10	6.48	0.68	4.21
i-Butane	58.12	1.25	0.38	0.91
n-Butane	58.12	2.79	1.38	2.24
i-Pentane	72.15	0.77	1.03	0.87
n-Pentane	72.15	0.98	1.82	1.31
Hexanes	85.48	0.76	4.10	2.07
Heptanes	93.03	0.34	5.36	2.31
Octanes	106.27	0.10	8.33	3.33
Nonanes	120.99	0.01	6.56	2.58
C_{10+}	293.50	0.00	70.15	27.51
Total		100	100	100

By performing corresponding mathematical recombination, the composition of the recombined initial reservoir oil was determined and the results are also shown in Table 3.13. The corresponding volumetric data obtained in the single flash experiment for initial reservoir oil are shown Table 3.14.

Table 3.14 The single flash results for the depleted reservoir oil. The bubble point pressure was verified (pb= 242 bar) in the CCE experiments at reservoir temperature 130 ºC

Item	Initial fluid	Unit
The bubble point of oil	242.00	bar
The oil density at p_b	0.67	g/cm^3
Oil molecular weight	103.2	g/gmol
Gas oil ratio	133.2	sm^3/sm^3
Oil formation volume factor at p_b	1.48	cm^3/scm^3

Constant composition expansion experiments

Constant composition experiments (CCE) were performed and the density, compressibility, and bubble point pressure of the depleted reservoir oil at 130 ºC was determined. Using the oil density measured in the single flash and the oil compressibility data, the oil density as a function of pressure was calculated and the result is shown in Figure 3.3.

The CO_2/oil swelling experiments at 130 ºC

A pVTx diagram at the initial reservoir temperature 130 ºC for the depleted reservoir oil and CO_2 system has been determined. This was done by mixing a known amount of initial reservoir oil and CO_2 in the pVT cell. The pVT cell was charged with known quantities of the depleted reservoir oil as shown in Table 3.15 then a known amount of CO_2 was added in separate steps as given in Table 3.16.

Table 3.15 The pVT cell initial conditions before the addition of any CO_2 at 130 ºC

Pressure	250.38	bara
Temperature	130.45	º C
Oil volume	40.20	ml
Molar volume of oil:@450 bar	158.14	ml/mole
Oil molecular weight	106.33	g/gmol
Mole of oil in the pVT cell	0.254	gmol

For each step in Table 3.16 the oil and CO_2 were mixed and the system pressurized into the one phase region. A constant mass expansion was performed. Below the bubble point the gas and liquid volumes were measured at several pressures. The percentage of the liquid volume versus pressure for each step is shown in Figure 3.7. As shown in this figure, all points having 100 % liquid volume are placed in the bubble point.

Finally similar tests have been done by starting with pure CO_2 in the cell for several successive oil additions. The pVT cell initial conditions before the addition of any oil is shown in Table 3.17.

Table 3.16 The mole fraction of the CO_2 in the pVT cell after the addition of CO_2 in each step

Step	Mole of oil in the pVT cell:	Cumulative mole of added CO_2	X, Mole fraction of CO_2
	gmol	gmol	fraction
0	0.254	0.000	0.000
1	0.254	0.096	0.260
2	0.254	0.153	0.360
3	0.254	0.213	0.438
4	0.254	0.365	0.573
5	0.254	0.445	0.620
6	0.254	0.564	0.674

Table 3.17 The pVT cell initial conditions before the addition of any depleted reservoir oil

Pressure	450.0	bara
Temperature	130.45	^{o} C
pVT cell volume	41.72	ml
CO_2 density at T, P	0.70	g/cm^3
Molecular Weight	44.01	g/gmol
Mole of CO_2	0.67	gmol

Starting with pure CO_2 in the pVT cell as shown in Table 3.17, a known amount of mole of oil was added in separate steps as given in Table 3.18.

For each step given in Table 3.18 the oil and CO_2 were mixed and the system pressurized into the one phase region (gas phase). A constant mass expansion was performed. Below the dew point the gas and oil volumes were measured at several pressures. The results for each step are shown in Figure 3.7.

Using the volumetric values given in Figure 3.7, the phase diagram for CO_2-oil system was made and is shown in Figure 3.8. This figure demonstrates that the critical point for this system is at $X_{CO2} = 0.63$. As shown in this figure all data with zero percent liquid volume are in the dew point line.

Table 3.18 The mole fraction of the CO_2 in the pVT cell after each addition of oil

Step	Mole of CO_2	Cumulative mole of added oil	X, Mole fraction of CO_2
	gmol	gmol	fraction
7	0.67	0.039	0.945
8	0.67	0.096	0.874
9	0.67	0.214	0.757

Viscosity measurement

The Ruska rolling ball viscometer was used to determine the viscosity of the liquid phase of the different oil/CO_2 mixtures. The measurements were performed at a temperature of 130 ºC at a fixed pressure of 300 bar. This instrument operates on the rolling ball principle, where the roll time of a 0.252 inch diameter ball is used to obtain viscosity data. The viscosity is calculated as

$$\mu = K.t\left(\rho_{ball} - \rho_{fluid}\right)$$

where:

μ viscosity

K constant

ρ_{ball} Density of the ball

ρ_{fliud} Density of the fluid

t Roll back time

The driving force in this instrument is the difference in density between the fluid and the ball. At a fixed temperature, the difference in the ball and fluid density will be constant. The viscosity will be directly proportional to the roll back time. The constant of the viscometer must be determined by previous calibration using a liquid of known viscosity.

Different mixtures from the depleted reservoir oil and CO_2 were prepared with composition as shown in Table 3.19. Then each mixture was flashed to the pressure of 300 bar and the resulting liquid phase with densities given in Table 3.19 were transferred to viscometer. The roll time of the ball for each step was measured while adjusting the whole assembly to the desired angle (70°, 45°, or 23°).

Using the predetermined constant K for each angle, the, liquid viscosity for each step was calculated and the results are shown in Figure 3.6. This figure shows a value of 0.35 cp for pure oil ($X_{CO2} = 0$) and reduction of mixture viscosity to a minimum value of 0.18 cp for CO_2 concentration of $X_{CO2} = 0.27$ and then increasing the liquid phase viscosity beyond this concentration. Mixture with CO_2 concentration $X_{CO2} = 0.27$, is in

its bubble point at pressure 300 bar and temperature 130ºC. Adding more CO_2 brings the mixture to its two phase region where the liquid become more viscous. This behaviour was due to extraction of the light components from liquid phase into the gas phase. This easily can be verified by comparing the density of the liquids as it shown in Table 3.19

Table 3.19 Different mixture of depleted oil and CO_2, which was prepared for measurement of liquid viscosities at pressure 300 bar and temperature of 130 ºC

Step	Mole fraction of the CO_2 in the mixture X_{CO2}	Liquid density@ 300bar , 130ºC
		g/cm^3
1	0.000	0.680
2	0.060	0.665
3	0.118	0.650
4	0.178	0.635
5	0.272	0.612
6	0.468	0.624
7	0.581	0.735
8	0.659	0.759

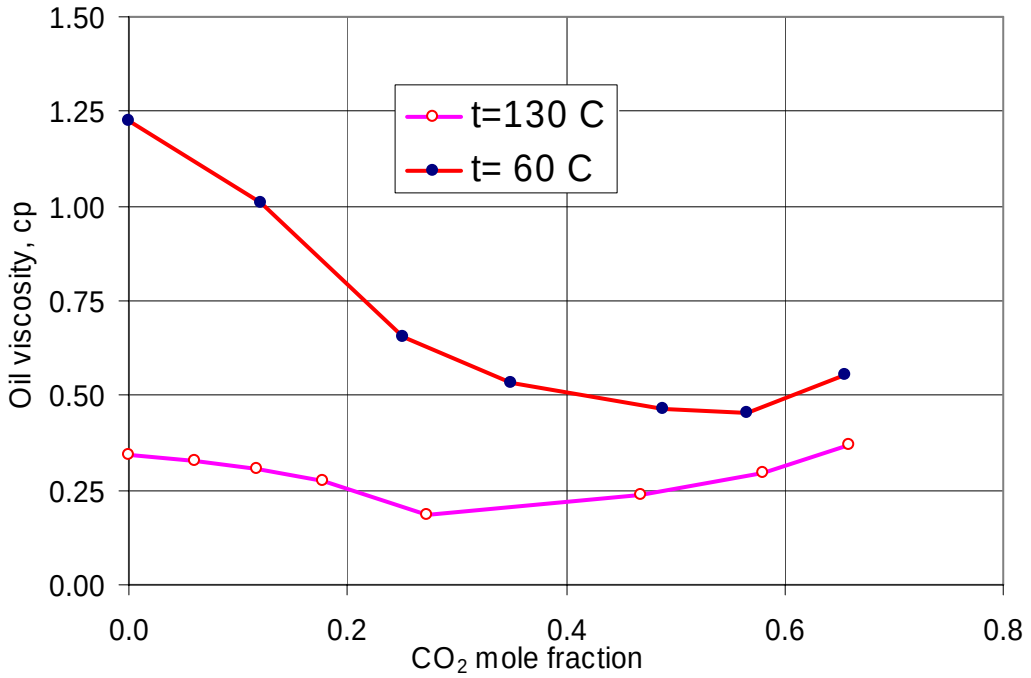

Figure 3.6 The liquid viscosities measured for depleted reservoir fluids at a pressure of 300 bar.

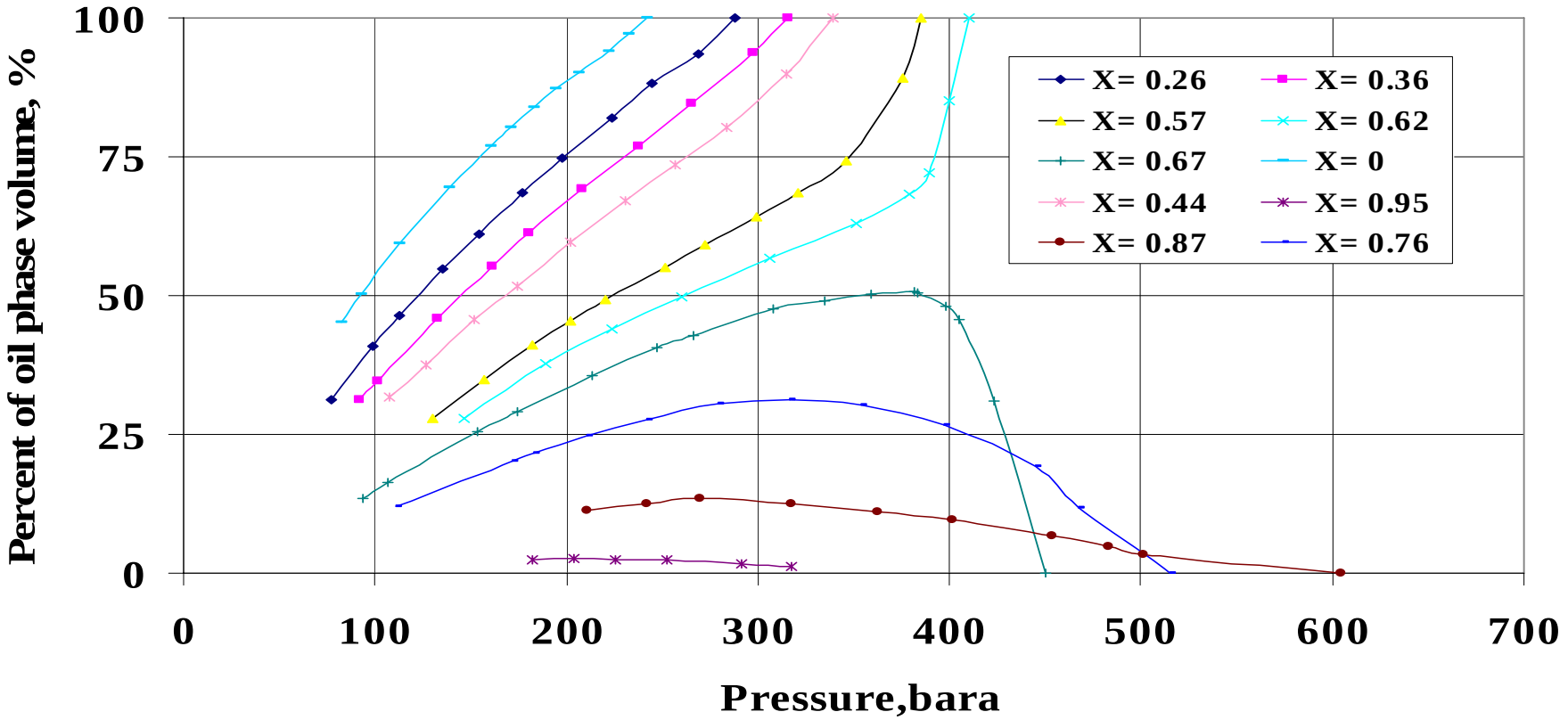

Figure 3.7 The oil-CO_2 volumetric values measured in swelling followed by the CCE experiment. The experiments were conducted at 130 ºC and used the depleted reservoir fluid.

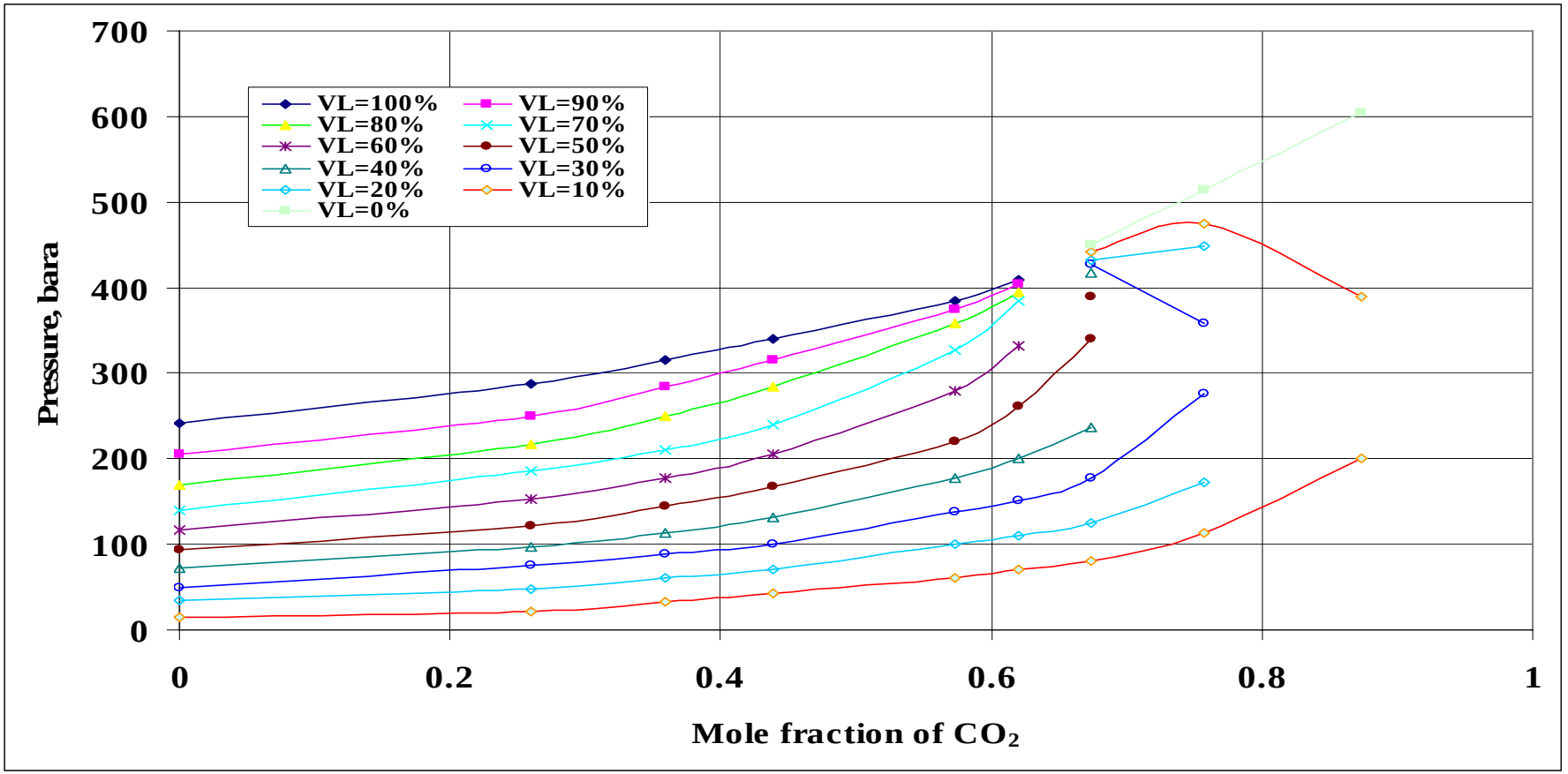

Figure 3.8 The pVTx diagram for the depleted reservoir fluid with pb=242 bar @T=130.4° C

3.3.3 Characterization of depleted reservoir oil at 60º C

Based on the field production history, in order to increase and maintain the reservoir pressure, water was injected into the reservoir. Sea water were used and consequently the reservoir temperature in the water flooded zone was reduced from its initial value of 130 ºC to 60 ºC. Therefore it is necessary to characterize the depleted oil at this new reservoir temperature. The same experiments as was done at 130 ºC were repeated at 60 ºC and all results are explained in the following sections.

Single flash

The pVT cell was charged with depleted reservoir oil at pressure and temperature of 300 bar and 60 ºC respectively. The single flash operation was performed by flashing a known volume of the reservoir oil to atmospheric conditions. The weight, volume, composition, and molecular weight of the flashed oil and gas were measured. The single flash fluid compositions and the resulting initial reservoir oil composition are shown in Table 3.13.

The corresponding volumetric data obtained in the single flash experiment for initial reservoir oil are shown Table 3.14.

Table 3.20 The single flash results for the depleted reservoir oil. The bubble point pressure was determined (pb=204 bar) in the CCE experiments at reservoir temperature 60 ºC

Item	Initial fluid	Unit
The bubble point of oil	204.00	bar
The oil density at p_b	0.712	g/cm^3
Oil molecular weight	103.2	g/gmol
Gas oil ratio	133.2	sm^3/sm^3
Oil formation volume factor at p_b	1.40	cm^3/scm^3

Constant composition expansion experiments

Constant composition experiments (CCE) were performed and the density, compressibility, and bubble point pressure of the depleted reservoir oil at 60ºC was determined. Using the oil density measured in the single flash and the oil compressibility data, the oil density as a function of pressure was calculated and the result is shown in Figure 3.3

The CO_2/oil swelling experiments at 60 ºC

A pVTx diagram at the reservoir temperature 60 ºC for the depleted reservoir oil and CO_2 system has been determined. This was done by a mixing known amount of initial reservoir oil and CO_2 in the pVT cell. The pVT cell was charged with known quantities of the depleted reservoir oil as shown in Table 3.21 then a known amount of CO_2 were added in separate steps as given in Table 3.22.

Table 3.21 The pVT cell initial conditions before the addition of any CO_2 at 130 ºC

Pressure	300	bara
Temperature	60	º C
Oil volume	36.21	ml
Molar volume of oil:@450 bar	124.94	ml/mole
Oil molecular weight	106.33	g/gmol
Mole of oil in the pVT cell	0.289	gmol

For each step in Table 3.22 the oil and CO_2 were mixed and the system pressurized into the one phase region. A constant mass expansion was performed. Below the bubble point the gas and liquid volumes were measured at several pressures. The percentage of the liquid volume versus pressure for each step is shown in Figure 3.7. As shown in this figure, all points having 100 % liquid volume are placed in the bubble point.

Table 3.22 The mole fraction of the CO_2 in the pVT cell after the addition of CO_2 at each step

Step	Mole of oil in the pVT cell:	Cumulative mole of added CO_2	X, Mole fraction of CO_2
	gmol	gmol	fraction
0	0.289	0.000	0.00
1	0.289	0.040	0.12
2	0.289	0.090	0.24
3	0.289	0.159	0.35
4	0.289	0.282	0.49
5	0.289	0.382	0.57
6	0.289	0.545	0.65
7	0.289	0.911	0.76
8	0.289	1.841	0.86

Using the volumetric values given in Figure 3.9, the phase diagram for the CO_2-oil system was made and is shown in Figure 3.10. This figure illustrates that the critical point for this system is at $X_{CO2} = 0.58$. As shown in this figure all data with zero percent liquid volume are in the dew point line

Table 3.23 The mole fraction of the CO_2 in the pVT cell after each addition of oil

Step	Mole of CO_2 gmol	Cumulative mole of added oil gmol	X, Mole fraction of CO_2 fraction
7	0.67	0.039	0.945
8	0.67	0.096	0.874
9	0.67	0.214	0.757

Viscosity measurement

Different mixtures from the depleted reservoir oil and CO_2 were prepared with the composition shown in Table 3.19. Then each mixture was flashed to the pressure of 300 bar and temperature 60 ºC and the resulting liquid phase with densities given in Table 3.24 were transferred to the viscometer. The roll time of the ball for each step was measured while adjusting the whole assembly to the desired angle (70°, 45°, or 23°).

Table 3.24 The mixtures of oil and CO_2 which were used for the viscosity measurement. Each mixture was flashed to 300 bar and 60 ºC, and the separated liquid phase was used for the viscosity measurement. The density in this table corresponds to separated liquid density at 300 bar and 60 ºC.

Step	Mole fraction of the CO_2 X_{CO2}	Liquid density @ 300 bar , 60ºC
		g/cm^3
1	0.00	0.730
2	0.12	0.700
3	0.25	0.680
4	0.35	0.635
5	0.49	0.612
6	0.57	0.600
7	0.66	0.630

The calculated viscosities for each step are shown in Figure 3.6.

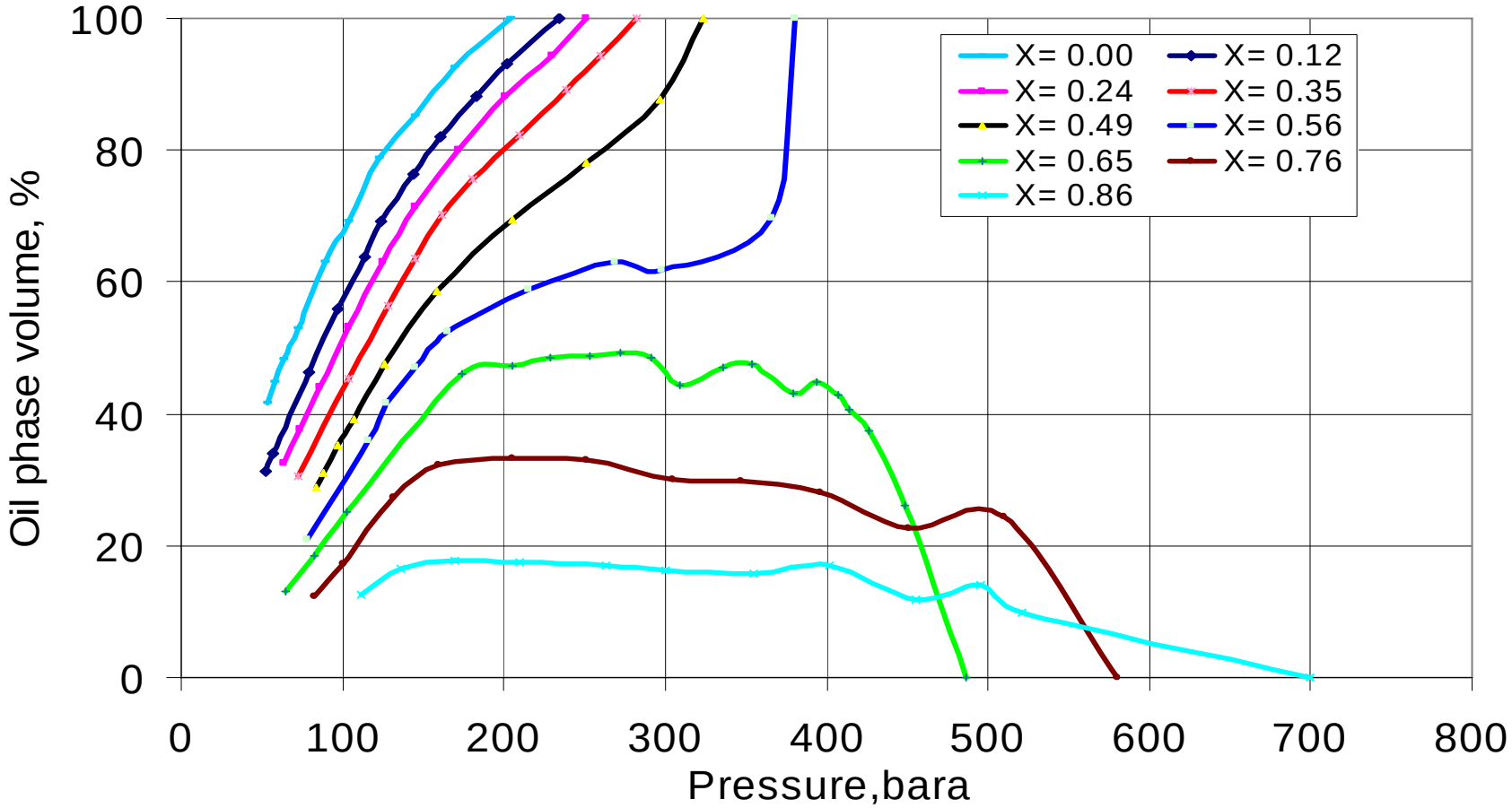

Figure 3.9 *The oil-CO_2 volumetric values measured in swelling followed by CCE experiment. The experiments were conducted at 130 ºC and using the depleted reservoir fluid.*

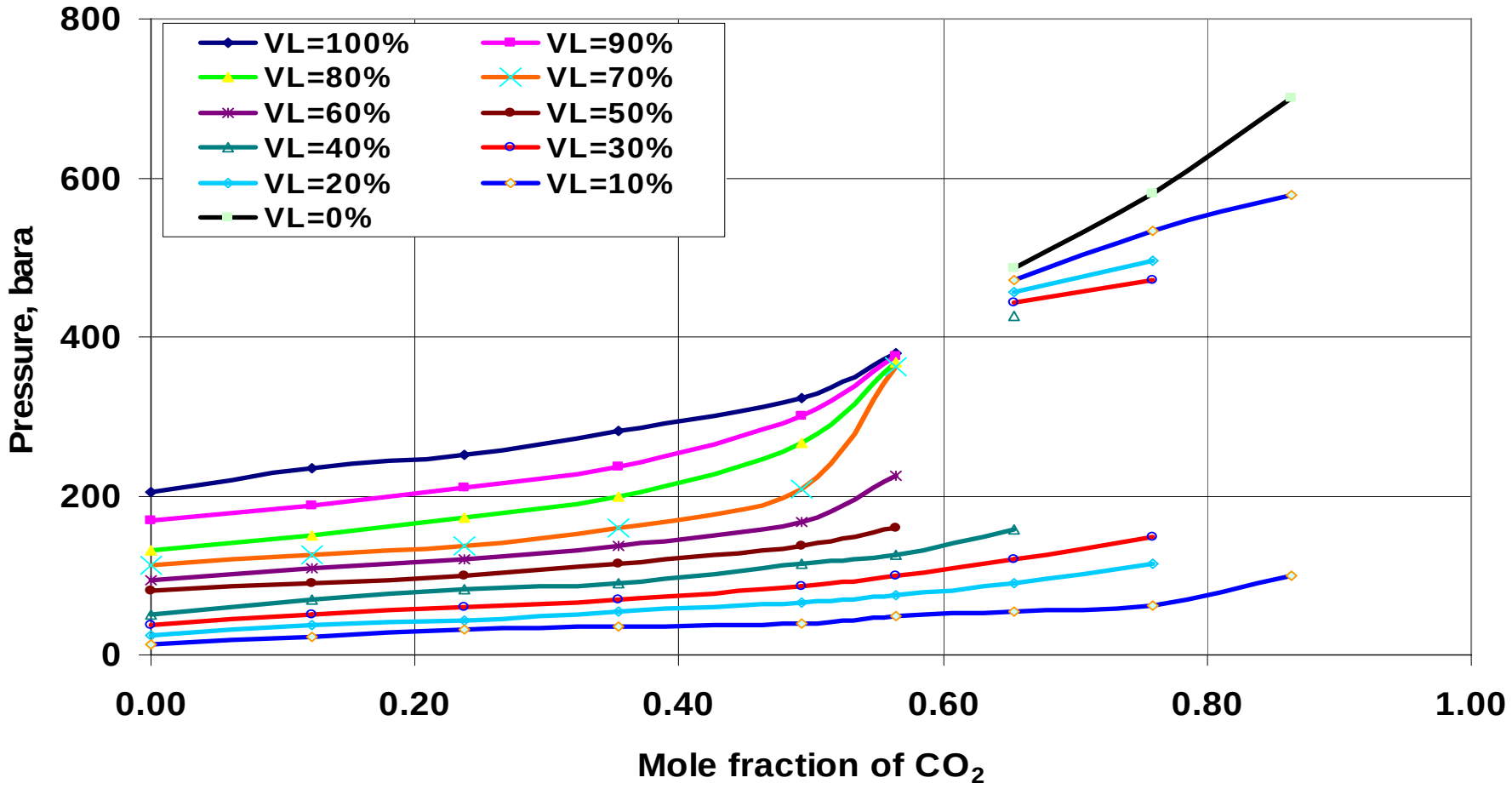

Figure 3.10 The pVTx diagram for the depleted reservoir fluid with pb = 242 bar @T = 130.4° C

3.4 EOS characterization

Saturation pressures, compositional data and volumetric pVT data were given in the previous sections used to construct the required EOS model for using in the compositional simulation of the CO_2 injection experiments. Since all CO_2 injection experiment was performed by using the depleted reservoir fluid, the EOS models for this fluid were prepared for temperatures of 130 ºC and 60 ºC.

3.4.1 EOS characterization for depleted reservoir oil at 130 ºC

The fluid description was made using the pVT simulator PVTsim (Calsep A/S, 2005). The Soave-Redlich-Kwong equation (Soave, 1972) with temperature dependent Peneloux volume correction (Peneloux et al., 1982 and Pedersen et al., 2004) was used as the equation of state. Using the depleted oil composition given in Table 3.13, the component iC_4 was lumped with nC_4, and iC_5 was lumped with nC_5. The number of C_{7+} pseudo-components was chosen to be 6. This gives a total of 14 pseudo components which can properly model the complex phase behaviour of the oil and CO_2 mixtures. The optimum EOS parameters for depleted fluid at 130 ºC are shown in Table 1.13. Non zero binary interaction coefficients are shown in Table 3.26

Table 3.25 Optimum EOS parameters for depleted fluid at 130 ºC

Component	Mole%	MW g/gmol	T_c (°C)	p_c (bar)	ω	Peneloux (cm^3/gmol)	Peneloux-T (cm^3/gmol K)
N_2	0.12	28.00	-147.00	33.94	0.04	0.92	0.000
CO_2	0.83	44.00	31.10	73.76	0.23	3.03	0.005
C_1	44.15	16.00	-82.60	46.00	0.01	0.63	0.000
C_2	7.56	30.10	32.30	48.84	0.10	2.63	0.000
C_3	4.21	44.10	96.70	42.46	0.15	5.06	0.000
C_4	3.15	58.10	147.10	37.56	0.19	7.70	0.000
C_5	2.19	72.20	192.80	33.78	0.24	11.68	0.000
C_6	2.07	86.20	234.30	29.69	0.30	17.98	0.000
C_7-C_9	8.21	108.30	272.60	28.31	0.51	18.36	0.021
C_{10}-C_{15}	11.58	166.00	358.10	19.98	0.67	44.84	-0.022
C_{16}-C_{22}	5.51	247.10	444.10	15.86	0.87	55.28	-0.084
C_{23}-C_{34}	4.65	336.20	523.80	14.30	1.06	37.24	-0.150
C_{35}-C_{41}	3.34	484.00	633.90	13.35	1.28	-25.67	-0.240
C_{42}-C_{80}	2.43	659.20	755.60	13.14	1.33	-121.72	-0.330

With Peneloux volume correction the Soave-Redlich-Kwong equation takes the form shown in Eq. 3-1:

$$P=\frac{R.T}{V-b}-\frac{a(T)}{(V+c)(V+b+2c)} \quad \text{.....3-1}$$

The parameters *a* and *b* are the function of T_c, p_c and acentric factor (ω). For the C_{7+} fractions the below property correlations are used (Pedersen et al., 1992)

$$T_c = c_1\rho + c_2\ln(M) + c_3 M + \frac{c_4}{M} \quad \text{3-2}$$

$$\ln(P_c) = d_1 + d_2\rho^{d_s} + \frac{d_3}{M} + \frac{d_4}{M^2} \quad \text{3-3}$$

$$m = e_1 + e_2 M + e_3\rho + e_4 M^2 \quad \text{3-4}$$

$$m = 0.480 + 1.574\omega - 0.176\omega^2 \quad \text{3-5}$$

In above equations, M stands for molecular weight, ρ for density at atmospheric conditions. The C_{7+} fractions are usually lumped into 3-12 pseudo-components. The Peneloux volume shift parameter may be a constant or as in this work a function of temperature.

$$c_i = c_{oi} + c_{1i}\left(T - 288.15\right) \quad \text{3-6}$$

where T is the absolute temperature in K.

Table 3.26 Non-zero binary interaction coefficients applied for depleted fluid at 130 ºC

	CO_2	C_1	C_2	C_3	C_4	C_5	C_6
N_2	-0.0315	0.0278	0.0407	0.0763	0.0700	0.0878	0.0800
CO_2		0.1200	0.1200	0.1200	0.1200	0.1200	0.1200
	C_7-C_9	C_{10}-C_{15}	C_{16}-C_{22}	C_{23}-C_{34}	C_{35}-C_{41}	C_{42}-C_{80}	
N_2	0.0800	0.0800	0.0800	0.0800	0.0800	0.0800	
CO_2	0.0800	0.0800	0.0800	0.0800	0.0800	0.0800	

In optimum EOS, the parameters given in Table 3.25, the temperature dependent term of the Peneloux parameter (c1 Eq.3-6) was slightly modified to match the Bo data given in Table 3.14. PVTsim by default uses a binary interaction parameter (k_{ij}) of 0.10 between CO_2 and C_{7+} pseudo-components. In order not to simulate too high a saturation point for the highest CO_2 concentration, the value of k_{ij} for these component pairs was decreased to 0.08 as it is shown in Table 3.26.

EOS model predicted phase behaviour

Figure 3.11 shows the measured and simulated Bo-factors for the depleted reservoir oil. Figure 3.12 shows the measured and simulated saturation pressures plotted against CO_2 mole% for the depleted reservoir oil. The saturation points for the highest CO_2 concentrations are at dew point while those for the lower CO_2 concentrations are bubble points. The experimental saturation points are matched quite well in the simulations.

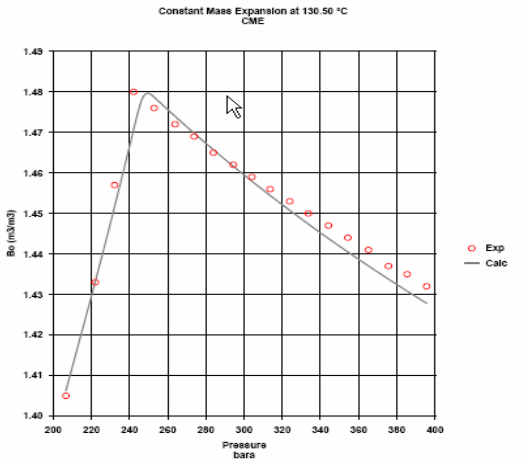

Figure 3.11 EOS model predicted Bo factors for depleted fluid at 130.5 °C

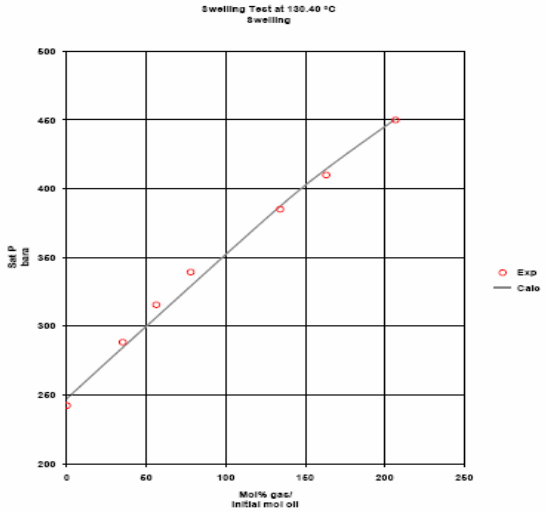

Figure 3.12 EOS model predicted CO_2 swelling saturation point data and simulation results for depleted fluid at 130.4 °C

The liquid volume percent versus pressure for different mixture of the depleted reservoir oil and CO_2 at 130 ºC are shown in Figure 3.11 to Figure 3.16.

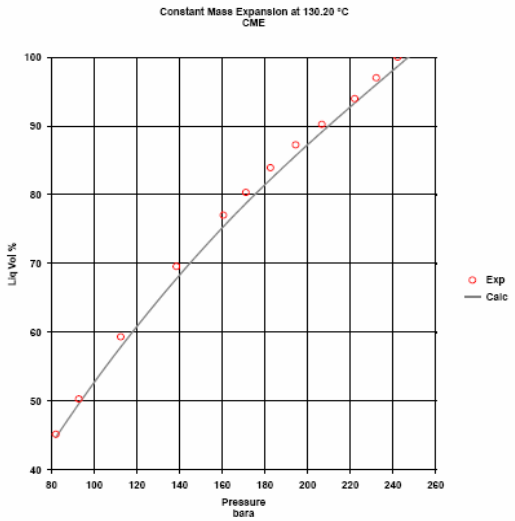

Figure 3.13 EOS model predicted liquid volume% versus pressure for depleted fluid at 130.2 °C ($XCO_2 = 0$)

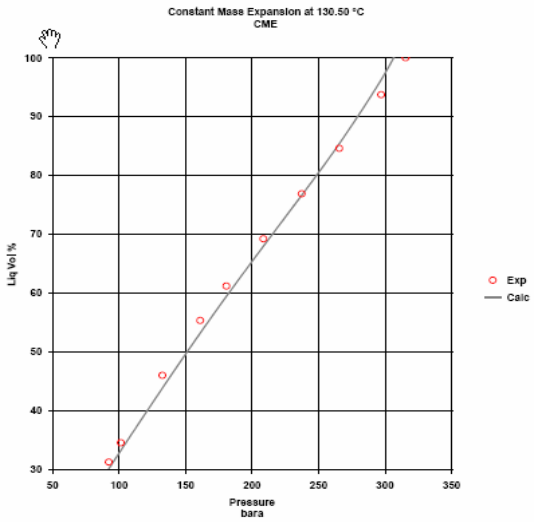

Figure 3.14 EOS model predicted liquid volume% versus pressure for a mixture of 64 mole% depleted fluid and 36 mole% CO_2 at 130 ºC

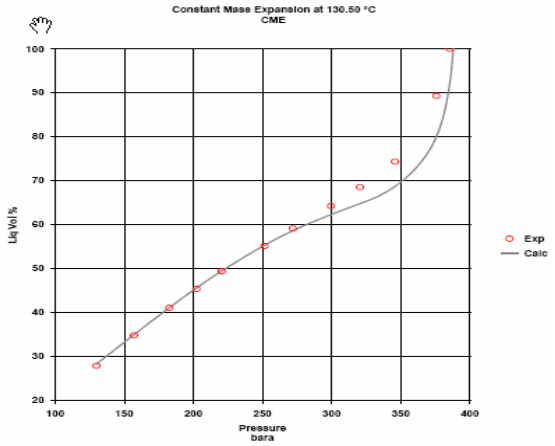

Figure 3.15 EOS model predicted liquid volume% versus pressure for a mixture of 42.7 mole% depleted fluid and 57.3 mole% CO_2 at 130 ºC

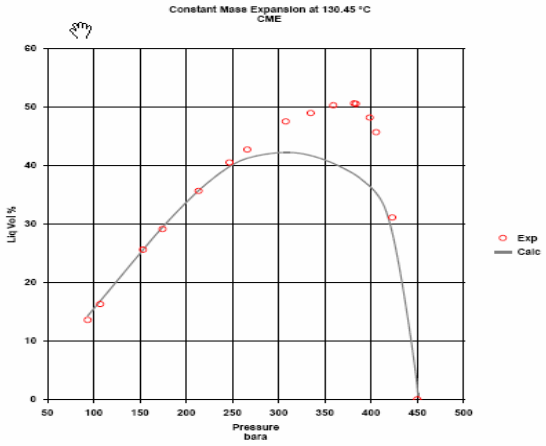

Figure 3.16 EOS model predicted liquid volume% versus pressure for a mixture of 32.6 mole% depleted fluid and 67.4 mole% CO_2 at 130 ºC

Figure 3.13 to Figure 3.16 show the EOS model match to the critical point on the swelling curve where the saturation point changes from a bubble point to a dew point.

Viscosity calculation

The viscosity of oil above its Wax Appearance Point (WAP) is calculated using either the corresponding states model (CSP), or the Lohrenz-Bray-Clark (LBC) model.

The LBC method is still the most common method employed in the petroleum industry for estimating the viscosity of petroleum fluids. It is based on the observation that excess viscosity of a fluid is primarily a function of density and that for the first approximation it can be assumed to be independent of temperature. The LBC method incorporates this finding into a general two parameter corresponding states methodology for estimating the viscosity of petroleum fluids from critical parameters of its constituent species. The viscosity of a fluid mixture is thus given by:

$$\left[\left(\eta-\eta^{0}\right)\xi+10^{-4}\right]^{-0.25}=\sum_{j=0}^{4}a_{j}\left(\frac{\rho}{\rho_{c}}\right)^{j} \quad \text{.....3-7}$$

$$\xi^{6}=\left[\sum x_{i}T_{ci}\right]\left[\sum x_{i}M_{ci}\right]^{-3}\left[\sum x_{i}P_{ci}\right]^{-2} \quad \text{.....3-8}$$

where x_i is the mole fraction of each pure species i, while T_{ci}, p_{ci} and M_i are the critical temperature, pressure and molecular weight respectively. The coefficients a_j are temperature independent and are those already suggested by (Jossi et al., 1962). The zero density mixture viscosity is given by a simple mixing rule:

$$\eta^0 = \frac{\sum_{i=1}^{N} x_i \eta_i^0 M_i^{1/2}}{\sum_{i=1}^{N} x_i M_i^{1/2}} \quad \text{..... 3-9}$$

While the critical density is calculated from the critical volume obtained from a mole fraction average mixing rule Lohrenz-Bray-Clark (LBC). In principle the zero density viscosity, 0, of each pure species can be obtained from a number of reliable sources. In this work the original expressions employed by (Lohrentz et al., 1987) are used, where the viscosity is calculated by means of a simple corresponding states expression in terms of reduced temperature.

The Lorenz-Bray-Clark (LBC) a_j correlations were tuned to the viscosity data and they were used to calculate viscosities as shown in Figure 2.1. Table 3.27 shows the coefficients a_j which were tuned against experimental data.

Table 3.27 The coefficients a_j are temperature independent and they are tuned to get a match to the experimental data.

a_0	a_1	a_2	a_3	a_4
0.1023	0.023364	0.058533	-0.04076	0.009332

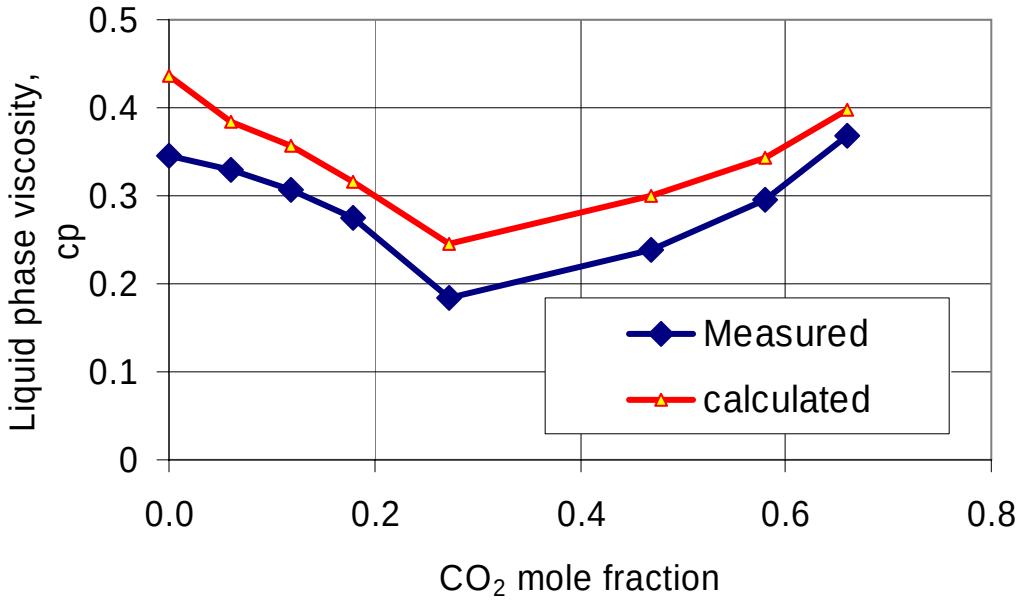

Figure 3.17 LBC calculated liquid phase viscosities for different mixture of depleted oil and CO_2 compared with experimental data at 130 ºC

Minimum miscibility pressure

The minimum miscibility pressure (MMP) for CO_2 and the depleted reservoir fluid at 130 ºC was calculated by using the EOS parameters given in Table 3.25 andTable 3.26 based on the compositional reservoir simulator and the method described in Section 2.9.

Stalkup (1992). This was done by running slim tube simulations in which the number of grids were 500, 1000, 1500, 2000, 10000. After eliminating the numerical dispersion, the MMP for this system was calculated to be 275 bar.

The simulation results and the extrapolated MMP after eliminating numerical dispersion for the CO_2 and oil are shown in Figure 3.18 (blue line indicated as N = Infinite).

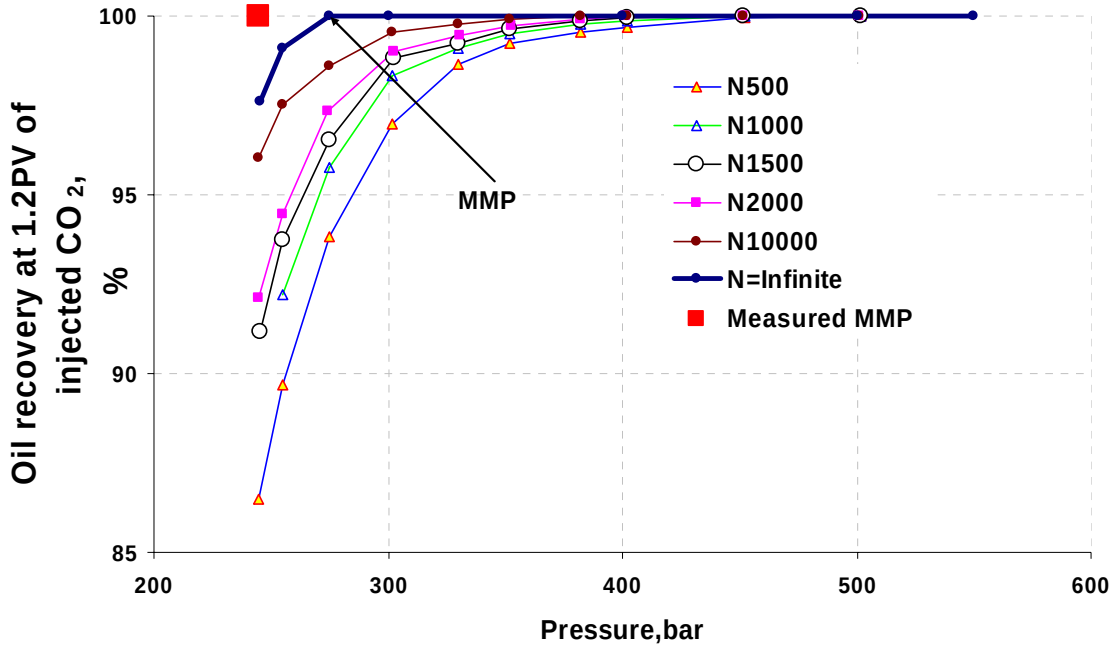

Figure 3.18 The slim tube simulation results for CO_2 and depleted reservoir oil at 130 ºC. The MMP at infinite number of grids is obtained by extrapolation and it is calculated to be 275 bar.

In Figure 3.18 the point indicated by a red square indicating the MMP which was measured through the slime tube experiment using CO_2 as injection gas. It is obvious that the calculated MMP is in very good agreement with the experimental value and confirming that the developed EOS model is able to predicate the behaviour of the heavy end components in the oil.

3.4.2 EOS characterization for depleted reservoir oil at 60 ºC

The fluid description was made using the pVT simulator PVTsim (Calsep A/S, 2005). The Soave-Redlich-Kwong equation (Soave, 1972) with temperature dependent Peneloux volume correction (Peneloux et al., 1982 and Pedersen et al., 2004) was used as the equation of state. Using the depleted oil composition given in Table 3.13, the component iC_4 was lumped with nC_4, and iC_5 was lumped with nC_5. The number of C_{7+} pseudo components was chosen to 6. This gives a total of 14 pseudo components which can properly model the complex phase behaviour of the oil and CO_2 mixtures at 60 ºC. The optimum EOS parameters for depleted fluid at 60 ºC are shown in Table 3.28. Binary interaction coefficients are shown in Table 3.29

Table 3.28 Optimum EOS parameters for depleted fluid at 60 ºC

Component	Mole%	MW	T_c	p_c	ω	Peneloux	Peneloux-T
N_2	0.12	28.00	-147.00	33.94	0.040	0.92	0.000
CO_2	0.83	44.00	31.10	73.76	0.225	3.03	0.005
C_1	44.15	16.00	-82.60	46	0.008	0.63	0.000
C_2	7.56	30.10	32.30	48.84	0.098	2.63	0.000
C_3	4.21	44.10	96.70	42.46	0.152	5.06	0.000
C_4	3.15	58.10	147.10	37.56	0.188	7.7	0.000
C_5	2.19	72.20	192.80	33.78	0.241	11.68	0.000
C_6	2.07	86.20	234.30	29.69	0.296	17.98	0.000
C_7-C_9	8.21	108.30	272.60	22.7	0.659	18.38	0.021
C_{10}-C_{15}	11.58	166.00	358.10	17.36	0.911	43.57	-0.022
C_{16}-C_{22}	5.51	247.10	444.10	16.17	1.065	55.3	-0.084
C_{23}-C_{34}	4.65	336.20	523.80	14.25	1.124	37.24	-0.150
C_{35}-C_{41}	3.34	484.00	633.90	13.34	1.357	-25.7	-0.240
C_{42}-C_{80}	2.43	659.20	755.60	13.85	1.365	-125.29	-0.330

EOS model predicted phase behaviour

Figure 3.19 shows measured and simulated Bo-factors for the depleted reservoir oil. Figure 3.20 shows the measured and simulated saturation pressures plotted against mole% CO_2 per each mole of oil for the depleted reservoir oil. The saturation points for last two CO_2 concentrations are at dew point while those for the lower CO_2 concentrations are bubble points. The experimental saturation points are matched quite well in the simulations.

Table 3.29 Binary interaction coefficients applied for depleted fluid at 60 ºC

-0.032										
0.0278	0.12									
0.0407	0.12	0								
0.0763	0.12	0	0							
0.0700	0.12	0	0	0						
0.0878	0.12	0	0	0	0					
0.1000	0.12	0	0	0	0	0				
0.2034	0.1016	-0.002	0	0	0	0	0			
0.2034	0.1016	-0.002	0	0	0	0	0	0		
0.2034	0.1016	-0.002	0	0	0	0	0	0	0	
0.2034	0.0917	-0.002	0	0	0	0	0	0	0	
0.2034	0.0917	-0.002	0	0	0	0	0	0	0	0
0.2034	0.0917	-0.002	0	0	0	0	0	0	0	0	0

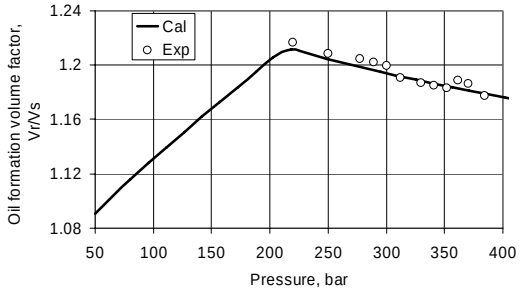

Figure 3.19 EOS model predicted Bo factors for depleted fluid at 60 °C

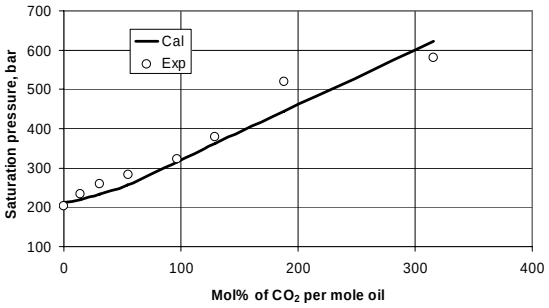

Figure 3.20 EOS model predicted CO_2 swelling saturation point data and Experimental results for depleted fluid at 60 °C

The liquid volume percent versus pressure for different mixtures of the depleted reservoir oil and CO_2 at 60 ºC are shown in Figure 3.21 toFigure 3.24.

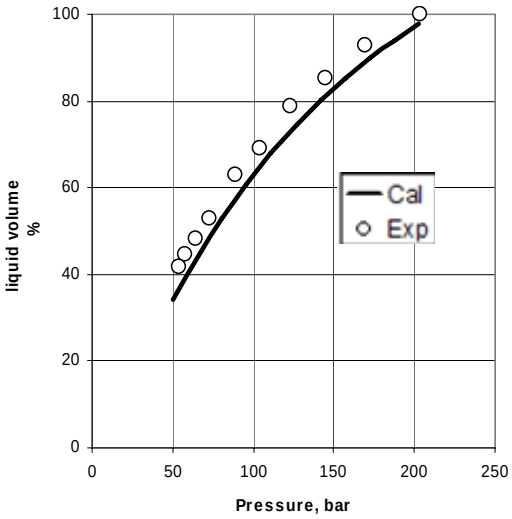

Figure 3.21 EOS model predicted liquid volume% versus pressure for depleted fluid at 60 °C ($XCO_2 = 0$)

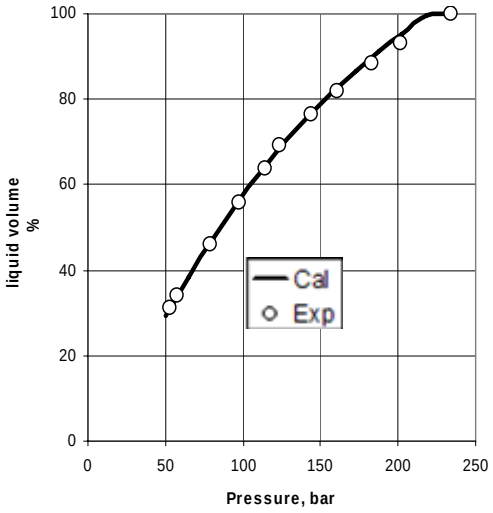

Figure 3.22 EOS model predicted Liquid volume% versus pressure for a mixture of 13.9mole% CO_2 per mole of depleted oil at 60 ºC ($XCO_2 = 0.12$)

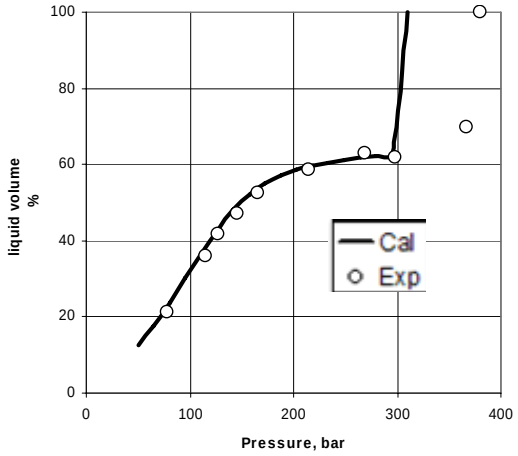

Figure 3.23 EOS model predicted Liquid volume% versus pressure for a mixture of 129mole% CO_2per mole of depleted oil at 60 ºC $XCO_2 = 0.56$

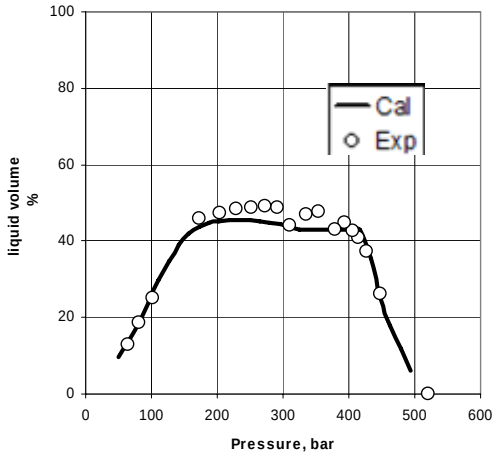

Figure 3.24 EOS model predicted Liquid volume% versus pressure for a mixture of 188mole% CO_2per mole of depleted oil at 60 ºC $XCO_2 = 0.65$

Figure 3.21 toFigure 3.24 show the EOS model match to the critical point on the swelling curve where the saturation point changes from a bubble point to a dew point.

3.5 North Sea chalk and rock characterization

In fractured reservoirs the fissures system constitutes the primary conduit for flow while the gross fluid volumes are contained in the matrix blocks which must be transferred to the fracture system and eventually to the production wells. The matrix-fracture fluid exchanges are functions of both fracture intensity and the capillary continuity. High fracture intensity increases the oil and gas exposure surface area, and consequently a higher diffusion drive mechanism, while capillary continuity increases the chance for gravity drainage (assuming the gas and oil are not in equilibrium).

The matrix properties such as permeability also control the gravity drainage contribution. In the case of small matrix block height, there is no capillary continuity, a very high gas-oil interfacial tension and low matrix permeability, thus the gravity drainage contribution can be neglected.

These and other types of matrix fracture fluid exchange behaviour must be studied in a set of reservoir conditions experiments in which representative reservoir rock and fluids are used. Due to some limitations to get reservoir core material for experiments, rock material from the Faxe outcrop in Denmark which has similar rock properties to the reservoir under study have been used. However it was important to check the basic rock properties. The next following sections show the summary of the geneses, mineralogy of chalk in the North Sea and the rock and its characterization which was used in all the CO_2 injection experiments.

3.5.1 Geneses of chalk in the North Sea

The chalk is primarily pelagic sediment of accumulation rather than mechanical deposition. It is a rock composed mainly of skeletal calcite of the phylum Haptophyta with minor amounts (<10 %) of other biogenic fragments (Mortimore 1990). Therefore it is extremely pure limestone. Chalk was deposited over large areas of NW Europe during the Cretaceous Period as pelagic sediment (deep-sea ooze) and through a series of digenetic processes the sediment became lithified.

In the North Sea the chalk attains a maximum thickness of 2000 m in the Viking Graben and Central Trough, but 300 - 350 m is more usual on the flanks and in the areas where it outcrops. The considerable thickness of chalk in the Central Trough is due to redeposition following sliding, slumping and the formation of debris flow and turbidity. Tectonic movements initiated large scale displacement of unstable chalk down the flanks of the Trough to accumulate in the Trough itself as complex allochthonous sequences.

Burial and subsequent uplift of the lithified sediments caused fractures to form (Downing et al., 1993). Figure 3.25 shows chalk distribution in Europe (FRACFLOW 2000).

3.5.2 Mineralogy

Chalk is an extremely soft and pure limestone consisting mainly of calcium carbonate with small portions of other constituents. Clay minerals mainly include the smectite group usually in the form of Ca-montmorillonite. The mica group is less important and chlorite is rare. In the white-chalk facies such as in English and Danish chalk, the clay content is typically less than 2 % (Hancock 1993). Quartz occurs as clay and silt-grade particles and as pseudomorphs after foraminifera throughout the chalk. Most of the original biogenic silica has undergone a series of digenetic changes to become concentrated into chert-nodules called flints (Hancock 1993).

Figure 3.25 Chalk distribution in Europe (FRACFLOW 2000).

3.5.3 Chalk porosity and permeability

The chalk with its depositional, digenetic and tectonic setting is translated to a typical dual-porosity or double-porosity formation, with porosity due to the matrix pores (30-40 %) and the other due to the fractures (probably ≤1%). In these formations the chalk-matrix pores provide the storage capacity and the fractures provide the permeable pathways for fluid transport.

In hydrocarbon bearing North Sea chalk, microfossils may be filled with cement and mud particles mature to equant shape while the mud matrix itself remains uncemented as a consequence of hydrocarbon lubrication. Uncemented North Sea chalk with mature mud may have porosities near 20% where the effective burial stress is large enough. In several North Sea fields the effective burial stress is so low that porosities of 40%-50% are maintained.

The permeability of the chalk is critically controlled by the size of the constituent coccoliths, which are various in the chalk deposits. The Maastrichtian Tor Formation contains the largest coccoliths, followed by the Danian Ekofisk formation. The porosity and matrix permeability of the chalk are influenced by many factors, such as; burial depth, overpressure, re-deposition, clay content and porosity preservation due to hydrocarbon saturation. Figure 3.26 shows the porosity-permeability relationship for two typical chalk systems in the uppermost Niobrara and North Sea chalk (Lockridge and Scholle 1978).

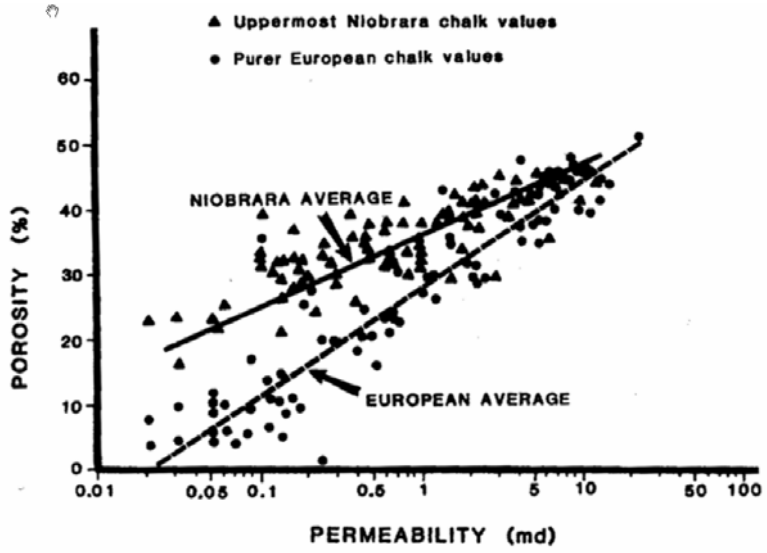

Figure 3.26 Porosity and permeability relationship for North Sea and Niobrara chalk (From Lockridge and Scholle 1978)

3.5.4 The Faxe chalk outcrop

For the CO_2 injection experiment which will be discussed in Chapter 4 it was decided to use rock material which is analogue to the one in the North Sea chalk reservoirs in this study. The Faxe outcrop in Denmark has similar rock properties comparing to North Sea chalk material. They can be used as a good candidate in any experiment investigating the matrix fracture fluid exchange in the case of CO_2 injection. The well-known limestone Rørdal outcrop chalk has been used by Graue and Bongnø (1990) for their

investigation on the oil recovery mechanisms in fractured chalk reservoirs. The basic measurements such as the brine permeability and porosity of the Faxe outcrop have shown similar rock properties as Rørdal outcrop chalk.

Porosity and permeability

The rock formation is of Maastrichan age and consists mainly of cocolitt deposits with about 99 % calcite and 1 % quartz. All the core samples were drilled in the same orientation relative to bedding planes or laminations. The chalk cores were dried at 130 °C for at least one week before being used. The brine permeability and porosity for the chalk cores ranged from 3-4 mD and 43–45 %, respectively.

Synthetic brine was prepared from the reservoir formation water composition shown in Table 3.30. The density and the viscosity of the brine were 1.09 g/cm3 and 1.19 cp, respectively, at 20 ºC and atmospheric pressure. The brine was filtered through a 0.45 mm paper filter membrane.

Vertical to Horizontal permeability ratio

To examine the rock heterogeneity several small block samples from the existing big block Faxe chalk have been taken. Using a gas Mini-Permeameter, the rock heterogeneity with reference to its orientation relative to bedding planes or lamination has been checked out.

Table 3.30 Synthetic brine prepared from the reservoir formation water composition

Component	weight (g)
NaCl	35.74
KCl	0.29
$CaCl_2 \cdot 2H_2O$	32.28
$MgCl_2 \cdot 6H_2O$	4.35
H_2O	927.34
Total	1000.00

In order to investigate the magnitude of the ratio of vertical to horizontal permeability (K_v/K_h), a small chalk block approximately 11 cm thick from the original big block has been cut. The chalk block with its correct orientation with respect to the outcrop is shown in Figure 3.27. The XY and YZ planes for the block that corresponds to its position in the outcrop are called planes F and B respectively.

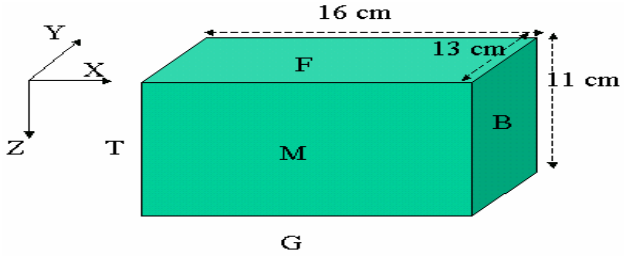

Figure 3.27 The horizontal and vertical direction for the chalk block with reference to its position in the outcrop

Planes F (XY) and B (YZ) were divided into 3×4 and 3×3 grid cell systems respectively as shown in Figure 3.28.

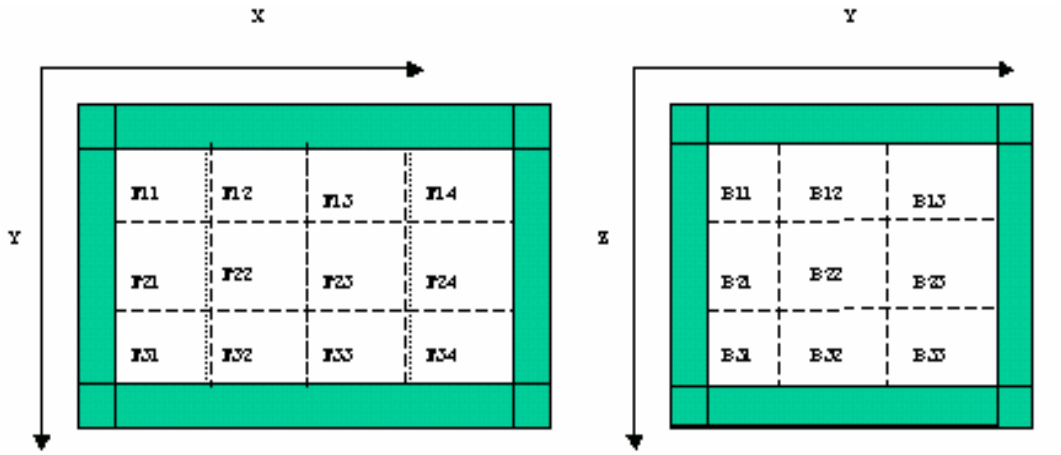

Figure 3.28 The grid system for F (YX) and B (YZ) planes of the chalk block

By using a Mini-Permeameter, the heterogeneity of the chalk block with respect to its permeability was measured. The procedure for measuring the heterogeneity would become very simple when using the flow equation applicable to the Mini-Permeameter equipment.

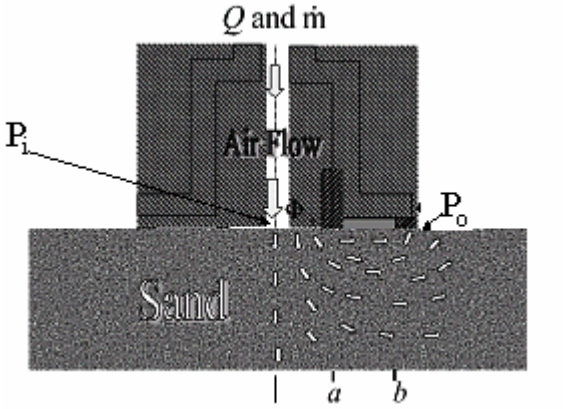

Figure 3.29 Typical Mini-Permeameter configuration

Figure 3.29 shows the typical Mini-Permeameter configuration. In this configuration the permeability of rock is characterized by the flow of gas Q and inlet pressure at the rock

face (back pressure P_i). The local permeability can be measured by knowing these two parameters and using Eq. 3-1

$$k_{measured} = \frac{Q\mu P_i}{G.\left(P_i^2 - P_o^2\right)} \quad \text{..... 3-1}$$

where Q is the gas flow rate and P_i is the inlet pressure to the block surface, P_o is the outer pressure and it is equal to zero and G is the shape factor, which is constant for all measurements. The gas flow rate is proportional to the value of deferential pressure measured across a packed column inside the equipment. The pressure at the inlet of the block P_i is directly measured by a very sensitive pressure transducer.

The ratio of the permeability of each point in the plane with respect of a reference point in the same plan is calculated by Eq. 3-2

The permeability of each point in plane F (F_{ij}) can be compared with the permeability of a reference point (F_{23}) in the same plane by using Eq. 3-2, and consequently the heterogeneity in the rock can be determined.

$$\frac{K_{F_{ij}}}{K_{F_{reff\_point}}} = \frac{\left(\frac{\Delta P}{P_i}\right)_{ij}}{\left(\frac{\Delta P}{P_i}\right)_{reff}} \quad \text{..... 3-2}$$

In Eq. 3-2 ΔP is the pressure drop across the packed column for a certain gas flow rate Q. The measured parameters in the F plane belong to the block vertical permeability while the values for the B plane are for the block horizontal permeability.

The same measurements also can be performed for plane B and the heterogeneity in the block for this plane can be determined by using Eq.3-3.

$$\frac{K_{B_{ij}}}{K_{B_{reff\_point}}} = \frac{\left(\frac{\Delta P}{P_i}\right)_{ij}}{\left(\frac{\Delta P}{P_i}\right)_{reff}} \quad \text{..... 3-3}$$

In Eq. 3-3 the reference point is B_{22} .The ratio of the vertical permeability to horizontal permeability of the block also can be calculated by using Eq.3-4.

$$\frac{K_{F_{ij}}}{K_{B_{reff\_point}}} = \frac{\left(\frac{\Delta P}{P_i}\right)_{Fij}}{\left(\frac{\Delta P}{P_i}\right)_{Breff\_cell}} \quad \text{..... 3-4}$$

The permeability variation can be obtained by using the measured values in the laboratory for each plan and using the above equations.

The heterogeneity of the vertical permeability (blue colour) for plane F is shown in Figure 3.30. This figure clearly confirms that the block has an isotropic behaviour and the measured permeability parameter for all points in plane F is almost equal. However there is still one point (F_{24}) in plane F that has a very large difference value comparing to the other point. Considering Figure 3.28, the position of this point (F_{24}) is near the edges of the block and because of the high value of the permeability at this point, this strange value could be due to induced fracture and mechanical damage produced during the preparation of the block.

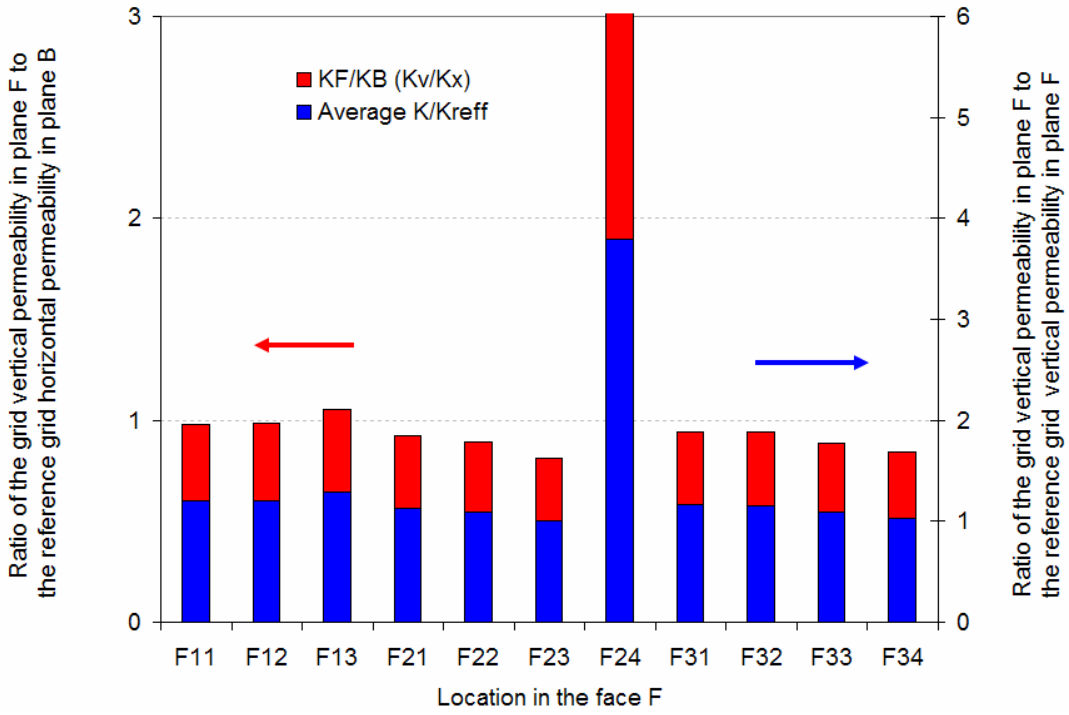

Figure 3.30 The ratio of the grid vertical permeability in plane F to the reference grid (F_{23}) vertical permeability in plane F (blue), ratio of the grid vertical permeability in plane F to the reference grid (B_{22}) horizontal permeability in plane B (red)

Figure 3.30 also shows that the ratio of vertical permeability to horizontal permeability (red) for all points in plane F is the same and has an average value of 0.8.

Figure 3.31 shows the ratio of the grid vertical permeability in plane B to the reference grid (B_{22}) vertical permeability in plane B (blue), and also the ratio of the grid vertical permeability in plane F to the reference grid (B_{22}) horizontal permeability in plan B (red).

This figure also confirms that the permeability distribution in this plane is almost isotropic and again the ratio of the vertical to horizontal permeability for the block is in the range of 0.78 to 0.9.

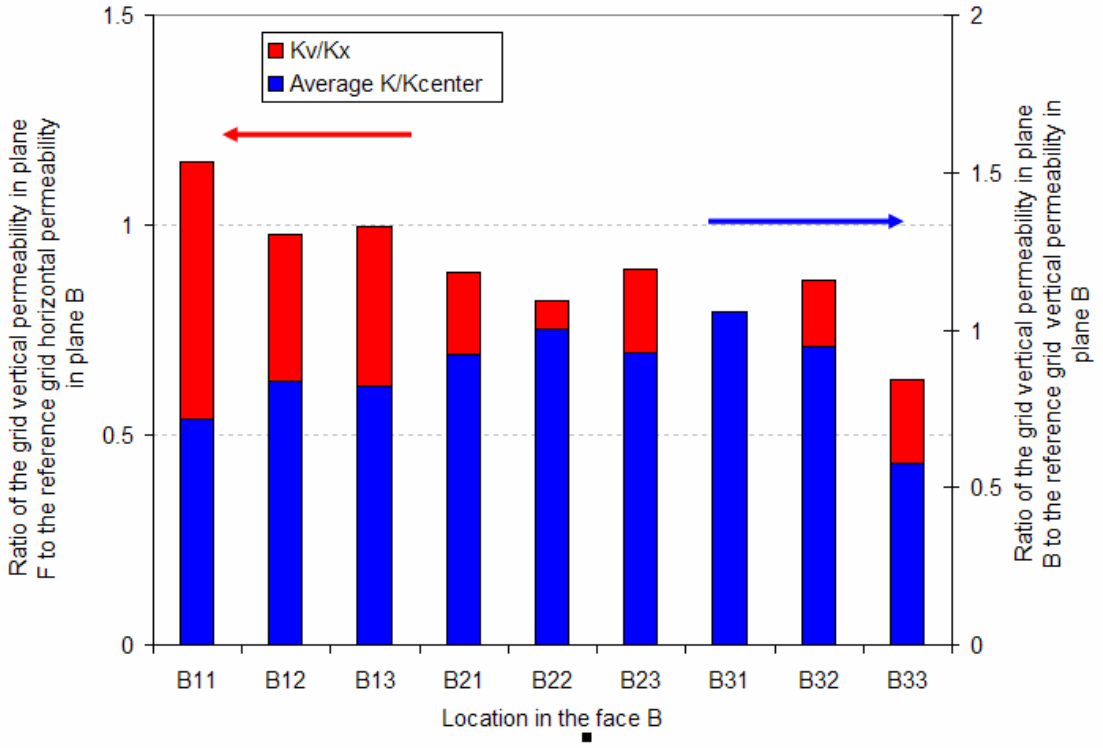

Figure 3.31 *Ratio of the grid vertical permeability in plane B to the reference grid vertical permeability in plane B and ratio of the grid vertical permeability in plane F to the reference grid horizontal permeability in plane B*

3.6 Conclusion

A comprehensive pVT fluid study was performed on the live oil similar to reservoir fluid from one of the North Sea fractured chalk reservoirs. The results from this study were used to develop 14 pseudo components SRK Equation of State model (SRK EOS) so that all the measured phase behaviour and volumetric of oil-CO_2 data are adequately matched

No attempt has been made to minimize the number of the pseudo components however for any field scale simulation the number of pseudo components has to be reduced to minimize the simulation time. The existing EOS model and pVT data are a very good base to make such EOS models.

Faxe chalk, an outcrop analogue to the reservoir rock, was used to conduct rock characterization. The cores from this outcrop later were used in all CO_2 injection experiments. Based on this study the selected outcrop has very similar rock properties to the reservoir rock with matrix permeability of 4 mD and rock porosity of about 44 %.

3.7 References

1) Calsep A/S. (1988-2003). pVTsim. Software Version 13.

2) Downing, R.A., Price, M. and Jones, G.P. (1993). The making of an aquifer. In: The Hydrogeology of the Chalk of North-West Europe, Downing, R.A., Price, M. and Jones, G.P.- pp. 1-13. Oxford University Press Inc., New York.

3) Feazel, c.T.' Keany, J. and Peterson, R.M.: "Cretaceous and Tertiary Chalk of the Central North Sea: A Major Petroleum Reservoir", in Carbonate Petroleum Reservoirs: A case book (1980)

4) Fracflow Third Annual Progress Report (Co-ordinators Summary Report (01.12.1999–30.11.2000). 197 (unpublished).

5) Graue, A., Aspenes, E., Bognø, T., Moe, R.W., and Ramsdal, J. "Alteration of Wettability and Wettability Heterogeneity", University of Bergen, Norway

6) Hancock, J.M. (1993). The formation and digenesis of chalk. In: The Hydrogeology of the Chalk of North-West Europe, Downing, R.A., Price, M. and Jones, G.P.- pp. 14-34, G.P. Oxford University Press Inc., New York.

7) Hujun, Li. "Experimental Investigation of CO_2 Gravity Drainage in a Fractured System," paper SPE 64510 presented at the SPE Asia Pacific Oil and Gas Conference and Exhibition held in Brisbane, Australia, 16–18 October 2000.

8) Jossi J.A., L.I. Stiel and G. Thodos, AIChE J. 8:59 (1962).

9) Lockridge, J. P., and P. A. Scholle. (1978). Niobrara gas in eastern Colorado and North-Western Kansas: Rocky Mountain Assoc. Geol. 1978 Symp. 35-49.

10) Mortimore, R.N. (1990). Chalk or chalk?. In: Chalk, pp.15-45.Thomas Telford, London.

11) Moritis, G. "EOR Continues to Unlock the Oil Resources", Oil & Gas Journal, 45-52, April 12, 2004.

12) Øyno, L, Uleberg K., and Whitson C.H. "Dry Gas Injection in Fractured Chalk Reservoirs- an Experimental Approach", paper SCA1995-27 presented at the International Symposium of the Society of Core Analysts held in San Francisco, California (1995).

13) Pedersen, A. Fredenslund, P.L. Christensen and P. Thomassen, Chem. Eng. Sci. 39:1011 (1984).

14) Peneloux, A., E. Rauzy., and R. Freze. "A Consistent Correction for Redlich-Kwong-Soave Volumes". Fluid Phase Eq. 8, 7-27 (1982).

15) Soave, G. (1972). "Equilibrium Constants from a Modified Redlich-Kwong Equation of State", Chem. Eng. Sci., 27:1197-1203.

16) Standing M.B. (1977). Volumetric and Phase Behaviour of Oil Field Hydrocarbon Systems.

4. CO_2 injection in fractured core

4.1 Introduction

Crude oil development and production in. oil reservoirs can include up to three distinct phases: primary, secondary, and tertiary (or enhanced) recovery. During primary recovery, the natural pressure of the reservoir or gravity drive oil into the well bore, combined with artificial lift techniques (such as pumps) which bring the oil to the surface. But only about 10 percent of a reservoir's original oil in place is typically produced during primary recovery. Secondary recovery techniques to the field's productive life generally by injecting water or gas to displace oil and drive it to a production well bore, result in the recovery of 20 to 40 percent of the original oil in place.

However, with much of the easy-to-produce oil already recovered from oil fields, producers have attempted several tertiary, or enhanced oil recovery (EOR), techniques that offer prospects for ultimately producing 30 to 60 percent, or more, of the reservoir's original oil in place.

One of the EOR techniques that is attracting the most new market interest is carbon dioxide (CO_2)-EOR. Carbon dioxide is a relatively cheap gas, which is produced in the petroleum industry as a waste gas. Performed projects during the last few years, as illustrated in Figure 4.1 (Moritis, 2004) have produced as much as 206 000 barrels per day.

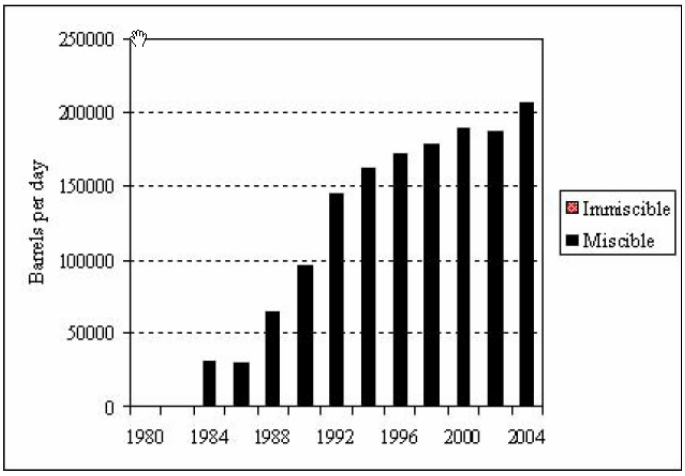

Figure 4.1 Petroleum production by miscible and immiscible carbon dioxide flooding in the United States (Moritis, 2004)

Naturally fractured reservoirs contain a significant portion of the world's oil reserves which also represents a significant geological storage potential for CO_2 as a means of greenhouse gas reduction. Geological CO_2 storage in oil reservoirs is the most likely target for CO_2 mitigation practices because of a number of reasons including additional economic benefit through EOR, the existence of abundant characterization data and utilizing at least part of the existing infrastructure.

For CO_2 injection in fractured oil, matrix blocks are assumed to act as sources of oil and fractures are a flow conduit through which the oil is flowing towards the producing wells.

Depends on the matrix blocks geometry and the reservoir fluid properties, oil from the matrix block is transferred to the fracture system by different mechanisms. Based on classical fractured reservoir production mechanisms, when a tall and permeable oil-saturated matrix block is surrounded by gas in the fracture, oil drains from the matrix as a result of the density difference between the gas in the fracture and the oil in the matrix (gravity dominated mechanism). In case of low permeability and small size matrix blocks with high capillary pressure, the gravity drainage mechanism is inefficient and molecular diffusion mechanism will dominate.

The diffusion calculations in the current commercial compositional simulators are based on models of gas-gas and liquid-liquid diffusion at the fracture-matrix interface and for black oil simulators the diffusion calculation is performed inconsistent models of gas to liquid diffusion at the fracture-matrix interface (Cross phase diffusion)

Coat (1989) has modeled the effect of diffusion in dual-porosity models by the above concept. In his work, he has suggested the diffusion flux to be related to gas-liquid diffusion coefficients and the concentration difference between the matrix and the fracture. The latter is divided by the matrix width to account for concentration gradient. Unfortunately, the proposed formulation is inconsistent with both equilibrium and irreversible thermodynamics and has no physical basis, Hoteit and Firoozabadi (2006).

Hoteit and Firoozabadi (2006) presented a consistent model to incorporate physical diffusion of multicomponent mixtures for gas injection schemes in fractured reservoirs. In their work, the multicomponent diffusion flux was related to multicomponent diffusion coefficients, which are temperature, pressure and composition dependent. These coefficients are calculated from a model based on irreversible thermodynamics.

In their model, the concept of gas to liquid diffusion at the fracture-matrix interface was avoided by assuming that the gas and liquid phases are in equilibrium at the interface. The concept of cross flow equilibrium (that is, vertical equilibrium) is invoked in their model to avoid the use of transfer functions.

In order to verify and examine the accuracy of the above concepts and also understand the contribution of the above mechanisms for oil recovery during CO_2 injection in highly fractured under-saturated light oil reservoirs, it is necessary to perform laboratory experiments at reservoir conditions. Due to the large compositional space involved in this process it is also necessary to initialize the matrix and fracture system with the representative reservoir fluids.

However, in this kind of experiments saturating the pore system with live oil is very difficult. Due to large permeability contrast between the matrix and fracture, normal core flooding can not be used for saturating the pore system. Oil would flow through the fracture and only partially saturate the pore system. Because of this problem, dead oil was used for saturating the pore system in most of the experimental studies reported in literature.

For example in the CO_2 gravity drainage experiments performed by Hujun, Li (2000), the core was saturated by dead oil while the experiment was supposed to be at the reservoir conditions.

Dry gas injection in fractured chalk by Øyno (1995) conducted by saturating the matrix system with live oil, but still their method for initialization of the pore system with live oil is not certain. In their experiment the oil recombination was carried out in the core holder where the matrix and fracture were placed. The oil/gas mixture was circulated in the system and pressure was monitored. Once pressure had stabilized, they assumed that the pore system is saturated with the live oil. In this method, since the pore system was saturated with oil by a very slow diffusion mechanism, the pressure stabilization over a short time interval will not guarantee the homogeneous initialization of the pore system with representative reservoir fluids.

This chapter presents the experimental results obtained during injection of CO_2 into an artificially fractured core which has been initialized with under-saturated live oil. For performing this experiment the core holder assembly was modified and, new methods for the initialization of the matrix and fracture systems with representative reservoir fluids have been developed.

4.2 Experimental set up

In this experiment, the porous medium is a cylindrical chalk core acting as a matrix block which is surrounded by an artificial fracture. The rock and fluid samples which were used in all experiments have been discussed in the previous chapter. The matrix and fracture system initially was designed based on the simulation study that is presented in Appendix A. In this simulation model the porous medium was a cylindrical chalk core which has a concentric hole through the middle of the core acting as an artificial fracture Figure 1 in Appendix A. Because of the weakness of the chalk and collapsing of the core, it was very difficult and sometimes impossible to run the experiments by having the fracture system in the middle of the core.

Therefore the 60 cm long and 46 mm in diameter core was inserted into a steel tube having an inside diameter of 50 mm. Then core was centralized inside the steel tube. The 2 mm annulus space between the outer boundary of the core and the wall of the steel tube was considered as artificial fracture. This configuration of matrix and fracture system prevented any collapsing of the core due to confining pressure and it was better than the first case studied in the Appendix A.

However this arrangement gives a smaller fracture volume compared to the first model and in the case of a high drainage rate the level of the oil in the fracture system may increase and consequently reduce the gravity forces in the experiments.

Therefore in order to find out the best fracture width, another simulation study using the second configuration has been carried out and the 2 mm annulus space between the outer boundary of the core and the wall of the steel tube was considered as best fracture width.

The 2 mm annulus space will create enough fracture volume to prevent any rising of the drained oil level in the fracture and at the same time less live oil will be used later as a displacing agent to clean the fracture system.

This was a criterion for the selection of the optimum fracture width in the performed simulations. The simulation models in this task were similar to the simulation models which were used for history matching of the experiments and will be discussed later in Chapter 5.

As mentioned before one of the most challenging steps in this experiment is to establish representative reservoir oil saturation in the core with CO_2 in the fracture at all reservoir conditions. Existence of the very highly permeable artificial fracture causes oil to flow only in the fracture therefore the establishment of oil in the matrix will be impossible. To resolve this problem, the fracture system was temporarily sealed with very low melting point material (70 ºC) having a high density 9.67 g/cm^3.

The woods metal had no effect on the surface area of the core or on the fluid which later was used for saturating the core. This was checked visually after finishing the experiment and also by measuring the core permeability. The core permeability before and after contacting the core with woods metal was 4 mad. Under this circumstance the artificial fracture filled with sealing material had zero permeability and the core (matrix) had an initial permeability of 4 mD.

Once the fracture system was sealed with woods metals, the core (matrix) can be initialized with proper fluids at a temperature below the melting point of the woods metal. This can be done by using the normal core flooding rig. However some small modifications have been applied on the end pieces of the core holder to facilitate removal of the woods metal from the fracture system after finishing the core initialization.

Figure 4.2 shows the set up that was used for all CO_2 injection experiments. As indicated in the figure the core (matrix) can be initialized with proper fluid saturation through the pink flow-line. In the pink flow-line the core which initially is saturated with brine at 300 bar and 40 ºC is flooded with the live oil and the outlet stream from the core is directed to a back pressure valve where the system pressure is controlled at 300 bar.

A very fine filter of 0.5 micron was installed on the upstream of the core to separate the existing particle in the oil stream and prevent any matrix permeability reduction. The outlet from the back pressure was diverted to a three phase separator working at atmospheric pressure and room temperature. The mass and volume of the liquid phases can be measured on line and the volume of the gas can be measured by the gas collection system.

The gas collection system includes two gas collection tanks in a parallel flow system. In this system one tank is in the filling condition while the other tank is in the evacuation mode. The gas collection system was also designed to monitor and measure the produced gas volume.

Once the desired oil saturation was established in the core, the flow-line system can be changed to the red flow-line system. In the red flow-line system, the outlet from the core

is transferred to a horizontal separator (sealing material separator) initially filled with water. The outlet of this separator is connected to the back pressure valve so that the system pressure can be maintained at the desired pressure.

At this stage the system temperature can be increased to the reservoir temperature 130 ºC. At this temperature the sealing material inside the fracture becomes liquid and can be displaced by the same live oil which was used for core initialization. The woods metal in the fracture then will flow to the separator where it can easily be separated from the oil. In order to be sure that all sealing material is removed from the fracture, 1.2 fracture pore volume of the oil must be injected through the fracture.

After removing the sealing materiel from the fracture system, both the matrix and the fracture system are initialized with live reservoir oil at 130 ºC and the desired pressure which in all experiments this pressure was set at 300 bar.

After removing all sealing material from the fracture, the flow system can again be changed to pink and the sealing material separator can be disconnected from the set up.

At this stage the system is ready to remove the fracture oil by any fluid depending on the injection strategy and the temperature and pressure of the system can be adjusted to the desired conditions.

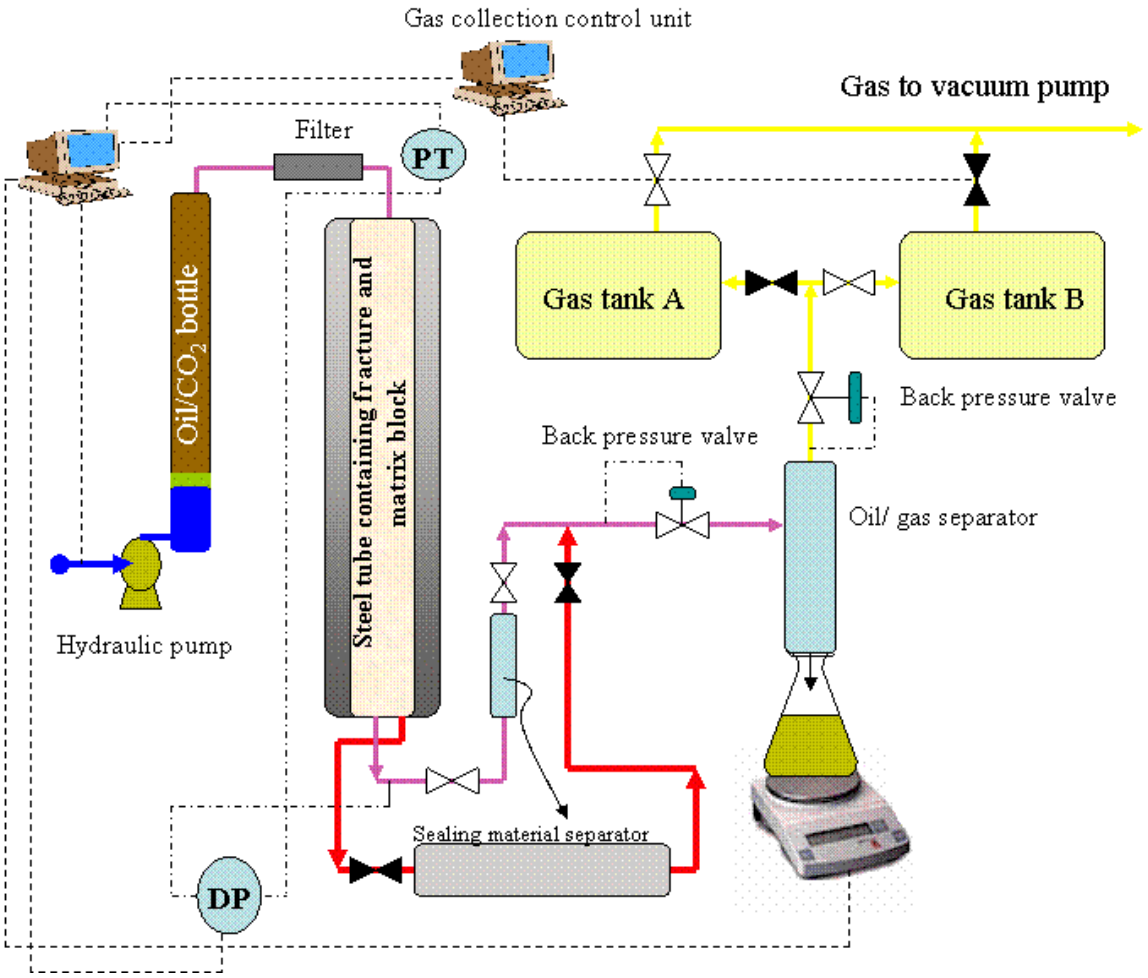

Figure 4.2 Schematic of the set up used for core initialization (red streams), displacement of sealing material from the fracture (pink streams) and CO_2 injection (red streams)

Using the above procedure for core initialization, several CO_2 injection experiments were done at different water saturation level at two temperatures 130 ºC and 60 ºC .The experiments are discussed in the following sections.

4.3 High temperature CO_2 injection experiments

Using the set up described in the previous section, two experiments were conducted at 130 ºC. In the first experiment (Exp1) the CO_2 was injected into the core with zero water saturation while in the second experiment (Exp2) the CO_2 injection was performed with the initial water saturation in the core equal to 26.3%. In both experiments the core was the chalk material was explained in the previous chapter and the depleted reservoir oil with the composition given in Table 3.13 was used. The procedure of core initialization for each experiment was different and is described in the following section.

4.3.1 Core initial water saturation

In the first experiment the steel tube containing the core as described in the previous section was assembled into normal core flooding rig and after complete evacuation of the system, the core was pressurized to 300 bar with mixture of 85 % toluene and 15 % exxsol.

This mixture had a higher density compared to the reservoir fluid and therefore by injecting the oil from the top of the core, a gravity stable miscible displacement was established. The core (matrix) was placed at the vertical position and was flooded from the top with 2 pore volumes of reservoir live oil with a very slow rate.

In the second experiment the steel tube and core was assembled into normal core flooding rig and after complete evacuation of the system it was flooded with brine with composition given in Table 3.30. Then reservoir oil was injected from the top and the produced water was measured. The water saturation of the core after flooding with 1.2 pore volume of oil was 26.3 %.

The core initial conditions before CO_2 injection and after removal of the sealing material, for both experiments are shown in Table 4.1.

Table 4.1 Core initial condition before CO_2 injection

Core initial conditions	Exp1	Exp2
Height, cm	59.7	59.7
Diameter, cm	4.6	4.6
Porosity, (%)	44.4	44.4
Pore volume, cm^3	440.5	440.5
Water saturation, (%)	0	26.3
Pressure, bar	300	300
Temperature, (ºC)	130	130
Initial oil In place, Scm^3	303.6	223.7

Once the core and fracture system were initialized with oil (Table 4.1), the fracture system was flooded with CO_2 to displace the oil inside the fracture system. The fracture oil was displaced with CO_2 with a very high flow rate 5.6 cm^3/min for 30 minutes and then the flow rate of CO_2 was reduced to 0.1 cm^3/min During the CO_2 injection the whole system was placed in a heating cabinet operating at the reservoir temperature of 130 ºC and the injection of CO_2 was continued for several days at a constant pressure and temperature of 300 bar and 130 ºC. The produced fluid at experimental conditions was diverted to a separator working at standard conditions. The composition and mass of produced oil, water and gas were measured and the results for both experiments are

described in the following section. The CO_2 injection rate for Exp2 for the first two days of experiments was a little higher compared to the first experiment. This was due to some miscalculation and it was corrected after two days. The injection rate for Exp2 in this period was 0.12 cm^3/min.

4.3.2 High temperature experimental results

The oil recovery versus time for both experiments is shown in Figure 4.3. This figure shows a rapid oil production rate for the first five days in both experiments.

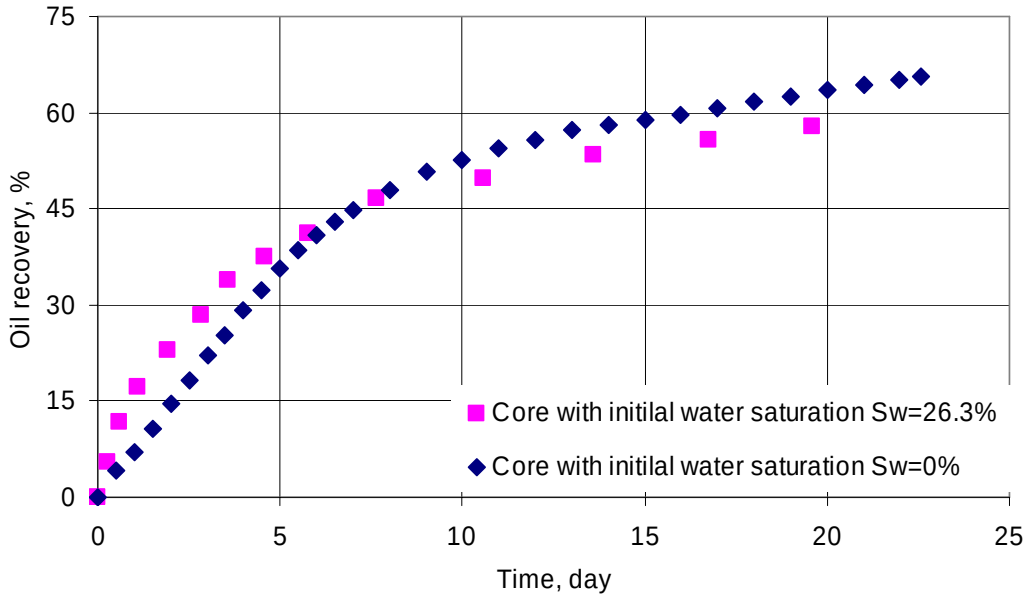

Figure 4.3 The oil recovery versus time at pressure of 300 bar and temperature of 130 ºC for experiments 1 and 2. The initial water saturation in experiments 1 and 2 were zero and 26.3 % respectively.

The oil recovery after 5 days in Exp1 and 2 are 35.6 % and 40 % respectively. In this period in the Exp2 the oil production rate was higher than the first experiment. For both experiments after five days the oil production rate start to decline but the decline rate for the Exp2 was more than Exp1 and eventually after 20 days of CO_2 injection more oil was recovered in Exp1 compared to Exp2.

In experiment 2, the cumulative water production versus time is shown in Figure 4.4. The initial water saturation (irreducible) was 26.3 % corresponding to 116 cm^3 water in the matrix block. This figure clearly shows that after start of the CO_2 injection the irreducible water starts to mobilize and after 19.6 days the water saturation was reduced to 19.5 %.

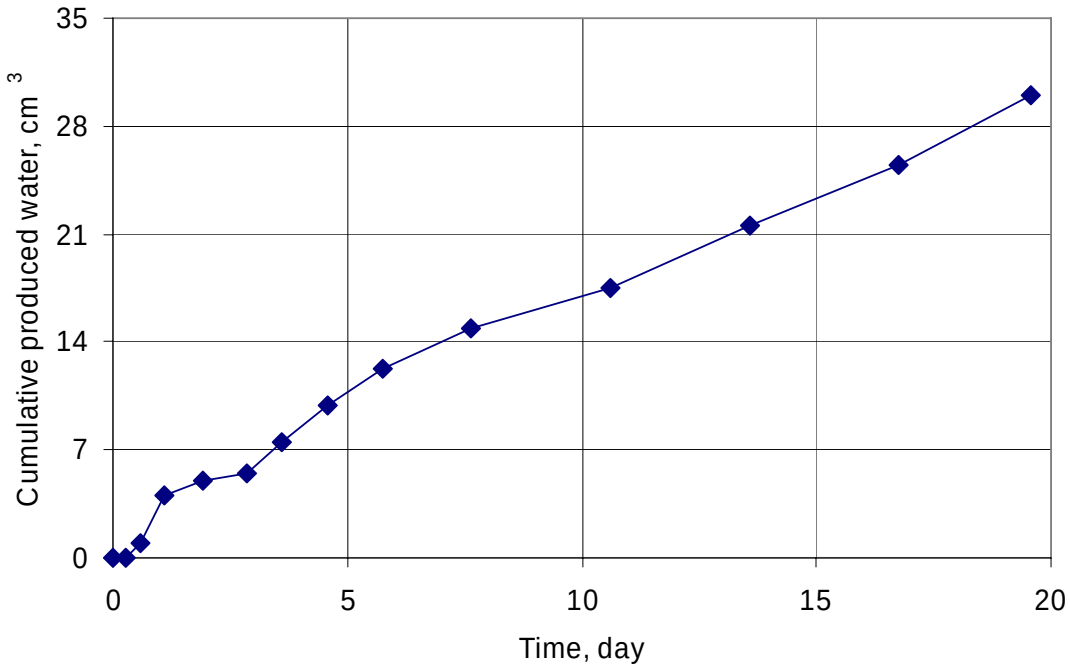

Figure 4.4 The cumulative water production in the Expt2 during CO_2 injection. The core initial water saturation (irreducible) was 26.3 % corresponding to 116 cm^3 water

The molecular weight of produced oil at standard conditions versus time for both Exp1 and Exp2 is presented in Figure 4.5. Also in this figure for comparison, molecular weight of the stack tank oil that was measured during a single flash of reservoir oil is shown at time zero (pink square). This figure clearly indicates that the molecular weight of produced oil for both experiments is changing with time. For Exp1 molecular weight of produced oil initially had a sharp reduction from its initial value of 250 g/gmol to 182 g/gmol followed by gradual increase with a very slop and then increasing with higher rate. But in Exp2, after a sharp reduction of molecular weight at time zero, the produced oil has experienced an almost a constant molecular weight for almost 3 days and then it rapidly started to increase. In the late stage of the experiments, the rate of increase of produced oil molecular weight in Exp2 is much more than Exp1.

Figure 4.6 and Figure 4.7 show the composition of the produced oil at standard conditions. These figures also reveal a variable composition of produced oil in both experiments. Initially produced oil is enriched with a light component and at the late stage the produced oil mostly contains C_{23+}.

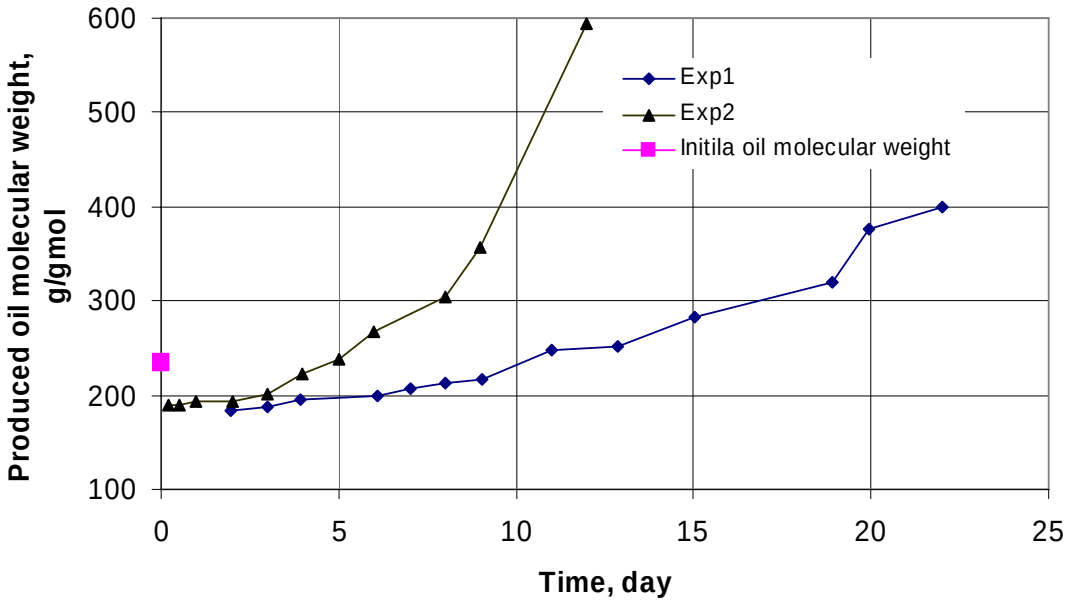

Figure 4.5 *Produced oil molecular weight for Exp1 and 2 versus time. In this figure, time zero value (pink square) belongs to molecular weight of initial stock tank oil taken from single flash experiment of initial reservoir oil.*

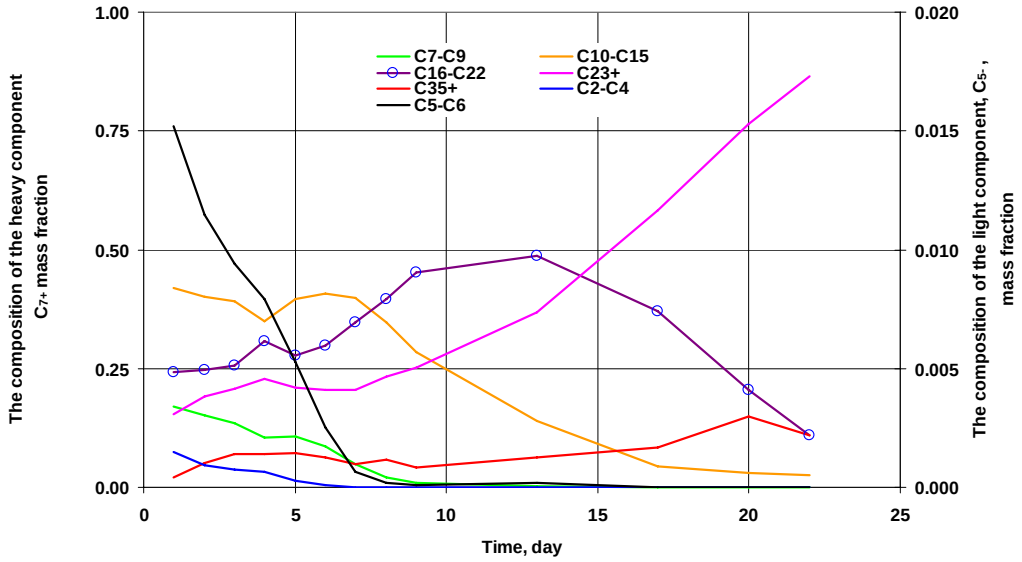

Figure 4.6 *The composition of produced oil at standard conditions for Exp1.*

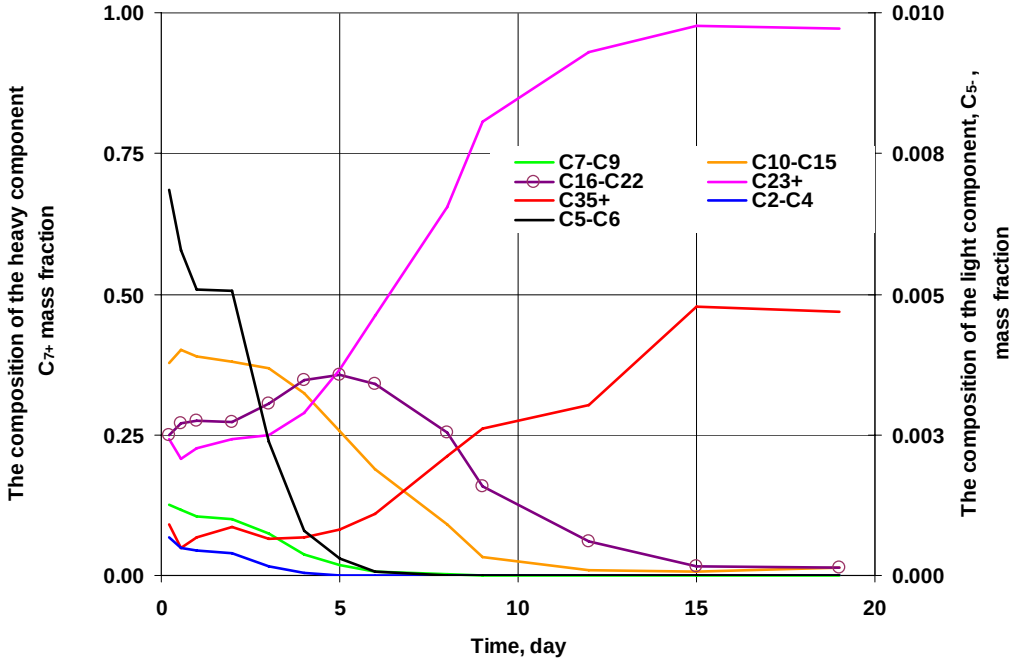

Figure 4.7 The composition of produced oil at standard conditions for Exp2.

For Exp2 the mass fraction of C_{23+} in the tail production period is almost 100 % which is in agreement with the measure molecular of produced oil. From these figures it can be concluded that the light and intermediate components initially have been produced the heavy components in the tail production. This behaviour of produced oil composition with time suggests the domination of diffusion mechanism over the other mechanisms such as gravity drainage

The hydrocarbon produced gas composition at standard conditions as function of time in Exp1 and Exp2 are shown in Figure 4.8 and Figure 4.9 respectively.

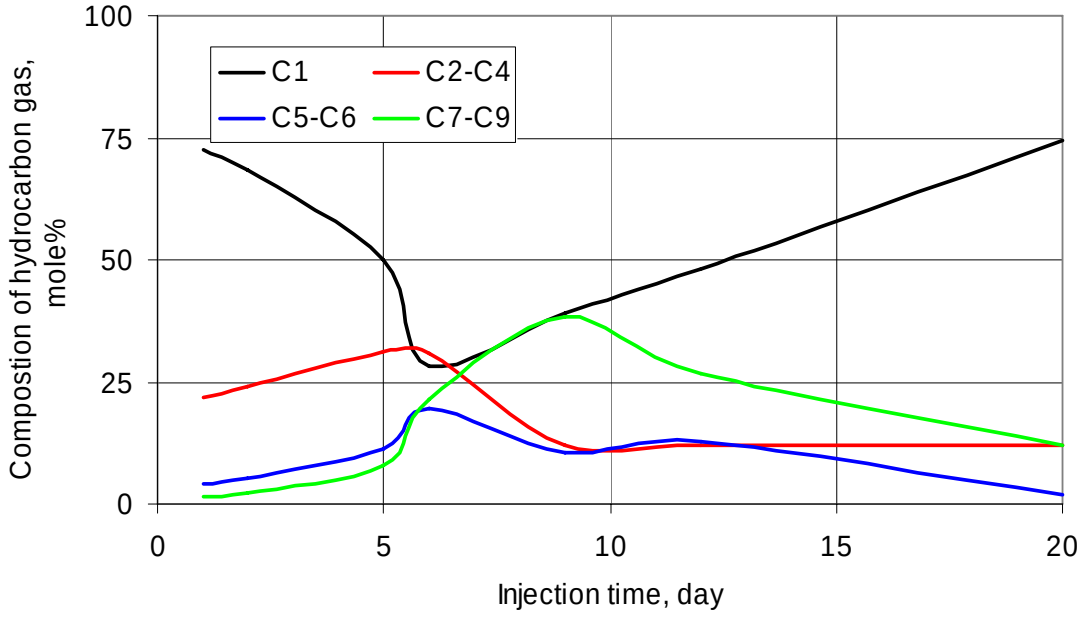

Figure 4.8 *The produced hydrocarbon gas composition versus time measured in Exp1. The produced stream from the experiments was flashed in an atmospheric separator and the composition of the gas from that separator is shown in the figure*

From the above figures it is obvious that hydrocarbon gas composition in both experiments have a similar trend. The produced gas is enriched with methane initially and then it is reduced to a minimum value and again starts to increase. The concentrations of heavy components (C_7-C_9) initially are low and then at the late stage their concentrations are increased. The intermediate components initially have a low concentration, and then their concentration increases to maximum and it start to reduce in the late stages. In the above figures the given compositions are calculated based on no CO_2 in the outlet gas stream. The total compositions of the gas stream including CO_2 for each experiment are given in Table 4.2 and Table 4.3.

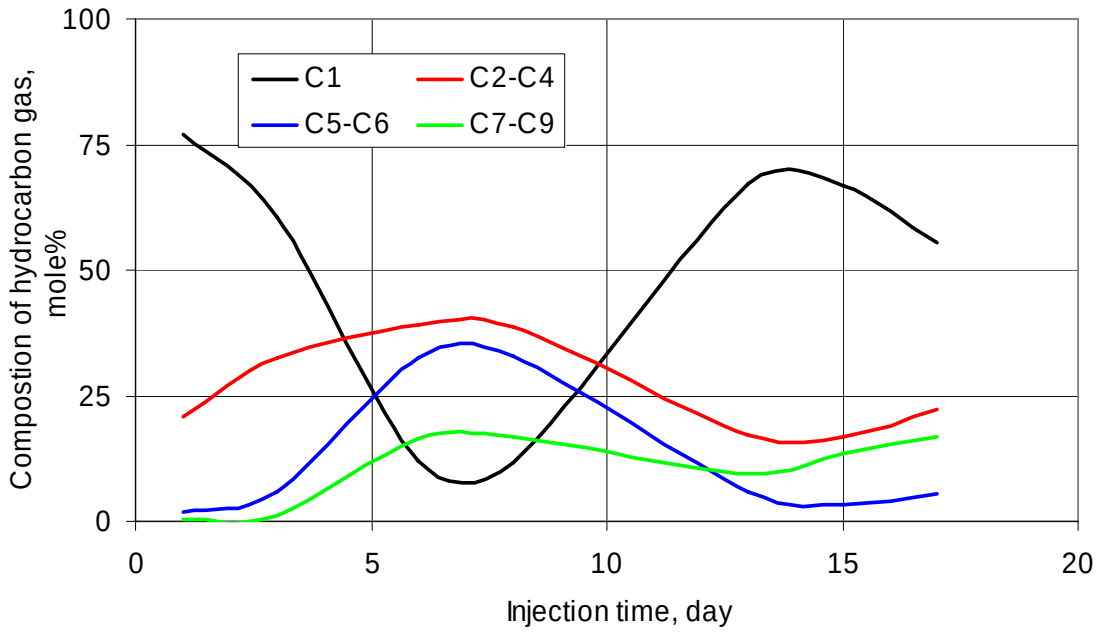

Figure 4.9 *The produced hydrocarbon gas composition versus time measured in Exp2. The produced stream from the experiments was flashed in an atmospheric separator and the composition of the gas from that separator is shown in the figure*

Table 4.2 *The outlet gas composition from atmospheric separator for Exp1.*

Day	1	2	5	6	9	12	20
Comp	mol%	mol%	mol%	mol%	mol%	mol%	mol%
CO_2	80.6981	87.2258	98.1519	99.642	99.9762	99.9883	99.994
C_1	14.0132	8.7181	0.9224	0.101	0.0093	0.0056	0.0044
C_2-C_4	4.1991	3.0775	0.5768	0.1097	0.0029	0.0014	0.0007
C_5-C_6	0.7847	0.6745	0.2062	0.0706	0.0025	0.0015	0.0001
C_7-C_9	0.3047	0.3041	0.1426	0.0766	0.0091	0.0031	0.0007
Total	100	100	100	100	100	100	100

Table 4.3 The outlet gas composition from atmospheric separator for Exp2

Day	1	3	6	8	13	15	17
Comp	mol%	mol%	mol%	mol%	mol%	mol%	mol%
CO_2	97.2987	98.7247	99.9823	99.9845	99.9947	99.9971	99.9728
C_1	2.085	0.7711	0.0021	0.0018	0.0035	0.002	0.001
C_2-C_4	0.5585	0.4135	0.0069	0.006	0.0009	0.0005	0.0004
C_5-C_6	0.0526	0.0753	0.0057	0.0051	0.0003	0.0001	0.0001
C_7-C_9	0.0053	0.0153	0.0029	0.0026	0.0005	0.0004	0.0003
Total	100	100	100	100	100	100	100

The higher CO_2 concentration in the Exp2 at the early stage was due to higher CO_2 injection rate compared to Exp1.

Material balance

After finishing the experiments, the pressure in the system gradually has been reduced from 300 bar to atmospheric pressure. During depletion period the mass of the produced oil at standard conditions was measured. Residual oil left in the core was recovered by using the distillation extraction method (Soxhlet apparatus). Dichloromethane CH_2Cl_2 was used in the Soxhlet apparatus as extractor solvent. The boiling point of dichloromethane CH_2Cl_2 is 40 ºC therefore the chance for losing any light component from the core was very low. Table 4.4 shows the material balance for both experiments. In this table, the weight of initial oil in place at standard conditions was calculated by:

$$m_{oil}^{s} = \frac{\rho_{oil}^{s}.(1-S_{wi}).V_{pv}}{B_o}$$

where:

m_{oil}^{s} The initial weight of the oil in the core at standard conditions, g

ρ_{oil}^{s} The oil density at standard conditions, g/cm^3

V_{pv} The pore volume of the core, cm^3

S_{wi} Initial water saturation of the core

B_o Oil formation volume factor measured at 130 ºC and 300 bar

For the first experiment (Exp1) the initial water saturation was zero, the weight of residual oil left in the core was measured by subtracting the weight of the core before and after cleaning.

For the second experiment (Exp2) the initial water saturation in the core was 26.3 % corresponding to 116 cm^3 (126.44 g). The total weight of the produced water during CO_2 injection and depletion of the core was 32.71 g. Using the water mass balance, the mass of the oil left in the core was calculated by measuring the weight of the core before and after cleaning.

Table 4.4 The material balance of the oil at standard conditions. The residual oil in the core was recovered by distillation extraction method (Soxhlet apparatus)

Exp	Weight of oil at standard condition inside the core	Weight of produced oil during CO_2 injection	Weight of produced oil during depletion	Weight of recovered residual oil	Error	Recovery
	g	g	g	g	%	%
1	259.2	170.3	4	78.4	2.5	65.7
2	192.5	111.4	0	76.6	2.4	57.9

4.3.3 Discussion

Diffusion drive production mechanism

The composition and molecular weight of the produced oil and gas in both experiments were changing with time. At the early stage the produced oil was enriched with light and intermediate components while at the late stage the heavy components have been produced. The variable composition of the produced oil is suggesting the domination of the diffusion mechanism.

The gravity drainage production mechanism can be interpreted as a phase movement in prose media and therefore the composition of the produced oil can be almost constant assuming constant injection rate. In this mechanism the density difference between gas and oil acts as a driving force to move the oil phase in the downward direction (assuming oil phase is heavier than the gas phase). Once the oil finds its way to the fracture network, it quickly evaporates in the gas phase which is flowing in the fracture system. With a constant production and injection rate (constant system pressure), the composition of the produced fluids will be constant.

In tight porous media such as chalk reservoirs with a matrix permeability of 3-4 mD, and very low gravity driving force between gas and oil phases in the matrix and fracture system and a high gas-oil interfacial tension the movement of the individual phases in the porous media is extremely difficult and sometimes is impossible. In this circumstance,

the transport of the components from the matrix blocks to the fracture system occurs through the diffusion mechanism. The driving force for transport in this mechanism is the concentration gradient of individual component and diffusivity of each component. The variable composition of produced oil in all experiments is something that is very interesting in terms of the oil recovery (up stream) and also down stream evaluation of the processing facilities. Therefore proper modelling of the oil recovery in this system where the produced oil has been experienced a very large compositional variation has to be developed.

The effect of water saturation (water bridge effect)

In the second experiment (Exp2), initial water saturation in the core was around 26.3 %. From the experimental results it is obvious that in the Exp2 at the early stage of CO_2 injection, the oil production rate was higher than the first experiment (Exp1) where there was no water in the core. This was reversed at the late stage and the oil production rate in the first experiment was higher than in the second experiment. The ultimate recovery in the case of no water in the core was almost 10 % more in Exp2.

The initial water saturation normally resides between the solid surface and oil phase as a thin film or is retained at the corners of the pores. In this case because of high solubility of CO_2 in water, the water film around the oil droplet will be quickly saturated with CO_2. Then due to the high concentration gradient of CO_2 between the water and the oil phase, the CO_2 is transported to oil through the liquid-liquid diffusion mechanism.

This causes swelling of oil and consequently expelling of the oil phase out of the matrix. Therefore due to the water bridge effect, at the early stage the oil production rate was higher in Exp2 compared to Exp1. In this case because of swelling production mechanism, the molecular weight of produced oil in Exp2 should be slightly higher than the produced oil in Exp1 at the very early stage and the produced oil will be enriched with more heavy components . This also was observed in Figure 4.5 and also can be seen by comparing the concentration of heavy components in both experiments Figure 4.10.

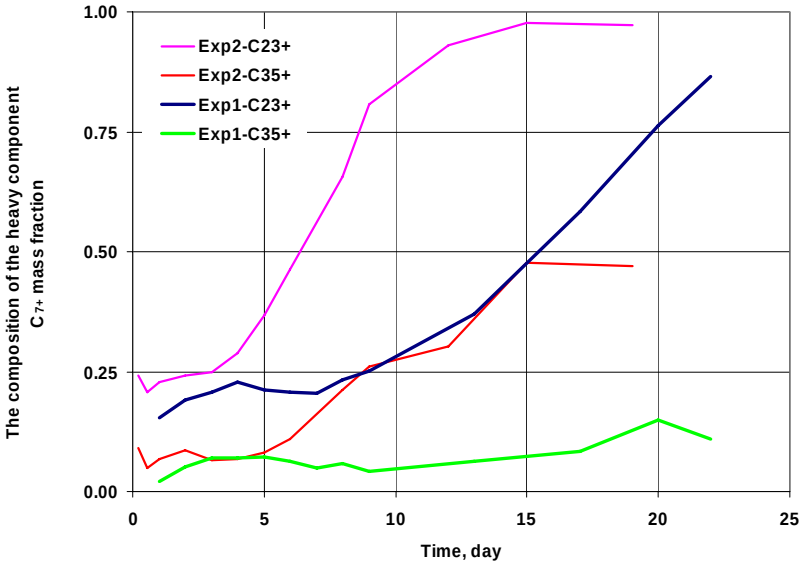

Figure 4.10 The concentration of heavy components versus time in Exp2 and Exp1 (concentrations are in the mass fraction)

Figure 4.10 clearly shows that the concentration of heavy components in Exp2 is higher than Exp1. This also was noticed by comparing the produced oil colours at the early stage of both experiments. The colour of produced oil at the early stage in Exp2 was black while in Exp1 it was light yellow.

The tail oil composition and oil production rate in Exp2 is very interesting. In this period the produced oil contains mainly C_{23+} and the produced oil is much heavier than the produced oil in Exp1. Comparing the tail production data in both experiments, it is obvious that the existence of water in the system reduced the ultimate oil recovery of the core and at the same time the produced oil was very heavy compared to the no water case.

How water has such an effect on the tail production is not clear at the moment and it must be investigated by compositional simulation of the experiments. Any simulation task in this respect must take into account the solubility of CO_2 in the water as well as the correct diffusion calculation in the three phase regions.

4.4 Tertiary CO_2 injection experiment

The reservoir under study in the North Sea is a fractured chalk reservoir producing from depths between 2900 and 3000 metres subsea. The predominant primary recovery mechanism was solution-gas drive and then the reservoirs have been extensively water flooded. Expected recoveries after water flood range from 30 to 45 percent of the original oil-in-place (OOIP). In the water flooded area the initial reservoir temperature is reduced from its initial value of 130 ºC to 60 ºC.

The reservoir pressure after water injection has been increased to 300 bar which is higher than the minimum miscibility pressure (MMP) 242 bar for CO_2. For this reservoir CO_2

injection could be the one with the greatest EOR potential since the reservoir temperature has been reduced and the reservoir pressure is above the MMP. Low reservoir temperature in the water flooded area increases the solubility of CO_2 in the oil and consequently oil swelling can be one of the major oil recovery mechanisms. The swelled oil easily expelled out from the matrix and it flowed to fracture system and production wells.

Using the experimental set up which was explained in the previous section the efficiency of tertiary CO_2 injection at reservoir conditions into fractured cores has been investigated experimentally. The experiment (Exp3) was designed to illustrate the process of water imbibition and CO_2 injection into a North Sea chalk reservoir.

Experimental results have shown that water injection proved to be an efficient method to recover oil from a water-wet low permeable chalk core. The oil recovery by water injection was 54 % of oil initially in place.

In this rock fluid system CO_2 injection could be considered as an effective EOR method for targeting the residual oil after water injection. The overall oil recovery was increased by 15 % of original oil in place. However, at the early stage of CO_2 injection, water production was much higher than the oil production

The full description of the experimental procedures, the results and conclusions for the tertiary CO_2 injection in Exp3 has been published as SPE paper 99649 and is presented in Appendix C.

4.5 Conclusion

The CO_2 injection experiment at the reservoir conditions has been performed under different water saturation. The rock and fluids used in the experiment were similar and analogous to rock and fluid from one of the North Sea chalk fractured reservoirs. The production data are showing a very high EOR potential in the case of CO_2 injection. The produced oil was experiencing a variable composition with time.

In Exp1 and Exp2, the variable produced oil compositions demonstrate the existence of the component movement rather than the phase movement. The light characteristic of produced oil at the early stage of the experiments shows that the light components have been produced first and the heavy components at the late stage.

In Exp2, the presence of water initially was causing a higher oil production rate. This was due to more effective means of transport of CO_2 into the oil phase. In this case because of the high solubility of CO_2 in water, the water film around the oil droplet will be quickly saturated with CO_2. Then due to the high concentration gradient of CO_2 between the water and the oil phase, more CO_2 is transported to oil through the liquid-liquid diffusion mechanism and consequently will be swelled and expelled out of the matrix at a higher rate.

In Exp3, the high initial water production rate was due to the high water saturation in the core as well as high water mobility. The mechanism by which the water was produced from the core was mainly water/CO_2 gravity drainage which was enhanced by swelling

oil. The injected CO_2 had a strong swelling effect on the oil at 60ºC and consequently it caused displacement of both oil and water from the matrix. Due to high water saturation, and also the higher density difference between water/CO_2 compared with oil/CO_2, the water production rate was higher than the oil production rate at the early stage of Exp3.

The strong compositional behaviour of produced oil in all experiments and its dependence on the domination of the diffusion mechanism must be considered in any EOR assessment which considers CO_2 as injection fluid.

The full description of the experimental procedures, the results and conclusions for Exp1 and Exp3 have been published as papers SPE 99650, SPE 99649 and are presented in Appendix B and Appendix C.

4.6 Reffrences

1) Hoteit H. and Firoozabadi A., "Numerical Modeling of Diffusion in Fractured Media for Gas Injection and Recycling Schemes ", SPE 103292, Sep 2006, Texas USA.
2) Hujun, Li. "Experimental Investigation of CO_2 Gravity Drainage in a Fractured System," paper SPE 64510 presented at the SPE Asia Pacific Oil and Gas Conference and Exhibition held in Brisbane, Australia, 16–18 October 2000
3) Moritis, G. "EOR Continues to Unlock the Oil Resources", Oil & Gas Journal, pp. 45-52, April 12, 2004.
4) Øyno, L, Uleberg K., Whitson C.H. "Dry Gas Injection in Fractured Chalk Reservoirs- an Experimental Approach", paper SCA1995-27 presented at the International Symposium of the Society of Core Analysts held in San Francisco California(1995)

5. Compositional simulation of the experiment

In order to study the recovery mechanism involved in the CO_2 injection experiments described in Chapter 4, these experiments must be simulated with a fully implicit compositional simulator that accounts for molecular diffusion and dynamic interfacial tension scaled capillary pressure.

For this simulation study, the compositional simulator Eclipse 300 (2004a1), and a two dimensional radial grid was used. The detail model description and the simulation results are discussed in the next section. The numerical design of the first experiment, in which the fracture system was considered in the middle of the core, also is explained in Appendix A.

5.1 Simulation of the two-phase experiment at 130 ºC

The first CO_2 injection experiment (Exp1), in which the initial water saturation in the core was zero, has been simulated. In this simulation model, a single matrix block surrounded by fractures was used to study the matrix-fracture component exchange. A two-dimensional radial grid 15x1x50 was used. Two equilibrium regions were defined: (1) the core with 10 grid blocks in a radial direction and (2) the last five outer radial grid cells corresponding to the surrounding fracture volume. In the vertical direction the core (matrix) was subdivided into 46 grid cells, two grid cells for the top and two grids for bottom fractures.

The fracture cells were assigned zero capillary pressure and straight-line relative permeabilities with zero endpoint saturations. Core region capillary pressure and relative permeability curves were taken from Uleberg (2002) these data were generated from Corey-type equation based on model parameters from relevant North Sea core data given in Appendix B.

Gas-oil capillary pressures in the model were scaled linearly with gas-oil IFT, where σ_{go} is calculated for each grid cell in the model using the parachor method. All pVT calculations were made using a 14-component pseudoized EOS characterization which was explained in Section 3.4.1. The gas and oil diffusion coefficients (D_{oi} and D_{gi}) for each component were calculated using the extended Sigmund correlation (Da Silva. 1989) and the value for each component can be found in Appendix B, Table 5.

5.1.1 Simulation model verification

In order to check the accuracy of the simulation model, the calculated oil recovery by analytical solution which was discussed in Section 2.6 is compared to the simulation results. For simplicity, it is assumed that there is no capillary pressure and no diffusion in the model that is corresponding to a pure gravity drainage mechanism. The analytical oil recovery for the core (single matrix block) was calculated by using Eq. 2-48 in which the Corey exponent is n = 3.8. In this equation the rock and fluid properties are given in Table 5.1.

Figure 5.1 shows the analytical solution (red) and simulation results (blue circle) for case where there is no gas-oil capillary pressure and no diffusion in the system. This figure shows that the simulation results and analytical solution are almost in good agreement. The mis-match between these two cases can be due to numerical dispersion and also the fluid properties calculated in the simulation model. In analytical solution the fluid properties are assumed to be constant, while in the numerical model, the fluid properties are calculated based on the component exchange in the front. For example the viscosity of the oil initially was calculated around 0.8 cp, but as CO_2 starts to dissolve into the oil the calculated viscosity was around 0.5 cp. Lower oil viscosity gave higher oil mobility and consequently more oil recovery. This behaviour was captured neatly in the simulation model. This means that higher oil recovery for lower viscosity compared to the analytical solution when the value of viscosity was set to the 0.8 cp. In Figure 5.1 the analytical solution for two oil viscosities of 0.8 cp and 0.6 cp are compared with numerical results.

Table 5.1 Rock and fluid properties for analytical solution of gravity drainage using Eq. 2-48

Porosity	44	%
Matrix permeability, k_m	4	mD
Oil viscosity at p=300 bar and T=130 ºC	0.8	cp
Oil density at p=300 bar and T=130 ºC	674.	kg/m^3
CO_2 density at p=300 bar and T=130 ºC	526	kg/m^3
Block height, H	0.6	m

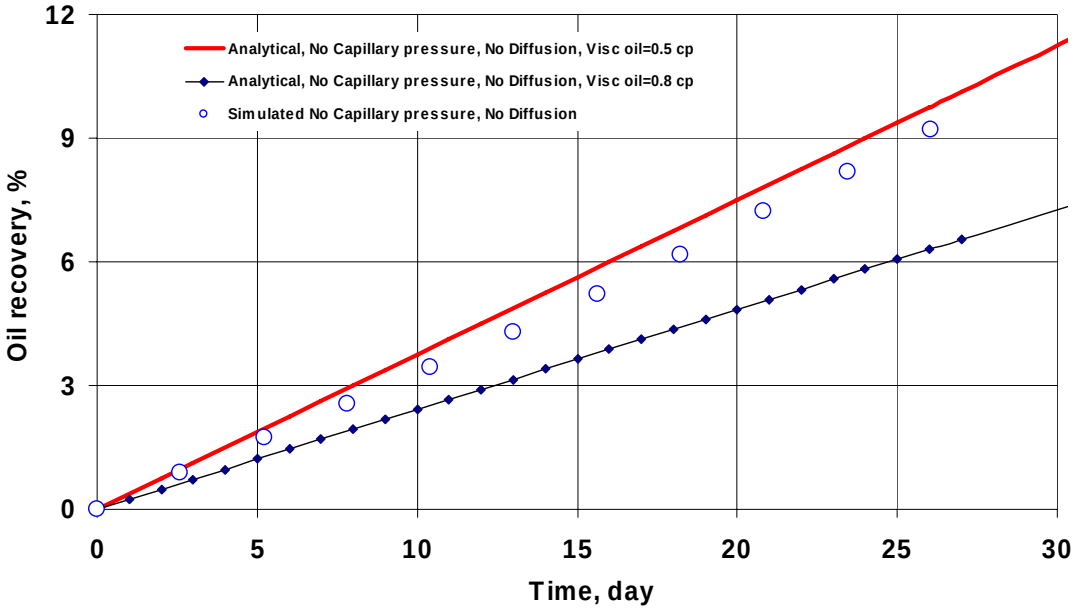

Figure 5.1 *Analytical and simulated CO_2 injection experiment assuming no capillary pressure and diffusion. Simulation was performed using a two-dimensional radial model and for the analytical solution Eq. 2-48 was used*

5.1.2 History matching of the two phase experiment

Using the model described in the previous section, the first experiment was simulated with the same boundary conditions as the experiment. The injection well was completed at the top of the core. This well was controlled by constant CO_2 injection rate 0.3 cm^3/min. The production well was completed at the bottom of the core and it was controlled by constant bottom hole pressure of 300 bar. The initial water saturation in the core was set to zero. Figure 5.3 shows the simulation results compared with the experimental data. This figure shows a very low oil recovery for the simulated case compared to experimental data. This mismatch can be due to:

- Incorrect gas-oil capillary pressure data
- Incorrect diffusion calculation

The effect of the above parameters was examined by performing sensitivity analysis by changing the capillary pressure curve and using different diffusion coefficients, the results are described below.

Effect of gas-oil capillary pressure

Core region capillary pressure data were taken from Uleberg (2002) these data were generated from Corey-type equation based on model parameters from relevant North Sea core data (Appendix B). The capillary threshold height of 62 cm as indicated in Figure

5.2 can not start any gravity drainage since the threshold height is greater than the block height in the experiment. Therefore these data were normalized with a very sharp slope to allow the injected CO_2 to enter into the core.

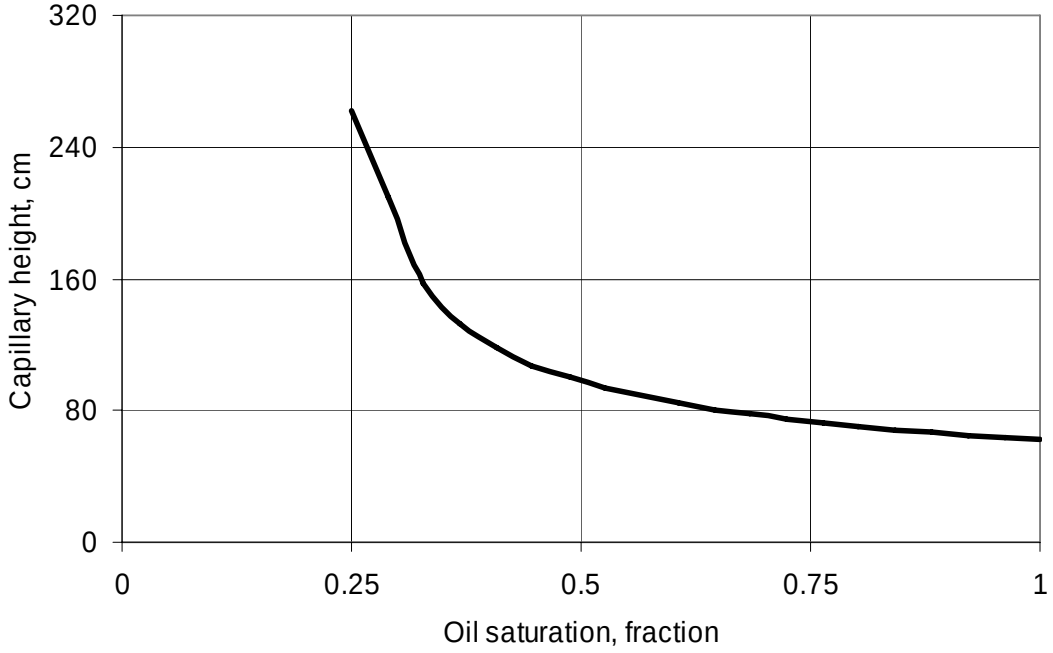

Figure 5.2 Core region capillary pressure curve was taken from Uleberg (2002, reference interfacial tension σ_{ref}=0.05 dynes/cm)

The low simulated recovery shown in Figure 5.3 can be due to incorrect capillary pressure data. This means for a small matrix block (60 cm) and a very high capillary threshold height of 62 cm in the model, the drainage is almost impossible and therefore the simulated results can be far from the actual experimental results.

In order to check the effect of the capillary pressure (surface tension), the case with the capillary pressure given in Figure 5.2 is compared with a case in which there was no capillary pressure in the model. The results of simulation are shown in Figure 5.3. This figure shows that even with no capillary pressure (zero threshold height and purely gravity drainage), the simulated oil recovery is far from the experimental results.

The variable composition of the produced oil during the experiment (Exp1) suggests that the oil was produced due to a diffusion mechanism rather than gravity drainage. The gravity drainage mechanism is somehow a phase movement, in which the oil or gas phases in the matrix block are moving downwards and consequently one should expect a constant composition of the produced oil, while in the experiment the produced oil was subjected to very strong compositional changes which was due to component movement and the diffusion mechanism. Therefore the mismatch between the simulated oil recovery and the experimental data should be due to the calculation of the diffusion in the model.

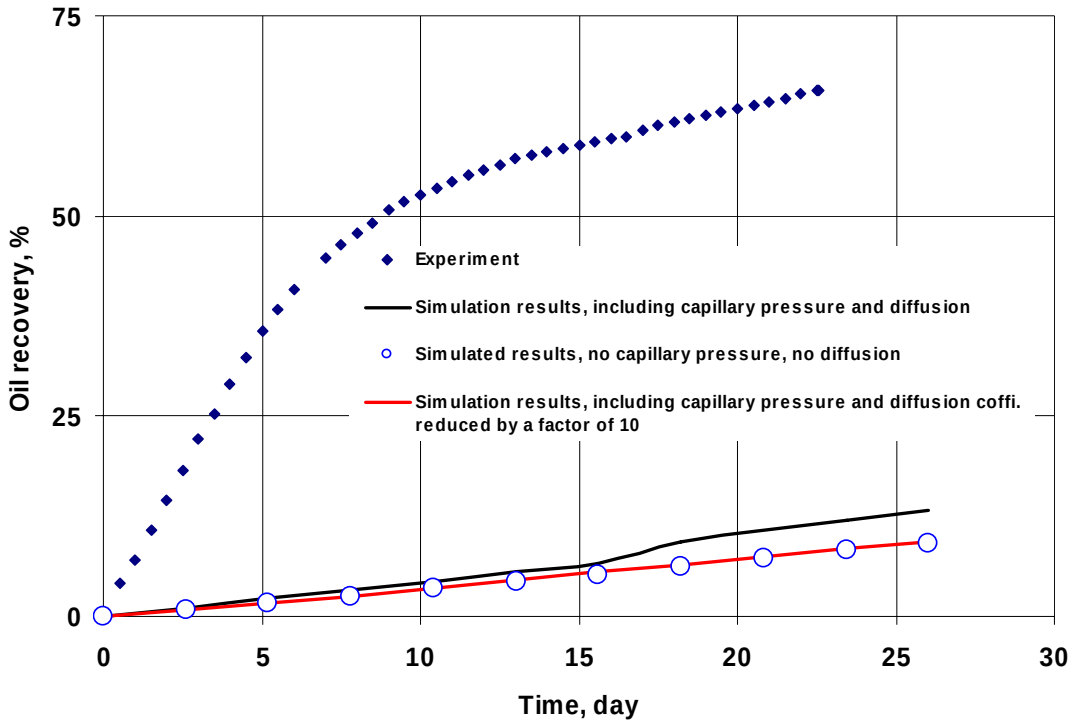

Figure 5.3 The simulation results for CO_2 injection experiment at 130 ºC compared to experimental results from Exp1

The effect of diffusion

The simulation results including diffusion option showed a very low oil recovery which is very far from the experimental results. The low simulated oil recovery in the case of having diffusion in the model might be due to:

- Incorrect oil and gas diffusion coefficient which was used in the simulation model
- Incorrect formulation regarding diffusion calculations in the software

In order to check the simulation performance with respect to the gas and oil diffusion coefficients, these coefficients were reduced by a factor of 10 and the results are compared with case where the diffusion coefficients were originally calculated from the Sigmund correlation (Da Silva 1989) (black and red results in Figure 5.3)

This comparison shows that the simulated results are not as sensitive to diffusion coefficients and a very small decrease in oil recovery was observed due to the reduction of these coefficients.

Therefore it was decided to check the diffusion calculation in the software by using a very simple one-dimensional model which is shown in Figure 5.4.

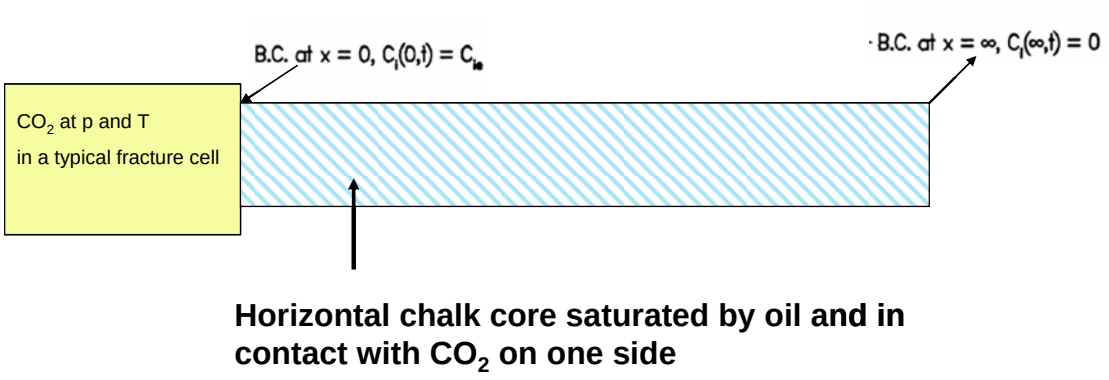

Figure 5.4 Schematic of transport process modelled by Eq. 5-1

In this model the oil-CO_2 interface is located at x = 0, while at the other end of the core x = ∞, the core initially was saturated with oil. At the interface x = 0 interfacial resistance to transport of CO_2 into liquid phase also is assumed to be negligible (no capillary pressure). To simplify the analysis further, the diffusion coefficients are assumed to be constant.

In this case, the change of concentration of CO_2 along the core in each time, can be calculated by using Fick's second law (Eq. 5-1) which was discussed in Section 2.10.1.The solution for Fick's second law when the area of diffusion is constant and two fluids have not any movement was presented in the form of Eq. 5-1 (Crank, 1975) with the initial and boundary conditions as shown in Figure 5.4

$$c_{CO_2} = \frac{1}{2}\left[1 \pm erf\left(\frac{z}{2\sqrt{D_{CO_2} t}}\right)\right] \quad \text{.....5-1}$$

The analytical and numerical solution for the concentration of CO_2 after 2000 days is shown in Figure 5.5.

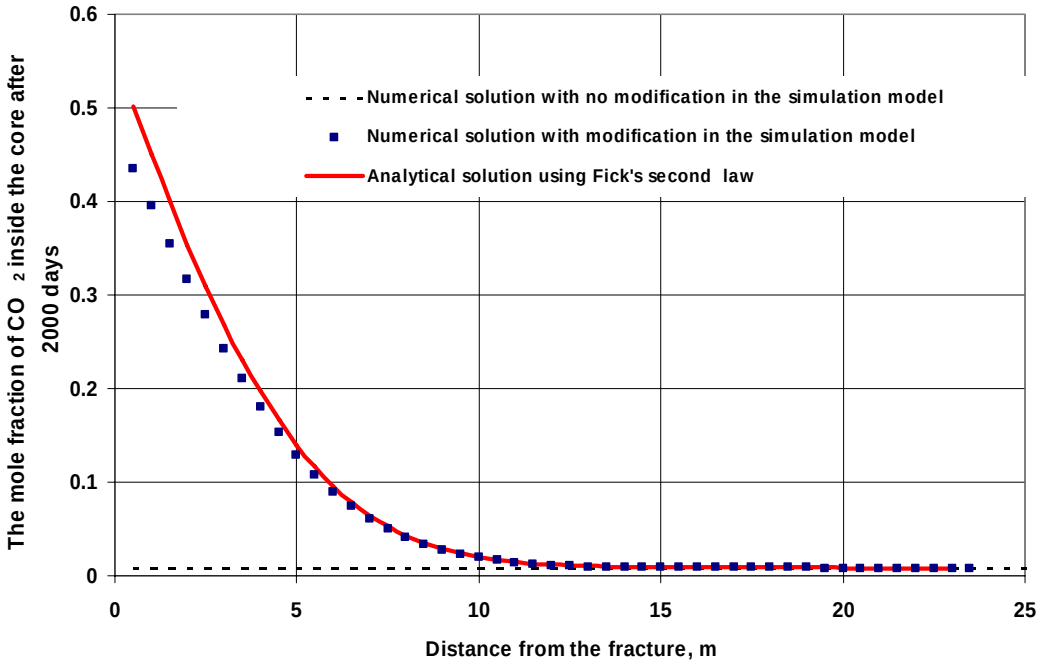

Figure 5.5 *The one-dimensional concentration change of CO_2 by molecular diffusion after 2000 days calculated by Eq. 2-2 and is compared with the numerical simulation of the same process for two different cases in which in one case the simulation model was modified with a grid cell initially was initialized with two phases in which in its liquid phase, the initial mole fraction of CO_2 was 0.5. In the other case the simulation model was not modified.*

Based on the analytical solution given in Figure 5.5 after 2000 days the concentration of CO_2 in the core at interface ($x = 0^+$) has been increased from 0.08 to 0.5 while by numerical solution this was constant. This unrealistic behaviour of the simulator also has been noticed in Figure 5.3 since the predicated oil recovery was very far below the actual oil recovery. Therefore considering both numerical results and also the analytical solution for this simple case, it is obvious that Eclips300 can not correctly calculate matrix-fracture component exchange by the diffusion mechanism.

Based on Eclips300 technical manual (2004a), for any two cells, the diffusive flow is proportional to the cross-sectional area between the cells, and inversely proportional to the distance between them. Integrating the flux and approximating the gradients between two grid blocks using differences, the diffusive flow between blocks is in the form of Eq. 5-3

$$F_i^{diff} = F_{io}^{diff} + F_{ig}^{diff} \quad 5\text{-}3$$

where:

$$F_{io}^{diff} = T_D D_{io} \left(S_o b_o^m\right)_u \Delta x_i$$
$$F_{ig}^{diff} = T_D D_{io} \left(S_g b_g^m\right)_u \Delta y_i \quad \text{.....5-4}$$

and (x_i, y_i) is the liquid and vapour mole fractions of component i respectively, $T_D = \phi A d^{-1}$ is the diffusivity, and $\left(b_o^m, b_g^m\right)$ is molar formation factors. The subscript u indicates that the values are evaluated upstream. The upstream evaluation of $\left(S_o b_o^m\right)_u$ and $\left(S_g b_g^m\right)_u$ give two major problems regarding diffusion calculations:

1. Strange results for strongly varying $S_o = 1 - S_g$ between neighbouring grid blocks. More correctly the delta should include more terms as indicated in

   $\Delta\left(\phi S_o b_o^m x_i\right), \quad \Delta\left(\phi S_g b_g^m y_i\right)$ .....5-5.

2. How is x_i determined in the gas phase and y_i in the oil phase? If these values are "arbitrary" the diffusive flows will be erroneous.

The upstream evaluation of this term is the major problem in the calculation of diffusion in Eclips300 and it should be modified by a better method.

In order to examine the existing problem in the software (Eclipse300), the previous simple one dimensional model was shown in Figure 5.4 was modified. This was done by introducing a two phase grid cell between the interface of oil and CO_2 as shown in Figure 5.6. In the two phase cell, the liquid phase has a very high CO_2 concentration which allows the CO_2 transport to the core from the two phase cell by a liquid-liquid diffusion process.

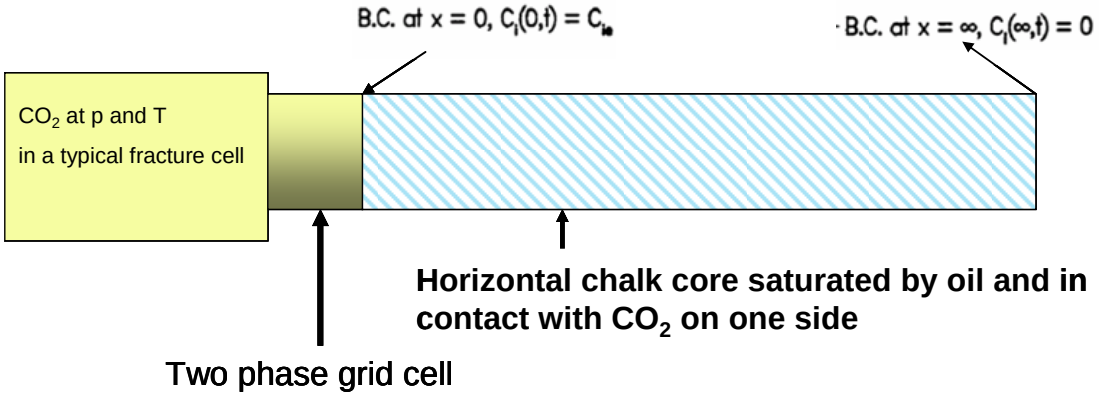

Figure 5.6 The modified simulation model to initiate the diffusion mechanism by introducing a two phase grid cell between CO_2 in the cell of the fracture and cells in the core saturated by oil

The simulation results for the modified model are compared with the analytical solution and shown in Figure 5.5. This figure clearly indicates that the analytical solution and simulated concentration of CO_2 along the core are in good agreement which confirms the

existing problem in the diffusion calculation in the software. As mentioned before, CO_2 is transported to the core through liquid-liquid diffusion and the two phase cell acts as a bridge.

Considering the above results and the weakness of Eclips300 for calculating cross phase diffusion, the simulation model used for history matching of the first experiment (Exp1) was modified by adding a two phase layer between the core and the surrounding fracture as shown in Figure 5.7.

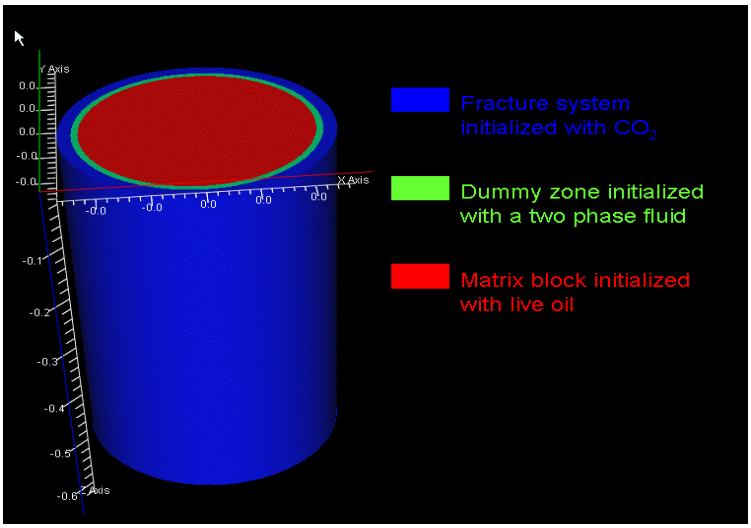

Figure 5.7 Modified simulation model used for history matching of the first two phase experiment (Exp1)

The sensitivity of the oil recovery with respect to concentration of CO_2 in the dummy zone (two phase grid cells) has been performed, and the results are shown in simulation part of Appendix B. The introduction of the two phase dummy zone around the core in the simulation model showed improvement in the simulation results. However since the numerical solution in the case of dummy zone are dependent on the size and the type of fluid in the dummy region, this method can not be a perfect solution to use for any predication scenario and the formulations in the software must be modified

5.2 Conclusions

Simulation and analytical solution (assuming no diffusion) for Exp1 show that even applying a zero capillary pressure between CO_2 and oil, the recovery performance is very far from the experimental results. By applying the diffusion option in the simulation model, it was possible to mach the experimental results. This proves the importance of diffusion as one of the important displacement mechanisms which causes the transport of components based on their diffusivities from a tight matrix to a fracture network.

Comparing the simulation and experimental results, diffusion in a fractured reservoir with very high fracture intensity, can be one of the main recovery mechanisms and it must be taken into account significantly in any CO_2 injection. Its high performance to recover oil

from the matrix system, similar to gravity drainage, results in a high EOR potential which have to be correctly modelled in any field scale modelling.

Simulation results also confirm the need of a consistent model to incorporate physical diffusion of multi component mixtures in a CO_2 injection schemes in fractured reservoirs. Diffusion calculations using the current simulation models such as Eclipse300 (2004a), are based on inconsistent upstream formulation of gas to gas and liquid to liquid component transport in both fracture and matrix domains. Simulations results have shown that, this incorrect formulation is not able to calculate the complex component exchange involved in the dominant diffusion mechanisms and result in very low underestimation of oil recovery.

5.3 References

1) Crank, J. (1975). Mathematics of diffusion. 2nd edition, Clarendon Press, Oxford

2) Eclips300 technical manual (2004a)

3) Silva Da., F.V. and Belery, P. ”Molecular Diffusion in Naturally Fractured Reservoirs: A Decisive Recovery Mechanism”, paper SPE 19672 presented at the 1989 Annual Technical Conference and Exhibition, San Antonio, TX, Oct 8-11

4) Uleberg, K, and Høier, L. “Miscible Gas Injection in Fractured Reservoirs”, paper SPE 75136 presented at the SPE/DOE Thirteenth Symposium on Improved Oil Recovery held in Tulsa, Oklahoma, USA (2002).

Appendix A: Numerical simulations for designing oil/CO_2 gravity drainage laboratory experiments of a naturally fractured reservoir

NUMERICAL SIMULATIONS FOR DESIGNING OIL/CO_2 GRAVITY DRAINAGE LABORATORY EXPERIMENTS OF A NATURALLY FRACTURED RESERVOIR

Gholam Reza Darvish[1], Erik Lindeberg[2] , Jon Kleppe[1], and Ole Torsæter [1]

[1)] Norwegian University of Science and Technology (NTNU), S.P. Andersensvei 15a, NO-7491 Trondheim, Norway
[2)] SINTEF Petroleum Research, S.P. Andersensvei 15b, NO-7465 Trondheim, Norway

Abstract

CO_2 EOR development offers the opportunity to reduce greenhouse gas emissions and at the same time, in suitable pools, to incrementally increase oil production. CO_2 injection is evaluated as a method to enhance oil recovery from one of the North Sea's naturally fractured reservoirs.

A fully compositional simulation model has been applied to a numerical experiment to investigate the drainage of CO_2 from a chalk core with artificial fractures. The effects of molecular diffusion and interfacial tension have been included. The simulated oil recovery for CO_2 as injection gas has been compared with the results of a conventional hydrocarbon gas injection recovery scheme. The objective of these simulations was to design a laboratory experiment on gravity drainage at reservoir conditions. The simulations were therefore performed with different core dimensions in order to find the optimal geometry for the experiment. The results obtained from this simulation have been used to: (1) tune the laboratory set-up for better monitoring of the displacement process via CO_2 gravity drainage, and (2) study oil-recovery efficiency by gravity drainage under CO_2 injection. In these experiments, the porous media are cylindrical chalk cores and the artificial fracture initially filled with hydrocarbon gas or CO_2.

Introduction

In order to investigate multiphase flow behaviour within a CO_2-oil gravity-drainage mechanism, laboratory experiments at reservoir conditions are often necessary to provide data for the modelling. Such experiments are difficult and time consuming. To ensure that an experiment's set-up is feasible and can give data within a specific time-frame, an estimate of the recovery will help to design the experiment for execution within a realistic lab time scale. In this circumstance, the laboratory experiment should be simulated using a compositional simulator. Simulation results will provide the required information for the best laboratory set-up configuration. The objective of the work described in this paper is to design the optimum core geometry and laboratory set up suitable for modelling CO_2 injection in fractured reservoirs using the compositional numerical simulator Eclipse 300 [1].

CO_2 gas is a favourable alternative injection fluid for increasing oil recovery in conventional reservoirs. Like hydrocarbon gases, CO_2 can be used as an immiscible or a miscible displacing agent, depending on the reservoir conditions and the properties of the crude oil. In this respect naturally fractured reservoirs do not meet classic CO_2 injection screening criteria due to excessive channelling of low viscosity CO_2 through the natural fractures. However, laboratory results indicate that if the fractures have sufficient vertical relief and significant density, CO_2 injection can give significant oil production by a gravity-drainage displacement mechanism [2].

In the case of gas injection in a fractured reservoir, gravity drainage plays an important role. This effect can be also significant when there is a high enough density difference between gas in the fractures and oil in the matrix blocks. In high-pressure reservoirs, the density of CO_2 at reservoir conditions is of the same order of magnitude as that of oil. This may reduce the gravity force and consequently the final recovery may be reduced compared to a similar case where hydrocarbon gas is used as an injection gas. However, CO_2 is highly soluble in crude oil, and its solubility increases as pressure increases. The dissolved CO_2 swells the oil and reduces the oil viscosity; these swelling and viscosity-lowering phenomena make the oil flow more easily and compensate for lack of gravity force between oil and CO_2.

Gravity-Drainage Experiment Description

In this experiment, the porous medium is a cylindrical chalk core which has a concentric hole through the middle of the core acting as an artificial fracture Figure 1: One of the most challenging steps in this experiment

Gholam Reza Darvish: Tel. (+47) 73594984, Fax. (+47) 73591246, Email: Gholam.darvish@iku.sintef.no

is to establish representative reservoir oil saturation in the annulus core with CO_2 in the fracture all at reservoir condition. Existence of the very highly permeable artificial fracture causes oil to flow only in the fracture so the establishment of oil in the annulus part will be impossible. Because of this difficulty, a previous CO_2-oil gravity-drainage experiment done by Schechter [2] did not initialize the matrix with the reservoir oil.

In order to initialize the annulus matrix block with the reservoir oil and using the advantage of normal core flooding, it is planned to use a low-melting-point metal. This metal can be melted over the fractures thus sealing them. Therefore by applying normal core flooding procedure, oil flows only through the matrix since the permeability of the fracture has been changed to zero. After establishment of oil saturation at reservoir conditions this low-melting-point material can be easily removed from the fracture by increasing the system temperature above its melting point. Then the hole in the middle of the core (the fracture) can be exposed to CO_2 from all sides, the relatively large hole ensures negligible rise of the oil level in the fracture and the gravity-drainage mechanism will start.

Numerical Experimental Model Specification

The development of a numerical model for this type of experiment must address the most important fluid exchange processes that occur in the actual experiment. These processes are gravity, diffusion and interfacial tension (IFT) effects. As gas advances through the core, the IFT will change at the front. The numerical model should have enough resolution to reflect this. The numerical gravity-drainage experiment has been simulated using a fully compositional simulator Eclipse 300 from Geoquest [1], and all fluid exchange mechanisms are captured using the available molecular diffusion and dynamic IFT-scaled capillary pressure options. The main stages in the development of this model are grid, fluid, rock properties and model initialization which are discussed in the following sections.

Rock Data

The fracture system is assigned a high permeability (1000 md) to minimize the viscous forces and secure complete phase segregation in the fracture system. This causes the matrix block to be surrounded by CO_2 at all time steps. Drainage gas and oil relative-permeability and capillary-pressure data for the matrix are shown in Figure 2. In the fracture system, zero capillary pressure and straight-line relative permeabilities with zero critical and residual saturation were used.

PVT Data and 13-Component Peng Robinson Equation of State (PR EOS) Model

A North Sea reservoir fluid with a bubble-point of 242 bars was used. Using an equation of state (EOS) tool pVTsim from Calsep [3] and the volumetric oil and gas laboratory data, a 13-component Peng Robinson (PR) EOS fluid model has been generated which gave an acceptable match to the measured laboratory data. The reservoir oil and hydrocarbon gas compositions together with EOS component critical properties are shown in Table 1.

The calculated CO_2 densities modelled by PR and Span and Wagner (SW) [4] EOS together with the calculated and measured laboratory oil densities and viscosity data are shown in Figure 3. This figure shows that both the PR and SW equations of state calculate the same CO_2 density and also confirm reduction of CO_2/oil density difference as the pressure increases.

Grid Data and Optimum Number of Grids in the Z-Direction

A two-dimensional 15 x 1 x 50 radial grid with two regions was defined: (1) the matrix block, (2) the fracture. The fractures grid are numbered from 1 to 5 in the R-direction and initialized with CO_2 while the rest of the grid was assigned as matrix block and initialized with oil. A matrix permeability of 4 md and a porosity of 40% were used for the matrix.

In order to check the effect of the number of grid in the Z-direction and to reduce the possible numerical dispersion, several radial configurations were tested. This was done by using 15 grids in the R-direction and different resolutions in the Z-direction, ranging from 25 to 100. The performance of the system for H=60 cm with different numbers of grid blocks in the Z-direction is shown in Figure 4. This figure clearly shows that at an early stage the predicted performance is very sensitive to the number of grid blocks in the Z-direction. The model with the lowest number of grid blocks has a higher recovery at an early stage while the ultimate recovery for all cases is equal. Considering Figure 4, the case with 15 grids in R-direction and 50 grid cells in the Z-

direction has enough resolution to reduce the numerical dispersion and at the same time capture all important recovery mechanisms.

Simulation Case Studies and Simulation Results

Considering the effect of different parameters on the drainage rate, several cases have been simulated. These cases include the block height (H), matrix permeability (K), system pressure (p) and effect of diffusion. The detail and the boundary conditions for each case are shown in Table 2. In this table, the case with block height of 60 cm, core diameter of 2 inches and system pressure equal to 328 bars is called the Base Case. All simulation results are compared with this case. In all cases the miscible option in the simulator was applied. In addition a test was also performed with a hydrocarbon gas for reference.

The Effect of Matrix Block Height

The size of matrix blocks will strongly affect the matrix-fracture fluid-exchange process and consequently the drainage rate. The drainage rate increases as the size of the matrix block increases. However, CO_2 enters the matrix if the height of the matrix is higher than the capillary entry height. As shown in Figure 2, for a capillary entry pressure of p_{cgot}=0.0018 bar, an oil density 697.4 kg/m^3 and a CO_2 density of 570.79 kg/m^3 at the reservoir condition (p=328 bars and T=134ºC), the capillary entry height will be 14.4 cm. Therefore the minimum block height for our study should be greater than 14.4 cm. This was also tested by running a case with a block height of 14 cm which resulted in zero recovery. The performance of the experiment under different core heights, H=60 cm (Base Case), 120 cm and 30 cm has been simulated. The simulation results for these three cases are shown in Figure 5. This figure shows that the drainage rate and the ultimate recovery for the biggest core will be greater than for the smallest one and that almost 10% of the oil can be recovered from the 60 cm core after 50 days.

The Effect of Diffusion

To investigate the combined effect of diffusion and lateral flow on the recovery performance, the Base Case simulation grid was selected. Three cases were compared: one where the diffusion in the model was disabled (denoted “NO DIFF”), one with the diffusion option activated (denoted “DIFF”) and one case where the diffusion coefficients were multiplied by a factor of ten (denoted “10DIFF”). The effective oil and gas diffusion coefficients (D_{oi}) and (D_{gi}) were scaled according to their components’ molecular weights from the oil and gas diffusion coefficients calculated by Uleberg [5]. The relationship between gas and liquid diffusion coefficient and molecular weight are shown in Figure 6. The effective diffusion coefficients for both gas and liquid were calculated [6] and used in all simulations.

The recovery performances for the above cases are shown in Figure 6. This figure clearly shows the importance of diffusion in all simulations. When the diffusion is taken into account in the model, the recovery increases due to both lateral flows (diffusion) and the gravity-drainage mechanism. The effects of diffusion are due to a reduction in the oil viscosity and swelling of the oil and also changing the frontal IFT in a positive or in a negative direction.

The viscosity reduction for both cases of diffusion and no diffusion along the middle of the core are compared at six different times and shown in Figure 7.

This figure shows that, in the case of diffusion, as the CO_2 diffuses laterally through the core the viscosity along the core reduces from 1.08 cp to 0.98 cp, but that, for the no-diffusion case, the reduction of oil viscosity is only at the front. Also this figure shows that the lateral reduction in oil viscosity stops after 50 days while the reduction continues along the core as the gas front moves downwards. The reduction of oil viscosity at the front ranges from 1.08 cp to 0.32 cp and causes an increase of oil mobility at the front. However, the reduction in the oil viscosity will be reversed when the front reaches that point. It means that the free gas which mostly contains CO_2 starts to extract the light-intermediate components of the residual oil left behind the front and then causes the increase in oil viscosity. The changes of oil viscosity and gas saturation *versus* time for two points at different heights in the middle of the block are shown in Figure 8.

Figure 8 clearly shows that the oil viscosities for these three points increase drastically as the gas saturation increases. The increase in oil viscosity reduces the oil mobility and consequently the gas saturation should remain constant at these points. But as shown in Figure 8, despite getting very high oil viscosity at these points, the gas saturation continues to increase. This introduces another recovery mechanism which is extraction of oil

by CO_2. As shown in the figure, the extraction mechanism is slow compared with the first part of the recovery which is due to a combined swelling and gravity-drainage mechanism.

The Effect of Pressure

The effect of pressure on the recovery performance was examined by running the model with two pressures, 400 and 250 bars. The recovery performance for these two cases are compared with the Base Case (328 bars) as shown in Figure 9, which clearly shows that, at early stage, the oil recovery reduces with increasing pressure while the ultimate recovery increases. The higher recovery at the early stage is due to reduction of gravity force, since the CO_2 density decreases with decreasing pressure. This results in a higher drainage rate and more recovery.

The Effect of Matrix Permeability

The actual experiment will be performed on cores taken from the Faxe chalk outcrop as the rock has properties that are similar to those of the reservoir rock under study. Laboratory measurements confirm a matrix permeability of 2 to 4 md and a porosity of 40% in a very homogenous rock. However, it is necessary to have a measure of the recovery performance for different permeabilities especially for the minimum value of 2 md. For this study, in addition to the Base Case permeability (K=4 md), two permeabilities – one with K=2 md and the other with K=10 md – have been simulated. The recovery *versus* time for these two cases are compared with the Base Case and shown in Figure 9. This figure clearly shows that the recovery will scale up as the permeability increases, the scaling factor depending on the permeability, and that the recovery rate for 4 md case is almost two times more than that for the 2 md case.

The Effect of the Injection Gas Type

In order to compare the performance of the system with respect to the type of injected gas, the fracture network in the Base Case model was initialized with a hydrocarbon gas with a composition as shown in Table 1.

The recovery performance for the hydrocarbon case is compared with the CO_2 case as shown in Figure 10. This figure clearly shows that the recovery for hydrocarbon gas at all stages is higher than in the CO_2 case. The high recovery for hydrocarbon is due to the low hydrocarbon gas density compared with the CO_2 density. The CO_2 density for P=328 bars is almost 1.2 times more than the hydrocarbon gas density.

Discussion of the Results

The simulation results examine the effects of core geometry, matrix permeability, pressure and the type of gas in the fracture system on oil recovery under CO_2-oil gravity drainage. The results show that the CO_2-oil gravity-drainage experiments at reservoir condition are promising and that such experiments can be carried out in a reasonable laboratory time scale. The oil recovery after 50 days is almost 10% for blocks with a height of H=60 cm and drainage rate increases with increasing core height. However, drainage only starts provided that the core height is higher than the capillary entry height.

The simulation results show that increasing pressure postpones the oil recovery. The density difference reduces as the pressure increases and consequently this reduces the gravity force and results in less recovery at an early stage. The ultimate recovery for a high-pressure case is more than for the low-pressure case and this is due to high extraction capability of CO_2 at high pressure [7]. The reservoir under study has a pressure of 328 bars and the experiment should be carried out at this pressure, although low pressure may be interesting as well, in order to examine the effects of pressure.

The simulated results indicate that in the case of CO_2 injection, the recovery mechanism can be divided into two production stages: (1) diffusion and gravity drainage and (2) the extraction mechanism. In the initial stage, transport of injection gas from the fracture into the annulus (matrix block) occurs primarily by lateral liquid-liquid diffusion between the undersaturated oil inside the annulus and the saturated oil with CO_2 at the inner surface of the annulus while at the same time the gas enters from the top of the block due to gravity drainage. This can be seen from the reduction of oil viscosity along the core in the diffusion case. The CO_2 diffusion into the core causes oil swelling followed by viscosity reduction and consequently less viscous forces and higher drainage rates. The swelling mechanism and viscosity reduction stop as soon as the oil inside the core becomes saturated with CO_2. The dominant mechanism becomes gravity drainage. In the next stage when the gas saturation at the core increases, the oil viscosity drastically increases which reduces the oil mobility to the

lowest possible level. Therefore, despite the existence of gravity force, the oil is not able to drain out of the block and the extraction mechanism has little impact compared with the first stage. In the extraction mechanism most heavy components of the residual oil vaporized into the gas phase.

Conclusions and Recommendations

A 13-pseudo component PR EOS model was developed to predict oil properties of one of the North Sea fractured reservoirs. Using the generated EOS model, a single porosity compositional numerical model for simple fracture-matrix systems has been developed. This model is able to capture the key recovery mechanisms involved in CO_2 injection in a fractured reservoir.

The model was run for different core geometries under CO_2 and hydrocarbon gas injection scenarios to quantify the optimum core geometry for future laboratory experiments. The sensitive parameters such as core height, fracture width, core diameters, the diffusion coefficients and pressure were checked. The optimum core geometry for laboratory setup has been determined. Simulation results confirm the importance of diffusion coefficients on the prediction of ultimate oil recovery as well as enhancing the different mechanisms involving in gas injection in fractured reservoirs. The key recovery mechanisms in these experiments are: (1) oil swelling and gravity drainage at the early stage followed by (2) a slow extraction mechanism which recovers the heavy-intermediate and heavy components from the residual oil saturation left behind the gas front.

The combined effect of diffusion and gravity suggests that the application of the oil and gas diffusion coefficients is critical in any field scale simulation of a fractured reservoir and the correct diffusion coefficients should be applied.

Acknowledgements

This work was performed under the CO_2-KMB project in SINTEF Petroleum Research and we thank Phillips Petroleum Company Norway for providing the fluid data and granting permission for publication.

References

1. Schlumberger. 2001. *Eclipse 300 Reservoir Simulation.* Software Version 2001a.
2. Schechter, D.S. 2000. Advanced Reservoir Characterization and Evaluation of CO_2 Gravity Drainage in the Naturally Fractured Spraberry Trend Area. *Fifth Annual Technical Progress Report, U.S. DOE Contract No. DE-FC22-95BC14942*.
3. Calsep A/S. 1988-2003. *pVTsim.* Software Version 13.
4. Span, R. and W. Wagner. 1996. A new equation of state for carbon dioxide covering the fluid region from the triple-point temperature to 100 K at pressures up to 800 MPa. *J. Phys. Chem. Ref. Data*, Vol. 25, No. 6: 1509-1596.
5. Uleberg, K. and L. Hoier. 2002. Miscible gas injection in fractured reservoirs. *SPE Paper 75136*, presented at the SPE/DOE Thirteenth Symposium on Improved Oil Recovery, 13-17 April, Tulsa, Oklahoma, USA.
6. Da Silva, F.V. and P. Belery. 1989. Molecular Diffusion in Naturally Fractured Reservoirs A Decisive Recovery Mechanism. *SPE Paper 19672*, presented at the SPE Annual Technical Conference and Exhibition, San Antonio.
7. Siagian, U.W.R. and R.B. Grigg. The extraction of hydrocarbons from crude oil by high pressure CO_2. *SPE Paper 39684*, presented at the SPE/DOE Symposium on Improved Oil Recovery, 19-22 April, Tulsa, Oklahoma, USA.

Table 1: Critical properties for the 13-component PR EOS model and oil composition with bubble point pressure 242 bars at 134ºC.

COMPONENT	MW	Oil composition	Gas composition	Tc	Pc	AF	Vc	Vshift	Parachor	omegha A	omegha B
		mol%	mol%	K	BARA		cm3/mol				
P1	28.0	0.213	0.3	126	33.9	0.04	90	-0.0299	41	0.45724	0.07780
CO_2	44.0	0.94	1.2	304	73.8	0.225	94	-0.0105	78	0.45724	0.07780
P3	16.0	59.5	77	191	46.0	0.008	99	-0.0330	77.3	0.45724	0.07780
P4	30.1	7.67	9.8	305	48.8	0.098	148	-0.0244	108.9	0.45724	0.07780
P5	44.1	4.14	5.2	370	42.5	0.152	203	-0.0192	151.9	0.45724	0.07780
P6	58.1	0.9	1.1	408	36.5	0.176	263	-0.0169	181.5	0.45724	0.07780
P7	58.1	2.12	2.4	425	38.0	0.193	255	-0.0153	191.7	0.45724	0.07780
P8	72.2	0.78	0.7	460	33.8	0.227	306	-0.0120	225	0.45724	0.07780
P9	72.2	1.17	1	470	33.7	0.251	304	-0.0097	233.9	0.45724	0.07780
P10	86.2	1.77	0.9	507	29.7	0.296	370	0.0021	271	0.45724	0.07780
P11	124.3	8.63	0.4	591	24.6	0.364	561	0.0173	359.3	0.45724	0.07780
P12	253.4	8.98	0	761	16.0	0.696	1136	0.0152	683.6	0.45724	0.07780
P13	531.2	3.16	0	1030	12.5	0.951	2621	-0.0085	1388.7	0.45724	0.07780

Table 2: Simulation case studies performed for both CO_2 and hydrocarbon for annulus core.

Simulation case	Core			System Pressure	Diffusion	Miscible
	Height	Diameter	Permeability			
	cm	Inch	md	Bar	Off/On	Off/On
Base case	60	2	4	328	On	On
H30D2K4P328DIF	30	2	4	328	On	On
H120D2K4P328DIF	120	2	4	328	On	On
H60D2K4P400DIF	60	2	4	400	On	On
H60D2K4P250DIF	60	2	4	250	On	On
H60D2K10P328DIF	60	2	10	328	On	On
H60D2K2P328DIF	60	2	2	328	On	On
H60D2K4P328NODIF	60	2	4	328	Off	On
*H60D2K4P328DIF10	60	2	4	328	*On	On

* The diffusion coefficients are multiplied with 10 to have one extreme case

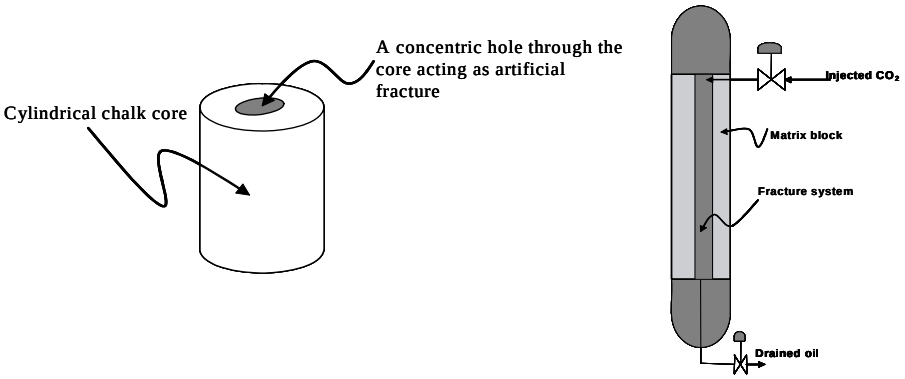

Figure 1: Set-up for the gravity-drainage experiment wherein a concentric hole is drilled acting as a fracture system.

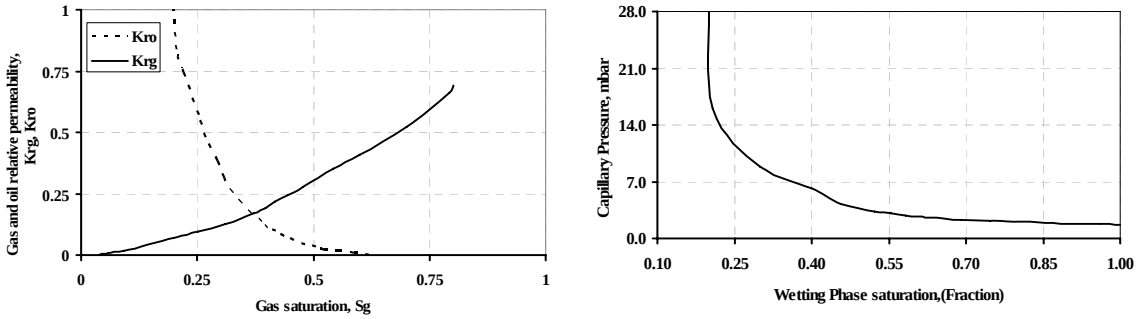

Figure 2: Gas and oil relative-permeability curves (left) and gas-oil capillary-pressure curve (right) with threshold pressure P_{cgot}=0.0018 bar used in all simulations for matrix.

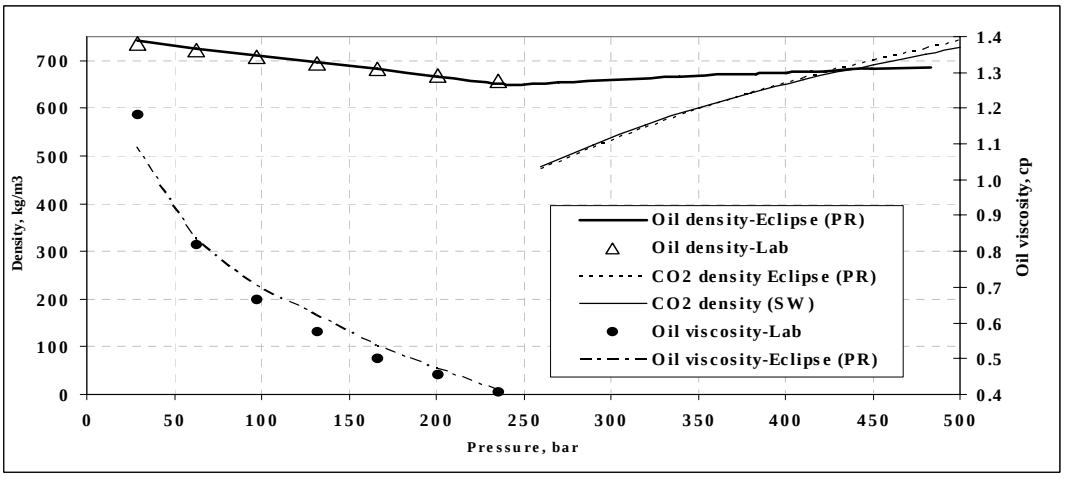

Figure 3: Calculated and measured oil densities and viscosities together with calculated CO_2 density by PR and SW equation of state.

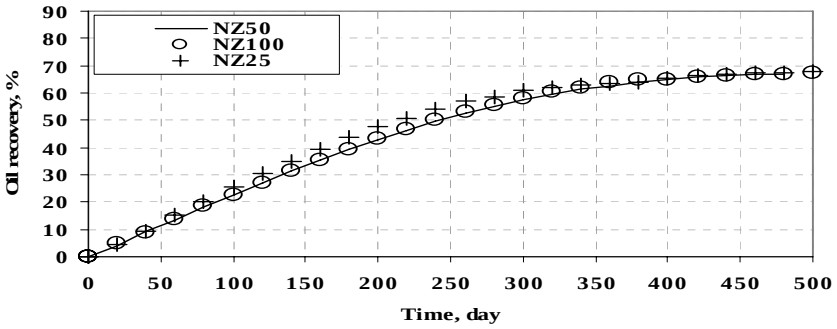

Figure 4: Simulation results for different numbers of grid in Z-direction (25, 50 and 100).

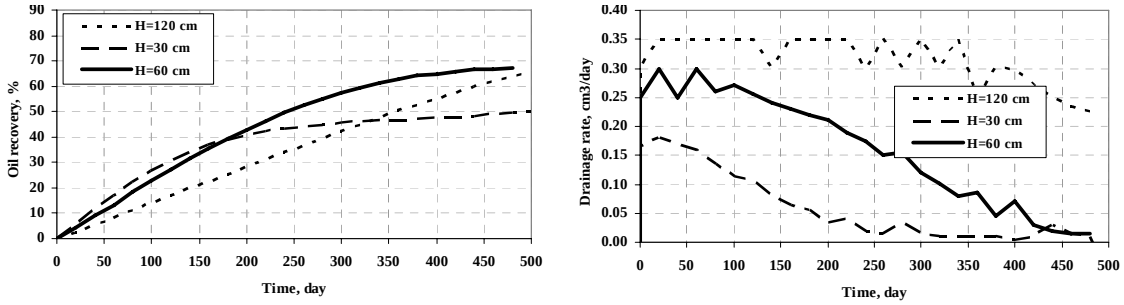

Figure 5: The oil recovery (left) and drainage rate (right) for numerical gravity-drainage experiment with different core height.

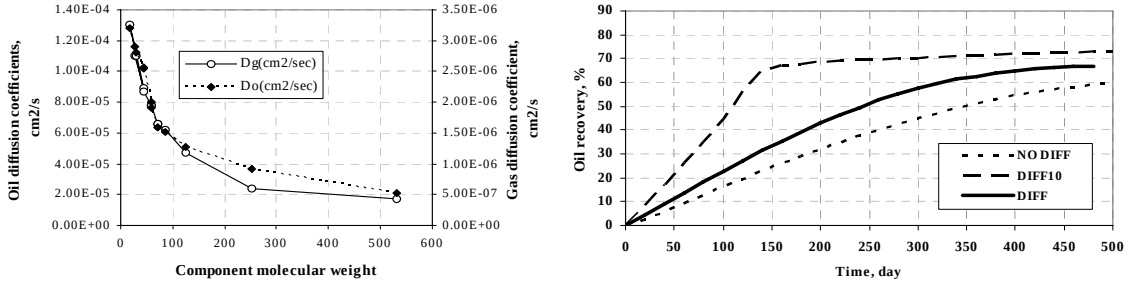

Figure 6: The oil and gas diffusion coefficients (left) and oil recovery when the diffusion coefficients in the model have been changed.

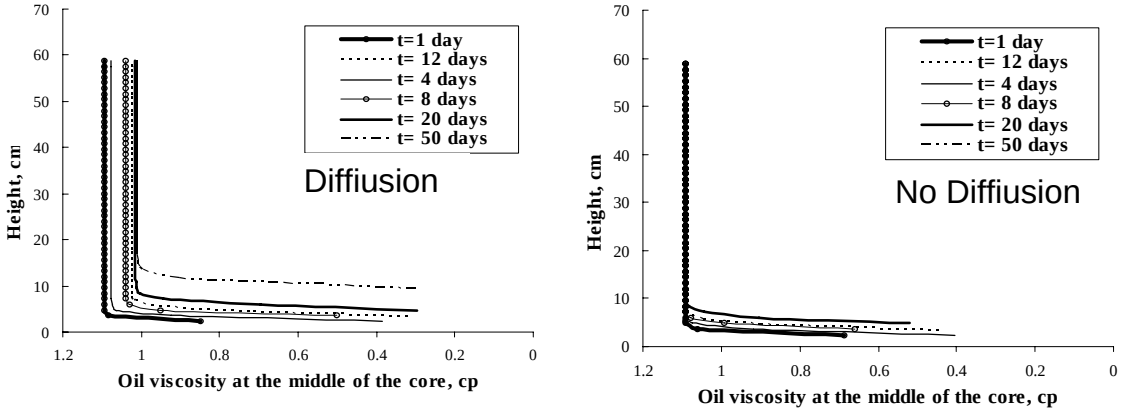

Figure 7: The effect of diffusion on the reduction of oil viscosity in the middle of the block.

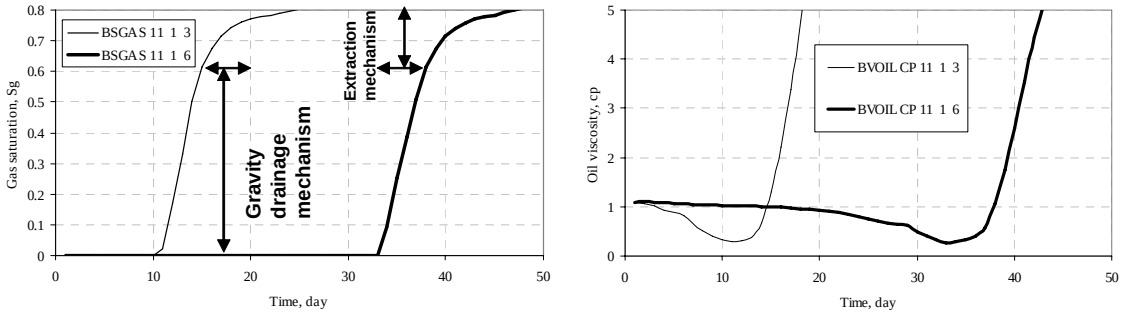

Figure 8*:* The gas saturation (left) and oil viscosity (right) *versus* time for two points at the middle of the core.

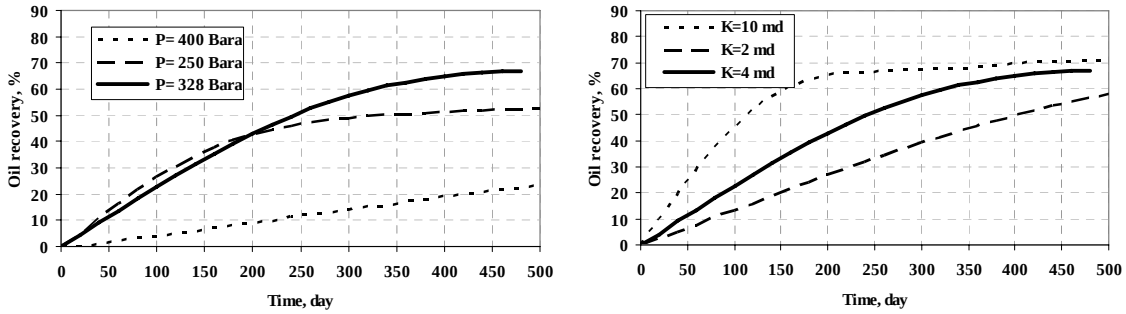

Figure 9: Simulation results for different pressures (left) and different matrix permeabilities (right).

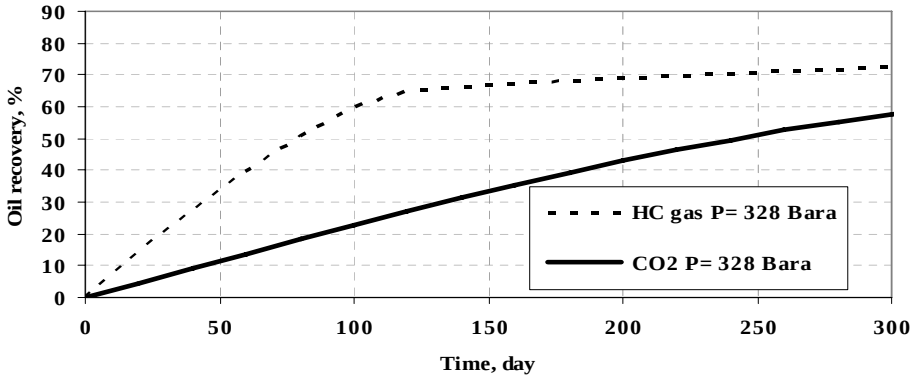

Figure 10: The effect of type of two different injection gases in a gravity-drainage experiment.

Appendix B: Reservoir conditions laboratory experiments of CO_2 injection into fractured cores

SPE 99650

Reservoir Conditions Laboratory Experiments of CO_2 Injection into Fractured Cores

Gholam Reza Darvish, SPE, SINTEF/NTNU, Erik Lindeberg, SPE, SINTEF, Torleif Holt, SPE, Reslab, Svein Arild Utne, SINTEF,Jon Kleppe, SPE, NTNU,

SPE 99650

Reservoir Conditions Laboratory Experiments of CO_2 Injection into Fractured Cores

Gholam Reza Darvish, SPE, SINTEF/NTNU, Erik Lindeberg, SPE, SINTEF, Torleif Holt, SPE, Reslab, Svein Arild Utne, SINTEF,Jon Kleppe, SPE, NTNU,

This paper was prepared for presentation at the SPE Europec/EAGE Annual Conference and Exhibition held in Vienna, Austria, 12–15 June 2006.

Abstract

During CO_2 injection into fractured reservoirs the overall oil recovery will be the result of the complex interplay of several mechanisms such as viscous flow, extraction by molecular diffusion and gravity drainage. In order to study the component exchange between the matrix and the fracture system during the CO_2 injection, CO_2 injection experiments at reservoir conditions have been carried out using 60 cm long 4.6 cm diameter composite cores from an outcrop analogue to one of the North Sea reservoir rock.

The core and core holder assembly were designed to allow a 2 mm fissure to surround the core plug simulating a fracture. Live reservoir fluid was prepared and used for saturating of the matrix system. Because of the large permeability contrast between core (4 mD) and fracture it is difficult to saturate the core by simply flooding the system with live oil. Oil would flow through the fracture and only partially saturate the core

To overcome this problem a unique technique has been developed for saturating the matrix system with reservoir fluids. This method ensures a homogeneous fluid composition within the pore system before the fracture system is initialized with the CO_2. During the experiments CO_2 was injected at a low and constant rate into the fractured system. The component exchange between the oil in the matrix and CO_2 in the fracture was monitored by analyzing the produced fluids. The recovery profiles and the fluid compositions were used to construct a compositional numerical model.

The results from the experiments in the long core as well as the simulation studies show the importance of the diffusion mechanism in these experiments. The results have proved that the key mechanism to recover oil from the tight matrix block was diffusion and the gravity drainage had no significant effect at the experimental conditions used.

Introduction

In fractured reservoirs, matrix blocks are assumed to act as sources of oil and fractures are a flow conduit through which the oil is flowing towards the producing wells. Depends on the matrix blocks geometry and the reservoir fluid properties, oil from the matrix block is transferred to the fracture system by different mechanisms. Based on classical fractured reservoir production mechanisms, when a tall and permeable oil-saturated matrix block is surrounded by gas in the fracture, oil drains from the matrix as a result of the density difference between the gas in the fracture and the oil in the matrix (gravity dominated mechanism). In case of low permeability and small size matrix blocks with high capillary pressure, the gravity drainage mechanism is inefficient and molecular diffusion mechanism will dominate.

To quantify and understand the contribution of the above mechanisms for oil recovery during CO_2 injection in highly fractured under-saturated light oil reservoirs, it is necessary to perform laboratory experiments at the reservoir conditions. Due to the large compositional space involved in this process it is also necessary to initialize the matrix and fracture system with the representative reservoir fluids.

However, in this kind of experiments saturating the pore system with live oil is very difficult. Due to large permeability contrast between matrix and fracture, normal core flooding can not be used for saturating the pore system. Oil would flow through the fracture and only partially saturate the pore system. Because of this problem, dead oil was used for saturating the pore system in most of the experimental studies reported in literature.

For example in the CO_2 gravity drainage experiments performed by Li et al[1], the core was saturated by dead oil while the experiment was supposed to be at the reservoir conditions.

Dry gas injection in fractured chalk by Øyno et al[2] conducted by saturating the matrix system with live oil, but still their method for initialization of the pore system with live oil is not certain. In their experiment the oil recombination was carried out in the core holder where the matrix and fracture were placed. The oil/gas mixture was circulated in the system and pressure was monitored. Once pressure had stabilized, they assumed that the pore system is saturated with the live oil. In this method, since the pore system was saturated with oil by a very slow diffusion mechanism, therefore the pressure stabilization over a short time interval will not guarantee the homogeneous initialization of the pore system with representative reservoir fluids.

This paper presents experimental results obtained during injection of CO_2 into an artificially fractured core which has been initialized with under-saturated live oil. For performing this experiment at the reservoir condition, a new method for initialization of matrix and fracture systems with representative reservoir fluids have been developed which secure the homogeneous initialization of the matrix block with oil while the fracture system was initialized with CO_2.
In addition to the experiment, special attention was given to the modelling of the experiments using single porosity compositional simulators. Therefore, comprehensive pVT studies on the reservoir fluid have been performed and the results were used for making an Equation of State (EOS) model which was used in compositional simulation. In the simulation part of the work, the cross phase diffusion was modelled and the effect of diffusion on the matrix oil properties during the experiment was studied.

Experimental Procedures

Core samples

Core samples from Faxe outcrop analogue to one of the North Sea fractured reservoirs rock were used. Cores were cut 60 cm long and 4.6 cm in diameter. The chalk is very homogenous and has an absolute permeability of 4 mD. The helium porosity is 44 % close to values for Maastrichtian chalk in this field. The experiment was conducted under two phase condition (oil/CO_2), and no attempt was done to establish initial water saturation in the core.

Fluid samples

Initial reservoir oil has been made by recombination of the stock tank (STO) oil with a synthetic gas mixture, and with addition of intermediate components (C_5 and C_6) as a liquid mixture. The initial reservoir oil had a bubble point pressure of 383 bar at 130 ºC with composition shown in Table 1.

The present reservoir fluid was prepared by lowering the pressure of the initial reservoir fluid and pushing off the gas cap. This operation has been started with initial pressure of 383 bar at the reservoir temperature of 130 ºC. The pressure was then reduced in a step-wise manner in steps of approx 35 bars down to the minimum reservoir pressure of 247 bar. The present reservoir fluid has a bubble point pressure of 247 bar at 130 ºC.

A comprehensive pVT fluid study on the present reservoir fluid has been performed. The reservoir oil was loaded in a pVT cell, and oil compressibility and the bubble point were determined. Then, a known volume of the reservoir oil was flashed to ambient conditions in a single step. The mass and compositions of the resulting oil and gas phases at standard condition was measured, and the composition of the reservoir oil has been calculated. The oil compositions as well as the key measured pVT data for both initial and present reservoir oil are shown in Table 1. The measured oil density as function of pressure for present reservoir fluid is shown in Figure 1.

Swelling tests were performed with different CO_2/oil ratios. The phase volumes in the two phase region were measured and the complete pVTx diagram for the CO_2/oil system as shown in Figure 2 was constructed.

Different mixtures of live oil/CO_2 were prepared and the resulting mixtures were flashed to pressure of 300 bar (current reservoir pressure) at temperature 130 ºC. The viscosities of the resulting liquid phase in the mixture were measured by Ruska Rolling ball viscometer. The results are shown in Figure 3.

Equation of state characterization

The measured basic pVT data as well as liquid volume versus pressure for different mixtures of reservoir oil and CO_2 were used to generate and tune a 14 pseudo components Soave-Redlich-Kwong Equation of State (SRK EOS) model. Figure 4 shows CO_2 swelling saturation point data and simulation results from the tuned EOS model for present reservoir fluid at 130 ºC. Figure 5 and Figure 6 show liquid volume% versus pressure for two mixtures (near critical point) of the present reservoir oil and CO_2. These figures show the EOS model match the critical point on the swelling curve where the saturation point changes from a bubble point to a dew point. The Lorenz-Bray-Clark (LBC) correlation tuned to viscosity data is used to calculate viscosities. The SRK EOS model developed with 14 pseudo components later was used for simulating the core flooding experiment. The EOS parameters for the current reservoir fluid are shown in Table2 and 3.

Experimental set-up and initialization of core and fracture with representative fluids

The first step for preparation of the setup was generating the matrix and fracture network. The core 60 cm long and 46 mm in diameter was inserted into a steel tube having an inside diameter of 50 mm. Then core was centralized inside the steel tube. The 2 mm annulus space between the core outer boundary and steel tube's wall was considered as artificial fracture. The fracture then was filled with sealing material. The core itself constitutes a single matrix block.

The sealing material had no effect on the surface area of the core and on the fluid which later was used for saturating the core. This was checked visually after finishing the experiment and by checking the core permeability. The core permeability at the outer boundary of the core where the core was contacted with this sealing material remained unchanged. Under this circumstance the artificial fracture filled with sealing material had zero permeability and the core (matrix) had an initial permeability of 4 mD.

The second step was to saturate the matrix block (core) with live present reservoir fluid at 300 bar. The steel tube and the core as described in the previous step was assembled into normal core flooding rig and after complete evacuation of the system, the core was pressurized to 300 bar with mixture of 85 % toluene and 15 % exxsol. This mixture has a higher density compare to the reservoir fluid and therefore by injecting the oil from the top of the core a gravity stable displacement was established. The core (matrix) placed at the vertical position and was flooded from the top with 2 pore volume of Reservoir live oil with very slow rate. This operation was done under low temperature (t=40 ºC) and high pressure (p=300 bar) where the oil was in its liquid phase condition and the sealing material was solid. Under these conditions the sealing material is still sealing the fracture and

all injected fluid is flowing through the core. The core initial condition after saturating with live oil is shown in Table 4.

As mentioned before this experiment was planned and conducted under no presence of water, therefore there was no extra attempt to establish initial water saturation in the core (matrix).

The third step was to remove the sealing material from the fracture while the core (matrix) still contains the live reservoir fluid. The core flooding rig temperature was increased to the reservoir temperature 130 ºC at the constant pressure 300 bar. At these conditions the sealing material inside the fracture was in its liquid condition and can be displaced from the fracture by flooding the fracture by the same live oil used for core initialization. The setup at this step was designed in such a way that during displacement of the sealing material from the fracture the system pressure and temperature were kept constant at 300 bar and 130 ºC respectively.

Once the sealing material from the fracture was removed, the setup could be used for injection of CO_2. First the oil inside the fracture has to be displaced with a very high flow rate of CO_2. The pore volume of the fracture was 169 cm^3. The fracture oil was displaced with CO_2 for 30 minutes and then the flow rate of CO_2 was reduced from 5.6 cm^3/min to 0.1 cm^3/min. Figure 7 schematically illustrates the setup used in the experiment for core initialization with live oil, removing the sealing material from the fracture and finally injecting CO_2: This includes backpressure regulator, pump, oil-gas separator, core holder, the gas collecting tanks and the scale for weighing the produced oil. During the CO_2 injection the whole system was placed in a heating cabinet operating at the reservoir temperature of 130 ºC and the injection of CO_2 was continued for 26 days at constant pressure and temperature of 300 bar and 130 ºC. The mass of produced oil and gas was monitored and the oil and gas samples on daily base were taken for gas chromatograph (GC) analysis.

Experiment results and discussion

The oil recovery versus core pore volume (PV) of injected CO_2 is shown in Figure 8. This figure shows a rapid oil production rate for the first 2 pore volumes of injected CO_2 followed by slow period of oil production (interval between 2-5 pore volumes injected) and finally a very slow oil production. Because of some practical problem the experiment was terminated after 22 days (8 pore volume injections) and as it is shown in this figure the oil recovery at the end of experiment is 68 %. The oil recovery would be more if the experiment has any chance to continue.

The composition profile and the molecular weight of the produced oil are shown in Figure 9 and 10. Figure 9 shows that the early production is enriched in light components, the produced oil initially was light with a very low molecular weight and it turns to production of component with heavy molecular weight.

Figure 11 compares the stock tank oil composition with the composition of oil samples taken in day one, day two and last day. This figure clearly shows the oil compositions for these three samples are completely different from the stock tank oil composition. At the early stage (day one) the produced oil was very light and includes 15 % (weight percent) of C_{23+} while in the last oil sample weight percent of C_{23+} was increased to 86 %.

In the case of gravity drainage mechanism produced oil would have almost a uniform composition profile through the experiment, while in this case, the produced oil have different composition from the stock tank oil composition. The variation of the produced oil composition suggests domination of the diffusion mechanism over the other mechanisms.

Simulation of the experiment and model description

A single matrix block surrounded by fractures was used to study the matrix-fracture component exchange.

The simulation model for this study has to be able to model the diffusion of oil and gas components within the oil and gas phases as well as diffusion of components directly from the gas phase to the oil phase (cross phase diffusion) from the sides. In the cross phase diffusion the CO_2 from the gas phase inside the fracture diffuse to oil phase inside the matrix. The commercial compositional reservoir simulator [3] that was used for this work was not capable to capture and model the cross phase diffusion. Therefore a special method was used for simulation of cross phase diffusion. This was done by constructing a two dimensional single porosity radial model 15x1x50 containing a two phase dummy zone located between matrix and fracture grids as shown in Figure 12.

The dummy zone was initialized with a mixture of 95 mol% CO_2 and 5 mol% of the heaviest component P14 which was called inert component in the EOS model given in Table2. A zero gas and oil diffusion coefficient was assigned for the inert component. The fluid inside the dummy zone has a two phase condition in which the liquid phase has a very high concentration of CO_2 (60 mol %). The presence of two phase condition in the dummy zone with a high concentration of CO_2 in its liquid phase would start the liquid-liquid diffusion from the dummy to the matrix. The gas and oil diffusion coefficients (Doi and Dgi) for each component were calculated using extended Sigmund correlation[4]. The effective diffusion coefficients for porous media (Deoi and Degi) were calculated using the expression:

$$D_{epi} = D_{pi} \cdot \phi^{m-1} \quad \text{.....(1)}$$

where $p=o$ or g, the cementation exponent m was used as a matching parameter for history matching the experiment. The value of m for the best match was 1.7. The calculated effective diffusion coefficients at 300 bar and reservoir temperature are given in Table 5.

The gas phases in the dummy cells contains 99.9 mol% CO_2 with a gas density almost the same as CO_2 density at the experiment conditions.

The matrix block is initially filled with oil and the fracture is initialized with CO_2 all at 130 ºC and 300 bar. The oil composition and the EOS parameters used in the model are shown in Table 1 and Table2.

Zero capillary pressure and high permeability (100 D) was assigned for the fracture and the dummy cells. The dummy cells have the critical gas saturation S_{gc} = 0.8 and the initial gas saturation for these cells were set equal to S_{gc}. This high critical gas saturation keeps the two phase conditions inside

the dummy cells for all time steps and prevents the movement of gas to the top grids in the dummy zone.

A large pore volume for the fracture was used in order to simplify the model and eliminate the injection and production wells. This means that there is sufficient supply of fresh CO_2 from the fracture and also there is sufficient space for drained oil to enter into fracture system. The dimensions and initial conditions for the matrix, the fracture and the dummy zone in the simulation model are shown in Table 6. The fluid compositions for matrix, fracture and dummy cells are shown in Table 7.

The saturation dependent data assigned to the dummy, fracture and matrix block are given in Table 8, 9 and 10 respectively. The capillary pressure and relative permeability curves were taken from Uleberg [5]. These data were generated from Corey-type equation based on model parameters from relevant North Sea core data.

The miscible option in the model was used to calculate the capillary pressure based on the calculated gas oil interfacial tension σ. The capillary pressures were scaled with IFT according to:

$$P_c = \frac{\sigma}{\sigma_{lab}} . P_{c_{lab}} \quad \text{.....(2)}$$

where $p_{c_{lab}}$ is lab-reported capillary pressure, σ_{lab} is the gas oil laboratory IFT, equal to 0.05 mN/m, and σ is reservoir gas oil interfacial tension calculated by

$$\sigma^{1/4} = \sum_{i=1}^{N} \left(\rho_l . [P]_i . X_i - \rho_v . [P]_i . Y_i \right) \quad \text{.....(3)}$$

In equation (3) the interfacial tension σ (in dyn/cm = 1 mN/m) is expressed in terms of the Parachors [P] of the individual components. ρ_l and ρ_v are the molar densities in mole/cm^3 (the density divided by the molecular weight) of the oil and gas phases respectively. X_i and Y_i are the mole fractions of component *i* in the oil and gas phases respectively. Oil recovery was calculated based on the mass balance performed on the matrix oil in place using relation:

$$RF = 100 - \frac{\text{Mass of oil in place at each time step}}{\text{Mass of initial oil in place}} \quad \text{...(4)}$$

Simulation results

The recovery as a function of time for both experimental data and simulation results with m=2 and m=1.7 at pressure 300 bar and temperature 130 ºC are shown in Figure 13. This figure shows a better match for m=1.7 compare to m=2 towards the end of the experiment.

The effect of the volume of the dummy on the simulation results has been verified by using m=1.7 and changing the pore volume of the dummy grids. The results are shown in Figure 14. These results show that the volume of the dummy almost has no effect on the simulation results.

The effect of fluid composition in the dummy cells on the simulation results were investigated by changing the composition of the inert component. The result is shown in Figure 15. This figure shows that the matrix block oil recovery is sensitive to the concentration of the inert component in the dummy cells. The recovery was increased as the concentration of the inert component in the dummy cells was increased. Increasing the concentration of the inert component in the dummy cells will increase the oil saturation and consequently more oil-oil diffusion. For case with zero concentration of the inert component in the dummy zone, the oil saturation in this zone is zero and as it shown in Figure 15 the calculated recovery is far from the experimental results. This difference between calculated oil recovery and experimental results shows the weakness of the simulator[3] for calculation of the cross phase diffusion. Therefore for any compositional simulation of fractured reservoirs the formulation for calculation of the cross phase diffusion in this simulator[3] must be modified.

At this point it is important to mention that using the concept of dummy is only applicable to quantify the contribution of the diffusion mechanism. This concept can not be used for predication of the produced oil composition when production and injection wells are applied in the model.

To investigate the contribution of the gravity drainage displacement mechanism (zero capillary pressure) on the oil recovery, the diffusion option in the model was turned off and the results were compared with the experimental data. Figure 13 compares the case with no diffusion (pure gravity drainage) and case with the diffusion option was turned on (both gravity drainage and diffusion). This figure shows that for case where diffusion is turned off in the model, the recovery is very low compared with cases where diffusion was active in the model.

The core oil saturation profiles for four different time steps in R-Z plan were shown in Figure 16. This figure clearly shows that the there is no gravity segregation of the oil phase as the displacement front is moving from all sides of the block.

Figure 17 shows the mole fraction of the CO_2 in the liquid phase for four different time steps. This figure shows that the CO_2 diffuses both laterally and vertically from the fracture system through the matrix.

Figure 18 shows the oil density for four different time steps. This figure clearly shows that the oil left inside the core becomes heavy as the CO_2 advance through the core centre.

The inert component has a zero diffusion coefficient therefore, its composition inside the matrix block should not change and it should stay at its zero value for all time steps. However because of the equilibrium calculation, the composition of the inert component in the boundary of matrix block start to increase and this is shown in Figure 19.The increase of composition for the inert component is not so big and therefore its effect on the oil in place calculation is not so big.

Conclusion

1. A very high oil recovery can be achieved by injection of CO_2 in fractured chalk reservoirs with high fracture intensity.
2. The maim oil recovery mechanism at the experimental conditions was concluded to be diffusion. This was confirmed by a variable produced oil composition through the experiment. The lighter components with higher diffusion coefficients were produced at the early stage of the experiments, while

the heavier components with very low diffusion coefficients at the late stage.

3. In addition to the experimental results, simulation results confirm that contribution of gravity drainage mechanism for recovery of the oil from the matrix blocks is very small at the experimental conditions.
4. Compositional numerical simulation of the experiment has shown the importance of the cross phase diffusion and the existing commercial compositional simulators have to be updated for modelling of this phenomenon.

Nomenclature

D_{eoi}= *oil effective diffusion*
D_{egi}= *gas effective diffusion*
EOS= equation of state
IFT= gas-oil interfacial tension, m/t^2, *dyne/cm*
GOR = gas oil ratio, cm^3/cm^3
k_{rg} = *relative permeability of gas*
k_{rog} = *relative permeability of oil*
LBC=Lorenz-Bray-Clark
m =cementation factor
MW = oil molecular weight
N = number of components
p = pressure, m/Lt^2, *bar*
p_b= *bubble point pressure,* m/Lt^2, *bar*
P_C = *capillary pressure,* m/Lt^2, *bar*
$P_{C_{lab}}$ = *measured capillary pressure,* m/Lt^2, *bar*
P_{cgo} = *drainage gas-oil capillary pressure,* m/Lt^2, *bar*
PV=pore volume
$[P]_i$ = *parachor of component i*
RF = oil recovery factor
S_g = *gas saturation*
S_{gc}= *the critical gas saturation*
SRK= Soave Redlich Kwong
t = temperature, ºC
X_i = *oil mole fraction of component i*
Y_i = *gas mole fraction of component i*
ρ_v =*gas density,* m/L_3, g/cm^3
ρ_l =*oil density,* m/L_3, g/cm^3
σ = *gas-oil interfacial tension,* m/t^2, *dyne/cm*
σ_{ref} = *reference gas-oil interfacial tension,* m/t^2, *dyne/cm*
ϕ = *porosity*

Acknowledgment

This work has been done as part of the CO_2-KMB project performed at SINTEF Petroleum Research and financed by the Research Council of Norway, Statoil, ConocoPhillips, Norsk Hydro, and Total. We would like to tank all partners for financing this study and allowing the results to be published.

References

1. Hujun, Li.: "Experimental Investigation of CO_2 Gravity Drainage in a Fractured System," paper SPE 64510 presented at the SPE Asia Pacific Oil and Gas Conference and Exhibition held in Brisbane, Australia, 16–18 October 2000.
2. Øyno, L, Uleberg K., Whitson C.H.: "Dry Gas Injection in Fractured Chalk Reservoirs- an Experimental Approach", paper SCA1995-27 presented at the International Symposium of the Society of Core Analysts held in San Francisco, California (1995).
3. ECLIPSE compositional simulator version 2004A, Schlumberger
4. Da Silva, F.V. and Belery, P.: "Molecular Diffusion in Naturally Fractured Reservoirs: A Decisive Recovery Mechanism", paper SPE 19672 presented at the 1989 Annual Technical Conference and Exhibition, San Antonio, TX, Oct. 8-11.
5. Uleberg, K, and Høier, L.: "Miscible Gas Injection in Fractured Reservoirs", paper SPE 75136 presented at the SPE/DOE Thirteenth Symposium on Improved Oil Recovery held in Tulsa, Oklahoma, USA (2002).

Table 1: Initial and current Reservoir oil composition

Component	Initial reservoir oil composition	Present reservoir oil composition
	(%)	(%)
N_2	0.232	0.124
CO_2	0.982	0.833
C_1	58.847	44.153
C_2	7.775	7.562
C_3	3.693	4.207
C_4	2.551	3.150
C_5	1.668	2.185
C_6	1.560	2.069
C_7-C_9	5.616	8.209
C_{10}-C_{15}	6.981	11.575
C_{16}-C_{20}	3.149	5.512
C_{21}-C_{29}	2.642	4.652
C_{30}-C_{34}	0.715	1.261
C_{35+}	3.589	4.508
C_{35+} MW g/gmol	527.806	592.434
GOR sm^3/sm^3	265.530	133.687
Bubble point pressure at 130 ºC (bar)	383.000	242.000
Oil formation volume factor at p_b rv/stc v	1.896	1.480

Table2:14 pseudo components SRK EOS parameters for present reservoir fluid.

Name	MW	Tc	Pc	ω	Peneloux	Peneloux-T
	g/gmol	(ºC)	(bar)		(cm^3/mol)	(cm^3/mol K)
N_2	28	-147	33.9	0.04	0.92	0
CO_2	44	31.1	73.8	0.23	3.03	0.0054
C_1	16	-82.6	46	0.01	0.63	0
C_2	30.1	32.3	48.8	0.1	2.63	0
C_3	44.1	96.7	42.5	0.15	5.06	0
C_4	58.1	147	37.6	0.19	7.7	0
C_5	72.2	193	33.8	0.24	11.68	0
C_6	86.2	234	29.7	0.3	17.98	0
P9	108.3	273	28.3	0.51	18.36	0.021
P10	166	358	20	0.67	44.84	-0.0221
P11	247.1	444	15.9	0.87	55.28	-0.0839
P12	336.2	524	14.3	1.06	37.24	-0.15
P13	484	634	13.4	1.28	-25.67	-0.24
P14	659.2	756	13.1	1.33	-121.72	-0.33
Inert	659.2	756	13.1	1.33	-121.72	-0.33

Table 3: Non-zero binary interaction coefficients

	N_2	CO_2
N_2		
CO_2	-0.0315	
C_1	0.0278	0.12
C_2	0.0407	0.12
C_3	0.0763	0.12
C_4	0.07	0.12
C_5	0.0878	0.12
C_6	0.08	0.12
P9	0.08	0.08
P10	0.08	0.08
P11	0.08	0.08
P12	0.08	0.08
P13	0.08	0.08
P14	0.08	0.08
Inert	0.08	0.08

Table 4: The core initial condition after saturating with Present reservoir oil

Core height	596.5	mm
Core diameter	46.0	mm
Porosity	44.4	%
Initial oil saturation	1.	
Pressure	300.	bar
Temperature	40.	ºC
Bubble point pressure of oil at 130ºC	242.	bar

Table 5: Effective diffusion coefficients using extended Sigmund correlation at 300 bar and 130 ºC

Component	Oil phase	Gas phase
	m^2/day	m^2/day
N_2	2.14E-06	1.08E-05
CO_2	1.20E-06	1.33E-04
C_1	2.83E-06	2.16E-05
C_2	1.30E-06	1.08E-05
C_3	1.07E-05	1.33E-05
C_4	5.47E-06	1.33E-05
C_5	5.47E-07	1.33E-05
C_6	2.21E-06	1.92E-05
P9	2.21E-06	1.92E-05
P10	1.44E-06	1.92E-05
P11	8.09E-06	1.92E-05
P12	3.21E-06	4.45E-05
P13	8.65E-08	7.04E-06
P14	6.00E-08	7.03E-07
Inert	0.00E+00	0.00E+00

Table 6: The dimensions and initial conditions for the matrix, the fracture and the dummy zone in the 2D simulation model

Item	Fracture system	Matrix system	Dummy
Number of grids in R-direction	2	12	1
Number of grids in Z direction	50	50	50
Pore volume, cm^3	100000	440	5
Initial oil saturation	0	1	0.36
Initial water saturation	0	0	0
Pressure, bar	300	300	300
Temperature, ºC	130	130	130

Table 7: The fracture, matrix and dummy fluid composition

Component	Fracture system	Matrix	Dummy
	mol%	mol%	mol%
N_2	0.0	0.1	0.0
CO_2	100.0	0.8	95.0
C_1	0.0	44.2	0.0
C_2	0.0	7.6	0.0
C_3	0.0	4.2	0.0
C_4	0.0	3.2	0.0
C_5	0.0	2.2	0.0
C_6	0.0	2.1	0.0
P9	0.0	8.2	0.0
P10	0.0	11.6	0.0
P11	0.0	5.5	0.0
P12	0.0	4.7	0.0
P13	0.0	3.3	0.0
P14	0.0	2.4	0.0
Inert	0.0	0.0	5.0

Table 8: Dummy cells relative permeability and gas-oil capillary pressure

Sg	K_{rog}	K_{rg}	P_{cog}
			(bar)
0.00	1.00	0.00	0.15
0.80	0.00	0.01	0.28

Table 9: Fracture relative permeability and gas-oil capillary pressure

Sg	K_{rog}	K_{rg}	P_{cog}
			(bar)
0.00	1.00	0.00	0.00
1.00	0.00	1.00	0.00

Table 10: Matrix block relative permeability and gas-oil capillary pressure

Sg	K_{rog}	K_{rg}	P_{cog}
			(bar)
0	1	0	0.009
0.039	0.8131	0.0003	0.0092
0.079	0.6534	0.002	0.0094
0.118	0.5181	0.0067	0.0097
0.158	0.4047	0.0155	0.0099
0.197	0.3108	0.0296	0.0102
0.237	0.2341	0.0499	0.0105
0.276	0.1723	0.0771	0.0109
0.316	0.1235	0.112	0.0113
0.355	0.0858	0.1549	0.0117
0.395	0.0573	0.2062	0.0123
0.434	0.0365	0.2661	0.0129
0.474	0.0219	0.3345	0.0136
0.513	0.0122	0.4111	0.0145
0.553	0.006	0.4955	0.0156
0.592	0.0026	0.5871	0.0171
0.632	0.0009	0.6848	0.0193
0.671	0.0002	0.7874	0.0228
0.711	0	0.8934	0.0304
0.75	0	1	0.038
1	0	1	0.038

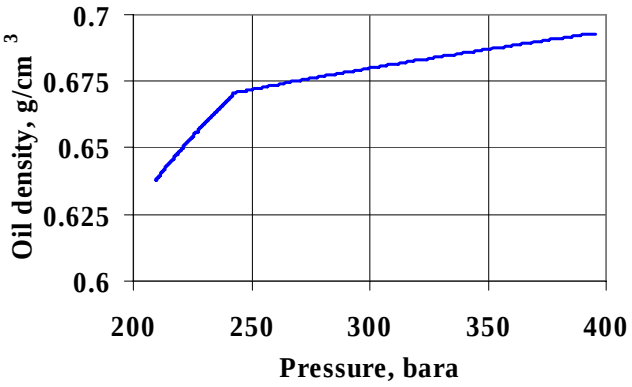

Figure 1: The measured the reservoir fluid density at 130 ºC.

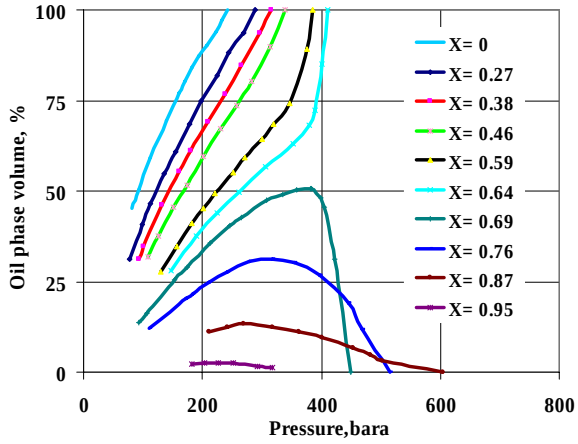

Figure 2: Liquid volume% versus pressure for different mixtures of the reservoir oil at 130 ºC (X is mole fraction of CO_2 in the mixture).

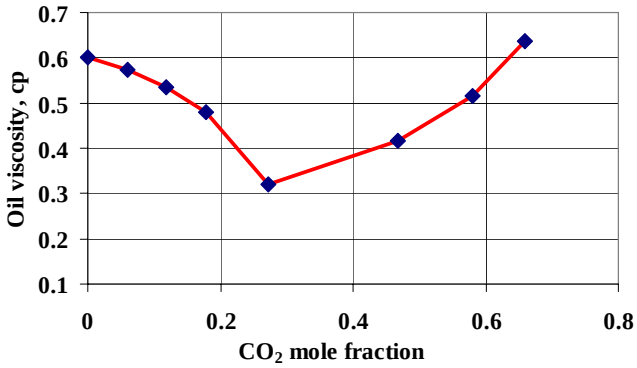

Figure 3: The measured oil phase viscosity (cp) for different mixtures of the reservoir oil and CO_2 at 130 ºC and pressure of 300 bar.

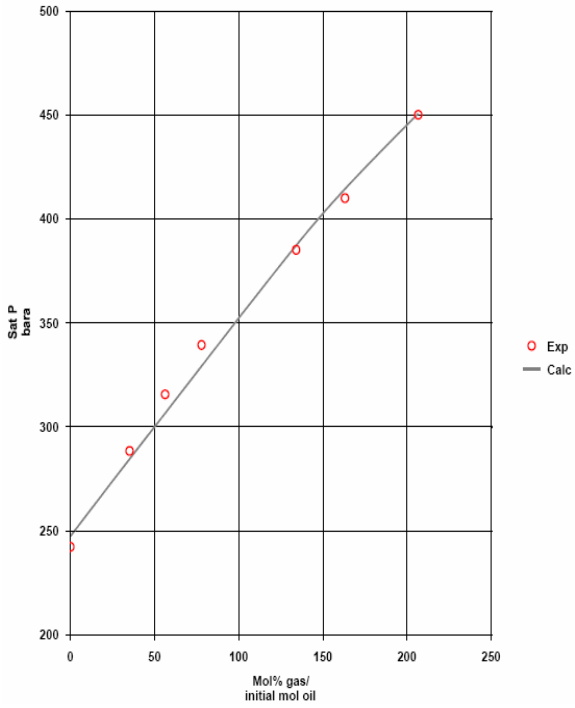

Figure 4: CO_2 swelling saturation point data and simulation results for the reservoir oil at 130 ºC

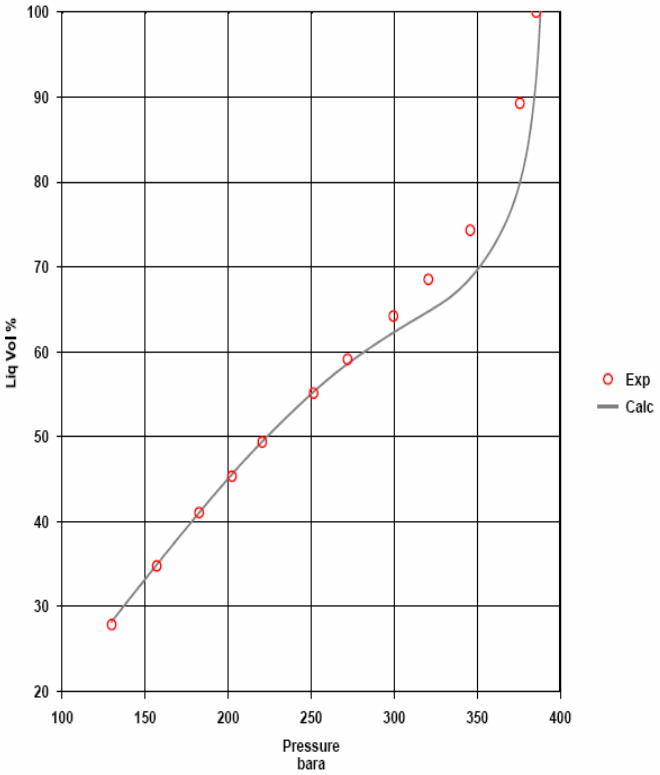

Figure 5: Liquid volume% versus pressure for a mixture of 42.7 mole% of the reservoir oil and 57.3 mole% CO_2 at 130 ºC

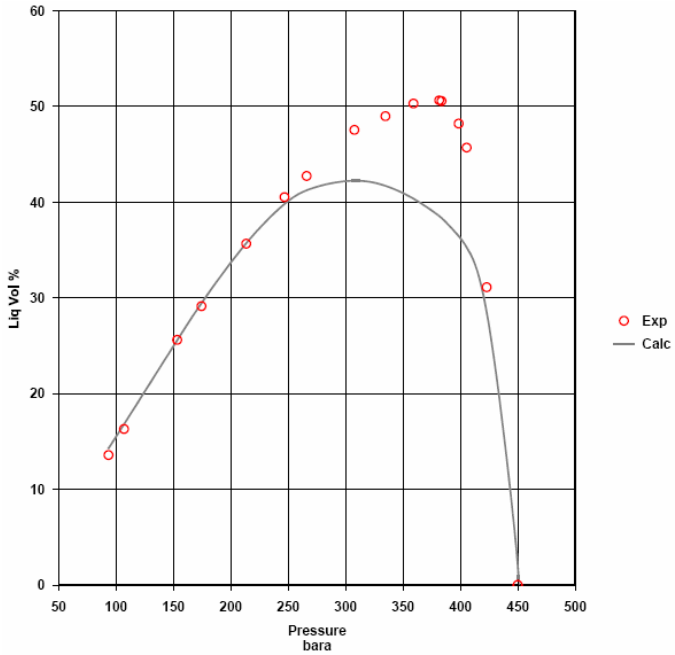

Figure 6: Liquid volume% versus pressure for a mixture of 32.6 mole% of the reservoir oil and 67.4 mole% CO_2 at 130 ºC

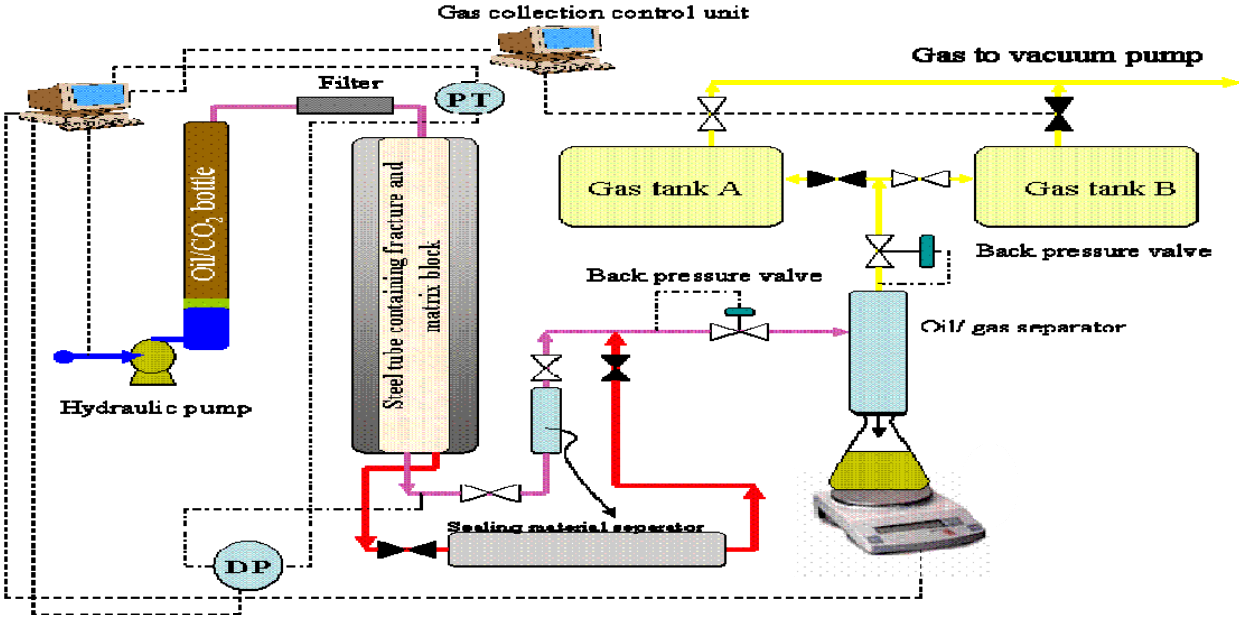

Figure 7: The schematic of the set up used for core initialization (red streams), displacement of sealing material from the fracture (pink streams) and CO_2 injection (red streams)

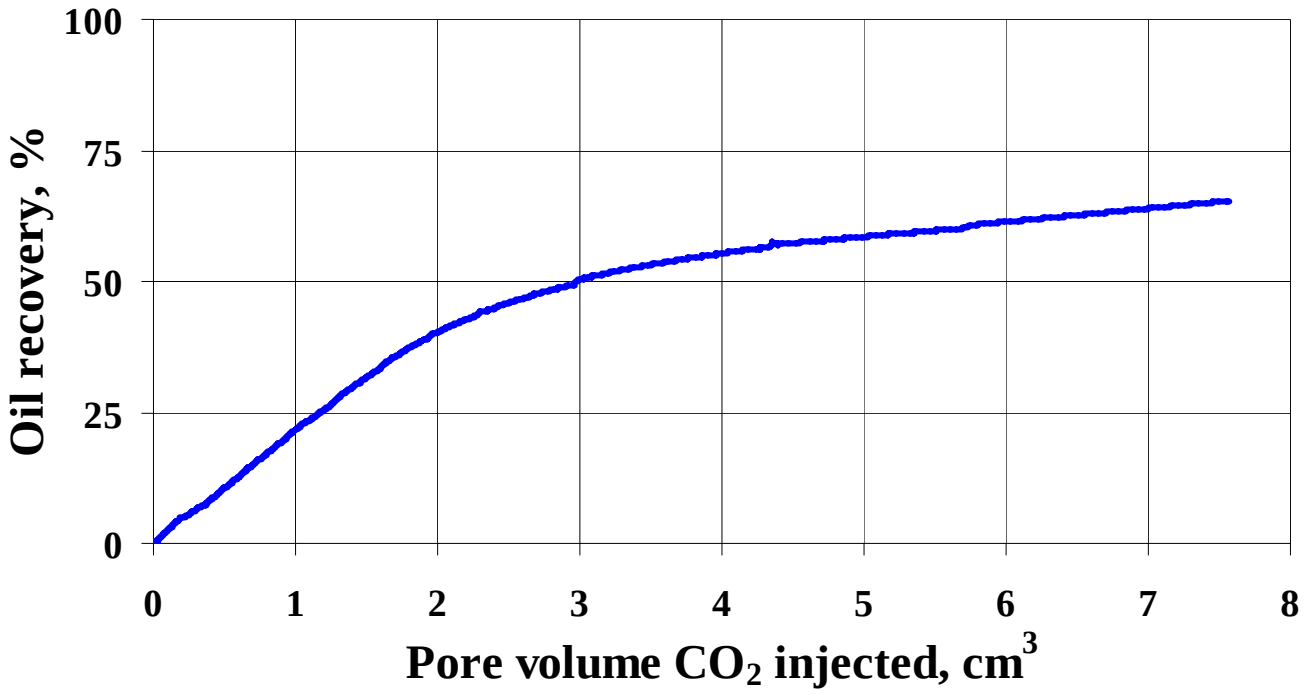

Figure 8: The core oil recovery versus pore volume of injected CO_2 at pressure of 300 bar and temperature of 130 ºC

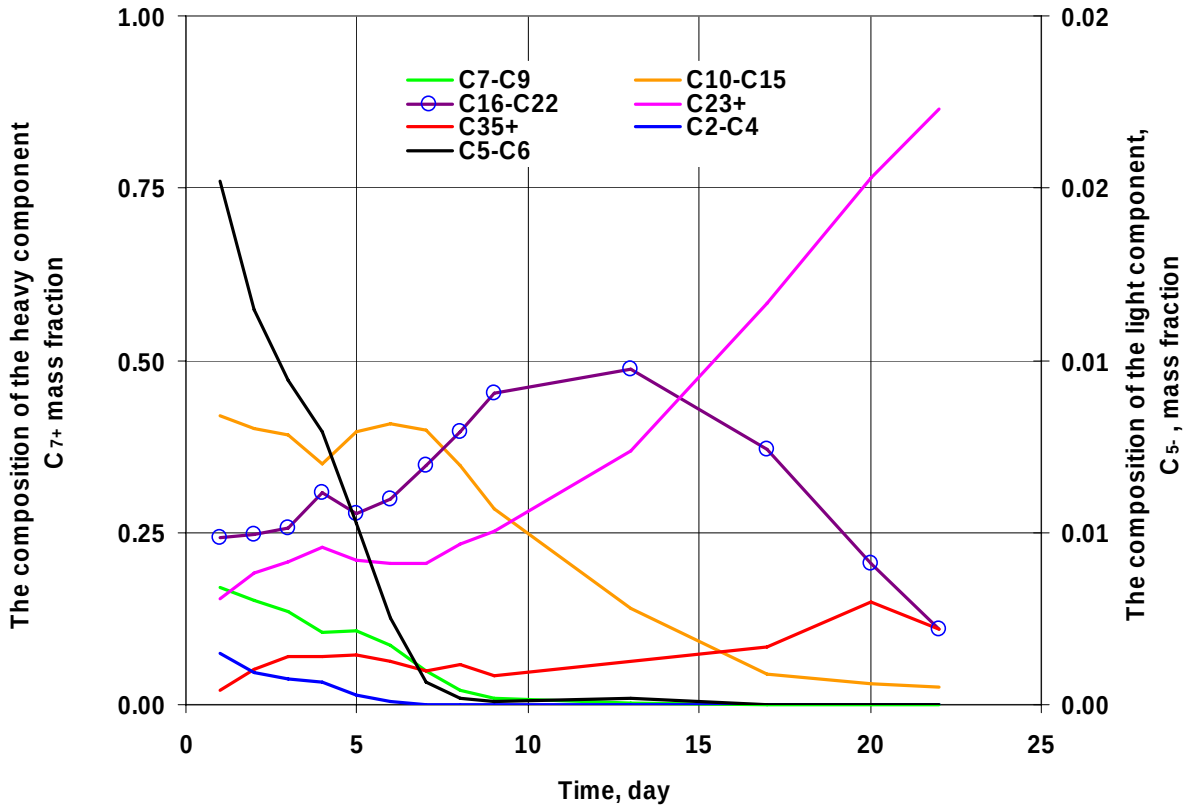

Figure 9: The composition of produced oil samples versus time all at ambient temperature 20 ºC and atmospheric pressure.

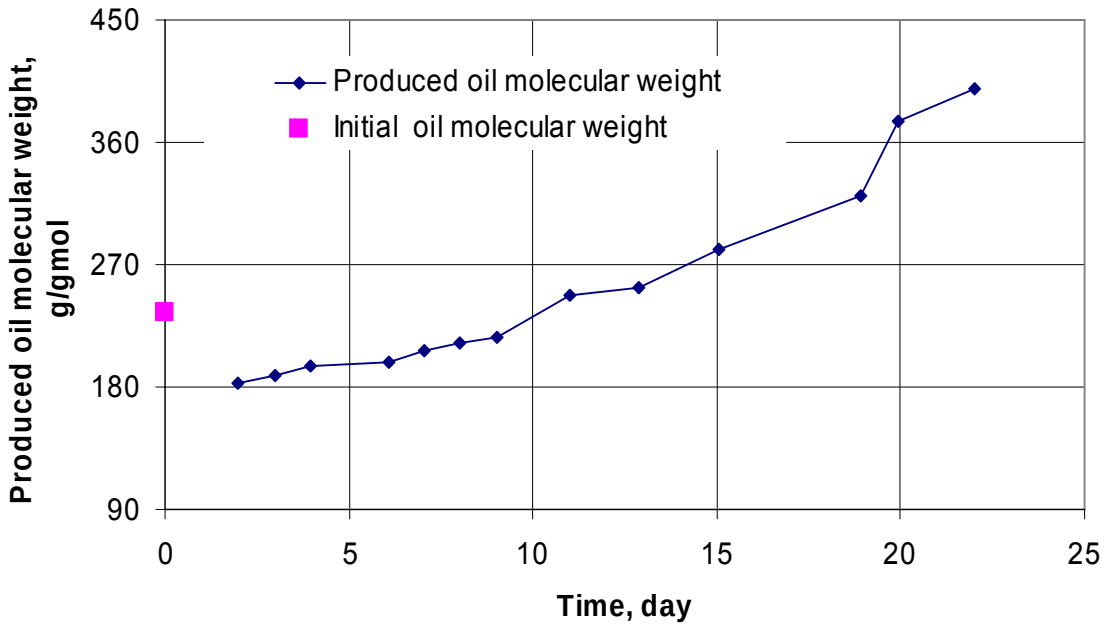

Figure 10: The molecular weight versus time for the produced oil at ambient temperature 20 ºC and atmospheric pressure.

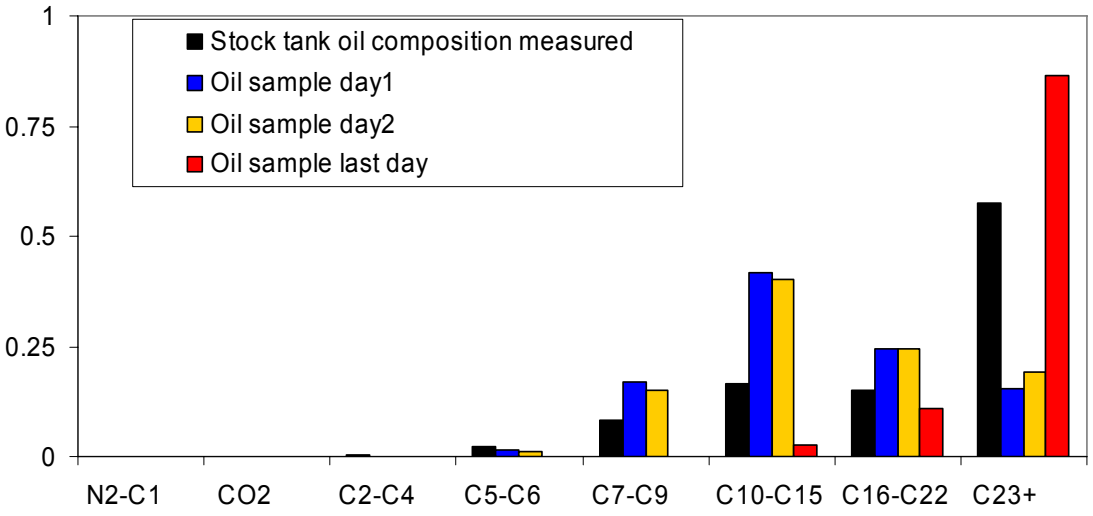

Figure 11: The composition of the produced oil samples at ambient temperature 20 ºC and atmospheric pressure.

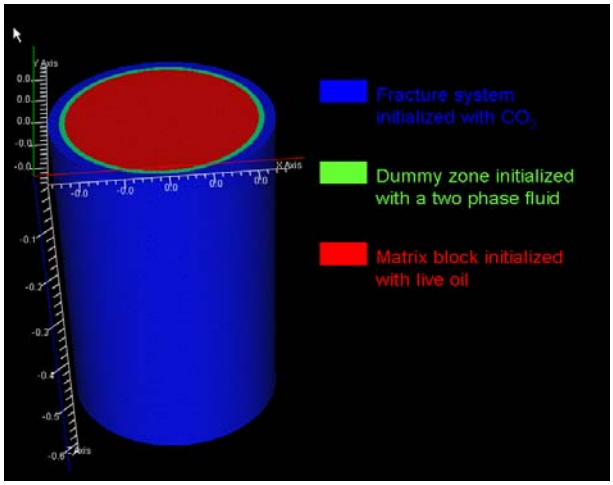

Figure 12: Two-dimensional single porosity radial model 15x1x50 containing a two phase dummy zone located between matrix and fracture grids.

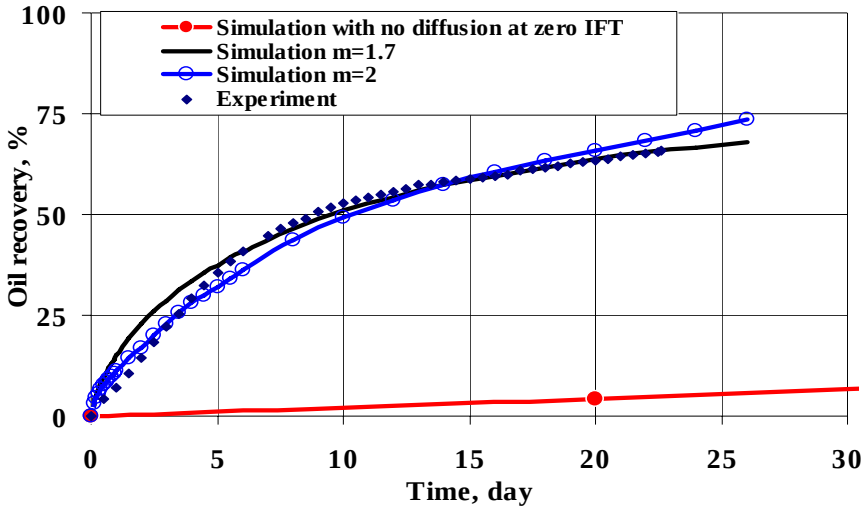

Figure 13: The experimental and simulated oil recovery of the core (matrix block)

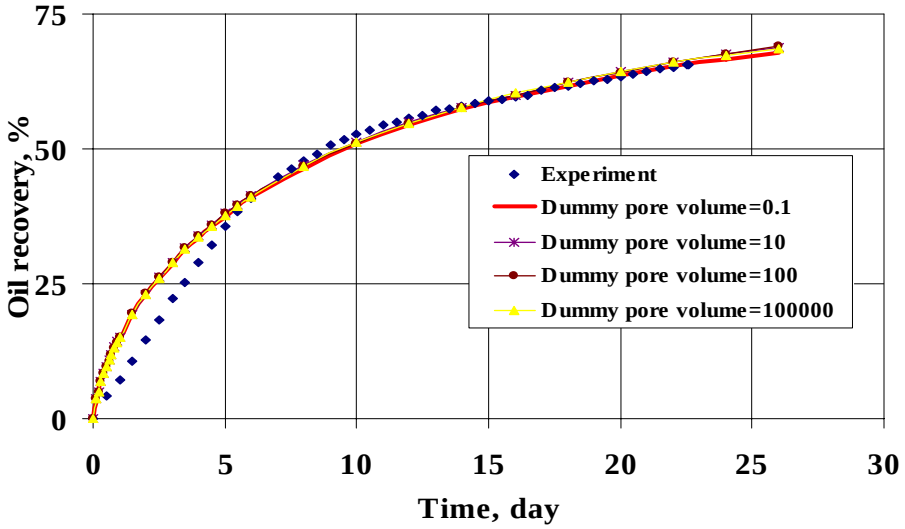

Figure 14: The sensitivity of the simulation results on the pore volume of the dummy grids (the pore volume is in m^3).

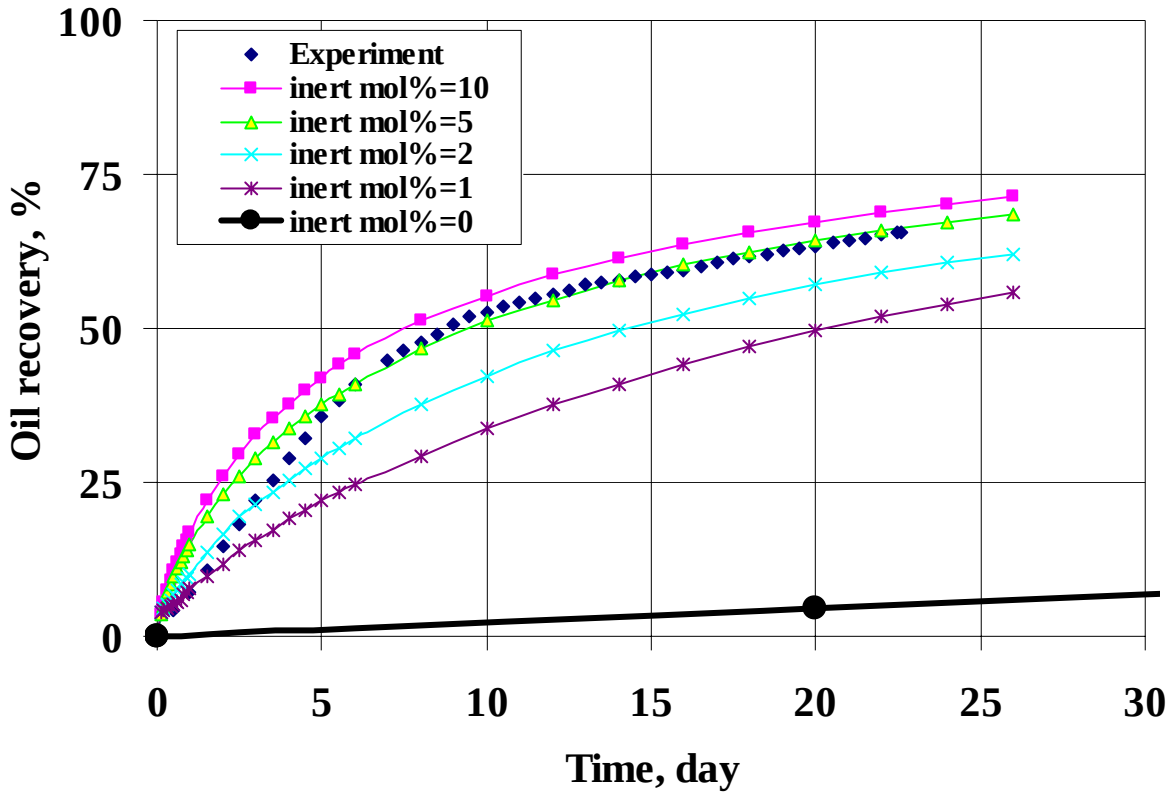

Figure 15: The sensitivity of the simulation results on the total composition of the inert component in the dummy cells.

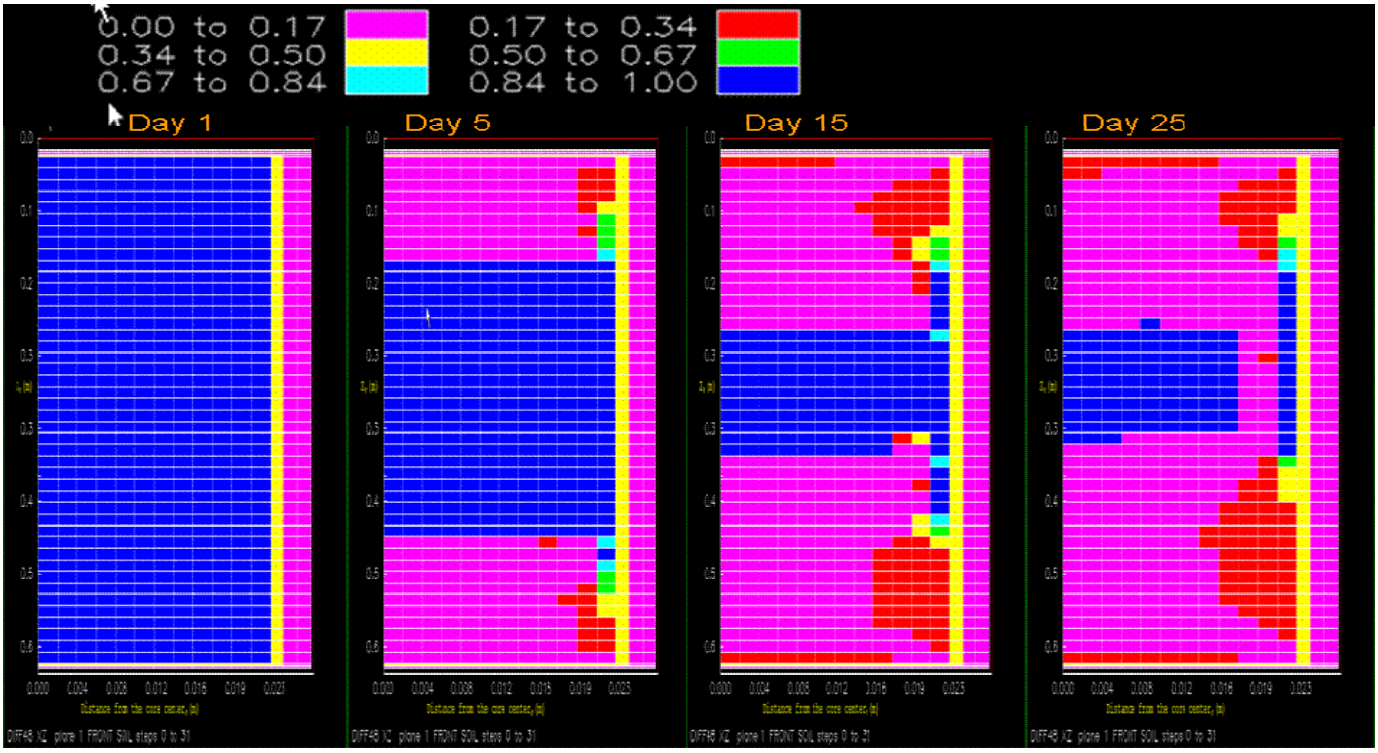

Figure 16: Simulated core oil saturation profiles for four different time steps in R-Z plan, m=1.7 (Horizontal axis is radial direction from the core centre and the vertical axis is the Z direction).

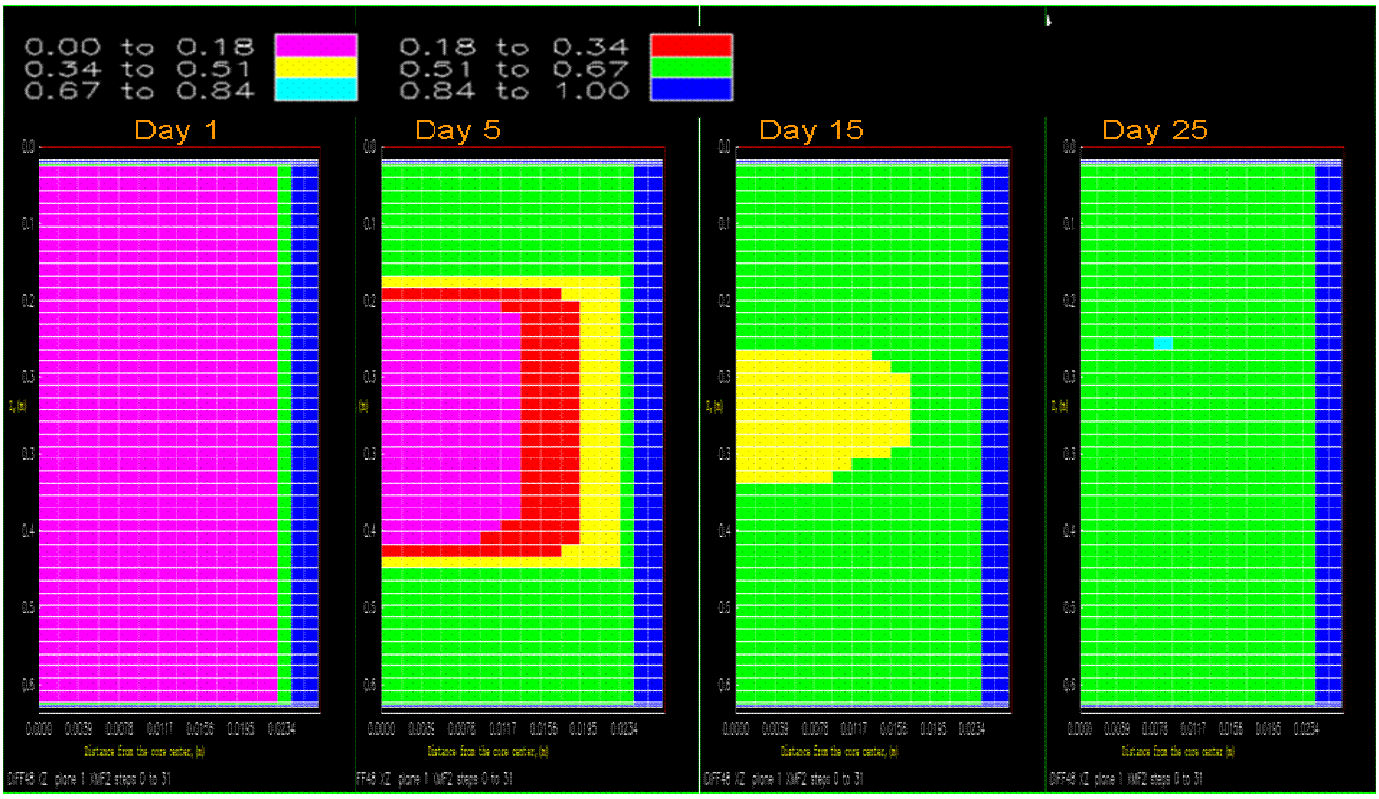

Figure 17: Mole fraction of the CO_2 in the liquid phase for four different time steps, m=1.7. (Horizontal axis is radial direction from the core centre and the vertical axis is the Z direction).

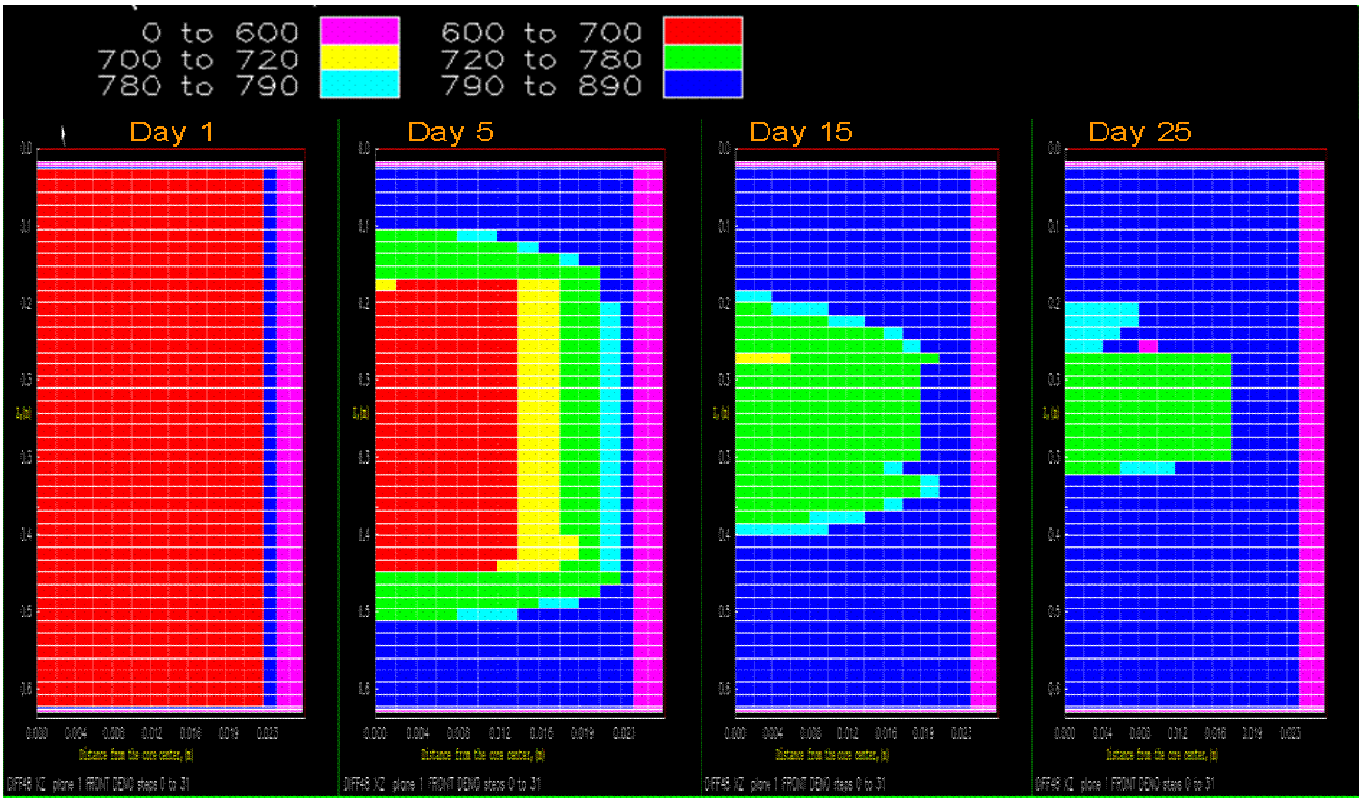

Figure 18: The oil density inside the core for four different time steps, m=1.7(Horizontal axis is radial direction from the core centre and the vertical axis is the Z direction).

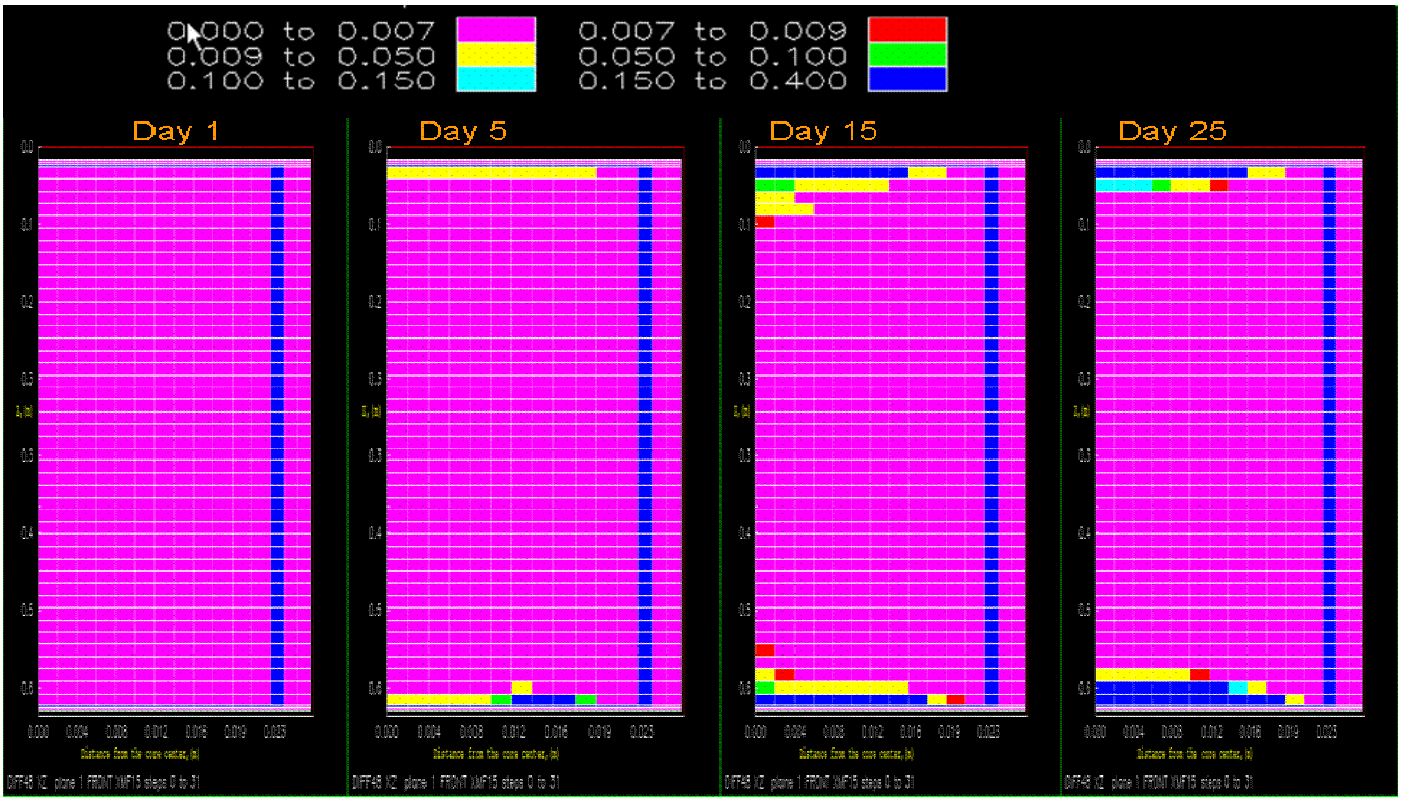

Figure 19: The mole fraction of inert component inside the matrix block at four different time step (Horizontal axis is radial direction from the core centre and the vertical axis is in the Z direction)

Appendix C: Tertiary CO_2 injection in fractured core

SPE 99649

Laboratory Experiments of Tertiary CO_2 Injection into a Fractured Core

Gholam Reza Darvish, SPE, SINTEF/NTNU, Erik Lindeberg, SPE, SINTEF, Torleif Holt, SPE, ResLab AS, Svein Arild Utne, SINTEF

SPE 99649

Laboratory Experiments of Tertiary CO_2 Injection into a Fractured Core

Gholam Reza Darvish, SPE, SINTEF/NTNU, Erik Lindeberg, SPE, SINTEF, Torleif Holt, SPE, ResLab AS, Svein Arild Utne, SINTEF

This paper was prepared for presentation at the 2006 SPE/DOE Symposium on Improved Oil Recovery held in Tulsa, Oklahoma, U.S.A., 22–26 April 2006.

Abstract

The efficiency of tertiary CO_2 injection at the reservoir conditions into fractured cores has been investigated experimentally. The experiment was designed to illustrate the process of water imbibition and CO_2 injection into a North Sea chalk reservoir.

The core and core holder assembly were designed to allow a 2 mm gap to surround the core simulating a fracture. Live reservoir oil was prepared and used to saturate the matrix system. Due to the large permeability contrast between the core (4 mD) and the fracture it is not feasible to saturate the core by simply flooding the system with live oil, since oil would flow through the fracture and only partially saturate the core. To overcome this problem a unique technique has been developed for saturating the matrix system with reservoir fluids. This method ensures a homogeneous fluid composition within the pore system before the fracture system is initialized by the injection fluids (water/CO_2).

During the experiment, the matrix system was first saturated with the live reservoir oil, during which the gap was blocked by a sealing material. In the next step the sealing material was removed and water was injected into the gap. Finally CO_2 was injected at a low and constant rate into the gap. Oil and water production and fluid composition were monitored and the results show that injection of CO_2 could significantly recover residual oil after water injection.

Introduction

To generate accurate predictions by field simulations of CO_2 injection into a fractured reservoir, a set of CO_2 injection experiments at reservoir conditions should be performed to check the compositional effects on the displacement process and to quantify the most important mechanisms. The results obtained can then be up-scaled to larger block sizes and finally allow development of the necessary transfer functions for any field scale simulation.

Performing laboratory experiments at reservoir conditions on fracture systems faces many challenges. The most important is to saturate the matrix and fracture with representative reservoir fluids. Therefore in previous experiments cores were not saturated with live reservoir oil. For example in the CO_2 gravity drainage experiments performed by Li et al[1], the core was saturated with dead oil while the experiment was supposed to be at the reservoir conditions.

Dry gas injection in fractured chalk by Øyno et al[2] was conducted by saturating the matrix system with live oil, but still their method for initialization of the pore system with live oil is not certain. In their experiment the oil recombination was carried out in the core holder where the matrix and fracture were placed. The oil/gas mixture was circulated in the system and pressure was monitored. Once pressure had stabilized, they assumed that the pore system is saturated with the live oil. In this method, since the pore system was saturated with oil by a very slow diffusion mechanism, pressure stabilization over a short time interval will not guarantee homogeneous initialization of the pore system with representative reservoir fluids.

The main objective of this work has been to investigate the efficency of the tertiary CO_2 injection into a fractured core, focusing on the mass transfer of CO_2 and hydrocarbons between the fracture and the chalk matrix.

The resulting recovery profiles and produced fluid compositions can later be used to construct a compositional numerical model. Using this model the magnitude of all forces as well as their contribution to the displacement mechanism during the experiments can be studied.

An important feature of CO_2 injection into fractured reservoirs is the potentially large component exchange between fracture and matrix system. This requires an accurate equation of state (EOS) for modelling purposes. Therefore a comprehensive fluid study of the CO_2/oil system including swelling tests has been performed.

Experimental

For a reservoir with a long water injection history, the reservoir temperature will typically be reduced. The highest reductions are seen in the proximity of the injection wells. In the field addressed by this study the initial reservoir temperature is reduced from its initial value of 130 ºC. For this experiment 60 ºC was chosen to represent the temperature of the water flooded zones. The current reservoir pressure is 300 bar.

The full detail of the core samples, fluids and experimental set up are described below.

Core material

Three core plugs from Faxe chalk, an outcrop analogue to the reservoir rock, were used to make a 60 cm long and 46 mm diameter composite core. The composite core was homogenous and had an absolute permeability of 4 mD. The helium porosity was 44 %, close to values for Maastrichtian chalk in the field under study. The core properties and dimensions are summarized in Table 1.

Fluid samples

An oil representative for the reservoir fluid was prepared and used in all experiments. The initial reservoir oil was made by recombination of stock tank oil with a synthetic gas mixture and with the addition of intermediate components (C_5 and C_6) as a liquid mixture. The initial reservoir oil had a bubble point pressure of 383 bar at 130 ºC with the composition shown in Table 2.

Reservoir oil corresponding to the present composition was obtained by stepwise lowering the pressure of the initial reservoir fluid and pushing off the gas cap in each step. This operation started with an initial pressure of 383 bar at 130 ºC. The pressure steps were approximately 35 bar. The lowest was 247 bar which corresponds to the lowest pressure in the production history. The present reservoir fluid thus has a bubble point pressure of 247 bar at 130 ºC.

A constant mass expansion and a subsequent single flash separation including compositional analyses were performed for both the initial and present reservoir oil. The results are summarized in Table 2. The measured reservoir fluid densities as a function of pressure at 130 ºC and 60 ºC are shown in Figure 1. The calculated CO_2 densities as modelled by the Span and Wagner[3] EOS model is shown in Figure 1

CO_2 swelling tests have been performed on the present reservoir oil for both temperatures. The phase volumes in the two phase region were measured to obtain complete pVTx diagrams for the two CO_2/oil systems (Figure 2 and 3).

Different mixtures of present reservoir oil and CO_2 were prepared and the resulting mixtures were flashed to a pressure of 300 bar. This was done at both temperatures. The viscosities of the resulting liquid phases were measured by a Ruska Rolling ball viscometer. The results are shown in Figure 4.

Matrix and fracture system

The dried core was inserted into a steel tube having inside diameter of 50 mm. Then core was centralized inside the steel tube. The 2 mm annular space between the core's outer boundary and steel tube's wall simulated the fracture. This artificial fracture was then filled with sealing material. The composite core simulated a single matrix block.

The sealing material had no effect on the surface area of the core or on the fluid which was used later for saturating the core. This was investigated by measuring core permeability before and after using sealing material. Measurements confirmed that the core permeability at the outer boundary where it was contacted the sealing material was the same as the core initial condition. Under this circumstance, the artificial fracture filled with sealing material had zero permeability and core had its initial permeability of 4 mD.

Establishing initial saturations

In the second step initial saturations were established. The steel tube and the core were assembled into a core holder and evacuated. The pore volume was measured by saturating the core with synthetic brine. Synthetic brine was prepared from the reservoir formation water composition shown in Table 3. The density and the viscosity of the brine were 1.09 g/cm^3 and 1.19 cp, respectively, at 20 ºC and atmospheric pressure.

The present reservoir oil, with a composition as shown in Table 2, was then injected into the top of the core at a rate of 1 cm^3/min. Oil broke through after 254 cm^3 of brine had been produced. The total live oil injected into the core was 658 cm^3 (1.5 PV) and the total volume of brine produced from the core was 312 cm^3. Thus, the initial water saturation, S_{wi}, and the initial oil saturation, S_{oi}, were 28.8 % and 71.2 %, respectively.

This initialisation was done at 45 ºC and 300 bar, at which the oil was in the liquid phase and the sealing material was solid. At this condition the fracture was still sealed and all injected fluid was forced to flow through the core. The core initial condition after saturating with live oil is shown in Table 4.

Removing the sealing material from the fracture system

The third step was to remove the sealing martial from the fracture while the core still contained the live reservoir fluid. The core flooding rig temperature was increased to the reservoir temperature of 130 ºC at a constant pressure of 300 bar. At these conditions the sealing material inside the fracture melted and was displaced from the fracture by flooding, using the same live oil as used for core initialization. The setup at this step was designed in such a way that during displacement of the sealing material from the fracture, the system pressure and temperature were kept constant. The core and fracture conditions after removing the sealing material are shown in Table 4

Results and discussion

Water Imbibition

Water injection was performed just after removing the sealing material from the fracture, still at 130 ºC and 300 bar. The whole set up shown in Figure 5. The core was placed vertically in a heating cabinet. Brine was first injected into the bottom of the core at a rate of 3 cm^3/min for 1.5 hour to displace the fracture oil. The injection rate was then reduced to 0.3 cm^3/min and the injection continued for six days. During this period the cumulative produced oil was 114Scm^3, corresponding to 54 % of the initial matrix oil. During water injection the oil saturation decreased from 71 % to 33 %. The major results obtained from the water imbibition are presented in Table 4. The recovery curve for water injection is shown in Figure 6.

The results show that almost 50 % of the matrix oil was recovered spontaneously after start of water injection. After six days of water injection another 4 % was recovered.

CO_2 injection at low temperature

The residual oil in the core after water injection was targeted by injecting CO_2. The system temperature was reduced from 130 ºC to 60 ºC during the end of the water flood. Then CO_2 was injected into the top of the core. The initial flow rate was 3 cm^3/min to displace water from the fracture and then decreased to 0.1 cm^3/min after 1.5 hours. The CO_2 injection continued for nine days. The total volume of produced oil and water from the core were 33 Scm^3 and 55 Scm^3, respectively. The core conditions after and before CO_2 injection are given in Table 4. The oil recovery versus time both for water imbibition and CO_2 injection are shown in Figure 6. This figure shows that after injection of CO_2, the oil recovery increased from 54 % to 69 %.

The cumulative oil and water productions during CO_2 injection are shown in Figure 7. This figure shows that after CO_2 injection the rate of water production is initially almost ten times higher than the oil production rate, and it eventually reduces to zero after 8 days. The high initial water production rate was due to the high water saturation in the core as well as high water mobility. The mechanism by which the water was produced from the core was mainly water/CO_2 gravity drainage which was enhanced by swelling oil. The injected CO_2 had a strong swelling effect on the oil at 60ºC and consequently it caused displacement of both oil and water from the matrix. Due to high water saturation, and also the higher density difference between water/CO_2 compared with oil/CO_2, the water production rate was higher than the oil production rate at the early stage.

The mass fractions of light and heavy components in the produced oil during CO_2 injection are shown in Figure 8 and 9. Figure 8 shows that the concentration of the components C_{10-20} in the produced oil was slightly increased at the early stage of CO_2 injection, while for the components C_{21-30} this increase was observed later in the experiment. The low concentration of the components C_5 to C_8 in the produced oil suggests that these components passed the separator. The compositional trend for produced oil show an almost constant composition at the early stage, and after continued injection of CO_2 the produced oil was enriched with heavy components.

The produced gas composition is shown in Figure 10. This figure shows that initially the produced gas at the early stage was enriched with methane and at the late stage it contains more intermediate components.

The molecular weight of the produced oil versus time is shown in Figure 11. This figure shows that the molecular weight was slightly reduced to a minimum value of 239 and then it started to increase. In this figure the value for time zero is the molecular weight of produced oil just after finishing the water imbibition. The change in the molecular weight complies with the compositional trend of the produced oil.

The constant produced oil composition at the early stage suggests that oil swelling and possibly some gravity drainage are the main recovery mechanisms. Because of low density difference between oil and CO_2 (Figure 1), and also the low matrix permeability, the gravity drainage mechanism contribution can be neglected and oil swelling is assumed to be the dominating mechanism at this stage.

At the late stage, the diffusion contribution to the oil recovery became more important since the oil was enriched with heavy components. Compositional simulation of the experiment would give a clearer picture about the contribution from the different recovery mechanisms.

Conclusions

1. A comprehensive pVT fluid study was performed on the oil from a fractured chalk reservoir. The results from this study can be used to make an equation of state model (EOS) for future modelling of the experiment.
2. A unique technique has been developed for saturating the matrix of a fractured core system with reservoir oil. This method ensures a homogeneous fluid composition within the pore system before the fracture is initialized with the injection fluids.
3. Water injection proved to be an efficient method to recover oil from a water-wet low permeability chalk core. The oil recovery by water injection was 54 % of oil initially in place.
4. In fractured reservoirs CO_2 injection could be considered as an effective EOR method for targeting the residual oil after water injection. The overall oil recovery was increased by 15 % of original oil in place. However, at the early stage of CO_2 injection, water production was much higher than the oil production.
5. During CO_2 injection the produced oil showed compositional changes. At the early stage the produced oil composition was constant for a short period and then it was enriched with light end components. Finally, at the late stage of the experiment the oil was enriched in heavy end components.
6. The change in the produced oil composition can be explained by the magnitude of the different recovery mechanisms involved in the mass transfer between the matrix and the fracture system, which should be investigated further by compositional modelling of the experiment.

Nomenclature

EOS= equation of state
GC= Gas chromatograph
MW = oil molecular weight
p = pressure, m/Lt^2, bar
p_b= bubble point pressure, m/Lt^2, bar
PV=pore volume
RF = oil recovery factor
S_g = gas saturation
S_{gc}= the critical gas saturation
S_{oi} = initial oil saturation
S_{wi}= Initial water saturation
SRK= Soave Redlich Kwong
t = temperature, ºC
ϕ = porosity

Acknowledgment

This work has been done as part of the CO_2-KMB project performed at SINTEF Petroleum Research and financed by the Research Council of Norway, Statoil, ConocoPhillips, Norsk Hydro, and Total. We would like to thank all the partners for financing this study and allowing the results to be published.

References

1. Hujun, Li.: "Experimental Investigation of CO_2 Gravity Drainage in a Fractured System," paper SPE 64510 presented at the SPE Asia Pacific Oil and Gas Conference and Exhibition held in Brisbane, Australia, 16–18 October 2000.
2. Øyno, L, Uleberg K., Whitson C.H.: "Dry Gas Injection in Fractured Chalk Reservoirs- an Experimental Approach", paper SCA1995-27 presented at the International Symposium of the Society of Core Analysts held in San Francisco, California (1995).
3. Span R. and W. Wagner. 1996. A new equation of state for carbon dioxide covering the fluid region from the triple-point temperature to 100 K at pressures up to 800 MPa. *J. Phys. Chem. Ref. Data,* Vol. 25, No. 6: 1509-1596.

Table 1: The core properties for experiments

Item	Exp.1
Core type	Fax chalk
Fractures location	Surrounding the core
Core orientation	Vertical
Core length, cm	60
Core diameter, cm	4.6
Core bulk volume, cm^3	997
Core pore volume, cm^3	439
Core porosity, %	44
Core absolute permeability, md	4
S_{wi}, %	28.82
S_{oi}, %	71.18

Table 2: Initial and present reservoir oil composition

Component	Initial reservoir oil composition	Present reservoir oil composition
	(%)	(%)
N_2	0.23	0.12
CO_2	0.98	0.83
C_1	58.85	44.15
C_2	7.78	7.56
C_3	3.69	4.21
C_4	2.55	3.15
C_5	1.67	2.19
C_6	1.56	2.07
C_7-C_9	5.62	8.21
C_{10}-C_{15}	6.98	11.58
C_{16}-C_{20}	3.15	5.51
C_{21}-C_{29}	2.64	4.65
C_{30}-C_{34}	0.72	1.26
C_{35}+	3.59	4.51
C_{35}+ MW g/gmol	528	592
GOR sm^3/sm^3	266	134
Bubble point pressure at 130 ºC (bar)	383.0	247.0
Oil formation volume factor at Pb rv/stc v	1.89	1.49

Table 3: Formation Water composition

Component	weight
	g
NaCl	35.736
KCl	0.298
$CaCl_2 \cdot 2H_2O$	32.281
$MgCl_2 \cdot 6H_2O$	4.350
H_2O	927.335
Total	1000

Table 4: The core and fracture saturation data

Item	Before imbibition	After imbibition	After CO_2 injection
Fracture water saturation, %	0	100	0
Fracture oil saturation, %	100	0	0
Fracture gas saturation, %	0	0	100
Core water saturation, %	29	67	54
Core oil saturation, %	71	33	22
Core gas saturation, %	0	0	24
Fracture oil in place, Scm^3	125	0	0
Matrix oil in place, Scm^3	211	97	65
Matrix oil recovery, %	0	54	69
System temperature, ºC	130	60	60
System pressure, bar	300	300	300

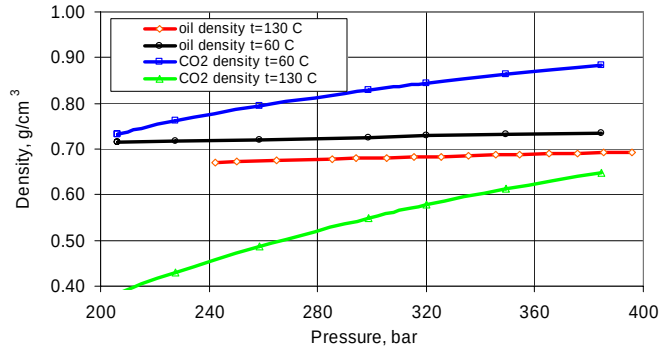

Figure 1: The measured density for present reservoir oil at two different temperatures and the CO_2 density calculated by Span and Wagner[3] EOS model.

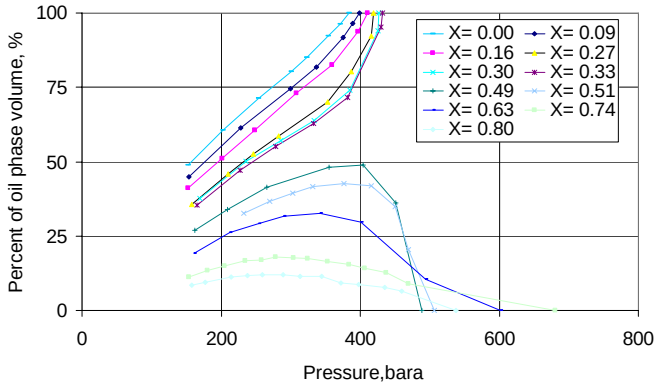

Figure 2: Liquid volume% versus pressure for different mixtures of present reservoir oil at 130 ºC (X is mole fraction of CO_2 in the mixture).

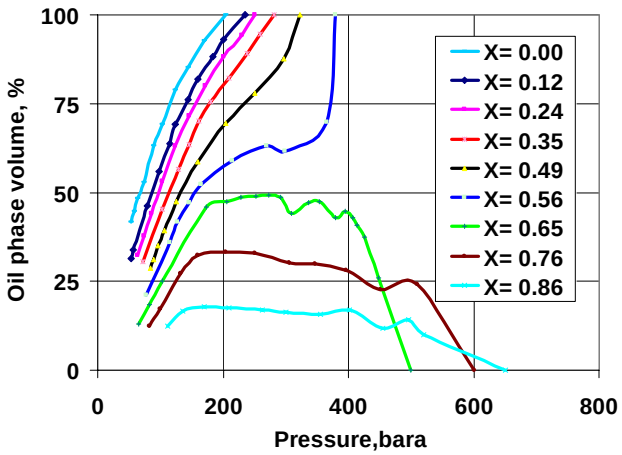

Figure 3: Liquid volume% versus pressure for different mixtures of present reservoir oil at 60ºC (X is mole fraction of CO_2 in the mixture).

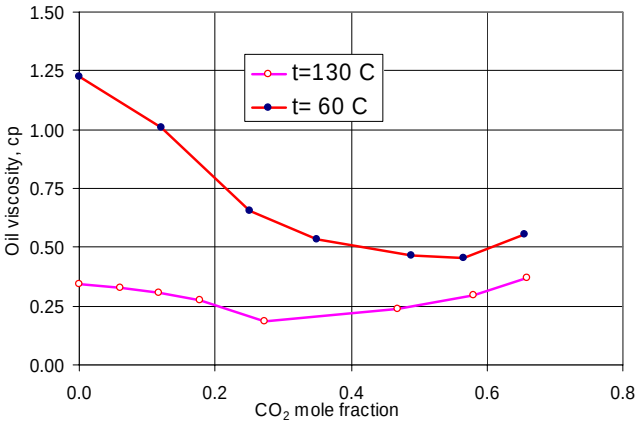

Figure 4: The measured oil phase viscosity (cp) for different mixtures of current reservoir oil and CO_2 at 130 ºC, 60 ºC and pressure of 300 bar.

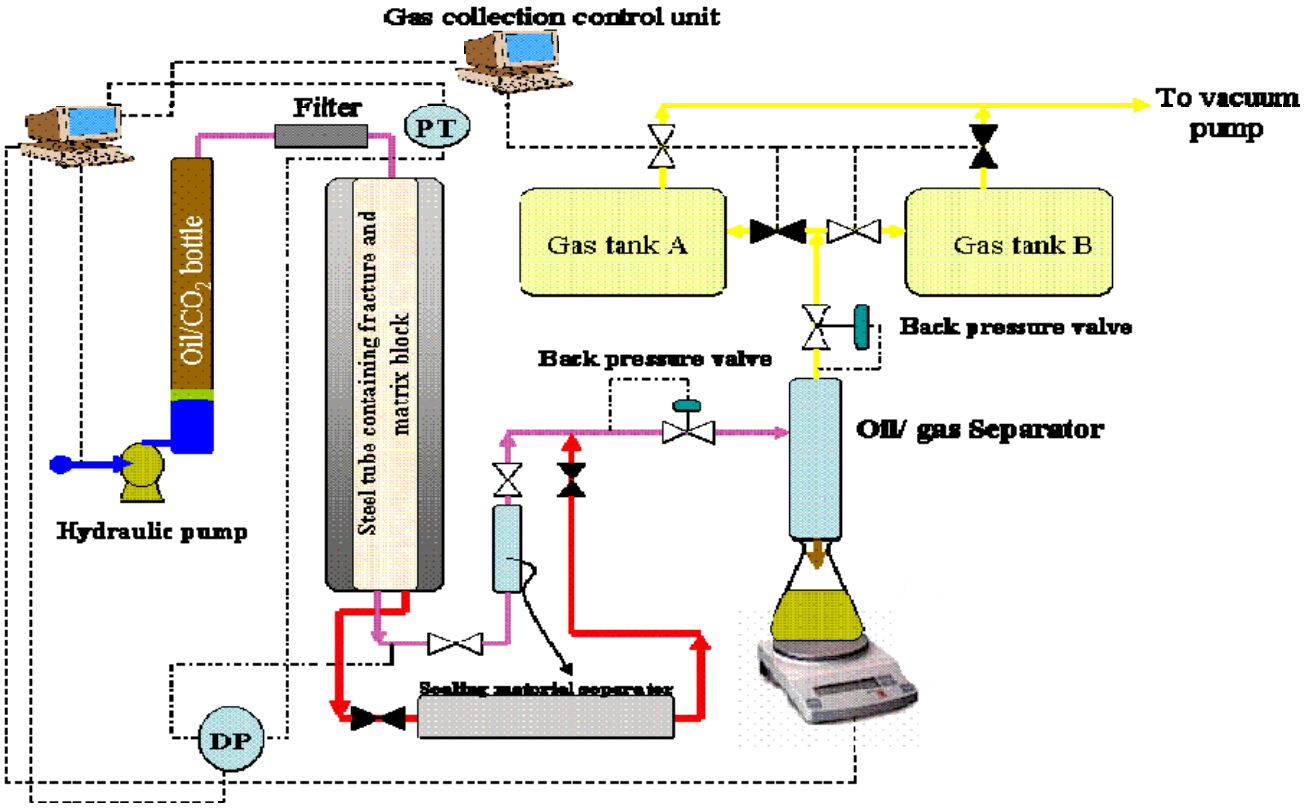

Figure 5: The schematic of the set up used for core initialization (pink streams), displacement of sealing material from the fracture (red streams) and water (pink steam from the bottom) and CO_2 injection (pink stream from the top).

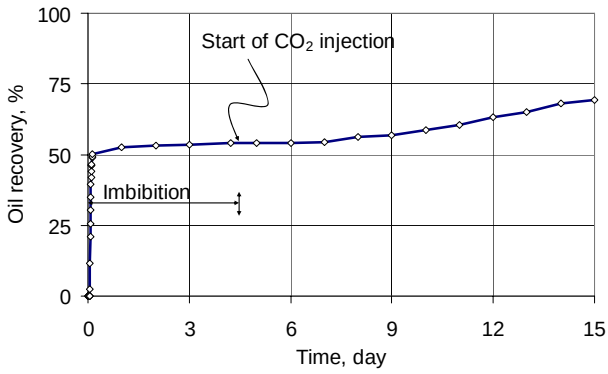

Figure 6: The oil recovery versus time for water injection and CO_2 injection period.

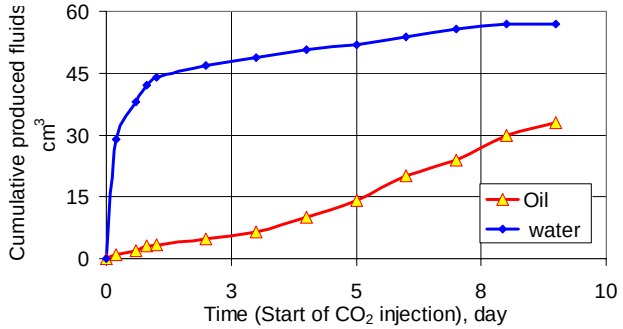

Figure 7: The cumulative produced oil and water during CO_2 injection at 300 bar and temperature 60 ºC.

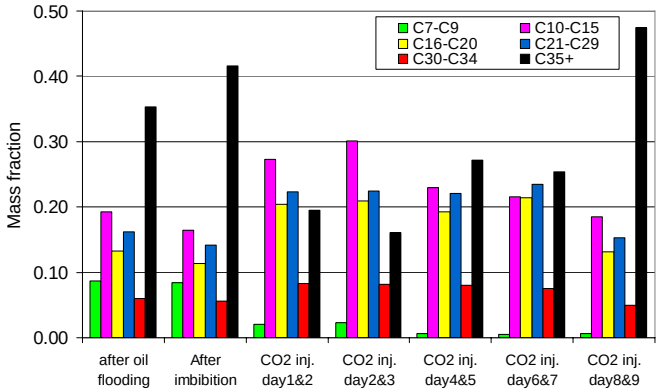

Figure 8: The mass fraction of C_7 and heavier components in the produced oil after water imbibition and CO_2 injection.

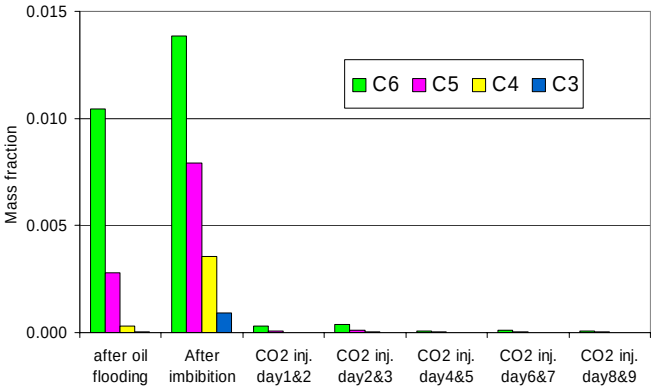

Figure 9: The mass fraction of C_6 and lighter components in the produced oil after water imbibition and CO_2 injection.

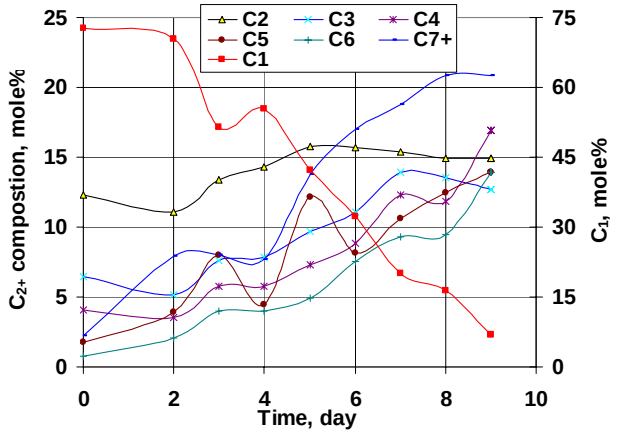

Figure 10: The measured produced gas composition (CO_2 is excluded). Time zero composition belongs to the produced gas after finishing the water imbibition.

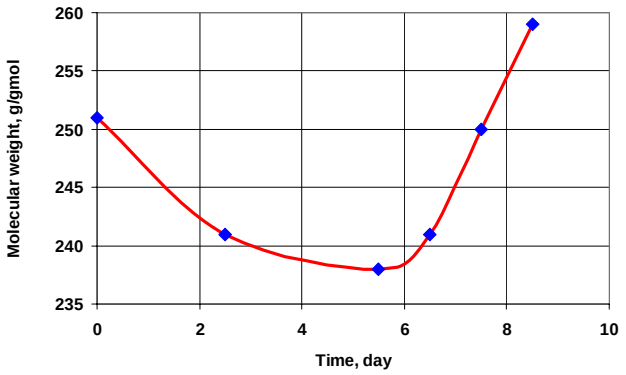

Figure 11: The measured molecular weight of the produced oil during CO_2 injection. The value at time zero showing the oil molecular weight after finishing water imbibition